Improving Biopharmaceutical Production of Chinese Hamster Ovary Cells using Targeted Genome Engineering Tools

A thesis submitted for the degree of PhD

Dublin City University

By

Kevin Kellner, M.Sc.

The research work described in this thesis was conducted under supervision of

Dr. Nga Lao and Prof. Martin Clynes
Dr. Niall Barron, University College Dublin

National Institute for Cellular Biotechnology
School of Biotechnology
Dublin City University

October 2018

I hereby certify that this material, which I now submit for assessment on the programme of study leading to the award of Ph.D. is entirely my own work, that I have exercised reasonable care to ensure that the work is original, and does not to the best of my knowledge breach any law of copyright, and has not been taken from the work of others save and to the extent that such work has been cited and acknowledged within the text of my work.

Signed: _____ (Candidate) ID No.: 14212905 Date: _____

Dedicated to my beloved parents

and friends

Acknowledgements

Almost 5 years ago when I moved to Ireland to write my master's thesis I would have never thought that I will stay a few years longer to do my PhD as well. With that I'd like to express my sincere gratitude to Dr. Niall Barron who gave me the chance to do my PhD in his lab. Thanks for never loosing your patience in every situation and for being always encouraging and positive even when experiments didn't go well. On the same hand I'd like to say thanks to Prof. Martin Clynes who is the most supportive and good person I've ever met! Thanks also to Dr Nga Lao for supervising the last year of my thesis as well as managing that bunch of students in the lab - what would we do without your magic cloning hands?

I would also like to thank the whole proteomics team with Dr. Paula Meleady, Dr. Micheal Henry, Orla Coleman, Dr. Shane Kelly and Dr. Mark Gallagher for helping and contributing so much towards my work. Thanks also to Dr. Clair Gallagher for spending a lot of hours on the FACS – still haven't figured out your secret of keeping the patience!

Of course, I would also like to thank all the postgrads and graduated doctors in our institute and School of Biotechnology for great lunch breaks, walks to Spar/Londis and coffee breaks. I am very glad to have made very good friends during my time in Ireland! Thanks Orla, Laura, Niamh, Giuseppe, Paul, Gemma, Andrew and Alan for the great company and laughs over the last few years. You have all been an amazing support over the last years especially in times of the reoccurring "PhD slumps".

Special thanks also to Justine Meiller, Mairead Callen, Emer Walsh, Gillian Smith and Carol McNamara for your support and help over the last years. The place would not run without you!

Especially I would like to express my sincere gratitude to David Willaert for being the most amazing mentor and manager. I feel like I learned more over the last year as part of your team than during my entire PhD. Besides that, my last year wouldn't have gone so smoothly without the motivating and inspiring speaches every second Friday. Thanks for always believing in me! I also want to thank everyone in the academia sales team for being outstanding and amazing - It was a pleasure to work with each of you and I am glad that I can call all of you friends by now.

I would also like to express my deepest gratitude and appreciation to my best friends: Evelyn, Mischa, Caio. Nora and Maggy. Even though we did not see each other as often as I would have liked to during my time in Ireland I am deeply grateful that you have all been there for me at any time and that I could always count on you! Thanks also for some awesome visits and travels through Ireland and the very best support during times of discouragement but also excitement.

There are no words which could express my gratitude to my beloved parents Angelika and Erwin for always supporting me at every stage during my life and not only throughout my PhD. Thanks for always having my back, inspring me to follow my dreams but also for pushing me always a little into the right direction! I could not have done it without you.

Scientific Talks, Posters, Publications and Graduate Training Elements

Graduate Training Elements:
- Leadership in Research
- Biopharma Industry Regulations and Management
- Posgraduate Tuter and Demonstrator
- Professional Skills for Scientists

Selected Scientific Talks:

Cell Line Development and Engineering US 12-14th June 2018 in San Francisco as invited speaker.

28th European Society for Animal Cell Culture Technology UK (ESACT-UK) 10-11th January 2018 in Leeds, Poster Flash Presentation

BioProduction Congress 2017 8-10th October 2017 in Dublin, Poster Flash Presentation

Publications:

Kellner K., Solanki A., Amann T., Lao N. and Barron N. (2018): "Targeting miRNAs with CRISPR/Cas9 to Improve Recombinant Protein Production of CHO Cells"; Methods Molecular Biology (David L. Hacker), 1850, - accepted for publication.

Kellner K., Lao N., Coleman O., Meleady P. and Barron N. (2018): “Molecular impact of the microRNA-23 cluster on bioprocess relevant attributes of Chinese hamster ovary cells”; BMC Proceedings 2018 **(**12 - Suppl 1).

Table of contents

List of figures

List of tables

Abbrevations

ADCC	Antibody-dependent Cell Mediated Cytotoxicity
AGO	Argonaut Protein
BCL	B-cell lymphoma protein family
BHK	Baby Hamster Kidney
Bp	Base Pair
CHO	Chinese Hamster Ovary
CRISPR	Clustered Regularly Interspaced Short Palindromic Repeat
Cas	CRISPR Associated Protein
CDC	Complement Dependent Cytotoxicity
CMV	Cytomegalovirus
DE	Differentially Expressed
DNA	Desoxyribonucleic Acid
DSB	Double Strand Break
DTE	Difficult to Express
DHFR	Dihydrofolate reductase
DOE	Design of experiments
ER	Endoplasmic Reticullum
ELISA	Enzyme-linked Immunosorbent Assay
EMA	European Medicines Agency
EPO	Erythropoietin
FDA	Food and Drug Administration
FUT	Fucosyltransferase
GS	Glutamine Synthetase
HEK	Human embryonic kidney

HPLC	High Performance Liquid Chromatography
HSP	Heat Shock Protein
HDR	Homology Directed Repair
Indel	Insertion/Deletion
KRAB	Krueppel associated box
LC-MS/MS	Liquid Chromatography – Mass Spectrometry
LDH	Lactate Dehydrogenase
MBS	MicroRNA Binding Sites
MOI	Multiplicity of Infection
MiRNA	MicroRNA
MYC	Myelocytomatosis
MAb	Monoclonal Antibody
MBS	MicroRNA binding sites
MGE	Mobile genetic elements
MTX	Methotrexate
MSX	Methionine Sulphoximine
MYC	Myelocytomatosis
NGS	Next Generation Sequencing
Nt	Nucleotide
NHEJ	Non-homologoues End Joining
NS0	Murine myeloma cell line
ORF	Open Reading Frame
PAM	Protospacer Adjacent Motif
PDI	Protein Disulfide Isomerase
PiRNA	PIWI-interacting RNA

RCME	Recombinase-mediated cassette exchange
ROS	Reactive Oxygen Species
RNA	Ribonucleic Acid
RISC	RNA-induced Silencing Complex
SEAP	Secreted Alkaline Phosphatase
SF9	Spodoptera frugiperda cell line
SiRNA/shRNA	Small interfering/small hairpin RNA
SgRNA	Single-guide RNA
SiRNA	Short-interferring RNA
TPA	Tissue Plasminogen Activator
TALEN	Transcription-like Effector Nucleases
TracrRNA	Trans-activiating crRNA
UCOE	Ubiquitous chromatin opening element
UPR	Unfolded Protein Response
UTR	Untranslated Region
XIAP	X-lonked inhibitor of apoptosis protein
ZNF	Zinc Finger Nucleases

Abstract

Title: Improving Biopharmaceutical Production in Chinese Hamster Ovary Cells using Targeted Genome Engineering Tools

Author: Kevin Kellner

Chinese Hamster Ovary (CHO) cells are the prominent cell line used in biopharmaceutical production. Over 70% of all therapeutically used recombinant proteins are produced by CHO cells with a market size predicted to exceed €250bn by 2021. Their favourable attributes over other cell lines are properties like resistance to viral infections, growth in chemical defined media, human like glycosylation patterns, good productivity and ease of genetic engineering. Due to the complexity of mammalian expression systems yields achieved are not phenomenal by any means. However, compared to 1986 with product concentrations of 50 mg/L, titres up to 10 g/L have been reported recently. Improvement of bioprocesses and media development contributed their part in facilitating higher titres but genetic engineering to improve host cells came to the foreground. MicroRNAs (miRNAs) have hereby been highlighted as attractive targets due to their involvement in processes like viability, secretion, productivity, product quality to mention only a few. MiRNAs are small non-coding RNAs which are about 22 nucleotides in length and were first discovered in the early 90's. A single miRNA can target 100-200 mRNAs which highlights them as key regulators for translational control. The miRNA-23 cluster was first identified as upregulated during induced hypothermic conditions. Hypothermia is a commonly used process to reduce growth and thrive CHO cells to improved productivities. Therefore, we hypothesised involvement of the miR-23 cluster or individual miRNA members in viability and productivity phenotypes. In this work we investigated the depletion of the miR-23 cluster as well as miR-23, miR-24 and miR-27 in a panel of industrially relevant cell lines expressing various recombinant products. In fact, miR-24 was identified as thriver of productivity and growth by upregulating ribosomal biogenesis, assembly of ribosomal subunits, translation as well as unfolded protein response (UPR). This was demonstrated in several cell lines and was not product specific. Furthermore, the depletion of the whole miR-23 cluster as well as miR-27 has been shown to improve productivity although in a cell line specific context. To overcome challenges of sponge technology we also implemented the recently developed CRISPR/Cas9 system to target miRNAs. When phenotypes after sponge and CRISPR/Cas9 mediated depletion of members of the miR-23 cluster were assessed, it was demonstrated that even enhanced properties were exhibited using CRISPR/Cas9 in case of miR-24 and miR-27 regarding productivity and longevity. Furthermore, we implemented a CRISPR/Cas9 library for genome wide recessive knockout screens to identify proteins involved in high productivity phenotypes or are important for survival of stress conditions i.e. hyperosmolality. Mixed populations expressing the sgRNA-library were sorted for high productivity using low temperature stains and were adapted to high salt conditions. Enrichment or depletion of sgRNAs was subsequently analyzed using Next-Generation Sequencing. SgRNA abundance analysed after low temperature stain showed enrichment of distinct populations. Functional annotation of enriched genes showed no evidence in relation to productivity. Exploiting miRNAs and genome-wide knockout studies to improve the bioprocess phenotype highlights these methods as interesting tools for further investigation regarding applications within biopharmaceutical industry.

1.0 Introduction

1 Introduction

1.1 CHO cells in biopharmaceutical industry

The first recombinant protein expressed by mammalian cells was tissue plasminogen activator (tPA) in 1986 used for the treatment of thrombosis and myocardial infarctions. The production of recombinant proteins by mammalian cells offered a wide field of possibilities for therapeutic applications in treatment for cancer, infectious diseases and diseases like haemophilia. The volumetric yields reached about 50 mg/l over a period of 7 days. Nowadays yields up to 5-10 g/L were reported (F. M. Wurm, 2004) and 70% of all recombinant proteins used as biopharmaceuticals are produced by mammalian cell lines. Prominent cell lines used for their production are Chinese hamster ovary (CHO), Mouse myeloma (NS0), baby hamster kidney (BHK) and human embryonic kidney cells (HEK293). The market size reached up to €140bn in 2013 and is predicted to exceed €250bn by 2021 (Walsh, 2014). Approved recombinant proteins are for example Erythropoietin (EPO), Cetuximab and Trastuzumab which are used as common therapeutics for the treatment of anaemia, colorectal cancer and breast cancer. However, recombinant proteins describe a diversity of different molecules like cytokines, monoclonal antibodies (mAb), Fc fusions, antibody fragments and enzymes.

CHO cells are the most commonly used cell line due to their beneficial properties like resistance to viral infections, growth in chemical defined media, human like glycosylation patterns, medium productivity and ease of genetic engineering. CHO cells are genetically well known and different selection systems like dihydrofolate reductase deficient (DHFR) or glutamine synthetase deficient (GS) strains are well established and studied. However, the optimisation approaches like improvement of media formulations and bioprocess regimes are limited pathways and genetic engineering to identify beneficial phenotypes and improve the bioprocess behaviour came to the foreground and was highlighted as a promising research field. Furthermore, the demand of more therapeutic proteins with high qualities and yields drive the development of new strategies. The focus of cell line engineering lies hereby not only on a phenotype with high productivities but equally important are other features like growth behaviour, apoptosis and stress resistance, glycosylation pattern, viability and improved secretion of products.

The development of new therapeutic proteins follows a distinct route from start to the finished approved product. Firstly, the host producer cell is transfected with the transgene of interest and cells are selected due to a selection marker which is usually

encoded by the same vector. The selection method depends hereby on the expression system. If DHFR deficient cells ($dhfr^-$) are used the selection and amplification process is performed with the help of methotrexate (MTX). MTX inhibits the dihydrofolate reductase (DHFR) which is an essential gene for the conversion of dihydrofolate to tetrahydrofolate. Tetrahydrofolate is required for purine and pyrimidine synthesis and therefore plays an essential role in cell growth by providing DNA precursors. The GS gene is a vital gene and is crucial for the synthesis of glutamine out of glutamate and ammonia. A GS deficient strain can be transfected with the gene of interest and the GS gene which allows the selection in glutamine free medium of positively transfected cells. Methionine sulphoximine (MSX) is a potent GS inhibitor and can be used for amplification processes but is often not necessary. Amplification processes are mainly based on the genetic instability of CHO cells which leads to genetic aberrations like for example gene amplifications (Derouazi et al., 2006). This genetic instability is used for the amplification of transgenes as higher copy numbers are usually associated with higher product expression (Schuster-Bockler et al., 2010; Stranger et al., 2007). Following selection and amplification clonal cell lines are established and individual clones are assessed for high productivities as well as their growth performance. Once high producers are identified the further development and screening is based on the cultivation process optimisation and individual growth characteristics. Design of experiments (DoE) is nowadays a vital part of process optimisation. DoE can be for example used to predict the growth behaviour of cells and to optimise media as well as feed characteristics without the need of large scale experiments. Only initial and final experiments are needed to assess the bioprocess at its best (Horowitz et al., 2009; Mandenius & Brundin 2008). After the bioprocess is defined and pilot-scales were successfully completed the commercialisation process begins which involves scale-ups and validation of manufacturing as well as clinical studies with the therapeutic protein (F. Li et al., 2006).

Besides the process development the major cost factor are clinical trials for the approval of the newly developed therapeutic protein by the regulatory authorities like FDA and EMA. Clinical trials are studies important for the investigation of the functional bioprocess product and are divided into three different phases (I, II and III). All trials aim to study the potential of the developed therapeutic drug with hindsight on potential side effects and efficacy. Total development costs of only one biopharmaceutical are estimated to be ~ US $ 1 billion including development, pre-clinical and clinical trials (DiMasi & Grabwoski, 2007). However, phase II and phase III are critical and success rates are in general very

low (~18% for II, ~5% for III) leading to high risk factors for the developing company. This explains why one of the main focuses is to reduce development and process costs implementing genetic engineering which are linked to immense amounts of savings potential.

1.1.1 Cell culture regimes and formats

For the large-scale production of recombinant proteins, bioprocesses are usually performed in dimensions up to 20,000 L. However, for process optimisation and development usually smaller scales are applied as up-scaling effects are well characterised and follow distinct rules. Furthermore, costs of goods increase drastically for larger scales e.g. media costs. The optimisation is usually performed in small scale cultures e.g. 96-well plates, shake flasks and benchtop bioreactors which allows process development in high-throughput (Li et al., 2010). One important factor hereby is the optimisation of the basal media and feed for fed-batch modes. These media are chemically defined for suspension cultures without the usage of animal derived components but including recombinantly derived products like albumin in exact concentrations. Defined media is optimal as process environments are defined and downstream applications are straight forward if no serum or other animal compounds are involved. Common carbon sources used are high levels of glucose and glutamine as well as other essential amino acids. Lipid sources are usually sterol, glycerol phospholipids and sphingolipids. Lipids are essential for energy storage and as structural element for e.g. membranes (Landauer, 2014). However, carbon sources are consumed very easily and waste products like lactate and ammonia have been shown to influence product quality as well as growth (Altamirano et al., 2000; Hansen & Emborg 1994; Lao & Toth 1997).

For the ideal production of the biopharmaceutical the choice of the bioprocess regime is essential. Besides batch and perfusion, the fed-batch culture is the most commonly used bioreactor mode for the production of recombinant proteins. However, the choice of the culture system can have significant influences on the product qualities and properties. It was reported that different culture conditions have an influence on the glycosylation pattern of IgGs (Patel et al., 1992). Furthermore, it was described that the pH influences the glycosylation of the product leading to the addition of buffering solutions in fed-batch cultivation to maintain a constant pH over the whole period of the bioprocess (Muthing

et al., 2003). Counteracting a pH drop using bases will however, ultimately increase burden on cells due to high osmolality conditions. Cultivation under high osmotic conditions has been considered to influence glycosylation pattern as well (Schmelzer & Miller, 2002) making the understanding of processes inalienable. The glycosylation pattern of a recombinant protein is essential to ensure efficacy, pharmacokinetics and prevent immune system response. Many process related factors were described to alter glycosylation pattern of the therapeutic product including the cell type, medium and feed supplements (Hossler, Khattak, & Li, 2009a).

Traditional cultivations in batch have become very uncommon over the past few years for mammalian cells due to major disadvantages of fast nutrient depletion, low cell densities and high waste accumulation. However, a batch-refeed strategy was applied for the removal of toxic waste products and has been shown to be applicable in small scale bioreactors up to 200 L (Xie et al., 2003) as a strategy to simplify perfusion.

Two major bioreactor systems are commonly used for the large-scale production of recombinant proteins using mammalian cells: fed-batch and perfusion cultivation. Fed-batch cultures are applicable with working volumes up to 20,000 L. The fed-batch mode works in two phases: initial cell growth is supported by basal media. Once a certain cell density is reached a concentrated nutrient feed is added to prevent nutrient depletion which would ultimately lead to declining cell densities and viability (Birch & Racher, 2006). Feed strategies have to be optimised for each cell line which is implemented by using small scale experiments and DoE (Horowitz et al., 2009; N. Ma et al., 2009). Optimisation of feed strategies and supplements has been shown to increase product yields. A DoE study implementing several different feeds and supplements showed increased yields of about 167 %, respectively (Kochanowski et al., 2011). However, the effect on the protein product itself was not investigated. DoE involves mathematical approaches linking the effect of the inputs given into the bioprocess on the output variables. It involves the inclusion of several parameters e.g. metabolism, media supplements and stress factors which can be extrapolated using stoichiometric calculations (Mandenius & Brundin, 2008b). However, even though input variables are constant a biological system usually never behaves the same but DoE is essential to reach the regulatory demands set by medical safety agencies. Fed-batch has been proven to be a consistent bioprocess system leading to high yields of up to 5-13 g/L (Huang et al., 2010; F. M. Wurm, 2004). The stationary phase in batch cultures is usually very short but is highly prolonged in fed-batch cultures and is usually associated with

high productivities due to inhibited proliferation. A common fed-batch process continuous on for 12-14 days in total. Nevertheless, due to enhanced cell number and the long cultivation times, accumulation of toxic catabolites like ammonia and lactate is one of the major problems of this bioprocess mode. Due to high lactate levels the pH starts to decrease over culture time and furthermore the osmolality increases due to feed addition of pH additives which are necessary to maintain constant bioprocess parameters. Low pH values and high osmolality have been shown to influence the glycosylation pattern as well as growth and ultimately lead to reduced quality of the bioprocess product. Furthermore, ammonia has been reported to impact the glycosylation pattern of IgGs. Gawlitzek and colleagues (Gawlitzek et al., 2000) reported a decrease in N-acetylneuraminic acid and galactose residues with increased levels of ammonia in the bioprocess. It was suggested that the alteration of galactosylation and sialyation is dosage dependent on the concentration of ammonia in the media. Several strategies have been described to control the waste accumulation due to controlled stoichiometric feeding of key metabolites like glutamine and glucose (Glacken et al., 1986).

Besides, controlling feeds to overcome high concentrations of catabolites in the culture media over time the perfusion bioprocess mode was developed. In comparison to fed-batch cultivation, perfusion can last up to months, whereas cells are fed constantly with fresh media whilst old media and product is removed. Cells remain in the bioreactor and different approaches have been proven to be successful. One way for example is to use polyester matrices, fibres or membranes to keep cells entrapped in the bioreactor (Meuwly et al., 2007; Zhang et al., 2015). Another approach is the usage of filtrations systems like tangential flow filters to maintain cells in the bioreactor (Clincke et al., 2013) or centrifugation. The removal of toxic waste products ensures optimal growth conditions for cells in the perfusion bioreactor. Furthermore, cells are usually cultivated in high cell densities up to 2 x 10^8 cells/mL (Y. Zhang et al., 2015) increasing yields drastically. One major advantage is as well that perfusion reactor scales are considerably smaller in comparison to fed-batch reactors. It was observed that the perfusion bioreactor with a working volume of 50 L can achieve same yields compared to a fed-batch reactor with a volume of 1,000 L. However, cultivation times regarding perfusion reactors are much longer compared to fed-batch cultures and fed-batch cultures are the most prominent cultivation methods in industry. Another advantage of the perfusion bioreactor is as well that the process conditions are not changed over time. Waste accumulation and addition of feed as well as alkali changes osmolality in a fed-batch cultivation process. Using

basal media or media with low percentages of feed for the perfusion reactor maintains the bioprocess constant. Furthermore, removal of therapeutic product out of the bioprocess environment increases the product stability as the product might be prone to degradation or cleaving by proteases in a closed bioprocess at late stages of the culture.

Studies showed that the perfusion reactor led to dramatically increased yields of an IgG when compared to the same product using the same cells in cultures. Zhang and colleagues showed a final IgG yield of 1.42 g in comparison to only 40.5 mg for a batch process. Same drastic impact on the titre was shown using Drosophila Schneider 2 cells with a final yield of 8 g for perfusion and 200 mg for batch cultures (L. Wang et al., 2012). However, cultivation times using the perfusion reactor are significantly longer.

Bioprocesses under hypothermic conditions is a well-established method for the production of recombinant proteins in biopharmaceutical industry. Commonly known as “biphasic culture” process the initial growth is promoted by a temperature of usually 37°C (cell line dependent). After reaching a critical cell density the temperature is decreased to 30-31°C. This hypothermic condition arrests cells in G_0/G_1 phase and ultimately reduces proliferation. However, due to inhibited growth the productivity is highly elevated as energy is shifted towards protein production instead of growth (Kaufmann et al., 1999; Trummer et al., 2006; Yoon et al., 2003). Furthermore, the nutrient consumption rate, protease activity as well as the O_2 consumption are reduced and thus longevity of the culture is significantly prolonged (Barnabe & Butler, 1994; Moore et al., 1997). In addition, lower nutrient consumption leads ultimately into lower accumulation of toxic waste products. Temperature shift can be applied in combination with fed-batch or perfusion bioprocesses and showed highly increased product titres in the past (Y. Zhang et al., 2015). However, it has been shown that the beneficial effect using temperature shift can be cell line and product specific as well the optimal temperature can vary from cell line to cell line (Yoon et al., 2003; Yoon et al., 2004). It has also been shown that low temperature can alter the abundance of glycosylation pattern which are exhibited on certain residues of the product (Andersen et al., 2000; Gawlitzek 2009) and certainly can influence the product quality as well as efficacy in vivo.

1.1.2 CHO cell heterogeneity

The diploid CHO genome consists of 22 chromosomes (2n=22) and its genome size is about 2.45 billion bases (haploid). The total number of predicted genes is 24,383 and most show sequence homology to human (19,711) and mouse (20,612) genes (Xu et al., 2011). The CHO genome shows a high level of genetic instability and the frequency of chromosome rearrangements as well as homologous recombination is higher than in other immortalised cell lines. However, their ease of genetic manipulation makes them a favourable cell line for recombinant protein production. These genetic changes are often exploited in gene amplification procedures used for the generation of stable, high producing cell lines.

The original cell line was first described in 1958 by Dr. Theodor Puck (Puck et al., 1958). The cell line was established out of 0.1 g Chinese hamster ovary tissue and exhibited a fibroblast like cell morphology. CHO cells were very popular for studies due to their large chromosomes and their ease of cultivation under simple media conditions. Furthermore, researchers were able to select cells for mutations in genes involved in metabolism due the usage of selective media. The original diploid cell line exhibited 11 chromosome pairs and only 1% of the total population exhibited an unusual number of chromosomes. After ten month of sub-cultivation the cells in the population changed morphology (epithelioid) and cells became spontaneously immortalised. However, CHO cells were distributed to many labs and were able to be grown with low concentrations of serum and in protein free media (Hamilton & Ham, 1977). Ten years after describing the original cell line the first CHO-K1 cell line as we know it was established and further distributed to other researchers as well as to the American tissue and cell culture collection (ATCC) (Kao & Puck, 1967; Kao & Puck, 1968) (Figure 1).

Ever since many different CHO cell lines were established and can be described nowadays as their own cell line (“Quasispecies”) exhibiting different phenotypes and genetic variations (M. F. Wurm, 2013). The genetic instability is most likely a result of gene aberrations like deletions and rearrangements as well as epigenetic events (Kim et al., 2011; Yang et al., 2010). Common CHO cell lines like CHO-S, DG44i, CHO-DXB11 and CHO-K1 were established and they exhibit different traits as well as phenotypes. CHO-S for example was first described to grow in suspension and was isolated from a sister cell line of CHO-K1 (Thompson & Baker, 1973). The DG44i cell line originated from CHO-K1 and both loci of the DHFR gene were deleted which were located on

chromosome 2 (Urlaub et al., 1983). This allows the rapid generation of stable cell lines transfected with a transgene and amplification using the DHFR inhibitor MTX.

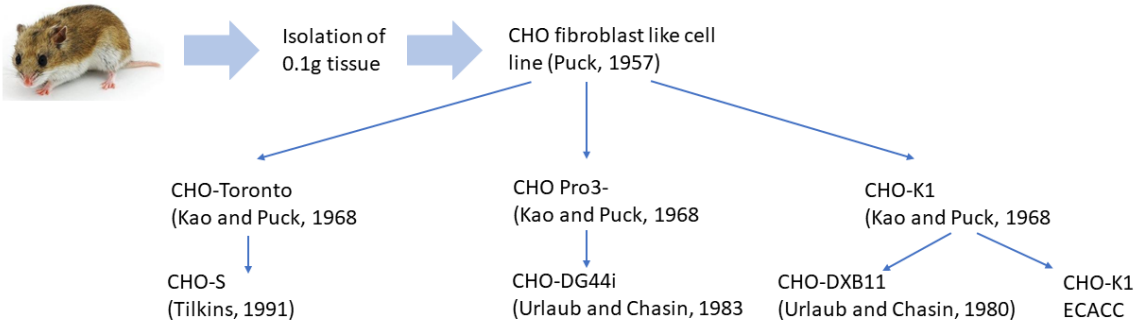

Figure 1: Summary of CHO cell quasispecies and variations. The original fibroblast like cell line was isolated out of 0.1g tissue originally in 1957 and had a near diploid state. Over cultivation of 10 month and spontaneoues immortalisation the first CHO progenitor cell line was described in 1958. Different CHO cell lineages were developed by adaption to suspension (CHO-Toronto and CHO-S) or deletion of the DHFR gene (DG44i).

Due to their ease of growth in chemically defined media and their ease in genetic engineering CHO cells are the commonly used production cell line in industrial production of recombinant proteins. Hereby, tPA was the first approved therapeutic for the treatment of thrombosis marketed by Genentech on 1986. In 2014 the total amount of approvals in Europe and the US has reached 246 overall (Walsh, 2014). Although media and bioprocess regime optimisation led to high yields and robust growing cells under defined conditions, the overall bioprocess including R&D, process optimisation, product commercialisation, pre-clinical trials and clinical trials requires tremendous amounts of capital. However, media and bioprocess optimisation are limited pathways and genetic engineering became one major tool to improve the bioprocess phenotype of CHO cells. This involves the better understanding of CHO cells gaining knowledge about the transcriptome, proteome, phospho-proteome, glycome, regulatory networks and metabolome (Datta, Linhardt, & Sharfstein, 2013a). That knowledge can be used to engineer pathways for improving secretion, growth, preventing apoptosis and many more applications. Recent advances and developments in targeted genome engineering tools led the way to a whole new path of genetically engineered cells and better understanding of global regulatory networks.

1.2 CHO cell engineering

The major limiting factor for the application of new techniques was the lack of sequence information for the Chinese hamster genome. A major breakthrough was achieved in 2012 when the complete sequence of the CHO-K1 ancestral cell line was published (Xu et al., 2011). The whole genomic sequence of other CHO cell lines i.e. CHO DXB11 (Kaas et al., 2015) or DG44 and CHO-S (Hefzi et al., 2016) followed consequently. The public availability of the genomic sequence led the way for the use of a variety of Next Generation Sequencing (NGS) approaches i.e. to identify transcripts and perform expression profiling under for example different growth conditions (Becker et al., 2011). Before the assembly of transcriptomics data, expressed sequence tags (EST) were used for the generation of expression data which limited the datasets to only hundred proteins (Wei et al., 2011). NGS and the comparison to *Mus musculus* and *Rattus norvegicus* enabled the analysis and identification of expressed genes and isoforms. Furthermore, it enabled first insight into the regulatory network of CHO which is essential for the analysis and application of integrated ‘omic approaches.

1.2.1 Implication of ‘omic approaches

The genomic sequence of the CHO genome combined with the rapid increase of transcriptomic data enabled the establishment of proteomic profiling studies using LC-MS/MS. The identification of thousands of proteins and studies to identify differential expression (DE) with regard to the bioprocess conditions like different media, stress environments, miRNA dysregulations and many more can give information about function or highlights engineering targets. In comparison to using ESTs, a proteomic study can give information about hundreds of differential expressed proteins which can be combined with transcriptomic datasets for gene expression to evolve deeper knowledge about regulatory networks (Clarke et al., 2012a; Xu et al., 2011). The identification of differential expressed proteins gives insight into many production relevant pathways like apoptosis, glycosylation, growth, translation as well as protein processing and metabolism (Baycin-Hizal et al., 2012). With the implementation of ‘omic studies and better understanding of pathways and protein regulatory networks as well as mRNA expression under certain conditions, more potential targets for cell line engineering were identified which can be used to improve the bioprocess phenotype of

CHO cells. Different approaches for cell line engineering exist and have been used for the improvement of the bioprocess phenotype.

1.2.2 Apoptosis engineering

Apoptosis engineering is based on the principle that genes are overexpressed which show anti-apoptotic functions or the downregulation/knockout of genes which function pro-apoptotic. The idea behind this approach is that cells exhibit higher viabilities in late stages of the culture which can improve the overall yield. Apoptosis in late stages of the culture is mainly induced by nutrient depletion, hyper-osmolality, shear stress or toxic catabolite accumulation. Furthermore, apoptosis has been shown to impair therapeutic protein quality regarding glycosylation. The overexpression of the apoptosis inhibitor Bcl-2 and Bcl-Xl has been shown to increase the resistance to apoptosis in many industrial relevant cell lines like CHO, NS0 myeloma and SF9 cells (Goswami et al., 1999; Mastrangelo et al., 2000; Mitchell-Logean & Murhammer 1997) due to numerous stress factors like shear stress, oxygen limitation, ammonia and nutrient depletion. However, it was also shown that the phenotype exhibited by the overexpression of both factors is cell line dependent. In some cases, a growth inhibition or an improved growth rate was observed (reviewed by Vives et al., 2003) suggesting a cell line dependent interaction of Bcl-2 and Bcl-Xl with the apoptosome. Both regulators mainly act by the inhibition of caspases which are the prominent proteases during induction of programmed cell death. Another interesting protein for the protection against apoptosis was shown to be X-linked inhibitor of apoptosis (XIAP). Sauerwald and colleagues showed that overexpression of XIAP or XIAP-mutants protect CHO and HEK293 cells from apoptosis induced by nutrient deprivation as well as programmed cell death induced by Sindbis-virus infections (Sauerwald et al., 2002; Sauerwald et al., 2003). Besides delaying apoptosis, XIAP has been demonstrated to be involved in productivity in two CHO-K1 cell lines (Griffith et al., 2018). XIAP is a specific inhibitor for caspase-3, -7 and -9 and interestingly it is a predicted target of miRNA-23a as well as miRNA-7 in CHO cells.

For the downregulation of pro-apoptotic genes, caspase-3 and caspase-7 were obvious targets for siRNA induced silencing. Studies showed an enhanced longevity due to the knockdown of caspase-3 and subsequent delay of apoptosis induction. However, no increase in productivity was reflected presumably due to lower mitochondrial function upon the knockdown of caspase-3 in a CHO mAb producing cell line. A co-silencing of

caspase-3 and caspase-7 showed increased product titres due to elongated culture times in a CHO cell line expressing thrombopoietin (Kim et al., 2002; Sung et al., 2007). However, the effect on expressing anti-apoptotic genes had a greater effect and seems to remain the prominent strategy in CHO cell engineering to prolong culture times with extended stationary phases to boost CHO cell productivity.

1.2.3 Metabolic engineering

Metabolic engineering involves for example the avoidance of toxic metabolite build-up which are exhibited in late stages of the culture e.g. ammonia and lactate. Lactate or lactic acid is a by-product of glycolysis and is enzymatically converted from pyruvate by lactate dehydrogenase (LDH). Glycolysis is usually enhanced in immortalised cell lines due to the Warburg effect. However, lactate in a bioprocess leads to low pH values which influences cell growth and product expression. To counteract low pH values alkali like NaOH is usually added to the medium which again changes the osmolality of the media and increases the stress levels on cells. Knockdown of LDH has been shown to limit lactate production and a decrease in glucose consumption rates was observed without effects on proliferation or expression of thrombopoietin or an IgG (Chen et al., 2001; Kim et al., 2007). Another group investigated the effect after transfection of a GLUT5 fructose transporter into CHO cells to use fructose as alternative primary carbon source which would ultimately lead to lower levels of lactate. Wlaschin and Hu identified clones which showed high product expression and reduced accumulation of lactate (Wlaschin & Hu, 2007).

Ammonia can inhibit cell growth at much lower concentrations compared to lactate and can also impair productivity. Furthermore, it was shown that ammonia possibly alters the glycosylation pattern of recombinant proteins (Gawlitzek et al., 2000) presumably due to inhibition of enzymes involved in providing sialic acid precursors. One approach to reduce ammonia was the use of CHO-K1 cells expressing GS and the addition of glutamate supplements to the media. Glutamate is enzymatically converted with ammonia to glutamine and Zhang and colleagues showed reduced ammonia formation (Zhang et al., 2006). The overexpression of two enzymes involved in the urea cycle which is most likely inactive in CHO-K1 showed beneficial effects on ammonium production as well. The expression of carbamoyl phosphatase synthetase I and ornithine

transcarbamoylase showed a 33% reduction of ammonium ions in CHO-K1 cell cultures and increased cell proliferation (Park et al., 2000).

1.2.4 Secretion and molecular chaperone engineering

Secretion engineering has been shown to be an efficient tool to enhance specific productivity. A common problem in industry resulting in low yields are difficult-to-express (DTE) mAbs. The difference in easy and DTE proteins are most likely related to protein processing. In a study two mAbs were selected and transfected, with Trastuzumab being easy to express and Infliximab being DTE. Trastuzumab showed higher expression compared to Infliximab over a panel of selected clones. This study showed that the processing of the DTE IgG is impaired due to lack of response of the unfolded protein response (UPR) ultimately leading to degradation and loss of the product (Le Foum et al., 2014). It was also demonstrated that the limitation shown in CHO cells due to high level expression of transgene can be solved by the simultaneous expression of human secretory proteins like SPR14. Furthermore, it was also shown that the expression of SPR14 not only restores the expression of the DTE IgG it also enhances the expression of the already highly produced Trastuzumab. This identified that bottlenecks in secretion can be overcome by the expression of limiting factors in that process. Further studies revealed that the introduction of other components of the secretory pathway like SNAP-23, VAMP8 and SM protein can improve secretion and boost the specific productivity in CHO cells (Peng & Fussenegger, 2009; Peng, Abellan, & Fussenegger, 2011). SNAP-23 and VAMP8 are proteins associated with the SNARE protein family which mediate the fusion of vesicles to the target membrane. It was shown that the introduction of SNAREs solves the bottleneck in secretion however, proliferation is impaired due to higher specific productivities. It is commonly observed that higher productivity is associated with lower investment of resources into the establishment of biomass resulting in lower proliferation rates.

A further bottleneck for the expression of proteins is the protein folding and processing machinery which is performed in the endoplasmic reticulum (ER). Chaperones are proteins which are involved in folding and unfolding of proteins and are also able to reduce protein aggregation which can occur due to high expression of recombinant proteins especially with high molecular weights. Common chaperone families are trigger factors, heat shock proteins and BiP. Overexpression of chaperones like

calnexin/calreticulin which are located in the ER has been shown to elevate specific productivity in CHO-K1 cells expressing thrombopoietin (Chung et al., 2004). Furthermore, overexpression of protein-disulphide isomerase (PDI) showed beneficial effects on recombinant protein expression in CHO cells. PDI is located in the ER and mediates the breakdown of randomly formed disulphide bridges to allow the peptide chain to form again. Enhanced productivity was observed CHO-K1 cells expressing IgGs, Fc receptor fusions and thrombopoietin (Borth et al., 2000; Davis et al., 2000; Mohan et al., 2007).

1.2.5 Promoter engineering and optimisation of expression systems

The reduction of transgene expression over time is a commonly observed phenomenon in cultures despite exhibiting multiple genomic copies (Kim et al., 1998; Strutzenberger et al., 1999) despite regular “pulsing” using selection agents. In one study a high producer was selected and cultivated for 18 months as well as routinely sub-cultivated twice a week (Kim et al., 2011). The transgene expression steadily declined over the 18-month period. The effect was investigated by several groups and it was observed that the commonly used CMV promoter is prone to DNA methylation at the 5’ and 3’ region of the promoter sequence which eventually led to a decrease in expression. Position -179 relative to the transcriptional start site off the CMV promoter is frequently methylated as well as positions -508, -41 and -13. However, it was reported that a single base pair mutation at position -179 can enhance and stabilise transgene expression over long cultivation times (M. Kim et al., 2011b; Moritz, Becker, & Gopfert, 2015; Osterlehner, Simmeth, & Gopfert, 2011). Besides DNA methylation, histone modifications may also play a role in the silencing of genes due to condensation of DNA and enabling DNA-binding factors to access the chromatin.

A promoter is defined by two regions: the proximal and the core elements. Both regions contain binding sites for proteins which are associated with transcription and the preinitiation complex formation. Transcription factors as well as transcription regulators bind to their target sequences and regulate the frequency of binding, the level of transcription and duration. Thus, promoters and their engineering are highlighted as potential tools for increasing stable expression over time. In CHO-K1 cells the promoter of a high and stable expressed protein (elongation factor-1α – EF-1α) was used including flanking regions and inserted into expression vectors. Six different genes were inserted

into the vector and transfected into CHO cells to investigate their expression. Four stable cell lines expressed 6 to 35-fold higher levels of transgenes compared to traditional, commercial plasmids (Running Deer & Allison, 2004).

The possible usage of synthetic promoters consisting of multiple elements from different origins in CHO cells have been proposed as potential tool for stable and high transgene expression. Transcription factor regulatory elements and binding sites were identified from viral promoters known to be active in CHO using bioinformatics tools. After transfection of constructed promoters with the SEAP gene downstream, one promoter was identified which showed increased transcriptional activity and yields (Brown et al., 2014).

The usage of site specific integration allows the prediction of target gene expression due to insertion into transcriptional active regions (hot-spots) which ensures the stable transcription of the transgene (Kuystermans et al., 2007). Recombinase-mediated cassette exchange (RCME) has been used for the site-specific integration of transgenes using viral recombinase systems like Cre/LoxP (Kito et al., 2002). Studies have also shown that the usage of ubiquitous chromatin opening elements (UCOE) can be beneficial due to resistance to DNA methylation which ensures high, stable expression of the gene of interest (F. Zhang et al., 2010). Gained knowledge about CHO cell promoters and regulatory elements will drive research and identify new possible synthetic promoters which can be used for stable long-term transgene expression.

1.2.6 Glycosylation-engineering

The dominant use of CHO cells in biopharmaceutical production is mainly because of the human-like glycosylation pattern. The attachment of saccharides to proteins can occur in two different distinct forms: N-linked glycosylation occurs on asparagine residues and O-linked glycosylation occurs on serine/threonine residues. N-linked glycosylation was demonstrated to be the more prominent posttranslational modification and the pattern is essential for the efficacy of the therapeutic protein as well as for possible side effects or pharmacokinetics (Elliott et al., 2003). To ensure quality over time in production of recombinant therapeutics, the bioprocess as well as the glycosylation pattern of the therapeutic protein must be investigated extensively to meet FDA regulations. Culture conditions as well as media components, the cell type and the

bioprocess itself can have a significant influence on the glycosylation pattern of therapeutic protein. The addition of N-linked glycoforms is mainly enzymatically catalysed in the ER and the addition of O-linked glycoforms is catalysed in the Golgi apparatus.

It has been demonstrated that different glycosylation patterns can influence the circulation half-life of IgGs and are potential engineering targets (reviewed by Hossler et al., 2009). Overexpression of human α2,6-sialyltransferase (ST6Gal1) for example has been used to enhance sialic acid content of erythropoietin in CHO-K1. The same approach was used for therapeutic products like tPA and Interferon γ (Fukuta et al., 2000; Minch, Kallio, & Bailey, 1995; B. Yin et al., 2015). The sialic acid residues are important for N-glycan capping which again plays a key role in the biological activity of recombinant proteins including adsorption, half-life and clearance (Bork et al., 2009).

Nevertheless, glycoforms are not only important for half-life of the recombinant protein but also can influence target binding efficiencies. The existence of N-linked glycans on heavy chains of mAbs have been shown to be important for the interaction of Fc receptors and their mediated function in the cell (Rothman et al., 1989). Fucosylation of antibodies has been shown to impair antibody-dependent cellular cytotoxicity (ADCC) and the knockout of fucosyl-transferases like α-1,6-fucosyltransferase (FUT8) was suggested to be clinical relevant for improved functions of recombinant proteins. Thus, production using CHO cells with knockouts of fucosyltransferases was highlighted as a “next-generation” for antibody engineering (Mori et al., 2007; Ronda et al., 2014a).

1.3 MicroRNAs

Small noncoding RNAs (20-30 nt) are classified into three groups: PIWI interacting RNAs (piRNAs), small interfering RNAs (siRNAs) and microRNAs (miRNAs). MiRNAs are highly conserved over species and have been shown to be extensive regulators of gene expression. After the discovery of the first miRNA by Ambros and colleagues in 1993 (Lee et al., 1993) in *Caenorhabditis elegans*, their function remained unknown for a long time. Studies revealed that miRNAs can regulate gene expression in a post-transcriptional manner by either inhibiting translation of its mRNA target or degradation of it. Sequencing data showed that over 1,800 conserved miRNAs are expressed in human cells and exhibited a high sequence complementary (~60 %) to many protein-coding mRNAs (Friedman et al., 2009; Kozomara & Griffiths-Jones 2014). MiRNAs are usually transcribed by RNA-Polymerase II and play an essential role in gene regulation by two different distinct mechanisms: degradation of the target mRNA or the repression of translation by inhibition of the polyribosome (Figure 2).

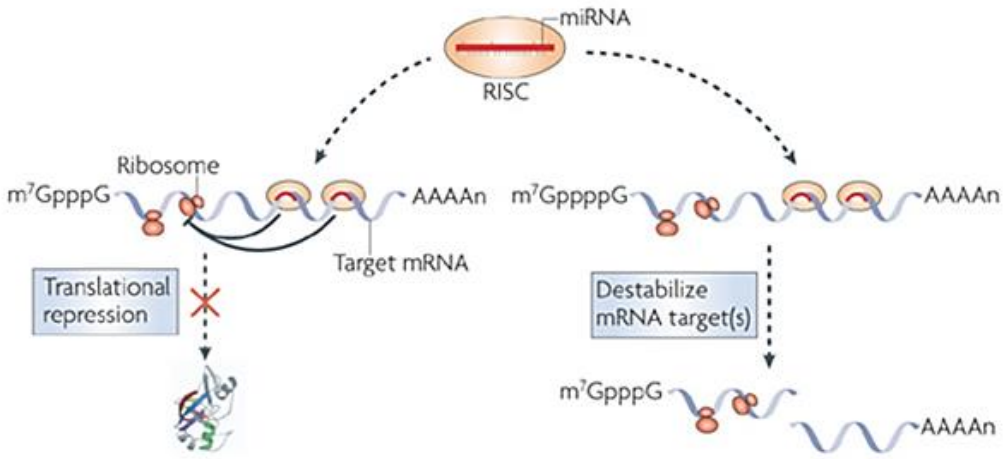

Figure 2: Mechanisms of translational inhibition of miRNAs. After guidance of the RISC by the incorporated mature miRNA the mRNA translation is inhibited by the physical hindrance of the polyribosome. The second act of mechanism is the destabilisation and degradation of the mRNA which usually occurs due to perfect binding of the miRNA. Figure was sourced and altered from Lodish and colleagues (Lodish et al., 2008).

The mature miRNA (~22 nt) is assembled into the RNA-induced silencing complex (RISC) which can act as an endonuclease whereas the miRNA acts as a guide, dictating target specificity (Hammond et al., 2000). Many proteins and domains are involved e.g. RNA binding domains which interact with dsRNA and single stranded RNA as well as

endonuclease domains, contributing to the RISC function (Pratt & MacRae, 2009). The loading of the RISC is supported by Ago2 and Dcr-2 proteins which binds to the premature miRNA duplex. The mRNA is specificly cleaved by the RISC if it shows a high complementary to the incorporated miRNA. Translational inhibition can also be exhibited by the binding of only the seed region (nucleotides 2 to 7 of the mature miRNA) to the mRNA target. If mismatches occur, the RISC prevents the translation of the mRNA by blocking the ribosomal propagation along the mRNA transcript. Furthermore, the 3´-untranslated region (3´UTR) is essential for translation due to regulatory elements and translation can be efficiently blocked by RISC binding to these regions or interfering with essential translation factors which bind to this highly regulatory region of the transcript (Doench & Sharp, 2004; Grimson et al., 2007; Humphreys, Westman, Martin, & Preiss, 2005). One mRNA can have several binding sites for miRNAs and it was also shown that one mRNA can be targeted by various miRNA families. The miR-23-24-27 constituting of three miRNAs with different seed families has been shown to target same mRNAs and pathways (Liang et al., 2004). Target prediction analysis showed further evidence that one single miRNA can have hundreds of targets by showing complementarity in the 3`UTR alone. Critical for the wide range of different targets is the seed region of the miRNA. This seed region is conserved in vertebrates and is located at the 5`-end of the mature miRNA. A requirement for the repression is the degree of matching of the seed region to the target mRNA but further factors seem to be involved such as sequence composition proximal to the seed region and position of miRNA binding sequence (MBS) (Grimson et al., 2007). The efficiency of miRNAs/mRNA binding and the miRNA acting mechanism seems to have alternative modes which are cell line and tissue dependent (Kulkami et al., 2016). Ten cell lines were co-transfected with miRNA mimics and a target sequence located in 3'UTR of a renilla reporter for the miRNA. All cells exhibited a lower level of fluorescence levels. However, five cell lines stabilised the mRNA transcript, three cell lines did not show any effect and two cell lines showed a translational inhibition due to degradation suggesting a cell and tissue specific preference of miRNA regulation mechanistic.

Target efficacy and number of binding sites on the mRNA transcript is proposed to vary dependent on the 3'UTR isoform usage which can show high variations across species. Alternative long and shorter isoforms have been reported in the same ORF due to different poly-A signals which can occur distal or proximal (Decker & Parker 1995; Miyamoto et al., 1996). Longer or shorter isoforms can exhibit a different number of

binding sites and the usage seems to be dependent on the cellular context to “fine-tune” expression (Nam et al., 2014). The difference in the 3’UTRs can strongly effect gene regulation in this context by adding or deleting miRNA binding sites and ultimately have tremendous impact on miRNA inhibitory function. It was also suggested that the amount of gene copies per cell influences miRNA regulation of the target mRNA. Studies showed that a dosage dependent effect of mRNA transcript effects the target selection of miRNAs (Shu et al., 2012).

1.3.1 Biogenesis of miRNAs

MiRNAs inhabit either their own genomic locus including promoter regions or are the results of mRNA splicing events when located intronicly of their host gene. Transcription of miRNAs is initiated by RNA-Polymerase II and the primary miRNA (pri-miRNA) transcript exhibits 5´- 7-methylguanosine caps as well as a 3´-poly-A tail. This nascent transcript forms a RNA-RNA duplex by complementary base pairing with several stem loops. The first step after transcription is the cleavage by Drosha RNase III which processes the pri-miRNA into a ~70 nucleotide long precursor miRNA (pre-miRNA). If the miRNA is located in introns, mRNA splicing can lead to formation of pre-miRNAs (Y. Lee et al., 2003). The pre-miRNA exhibits a 5´-phosphate and a 2 nucleotide 3`-overhang resulting from the RNase III cleavage. The second step is the export of the pre-miRNA into the cytoplasm mediated by exportin-5 which binds dsRNA and uses RanGTP as a cofactor (Lund et al., 2004). In the cytoplasm the pre-miRNA is further processed by the Dicer RNase III multi protein complex into a 22-nucleotide miRNA-miRNA* duplex with a two nucleotide 3`-overhang (Y. Lee et al., 2003) and the duplex is incorporated into a pre-RISC. The pre-RISC consists of Argonaute protein (AGO) and Dicer-2 which are supported by the chaperone machinery including HSP90 and HSC70. In this complex the miRNA-miRNA* duplex is separated to form the mature RISC. It is thought that the mature miRNA is selected from the miRNA-miRNA* duplex based on thermodynamic stability of their 5`-ends. The less stable 5´-end shows a preferential association with RISC due to the easier separation from the duplex (Schwarz et al., 2003). Assembled in the RISC, the miRNA plays its role in target recognition and binding by guiding the multiprotein RISC to the mRNA target.

The whole process of miRNA maturation is shown in Figure 3. Another type of non-coding RNA referred to as siRNA is similar in their target characteristics, their biogenesis

and their size. In the case of biogenesis, siRNAs and miRNAs share the Dicer complex as well as the RISC. Their difference is just related on their origin, as miRNAs are encoded in the host genome but siRNAs exhibit an exogenous source like viral genomes. However, the function of a siRNA lies in the perfect match of the target mRNA whereas miRNAs can exhibit mismatches in target binding.

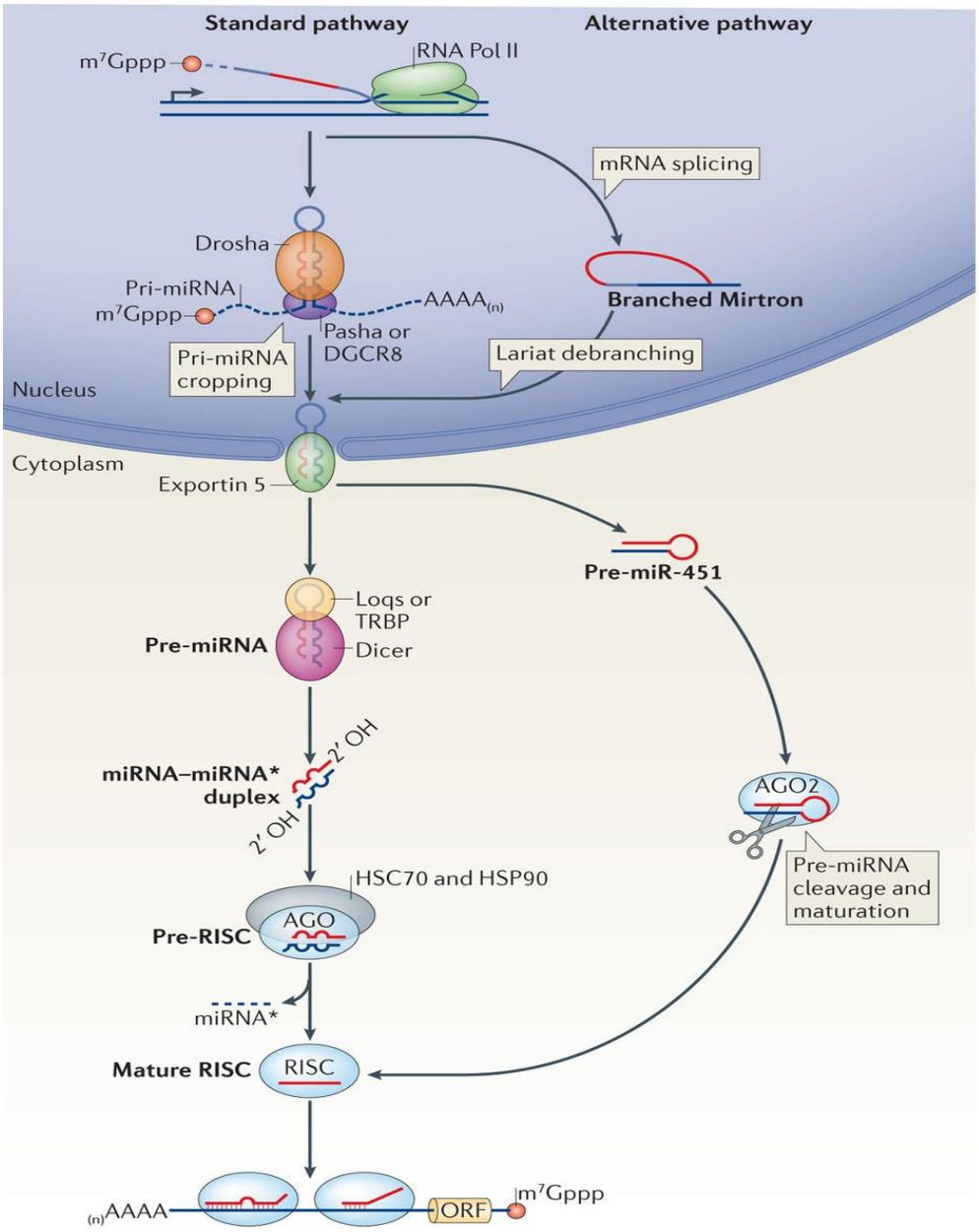

Figure 3: Biogenesis and processing of miRNAs. Firstly, the miRNA gene is transcribed by RNA-Polymerase II into pri-miRNA transcripts containing a 5'-7-methylguanosine cap and 3'-poly-A signal. The pri-miRNA is further processed into a ~ 70 nucleotide long pre-miRNA and is exported into the cytosol by exportin-5, a RanGTP dependent exporter. The pre-miRNA is further processes by a Dicer complex and incorporated into the pre-RISC with the help of molecular chaperones. Alternatively, the pre-miRNA can be processed by AGO2 before incorporation into the RISC. The pre-RISC matures by degrading miRNA* passenger strand and the final assembly of the mature miRNA before following its mechanistic function in translational inhibition. Figure was sourced and altered from (Ameres & Zamore, 2013).

1.3.1.1 Genomic organisation and nomenclature of miRNAs

Due to the rapidly increasing data which evolved with the development of NGS and better bioinformatics tools an organised nomenclature for miRNAs was proposed by Ambros and colleagues (Ambros et al., 2003). A mature miRNA is named in the way of discovery by continuous counting: miR-1, miR-2… and further. A gene which encodes for the miRNA is named in the same way with capital or lower-case letters (MIR-1 or mir-1) depending on the species. If a known miRNA is discovered in a new species and shows no difference or only a small discrepancy to the already known miRNA it is named equally (e.g. known miR-23 in human and recent discovered miRNA with the same sequence in CHO is named miR-23 as well). In addition, if miRNAs exhibit very similar sequences (homologs) in the same species a number or letter is added e.g. miR-23a and miR-23b. To name the origin of the miRNA also the species abbreviation was added e.g. hsa-miR-23a for human miRNA and cgr-miR-23a for the Chinese hamster miRNA-23a. Some of the known miRNAs are transcribed from a so-called cluster and are processed from one pre-miRNA precursor transcript. Several miRNAs can result from one pri-miRNA transcript (polycistronic) as well as from one precursor transcript (monocistronic). Examples for nomenclature of a cluster is the miR-23a-27a-24-2 cluster or miR-17-92 describing clustering of three miRNAs for the miR-23 cluster or six different miRNAs in case of the miR-17-92 cluster.

1.3.1.2 Identification of miRNA and validation of targets

MiRNAs are usually identified by miRNA profiling studies however, the validation of possible targets has been shown to be more difficult. Kuhn and colleagues (Kuhn et al., 2008) suggested an experimental approach for the experimental validation of possible miRNA targets. Bioinformatics tools like TargetScan, PicTar and miRanda are algorithms which can predict possible miRNA:mRNA interactions. Kuhn and colleagues showed a discrepancy as well in comparing these tools with each other leading to no overlaps and inconclusive identification of mRNA targets between the tools. Nevertheless, the interaction should be experimentally proven to be certain about the gene regulation by its target miRNA. The proposed workflow was to analyse possible mRNA targets using mentioned bioinformatics tools. Furthermore, a miRNA/mRNA co-expression study followed by an investigation of the miRNA effect on the protein and the assessment of the miRNA on the biological function.

1.3.2 MicroRNAs as potential tools for cell line engineering

As mentioned miRNAs regulate complex mechanism and a single miRNA can target ~100 mRNAs to prevent or “fine-tune” their translation. Thus, one miRNA regulates a whole network of proteins and plays a global role in cellular behaviour and phenotype. In addition, it is proven that miRNAs play an essential role in a variety of bioprocess related phenotypes like proliferation, apoptosis, protein expression and response to cellular stress such as hypoxia or low nutrient availability (Jadhav et al., 2013a). This highlights miRNAs as an interesting tool for cell line engineering to improve the bioprocess phenotype of CHO cells. Moreover, as miRNAs are processed from their non-coding precursors they do not impose translational burden if they are introduced on plasmids for overexpression.

Several studies prove the effects and benefits of dysregulating miRNAs on the phenotype of CHO cells. The depletion of miR-7 using sponge decoy technology for example showed positive effects like the increase of cell growth and specific productivity in CHO-K1 SEAP expressing cells (Sanchez et al., 2013). The inhibition enriched cells in G_2/M phase of the cell cycle enabling a faster progression through cell cycle steps. In contrast the overexpression showed an inhibition of cell cycle progression with cells enriched in G_1/S transition (Barron et al., 2011). Another interesting study showed that stable depletion of miR-23b can result in an increased productivity in CHO-K1 SEAP expressing cells. MiR-23b was identified to be differentially expressed in a panel of miRNAs identified using temperature shift to reduce cell growth and increase productivity (Gammell et al., 2007). Further investigation indicated that the depletion of miR-23b increases the mitochondrial oxidative phosphorylation capacity which ultimately led to higher specific productivity. However, the effect was inconsistent in a different CHO-K1 cell line expressing a mAb but nevertheless beneficial. Stable depletion of miR-23b led to increased viabilities during late stages of the culture possibly by higher intracellular XIAP levels which was confirmed to be targeted by miR-23 (Kelly et al., 2015). Overexpression of miR-17 increased the specific productivity and growth rate of CHO EpoFc expressing cells (Jadhav et al., 2012a; Jadhav et al., 2014)

Increased cell growth was also shown in HeLa cells due to inhibition of miR-21 and miR-24 (Cheng et al., 2005) and miR-24 and miR-27a have been shown to be up-regulated during hypothermia induced growth arrest in CHO-K1 cultures (Gammell et al., 2007). Transient inhibition of miR-24 in CHO-K1 SEAP expressing cells confirmed enhanced

growth rates and the effect was reversed by overexpressing miR-24 which led to growth inhibition. Clarke and colleagues investigated differential expressed miRNAs using an integrated approach combining microarrays and proteomic profiling (Clarke et al., 2012b). Sixteen miRNAs including miR-204, miR-338, miR-497, miR-30e, miR-206, miR-451 have been shown to be downregulated during high growth rates and 35 miRNAs were upregulated during high growth rates which turn them into potential aims for targeted proliferation engineering. A further study showed the link between miRNA expression patterns due to different phases in the culture process. Lag-, exponential and stationary phase were investigated and 117 miRNAs were found to be differential expressed displaying involvement in biological processes like cell growth and arrest (Hernandez Bort et al., 2012).

Other miRNAs like miR-15 and miR-16 can induce apoptosis by targeting Bcl-2 and a stable depletion of these miRNAs could be useful for preventing apoptosis in CHO cultures (Cimmino et al., 2005). More miRNAs linked to apoptosis in late stages of the cultivation process were investigated due to nutrient depletion. It was demonstrated that 70 miRNAs were differentially expressed in mouse including miR-466 and the miR-297-669 cluster which is possibly involved in initiating apoptosis (Druz et al., 2012). MiR-466 was further investigated and delayed activation of apoptosis in late stages of batch cultures was observed leading to increased maximum cell densities (Druz et al., 2013). More miRNAs which could be possibly used as engineering tools and studies which investigated the dysregulation under different culture conditions were summarised and reviewed by Jadhav and colleagues (Jadhav et al., 2013b).

Recent developed genome editing tools, such as transcriptional activator like nucleases (TALEN), zinc finger nucleases (ZNFs) and especially CRISPR/Cas9, opened a wide field of possibilities to target miRNAs more effectively for a possible application in industrial used cell lines. Beneficial phenotypes can exhibit for example higher specific productivities, lower apoptosis, increased cell viability and proliferation rates. It was shown, that targeted genome editing tools can be used for both, either gene knockouts or depletion of miRNAs. Thus, these tools might play an essential role in future cell line engineering approaches of CHO cells.

1.3.3 Biological function of the miR-23-24-27 cluster and its role in disease

Studies have shown that the miRNA cluster is derived from one primary transcript but the expression pattern of each member can vary possibly due to the specific biological

circumstances or diseases (Y. Lee et al., 2004). However, the paralogs are located on different genomic loci and are derived from different primary transcripts which would also suggest a different expression pattern (summarised by (Chhabra, Dubey, & Saini, 2010a). In human the miR-23a cluster is located intergenic (chromosome 9) and the miR-23b cluster is located intronic (chromosome 19). The appearance of two clusters is most likely due to gene duplication in evolution of mammals. In Chinese hamster the miR-23a cluster is similarly located intergenic and its paralog is located intronicly in the Aminopeptidase O-like gene (AMPO). The miR-23a cluster exhibits all core elements needed for a promoter region including TATA box and initiation sequences making transcription RNA-polymerase II dependent (Chhabra et al., 2010). The miR-23b cluster seems to lack common promoter elements which may suggest processing through intron splicing. The expression of both clusters seems to be highly variable over cell lines (Yu et al., 2006). In certain diseases each member can be simultaneously up- or downregulated i.e. in acute lymphoblastic leukaemia as well as acute myeloid leukaemia (Mi et al., 2007). In fact, several studies showed as well that single members of both miR-23 clusters were dysregulated in many diseases. For example, an upregulation of all single members was osberved in cardiac hypertrophy (Sayed et al., 2007) or a down regulation of each member was reported in schizophrenia and autism (Abu-Elneel et al., 2008; F. Wu et al., 2008). The function of each member or a co-operative function remains however, unclear. Although evidence exists that similar targets as well as pathways are targeted (T. Liang et al., 2014) which also may be the evolutionary result of why some miRNAs are clustered. Nevertheless, individual functions of each member were observed as well. Indicated differential expression could suggest that the function and a possible impact on a bioprocess phenotype in CHO cells is highly cell line or cell type dependent.

1.3.3.1 MicroRNA 23-24-27 cluster and its individual members

MiR-23a and miR-23b

With their role as posttranscriptional regulators it was observed that repression of miR-23a/b influences proliferation and metabolism of human B lymphocytes (Gao et al., 2009). Gao and colleagues showed also that high expression levels of the oncogene c-Myc represses the transcription of miR-23a as well as miR-23b. The repression leads to higher levels of mitochondrial glutaminase which is normally targeted by both miRNAs. Higher glutaminase levels led ultimately to enhanced mitochondrial capacity of Complex I/Complex II which again led to increased oxidative phosphorylation in CHO cells (Kelly et al., 2015). Due to the Warburg effect immortalised cells convert high amounts of glucose into lactate using glycolysis which increases cell proliferation but provides less substrate for mitochondrial based oxidative phosphorylation. While increased glutaminase levels strengthens the mitochondrial function by the conversion of glutamine to glutamate and subsequently to α-ketoglutarate which enters the TCA cycle. This reflects an alternative pathway to strengthen specific productivity in CHO-K1 SEAP expressing cells. However, the effect of miR-23 depletion seemed highly cell line and tissue specific. The dysregulation of miR-23 showed increased viability in late stages of the culture in a different CHO-K1 cell line expressing a mAb (Kelly et al., 2014). Another target for miR-23 is XIAP which is responsible for the inhibition of apoptosis by binding of caspase-3, -7 and -9 and could be responsible for observed prolonged cultures (Sauerwald et al., 2002). Furthermore, it was observed that miR-23a and miR-23b expression levels are decreased in some cancer types like prostate cancer and leukaemia (Porkka et al., 2007; Saumet et al., 2009). However, there is evidence that miR-23a/b can prevent apoptosis during hypoxia by targeting important key components of the apoptosis pathway like Bax-like BH3 protein (BID), caspase-7 or BCL2/Adenovirus E1B 19kDa Interacting Protein 3-Like (BNIP3L) (Agrawal et al., 2014). The positive effects of miR-23a/b on cell proliferation and apoptosis prevention highlights a possible strong tool for optimisation of cellular behaviour in a bioprocess dependent manner.

MiR-24

Similar to miR-23a/b, miR-24-1/2 has been shown to target essential proteins of the apoptotic pathway in human cells. The targets are pro-apoptotic proteins like Bim, FAF-

1, Caspase-9 and Apaf-1 (Agrawal et al., 2014; Cheng et al., 2005; Qin et al., 2010) as well as targets which are responsible for cell survival e.g. Bcl-2 (Singh & Saini, 2012a). It seems that the role of miR-24-1/2 in a pro- or anti-apoptotic manner depends on specific circumstances of the cell and is cell/tissue type specific. Overexpression of miR-24 inhibited cell proliferation of six different human cancer cell lines by inducing the expression of p53 and p21 (Mishra et al., 2009a). E2F2 and MYC are proteins which are involved in rapid cell cycle progression and a study showed that miR-24 targets both mRNAs and blocks uncontrolled proliferation. However, E2F2 and MYC do not exhibit binding sites for miR-24 in the 3'UTR (Lal et al., 2009). This was confirmed by transient overexpression of miR-24 using mimics in CHO cells resulting in significantly reduced cell growth (Noèlia Sanchez, 2013). Mishra and colleagues showed as well that miR-24 targets the DHFR gene which catalyses the reaction of dihydrofolate into tetrahydrofolate. Tetrahydrofolate is required for purine and pyrimidine synthesis and therefore plays an essential role in cell growth and proliferation. Consequently, a down regulation of miR-24 showed an increase of proliferation in human epithelial cells (Cheng et al., 2005). Dr. Sanchez showed in her thesis as well that transient inhibition of miR-24 resulted in increased proliferation in CHO-K1 SEAP expressing cells (Noèlia Sanchez, 2013). This suggests that deregulation of miR-24 could be used as potential target for improving bioprocess characteristics in CHO cells regarding growth behaviour.

MiR-27a and miR-27b

Several studies showed that miR-27 plays a role in apoptosis by either targeting pro-apoptotic or anti-apoptotic proteins possibly dependent on the specific circumstances of the cell environment. Agrawal and colleagues showed that miR-27 targets APAF1 which inhibits apoptosis under hypoxia (Agrawal et al., 2014). Further studies also showed that miR-27 negatively regulates FADD which interacts with caspase-8 in the apoptotic signalling pathway and prevents apoptosis in human cell lines (Chhabra et al., 2009). Up-regulation of miR-27a seems also to increase cell proliferation in human breast cancer cells by targeting the tumour suppressor FOXO1 (Guttilla & White, 2009). However, Guttilla and White reported an involvement of miR-96 and miR-186 as well which could involve a synergistic effect or shared targeting. Moreover, miR-27 stimulates cell survival by targeting Myt-1 which inhibits G_2-M phase progression (Mertens-Talcott et al., 2007). This leads to a higher percentage of cells in S phase and to higher

proliferation rates. Downregulation of miR-27a seemed to have an anti-apoptotic function by increased levels of Bcl-2 proteins. Interaction studies indicated that miR-27 targets are involved in many more cellular pathways like insulin signalling, Mitogen-activated protein kinase (MAPK) signalling and p53 signalling (S. Yang et al., 2012). Regarding CHO cells, the overexpression of miR-27a resulted in a decrease of growth (CHO-K1 mAb) but also increased proliferation in a different cell line (CHO2B6) showing mentioned cell type specific phenotype (Noèlia Sanchez, 2013). However, the involvement in proliferation and apoptosis highlights miR-27a and miR-27b as interesting engineering targets.

1.4 Targeted genome engineering tools

A better understanding of the genome and transcriptome with projects like the ENCODE consortium and recently developed targeted genome engineering tools have paved a whole era of new possibilities for treatment of diseases. Targeted engineering tools include transcriptional activator like nucleases (TALENs), zinc finger nucleases (ZNFs) and CRISPR/Cas9. For miRNA engineering and the investigation of miRNA function the common approach is either the overexpression of pre-miRNAs, transient mimics or the depletion using antisense molecules (antagomiRs) as well as sponge decoy vectors.

1.4.1 Sponge decoy technology for the stable or transient depletion of miRNAs

Sponge decoy technology is based on mimicking the natural binding sites of miRNAs using exogenous artificial miRNA binding sites (MBS) located in the 3'UTR of a reporter gene (reviewed by (Ebert & Sharp, 2010). A selection of reporters can be used e.g. destabilised GFP, mCherry or firefly luciferase. Reporter expression is usually driven by a CMV promoter located on a plasmid enabling transient screens as well as a permanent depletion by generating stable expressing cell populations. Transcription by RNA-polymerase II also increases mRNA stability due to the presence of a poly-A tail and a 5'-cap. Two different designs of the MBS have been utilised. The first approach is the perfect antisense sequence which can lead to degradation of the sponge mRNA. On the other hand, creating a four-base pair mismatch in the MBS between the mRNA and the miRNA has been shown to protect from AGO2 mediated endonucleolytic cleavage by

the RISC (Ebert et al., 2007; Kluvier et al., 2012). The same study showed that miRNAs sharing the same seed family can be targeted effectively by the same antisense sequence. The successful binding and function of the sponge is indicated by the reduction of the reporter signal (Figure 4).

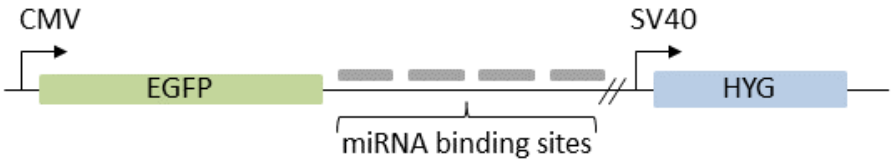

Figure 4: Basic mechanism of the sponge decoy approach. MBS can be cloned into the 3'UTR of a reporter gene. MiRNA binding and associated translational inhibition can be subsequently analysed and compared to a control without functional binding sites. The usage of a resistance gene allows the generation of stably expressing cell lines.

However, the function needs to be validated by quantifying target genes of the miRNA which should be higher abundant due to the depletion of its target miRNA. It has been reported that sponges containing ten binding sites are optimal as every binding site enhances the probability of mRNA cleavage. However, also dosage dependent effects and off target effects should be considered. High abundance of miRNAs with the same seed family require high amounts of sponge transcipt and can possibly influence the phenotype due to the posed transcriptional burden. Furthermore, the expression of sufficient levels of transgene can be challenging when stable cell lines are created as well as a decrease in transgene expression over time.

1.4.2 Clustered regularly interspaced short palindromic repeats (CRISPR)

Due to the challenge of mobile genetic elements (MGEs) such as plasmids or viral DNA several defence mechanisms have evolved in prokaryotes, eukaryotes and archaea. The CRISPR system is a common defence system used in ~39% of bacteria and ~88% archaea (Makarova et al., 2006). This system, first discovered in *Escherichia coli* by Ishino and colleagues in 1987 (Ishino et al., 1987), provides acquired immunity against invading viral and plasmid DNA by integrating foreign nucleic acid into the hosts chromosome (Grissa et al., 2007; Jansen et al., 2002). A CRISPR locus normally consists of variable foreign sequences, so called spacers which are separated by conserved repeats. The loci are flanked by genes encoding CRISPR-associated (Cas) proteins which are required for the processing of transcripts, the integration of new spacers as well as the cleavage of invading DNA (Haft et al., 2005; Makarova et al., 2006). CRISPR loci are conserved but the amount of spacer–repeats differs between loci and between species. Studies have revealed that spacers can have a length between 27-72 base pairs and repeats vary between 21-48 base pairs. Furthermore, the lead sequence upstream is A/T-rich and was shown to serve as the promoter region for the transcription of spacer-repeat sequences by RNA-Polymerase II (Horvath et al., 2008; Jansen et al., 2002; Kunin, Sorek, & Hugenholtz, 2007). A CRISPR locus is first transcribed into a pre-CRISPR-RNA (pre-crRNA). This transcript is further processed into small CRISPR-RNAs (crRNA) by cleavage of the pre-crRNA into spacers which are flanked by two repeats (Carte et al., 2008; Hale et al., 2009). Different systems have evolved over time and the maturing of the crRNAs depends on the classification of the system. Thereby CRISPR/Cas systems are divided into three major types: Type I, Type II and Type III. These types are further segmented into subtypes depending on their evolutionary relationship between the associated protein machinery and CRISPR/Cas clusters (Makarova et al., 2011). In addition, protospacers of crRNAs are flanked by short sequences which are called protospacer adjacent motifs (PAM). The PAM is essential for target recognition and varies between the species origin. To prevent self-targeting of chromosomal direct repeats CRISPR loci show a lack of PAM (Marraffini & Sontheimer, 2010b). The PAM used in *Streptococcus pyogenes* for example uses 5´-NGG whereas *Streptococcus thermophilus* uses 5´-NAAAAC. Depending on the type the PAM is located either at the 5`- (type I system) or 3`- (type II system) and is absent in the type III system (Marraffini & Sontheimer, 2010b). Repeat-spacer sequences are processed by CRISPR specific ribonucleases (Cas5 and Cas6) in type I and type III systems. In

type II systems a trans-activating RNA (tracrRNA), which is complementary to the repeat sequence of the crRNA binds and forms a double-stranded guide RNA (gRNA). In the *Streptococcus pyogenes* CRISPR/Cas system which is mainly used for targeted genome editing, two different tracrRNAs are expressed upstream of the CRISPR locus. The formed gRNA is recognized and cleaved by a cellular RNase III (Deltcheva et al., 2011). The whole crRNA biogenesis of the type II system consists of only four Cas proteins and Cas9 is described as playing the key role as endonuclease which is responsible for the cleavage of the target sequence (Deltcheva et al., 2011; Garneau et al., 2010). The mature gRNA forms a complex with Cas9 to follow its role in target binding and recognition. The recognition is followed through Watson-Crick base pairing and provides acquired immunity against invading MGEs by their recognition and cleavage. The process of cleavage and degradation of invading DNA is called CRISPR interference (CRISPRi). The adaption of new spacers, biogenesis of CRISPR and finally the interference is summarized in Figure 5 A and B.

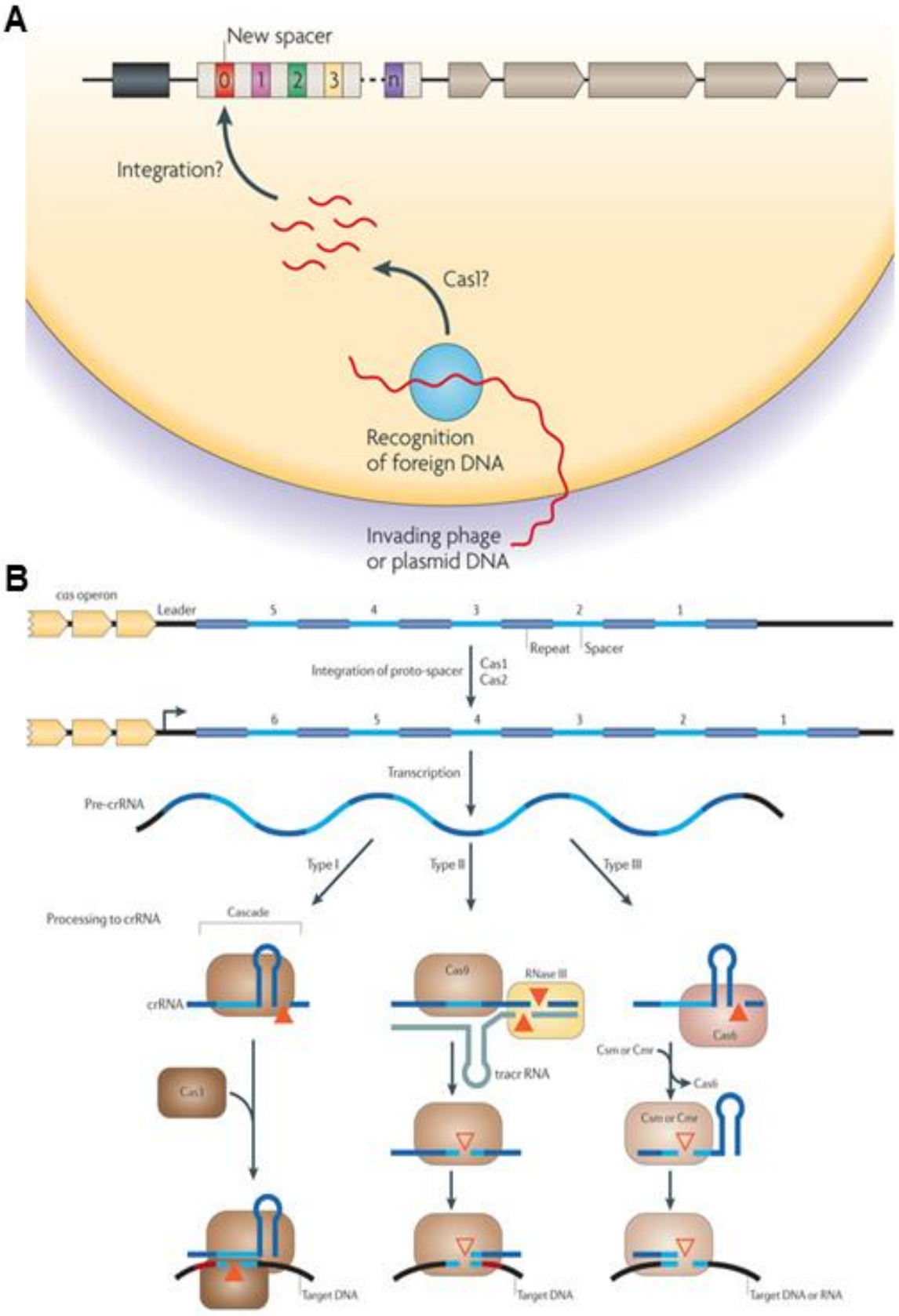
A
New spacer
0
1
2
3
n
Integration?
Cas1?
Recognition
of foreign DNA
Invading phage
or plasmid DNA
B
cas operon
Leader
5
4
3
2
1
Repeat
Spacer
Integration of proto-spacer
Cas1
Cas2
6
5
4
3
2
1
Transcription
Pre-crRNA
Type I
Type II
Type III
Processing to crRNA
Cascade
crRNA
Cas3
Cas9
RNase III
tracr RNA
Csm or Cmr
Cas6
Cas6
Csm or Cmr
Target DNA
Target DNA
Target DNA or RNA

Figure 5: Organisation of CRISPR loci, adaption and biogenesis. A) Adaption of new spacers is initiated by the recognition of foreign DNA with involvement of Cas proteins. The foreign DNA is cleaved and integrated as spacer into the host's genome with flanking repeats in 5'- and 3'-. The length of the spacer as well as the repeat depends hereby highly on the species. The CRISPR locus also exhibits the coding sequences proximal to the spacer-repeat region. The locus itself is transcribed by RNA-Polymerase II. B) After transcription of the pre-crRNA, the precursor is further processed by cleavage into repeat-spacer sequences. This step is proceeded by CRISPR specific ribonucleases in type I and type III systems. In type II systems a complementary trans-activating crRNA binds to the repeat sequence of the crRNA and the dsRNA is recognized and cleaved by RNase III. The mature gRNA forms dependent on the type a complex with a Cas protein to follow its role in target binding or recognition. Figures were sourced and altered from: (Makarova et al., 2011).

1.4.3 CRISPR/Cas9 as targeted genome engineering tool

For targeted genome editing the type II CRISPR system was adapted and a single guide RNA (sgRNA), which is a fusion of the protospacer containing crRNA and the tracrRNA, was introduced (Jinek et al., 2012). The sgRNA is usually under control of a U6 promoter and is transcribed by RNA-Polymerase III. The Cas9 endonuclease, with origin in *Streptococcus pyogenes,* incorporates the sgRNA and is guided to its target region by Watson-Crick base pairing between the target sequence and the protospacer. The PAM, essential for the target recognition, is located directly 3`- of the target region (Figure 6).

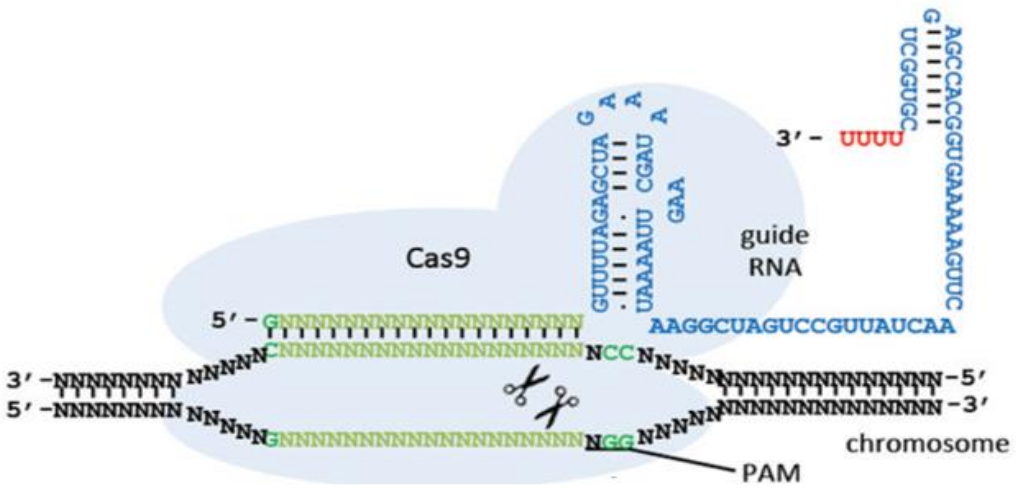

Figure 6: Overview of Cas9 targeting and function. The sgRNA is assembled into the Cas9 endonuclease which dictates the target specificity. The target specificity is exceptional high however, mismatches at the 5'-end of the sgRNA are tolerated which could possibly lead to off-target effects. After binding the target sequence, a double strand break (DSB) is induced by two DNA cleaving domains: RuvC-like and HNH-like nuclease domain. The DSB is catalysed between the base pairs 17 and 18 proximal to the PAM. Figure was sourced and altered from: (Mali et al., 2013).

Thus, Cas9 can possibly target every sequence in the host genome by altering the sequence of the 20 nucleotides protospacer. The only limitation is the PAM which must be present at the genomic target site. However, the PAM used by the *Streptococcus pyogenes* Cas9 (spCas9) can be found every 8 bp in the human genome (Cong et al., 2013). Furthermore, it was demonstrated that the region 1-12 nucleotides upstream the PAM is necessary to determine Cas9 target specificity whereas mismatches further

upstream the PAM region are more likely to be tolerated (Cong et al., 2013; Jinek et al., 2012). It was further shown that not only the complementarity of the sgRNA plays a role in target binding but also epigenetic features like DNA methylation as well as chromatin structures seem to be an important criterion. Genome-wide analysis of spCas9 binding predicts that 19% of binding variations occur due to epigenetic features like chromatin accessibility and DNA methylation pattern (Wu et al., 2014). As Cas9 was led to its target sequence the function relies on two domains: HNH-like nuclease domain and RuvC-like nuclease domain. Thereby the HNH-like nuclease domain cleaves the complementary strand and RuvC-like nuclease domain cleaves the opposite strand (Chylinski et al., 2013; Fonfara et al., 2014). Together the two domains mediate DSBs between the base pairs 17 and 18 of the target sequence. The DSB initiates two of the major DNA repair pathways, either non-homologous end joining (NHEJ) or homology direct repair (HDR). Due the fact that NHEJ requires no homologous sequence and is active during all phases of the cell cycle it is the prominent pathway.

DSBs are repaired by first creating a blunt end of the break if necessary (resection) and re-ligation by recruited ligases. Due to the process of NHEJ, indels of several base pairs are common which can lead to a shift of the open reading frame (ORF) in case of protein coding sequences. Alterations of the ORF are called frame-shift mutations and can have a significant effect on the target gene by changing the amino acid sequence. The introduction of a premature stop codon or the shift of the ORF can lead to nonsense mediated protein decay. However, the most common indels that seem to occur are deletions up to -9 and insertions of +1-2 base pairs (Canver et al., 2014; Hsu et al., 2013; Hwang et al., 2013). The CRISPR system allows also the introduction of repair templates which can be used to introduce a specific sequence at the DSB using HDR.

Several expression systems were established for the integration of Cas9 and the sgRNA into the host's genome. Thereby transient transfection methods e.g. lipid based reagents and electroporation as well as stable insertion into the host genome by viral delivery systems are applicable depending on the experimental design. After transfection, Cas9 and the sgRNA are co-expressed by corresponding promoters like human U6 RNA-Polymerase III promoter or cytomegalovirus (CMV) promoter. It was proven that CRISPR/Cas9 can target a wide range of endogenous genes in different organisms and cells. Cas9 was hereby used to edit genomes of e.g. Mouse (H. Yin et al., 2014), Chinese Hamster (Ronda et al., 2014b), Zebrafish (Hwang et al., 2013), Human (Mali et al., 2013) and many more organisms as well as cell lines.

As mentioned above, CRISPR/Cas9 needs only the PAM at the genomic target site to induce a DSB but also mismatches located upstream the PAM are likely to be tolerated. Up to five mismatches are tolerated which can lead to undesirable off-target effects on non-related sites (Fu et al., 2013a; Mali et al., 2013). To use the CRISPR system in industrial or therapeutic applications several strategies are available which can reduce potential off target effects. First, the usage of CRISPR design tools and second by using spCas9 nickases. A nickase induces a single strand break, which is referred to a nick and is quickly repaired. However, if two nickases cut proximal on opposite strands, the DNA damage is repaired as DSB and NHEJ is induced. The reduction of off-target effects is an essential issue for CRISPR/Cas9 in future therapeutic applications to use it as an efficient tool for genome editing. Several studies have shown that CRISPR/Cas9 could be applied for repairing mutation based diseases like cystic fibrosis (Schwank et al., 2013; Y. Wu et al., 2013) as well as the deletion/mutation of whole distinct loci (Ebina et al., 2013). Thus, the CRISPR system has been proven to be an easy, highly valuable system for cell line engineering and for applications in CHO cells to improve bioprocess phenotypes.

1.4.3.1 CRISPR/Cas9 variants

Since the first mentioning of CRISPR/Cas9 several different Cas9 variants have been described. The CRISPR/Cas9 system is in general not only limited to the induction of DSBs but can be used as transcriptional repressor/activator by recruitment or fusion to transcription factors, DNA or chromatin modifiers. Gilbert and colleagues performed investigations with two Cas9 fusions with Krueppel associated box (KRAB) and a so called “suntag” consisting of several VP64 repeats. KRAB hereby is a transcriptional repressor and VP64 is a transcriptional activator with viral origin (Gilbert et al., 2014). Another Cas9 variant is impaired in the DNA cleavage domains and is fused to FokI. The unspecific FokI endonuclease is only active as dimer and allows to target two proximal sequences to delete large DNA fragments or induce HDR (Tsai et al., 2014). As mentioned the PAM dictates the target sequence which can be used for sgRNA design. Another CRISPR class II system was recently developed using a single RNA-guided endonuclease named Cpf1. The species origin was *Francisella novicida* and the PAM used is 5’-TNN (Zetsche et al., 2015). Interestingly the PAM is located 3’- and not 5’- as for Cas9 and that the DSB exhibits a five nucleotide 5’-overhang. Cas9 induces blunt

end DSBs proximal to the PAM whereas Cpf1 mediates the DSB 18 nucleotides downstream the PAM. To reduce off-target effects and the possibility to mediate HDR rather than the NHEJ pathway Cas9 “nickases” were developed. This particular variant only cuts one strand and two nickases which target a sequence in a proximal distance can be used for the introduction of HDR using repair templates to insert exogenous DNA into the host’s genome. Due to double nicking the off-target effects are highly reduced.

1.4.3.2 CRISPR/Cas9 as potential tool to dysregulate miRNAs in CHO

Not only coding genes are potential targets but also miRNAs can be targeted which play an important role in gene regulation, disease and phenotypic behaviour (Zhao et al., 2014). It was recently demonstrated that miRNAs can be successfully targeted using CRISPR/Cas9 (Chang et al., 2016; Jiang et al., 2014). Targeted was the miR-27-92 cluster which consists of six induvial members with four different seed families. MiR-93 which is a member of the miR-106b cluster was targeted in the seed region and a successful reduced miRNA expression by over 90% was reported in single cell clones exhibiting various indel sizes. MiR-93 is critical in regulating cell growth and the expression of three targets (PTEN, E2F1 and p21) was assessed as well as the growth phenotype proving that miR-93 lost its function in regulating these proliferation relevant genes. It was also shown that small deletions can impair the Drosha processing and ultimately the maturation of miRNAs. Thus, CRISPR can be used as tool to stably deplete if not possibly knockout miRNAs besides using sponge decoy technology.

1.4.3.3 Genome wide studies using libraries

Due to the unique mechanism of the CRISPR/Cas9 system it provides high target specificity and is applicable for a wide range of different methods beginning with targeted knockouts of genes up to whole genomic screens using library-based methods to overcome pitfalls in RNAi libraries (Wang et al., 2014). Wang and colleagues hereby identified genes involved in etoposide protection as well as proliferation associated genes. Different library approaches were summarised recently by Shalem and colleagues (Shalem et al., 2015). Previously Shalem and colleagues performed a genome wide “loss of gene function” screen in human cells (HEK293T) using ~65,000

sgRNAs to target 18,080 genes. Investigated was the positive and negative selection with vemurafenib for the treatment of melanoma and already validated genes by RNAi were identified with high confidence using the CRISPR approach (Shalem et al., 2014). Another genome wide study identified unknown genes for the resistance to alpha-toxin and 6-thioguanine after the knockout of 19,150 genes using an 87,897 sgRNA-library in mouse embryonic stem cells. A total of 26 genes were identified including four unknown genes which are responsible for the resistance to mentioned toxins (Koike-Yusa et al., 2014). All known genes (22) were previously validated by an RNAi screen as well. A screen using two Cas9 variants with a transcriptional activator (VP64) and repressor (KRAB) using ~200,000 sgRNAs identified several unknown genes responsible for the sensitivity or resistance to diphtheria and cholera toxins (Gilbert et al., 2014). Mentioned studies highlight the power a genome-wide study for the investigation of genes using negative selection could potentially have for CHO cells to identify genes involved bioprocess relevant phenotypes.

2.0 Aims

2 Aims of the project

Stable depletion of the miR-23-24-27 cluster and each individual member to investigate the impact on the phenotype in industrially relevant cell lines with the aim to improve the bioprocess performance

- Investigation of the impact after stable depletion of miR-23, miR-27, miR-24 and miR-23-24-27 on a panel of cell lines expressing different modern biopharmaceutical products
- If a beneficial phenotype is observed further aim are the investigation of the molecular mechanisms and pathways in which the miRNAs are involved
- Highlight new targets for cell line engineering and ultimately increase CHO cell productivity

CRISPR/Cas9 as genome engineering tool to knockout miRNAs to improve the bioprocess performance of industrially relevant cell lines

- Functional assessment of CRISPR/Cas9 in CHO cells as an engineering tool for miRNAs
- Screen for single cell clones which show a significant knockdown/knockout of the targeted miRNA and the assessment of the bioprocess phenotype
- Comparison of the impact of a sponge decoy technology on miRNA depletion compared to CRISPR/Cas9 mediated depletion
- Investigation of interesting phenotypes obtained due to the depletion of miRNAs using CRISPR/Cas9 and investigation of what mechanisms are involved using proteomic profiling or transcriptomic analysis.

Genome-wide "loss of gene function" studies in Chinese Hamster Ovary cells using a CRISPR/Cas9 library to identify genes which are functionally involved in stress resistance or productivity

- Establishment of a stable cell line expressing human codon optimised spCas9 and investigation of function in CHO
- Investigation of the optimal delivery method for a sgRNA-library containing 87,897 different sgRNAs targeting 19,150 mouse genes to achieve low copy numbers per cell and optimal complexity of the library
- Enrichment of CHO cell population using stress exposure or isolation of clones which show high productivity due to knockouts which are functionally involved in such phenotype

3.0 Methods

3 Material and Methods

3.1 Cell culture techniques

3.1.1 Ultrapure water

Ultrapure water was prepared using Milli-RO 10 Plus system (Millipore) and it was used for the preparation of all media and buffer solutions if not otherwise specified. The water was pre-treated with activated carbon and purified by reverse osmosis. Water was sterilised prior use for 20 minutes at 121°C and 1 bar with saturated steam if used for cell culture purposes.

3.1.2 Glassware

Glassware was rinsed twice with ultrapure water prior sterilisation. To sterilise for cell culture purposes all glassware was autoclaved for 20 minutes at 121°C and 1 bar with saturated steam.

3.1.3 Cell culture cabinet

Cell culture work regarding Biosafety level 1 (BSL-1) was performed in class II laminar flow cabinets (LF, Holton). After a lead time of 15 minutes the surface was sterilized with 70 % denatured alcohol (IMS). All materials which were used in the laminar were prior autoclaved and wiped with IMS. To avoid cross contaminations only one cell line at a time was used. Prior use of next cell line, a 15 minutes break was given and all surfaces were sterilised with IMS again. Before switching off the cabinet all surfaces were sterilised with IMS and a 15-minute break was applied to allow a sterile, aerosol free air flow. Laminar flow cabinets were cleaned on regular basis which involved incubation of all surfaces with a detergent solution (Virkon® DuPont) followed by water and sterilisation with IMS.

3.1.3.1 Work with lentiviral systems in Biosafety level-2 environment

Lentiviral systems require work under Biosafety level 2 (BSL-2) conditions. Additionally, to the steps in BSL-I all materials which were in contact with virus containing liquids were treated with 1% Virkon® solution (DuPont) for 15 minutes and separately autoclaved as clinical waste. Additonally, waste solid waste required a pre-autoclavation step. The work was performed in a laminar flow cabinet class II (S@feflow 1.2). Spills were first incubated with 1% Virkon® solution for 15 minutes and rinsed with water before the surface was sterilised with IMS.

3.1.4 Culturing of mammalian cells

All cells used for experiments were in general cultured without the use of antibiotics. All solutions, glassware as well as tips were sterilised for 20 minutes at 121°C and 1 bar with saturated steam prior usage. Thermal labile solutions were filtered through 0.22 µm or 0.45 µm PVDF filters with the help of sterile syringes. Antibiotics were only used for the selection of cells after transfection or lentiviral transduction. Cells were also routinely "pulsed" with selection agent for three passages to maintain stable transgene expression. All cells were routinely assessed for mycoplasma contamination. In context of this PhD thesis no mycoplasma contamination was detected in any cell line used.

3.1.4.1 Trypsin/EDTA solution

For the subcultivation of cells growing in adherence Trypsin/EDTA (TV) solution was used. The TV solution consists of 0.25 % (w/v) Trypsin and 0.02 % EDTA. Trypsin is an endopeptidase normally found in the digestive system of mammals. It is commonly used in the detachment of monolayer cultured cells and is supported by the usage of EDTA which acts as chelator for divalent ions like Ca^{2+} or Mg^{2+}. The solution was prepared by dilution of 2.5 % (w/v) Trypsin (Gibco®) and 1% (w/v) EDTA solution in 500 ml of sterile phosphate buffered saline (PBS). The TV solution was aliquoted and stored at -20°C.

3.1.4.2 Incubators

Incubators were cleaned on regular basis which involved an incubation of all surfaces with a detergent solution (Virkon® DuPont) followed by water and sterilisation with IMS.

3.1.4.3 Anchorage dependent cells

Adherent cells were cultivated in a Steri-cycle® CO_2 incubator with heap-filter (Thermo Scientific). Cells were grown at 37°C, 5 % CO_2 and 80 % humidity. For the sub-cultivation media was removed into a sterile waste container using pipettes. The monolayer was washed with 5 mL of sterile PBS to remove residual media and serum. PBS was discarded and 2-5 mL prewarmed TV solution was added to the flask. Trypsin has its optimum at 37°C and cells were incubated for 2-5 minutes in an incubator. Cells were visually monitored using a microscope to observe detachment was observed. Serum containing media was added to neutralise TV and cells were transferred into sterile 30 mL universal containers and spun down for five minutes at 200 g. The supernatant containing TV was removed and the cell pellet was resuspended into fresh, prewarmed media. Cells were counted using Trypan Blue exclusion method and an aliquot was appropriately diluted as well as counted using a haemocytometer (Neubauer chamber). The required number of cells was then transferred into a new cell culture flask (Corning®) and the required amount of media was added.

3.1.4.4 Suspension cells

Cells were cultivated in a Kuhner Clima-shaker incubator (ISF1-X) with a process environment set to 37°C, 170 rpm and 80% humidity. Cells from Biogen Idec were cultivated in a Kuhner Clima-shaker incubator (ISF1-X) with a process environment set to 35°C, 170 rpm and 80% humidity. For routine growth TPP 50 ml TubeSpin® bioreactor tubes for 5 mL batch cultures or 250 ml Erlenmeyer shake flasks (Corning®) were used. For routine subcultivation cells were counted using Trypan Blue exclusion method and an aliquot was appropriately diluted as well as counted using a haemocytometer (Neubauer chamber). The number of cells was calculated and cells were seeded with initial cell density of $2x10^5$ cells/mL in TPP 50 ml TubeSpin® bioreactor tubes (5 mL culture volume) or 250 ml Erlenmeyer shake flasks (Corning®) (30 mL culture volume).

3.1.4.5 Counting cells and assessment of viability

Trypan Blue exclusion method

Trypan Blue is a method for the assessment of viability by staining dead cells and not viable cells. The dye does not permeate the membrane of viable cells whereas senescent and apoptotic cells are stained. For counting cells using Trypan Blue attached cells had to be trypsinised and an aliquot of the cell suspension was taken (as described in 3.1.4). The aliquot was diluted if necessary and the diluted sample was added to Trypan Blue (Gibco®) in a 1:1 ratio and incubated for ~3 minutes at RT. The sample/Trypan Blue mix was then transferred into a coverslip containing haemocytometer (Neubauer-chamber). All 16 squares for all four corner grids were counted using a light microscope. The average was multiplied by 10^4 and further by the dilution factor if used to obtain the amount of cells/mL. Trypan Blue exclusion method was usually used for routine subcultivation.

Guava™ ViaCount® reagent

The Guava ViaCount® assay (Merck Millipore, 4000-0040) is an easy, rapid and precise method for the assessment of dead and viable cells in a cell population. With the ViaCount® it is possible to read plates with replicates in high-throughput which is ideal for the assessment of viability and viable cell densities in small scale batch and Fed-batch bioprocesses. The assay uses two specifically DNA binding dyes: A nuclear dye binds to DNA in the nucleus (viable cells) and another dye binds to DNA of dying cells. Cell debris are excluded from this staining method. The ViaCount® reagent is supplied as 2x solution and cells were first appropriately diluted to obtain between $1x10^4$ and $5x10^5$ cells/mL. ViaCount® reagent was added afterwards and was incubated for at least 10 minutes at room temperature. The cell count was assessed in a Guava™ benchtop flow cytometer. A viable cell is detected if a positive fluorescence signal occurs when the forward light scatter (FSC) was positive as well. The FSC is produced and detected by a cell above a particular size. Cell debris are excluded that way by resulting in no or low FSC signal.

Guava™ ExpressPlus programme for assessment of GFP intensities

Measuring of GFP intensities was performed using a Guava™ benchtop flow cytometer with the Guava™ ExpressPlus programme. GFP negative cells were used to adjust settings and exclude the negative population. Cells were diluted appropriately using PBS and GFP was excited at λ 488 nm with a blue laser diode. The cell size is measured with the forward scatter, whereas the shape and the overall size is assessed with the forward scatter to exclude small cells or possible cell aggregates. The negative population was excluded by a rectangular gating and excited cells reaching the threshold were counted as positive. The gating had to be adjusted for every experiment.

Fluorescence assisted cell sorting (FACS)

For the sample preparation cells were trypsinised and trypsin was inactivated by adding basal media supplemented with 5 % foetal bovine serum (when cultures in adherent conditions). The pellet was resuspended and washed three times in particle free Dulbecco´s phosphate buffered saline (DPBS, Gibco®). After washing the cells were fixed in 3.7 % Paraformaldehyde solved in H_2O at 4°C for 10 minutes. After fixation the cells where washed again for three times in DPBS and samples were filtered through a cell strainer cap into a polystyrene falcon (5 mL, BD Falcon). A sample size of 300 µL was used for the analysis of viral integration events using a BFP reporter. The excitation wavelength was λ 402 nm and emission was measured at λ 457 nm. For the generation of single cell clones FACS was used as well. No fixation was necessary and cells were sorted for low, medium and high GFP intensities into 96-well plates (Corning®) containing prewarmed growth media supplemented with 10% conditioned media.

3.1.5 Cell lines and expressed products

All cells were routinely sub-cultivated as described in 3.1.4.3 and 3.1.4.4. The culture conditions and all used cell lines are listed in Table 1.

Table 1: Cell lines used for experiments and culture conditions

Cell line	Product	Media	Format	Selection	Concentration
CHO-K1 mAb	IgG	CHO-SFM II	Suspension	MTX/G418	350 nM/1mg/mL
CHO-K1 Fc	Fc	Biogen	Suspension	MTX	1000 nM
CHO-S Fc	Fc	Biogen	Suspension	MTX	1000 nM
DG44i Fc	Fc	Biogen	Suspension	MTX	1000 nM
DG44i mAb	IgG	Biogen	Suspension	MTX	1000 nM
HEK293T	none	DMEM	Attached	none	none
CHO parental	none	CHO-SFM II	Suspension	none	none

3.1.6 Cryopreservation of cells

For the cryopreservation of mammalian cells the storage condition is usually -196°C in the vapour phase of liquid nitrogen and cells can be stored for years under the right conditions. Firstly, cells were trypsinised (monolayer) and counted using Trypan Blue exclusion method. Depending on the cell line $2x10^6$ up to $1x10^7$ cells were used per cryopreservation vial (CRYO.S™ Greiner Bio One) in one mL. Cells were spun down at 200 g for 5 minutes and resuspended in basal media without serum. A pre-chilled 2x freezing media (e.g. DMEM, supplemented with 20% foetal bovine serum and 10-20% DMSO) was added to reach 1x concentration and cells were transferred into cryopreservation vials. DMSO hereby prevents the formation of ice crystals. Cells were transferred immediately into -20°C and stored for 2 to 3 hours as well as to -80°C for 24 hours before they were stored in the vapour phase of liquid nitrogen at -196°C.

3.1.7 Thawing of cryopreserved cells

Given the cytotoxic effect of DMSO in high concentrations long incubation with media containing DMSO was avoided. Cells were thawed in a pre-warmed water bath for two minutes and immediately transferred into 9 mL of pre-warmed media without

supplementation. Cells were spun down at 200 g for five minutes and the supernatant was discarded. The pellet was resuspended into appropriate media for suspension culture or cultivation in monolayer (3.1.5). Suspension cells were transferred into TPP 50 ml TubeSpin® bioreactor tubes or T75 cell culture flasks (Corning®) for adherent cells in a culture volume of 10 mL. To remove dead cells and debris the culture media was exchanged 24 hours after thawing and viability was assessed.

3.1.8 Lipid- and PEI-based transfection methods

Lipid-based transfection reagents are based on cationic liposomes which interact and form complexes with negatively charged DNA or RNA molecules. The transfection is usually highly efficient for some cell lines and can be used as transient approach or for the generation of stable cell lines. After the complex formation the liposome fuses with the phospholipid bilayer and the complex is taken up as vesicle by endocytosis. In the cytoplasm the vesicle can follow two routes: the formation of endosomes which results in degradation of the nucleic acid or the release which results into expression for e.g. plasmids with a transgene. Expression using the transient approach is usually maintained for up to 96 h. For the stable selection and integration into the host's genome, resistance genes e.g. hygromycin B phosphotransferase (hbh) or puromycin N-acetyl transferase (pac) can be used.

3.1.8.1 TransIT®-X2 Mirus for plasmid DNA

Cells were seeded with $5x10^5$ cells total for adherent cultures and $1x10^6$ cells for cells in suspension 24 hours prior transfection in 6-well plates (Corning®) or TPP 50 ml TubeSpin® bioreactor tubes. The complex formation was performed in CHO-S-SFMII media (Gibco®) without any supplements in 1.7 ml Eppendorf tubes. Firstly, the DNA was added to 250 µL of media and 1 µL Mirus transfection reagent (Mirus Bio® LCC, catalog number MIR6003) was added for every µg of plasmid DNA used. To allow the complex formation the reagent mix was incubated for 20 minutes at room temperature. The complexes were added drop wise to the cells and incubated for 3-4 hours before the media was refreshed. After 24 hours selection pressure was added for the generation of stable cell lines.

3.1.8.2 Lipofectamine® 2000

Cells were seeded with $5x10^5$ cells total for adherent cultures and $1x10^6$ cells for cells in suspension 24 hours prior transfection in 6-well plates (Corning®) or TPP 50 ml TubeSpin® bioreactor tubes. The complex formation was performed in CHO-S-SFMII media (Gibco®) without any supplements in 1.7 ml Eppendorf tubes. Firstly, the DNA was added to 250 µL of media and incubated for 10 minutes. For the complex formation 3 µL Lipofectamine2000 (Invitrogen, catalog number 11668) reagent was added for every µg of plasmid DNA used and the mix was incubated for 30 minutes at room temperature. The complexes were added drop wise to the cells and incubated for 6-8 hours before the media was refreshed.

3.1.9 Physical transfection methods – Electroporation

Not every cell line can be transfected using lipid-based reagents with high efficiencies. For those cell lines electroporation can be used to achieve higher efficiencies in delivery of the plasmid DNA or RNA. Media was refreshed the day before electroporation to ensure healthy growth. Adherent cultures were trypsinised and resuspended in basal media supplemented with 5% foetal bovine serum. Cells were washed with PBS and resuspended as well as counted. For the electroporation $1x10^7$ cells were spun down again and resuspended in 800 µL of HEBS (HEPES-buffered saline, Sigma-Aldrich, catalog number 51558). Cells were transferred into electroporation cuvettes (Bio-Rad Gene Pulser®, 0.4 cm gap, catalog number 1652088) and 10-50 µg plasmid DNA was added. Electroporation settings were set to 2.8 kV, 950 µF and ∞ Ω (Ohm, resistance) and cells were pulsed within 11-14 milliseconds. The suspension was acclimatised for 10 minutes at room temperature and cells were transferred into 10 mL of warm basal media and spun down for 5 minutes at 200 g. The supernatant was discarded and cells were resuspended in basal media and added into a T75 cell culture flask (Corning®). The media contained foetal bovine serum for adherent cells and only SFM media was used for suspension cells. However, cells grown in suspension were kept under static conditions for the whole selection period. After 24 hours the media was refreshed and selection agent was added. For the period of selection, the media was exchanged every 3-4 days and the cell density was adjusted to $2x10^5$ cells/mL. The selection pressure was maintained for 3-4 weeks. Nucleofection is another electroporation method which

was used according to the manufacturer's guidelines (4D-Nucleofector™ system, Lonza).

3.1.10 Generation of lentiviral particles

For the introduction of the sgRNA-library into CHO-K1 cells a lentiviral based approach was used. Therefore, HEK293T cells were seeded with a density of $2x10^6$ cells in a 10 cm Petri dish the day before transfection. Before transfection the media was refreshed and for the transfection lipid based Lipofectamine®2000 (Invitrogen) was used. As the cells are not able to produce lentiviral proteins two packaging plasmids were co-transfected (GeneCopoeia PLv-PK-01). Each of the packaging plasmids (6 µg) was transferred into 200 µl of serum free media together with 12 µg of the sgRNA-library plasmid. A total amount of 80 µl Lipofectamine®2000 reagent was transferred into 200 µl of serum free media and incubated for 5 minutes. Both solutions were combined in a 1:1 ratio. The mixture was incubated for 30 minutes at RT and added drop wise to the cells. After 24 hours the media was refreshed with DMEM supplemented with 2% foetal bovine serum. At 48 hours post transfection media was harvested and the volume of fresh media was decreased to 8 ml. At 72 hours post transfection the media was harvested again. To get rid of cell debris the conditioned media was filtered through 0.45 µm syringe low protein binding filters and the virus containing media was stored at -80°C until concentration was performed. Quantification of lentiviral particles was not performed.

3.1.10.1 Transduction of lentiviral particles

For the transduction of the sgRNA-library into CHO-KI mAb expressing cells the cells were seeded with $4x10^6$ cells into a T-75 vented flask and media was refreshed prior transduction. To ensure single copy integrations the used MOI was lowered to 0.04 and a dilution of 1:1 of the concentrated virus was performed. Media was removed and the virus containing media was added to the cells using 8 µg/ml polybrene. The virus was incubated for 8 hours to overnight and media was refreshed. After 48 hours post transduction cells were transferred into to T-75 vented flasks and selection pressure with

10 µg/ml puromycin was applied. The selection pressure was maintained for 7-10 days before integration events were analysed.

3.1.10.2 Concentration of lentiviral particles

To concentrate the lentivirus the conditioned media containing the virus was centrifuged. Therefore, the virus was transferred into sterile centrifuge tubes and pelleted at 4°C for 2.5 hours at 20,000 g. After centrifugation the supernatant was discarded and the virus pellet was solved in 5 ml of serum free media and stored at -80°C.

3.1.11 Limited dilution cloning

Limited dilution cloning besides FACS, is a suitable method for the generation of single cell clones and panels. However, the efficiency of single cell cloning is usually very low and several 96-well plates have to be seeded to obtain large numbers of clones compared to FACS. For limited dilution cloning the media was refreshed 24 hours before seeding to maintain healthy growth. Cells were counted as triplicate to ensure an accurate cell number. The cell suspension was diluted to obtain five cells per mL and 100 µL were transferred into each well (statistically 0.5 cells/well) to avoid colonies resulting from more than one cell. As the efficiency is generally very low, the final dilution contained 20% conditioned media which was harvested from the same culture after 24 hours. Conditioned media was prepared by removing cells by centrifugation for 5 minutes at 200 g. The supernatant was filtered through a 0.45 µm PVDF low protein binding membrane with the help of a sterile syringe. To ensure sufficient nutrients 100 µL basal media was added to the 96-well plate to obtain a final volume of 200 µL. The plates were sealed using ParafilmM® (Bemis) and positive wells were visually analysed using a microscope after 8-10 days. Adherent cells were trypsinised and transferred into a larger scale for further analysis.

3.1.12 Plasmid and vector maps

Plasmids which were used for the generation of stable cell lines for work related to CRISPR/Cas9, lentiviral library, assessment of transfection efficiencies and sponge

experiments are listed below. Plasmids were purchased from Addgene, Clonentech and Invitrogen.

SpCas9(BB)-2A-Puro (PX459)

PX459 contains two BbsI site downstream of a U6 promoter for the integration of gRNAs. Located downstream the cloning site the tracrRNA is expressed together with the protospacer forming the sgRNA. A Cas9 variant fused to pac with a 2A self-cleavage domain is driven by CMV promoter (Figure 7). Before ligating the gRNA the vector was digested with Bbs1 and gRNAs were designed with 5'- and 3'-overhangs to match the overhangs resulting out of restriction enzyme digest.

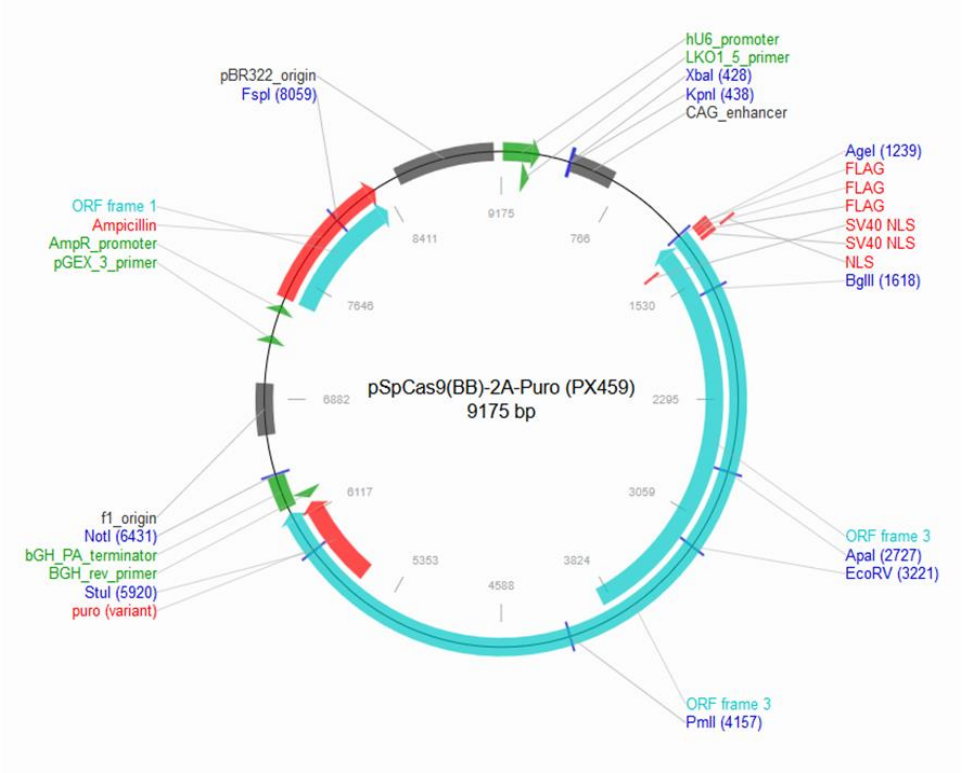

Figure 7: SpCas9(BB)-2A-Puro for the simultaneous expression of sgRNA and Cas9. The sgRNA is under control of a U6 promoter and the Cas9 fusion uses a CMV promoter. The mammalian selection marker is pac and ampicillin was used for the selection of positive clones after transformation of DH5-α.

pKLV-U6gRNA (BbsI)-PGKpuro-2A-BFP (lentiviral sgRNA-library)

Vector used for the generation of the sgRNA-library by Koike-Yusa and colleagues (Koike-Yusa et al., 2014). The backbone used was originated from pBlueScript. The sgRNA pool was created using 79 nucleotide long oligo sequences and obtained by CustomArray Inc. The sgRNA is under control of a U6 promoter whereas the puro-2A-BFP variant is PGK driven.

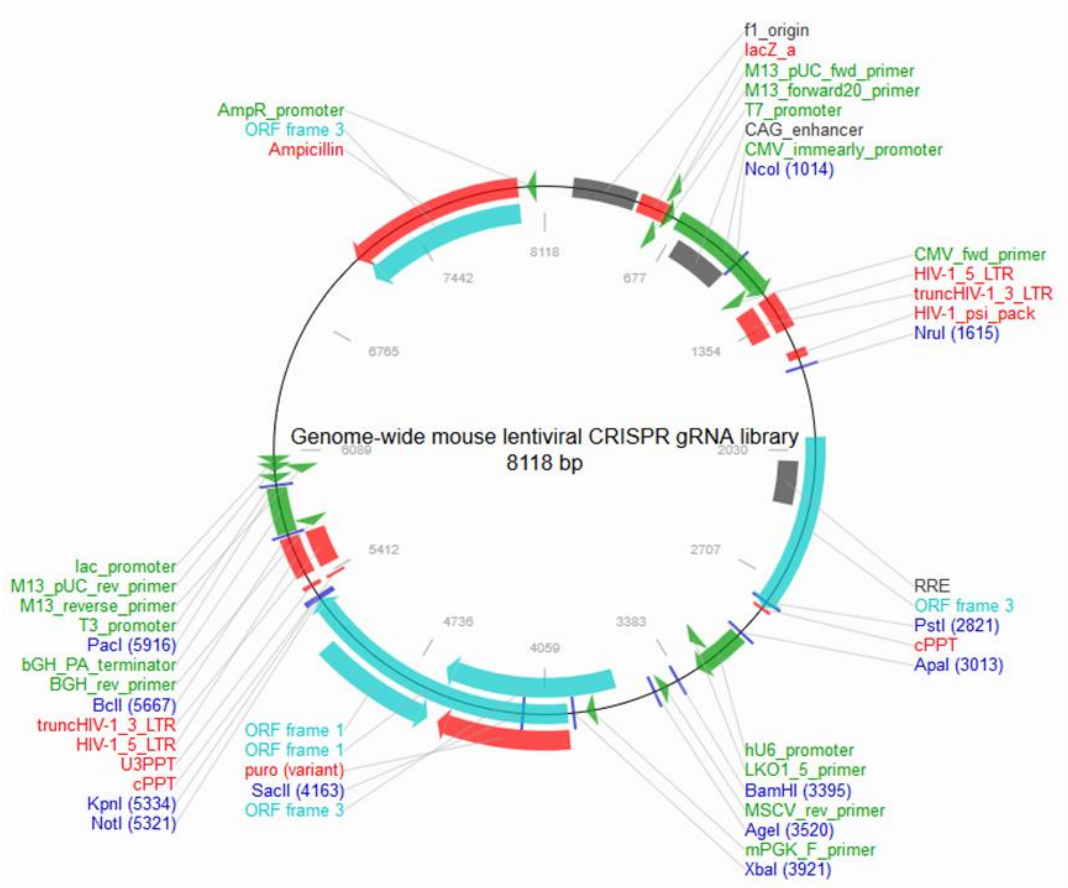

Figure 8: Vector used for the generation of the sgRNA-library containing 87,897 different sgRNAs targeting 19,150 *Mus musculus* genes. The sgRNA is expressed as chimeric construct under control of a U6 promoter. The backbone was sourced from pBlueScript. A pac variant fused to BFP by a 2A self-cleavage peptide.

pKLV-U6 (BbsI)-PGKpuro-2A-BFP (empty control vector)

Vector used for the generation of the sgRNA-library by Koike-Yusa and colleagues (Koike-Yusa et al., 2014). The vector exhibits BbsI sites for the integration of sgRNAs but was purchased as empty vector control for lentiviral packaging and transduction. The backbone used was originated from pBlueScript. The chimeric sgRNA would be under control of a U6 promoter whereas the puro-2A-BFP variant is PGK driven (Figure 9).

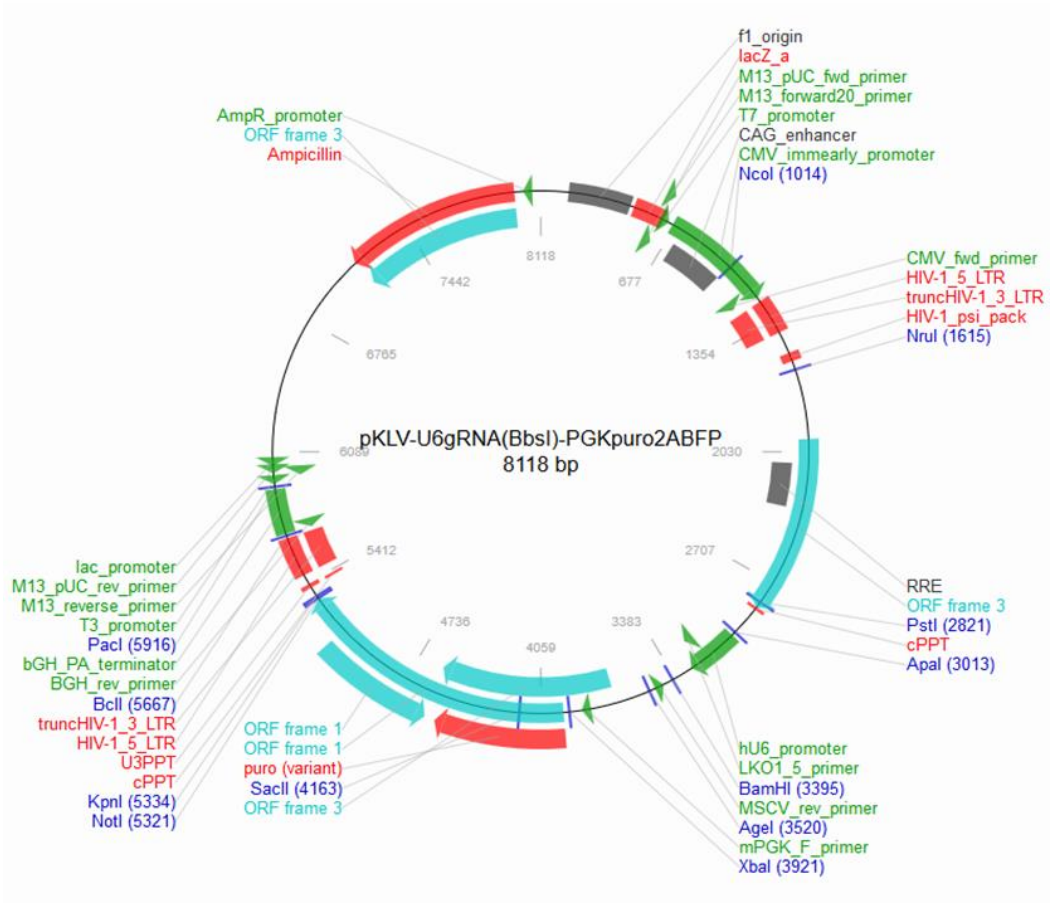

Figure 9: Vector used for the generation of the sgRNA-library without containing sgRNAs which was used as control for lentiviral transduction. The sgRNA (if used) would be expressed as chimeric construct under control of a U6 promoter. The backbone was sourced from pBlueScript. A pac variant fused to BFP by a 2A self-cleavage peptide.

pEGFP-C1 plasmid (Clontech Laboratories, Inc.)

Plasmid used for the assessment of transfection efficiency using the EGFP reporter. The EGFP is a red shifted variant with excitation maximum at λ 488 nm and emission maximum at λ 508 nm. The vector was originally designed for the cloning of fusion proteins which are then expressed with GFP to investigate their localisation. The MCS therefore is downstream the EGFP reporter. The vector can be selected in mammalian cells using the neomycin resistance gene (aph) which is also used for selection in bacteria using kanamycin (Figure 10).

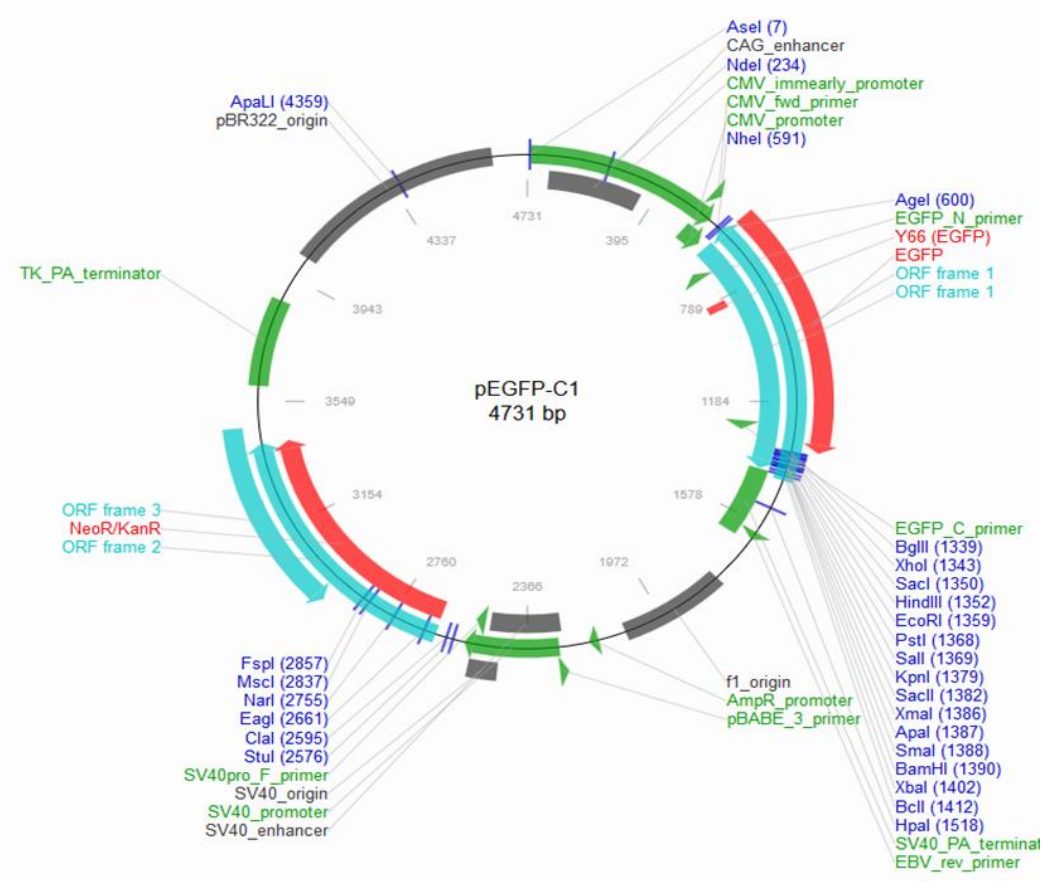

Figure 10: Plasmid used for the assessment of transfection efficiency using the EGFP reporter. The MCS therefore is downstream the EGFP reporter which can be used for the creation of fusion proteins. The vector can be selected in mammalian cells using the neomycin resistance gene (aph) which is also used for selection in bacteria using kanamycin.

pcDNA3.1/Hyg+ (backbone for the expression of destabilised GFP combined with sponge)

As backbone for the creation of sponge constructs pcDNA3.1/Hyg+ was the plasmid of choice. A destabilised EGFP reporter sequence (d2EGFP) was cloned into the MCS using NotI and BamHI. The spare MCS was removed and a new MCS was engineered using Not1 and EcoRI. The new MCS contained one SanDI site which allows the fast, site directed integration of sponge constructs with multiple fragments as previously reported by Kluiver and colleagues (Kluiver et al., 2012a). The d2EGFP-sponge construct is under control of a CMV promoter and the hph gene is driven by a SV40 promoter (Figure 11).

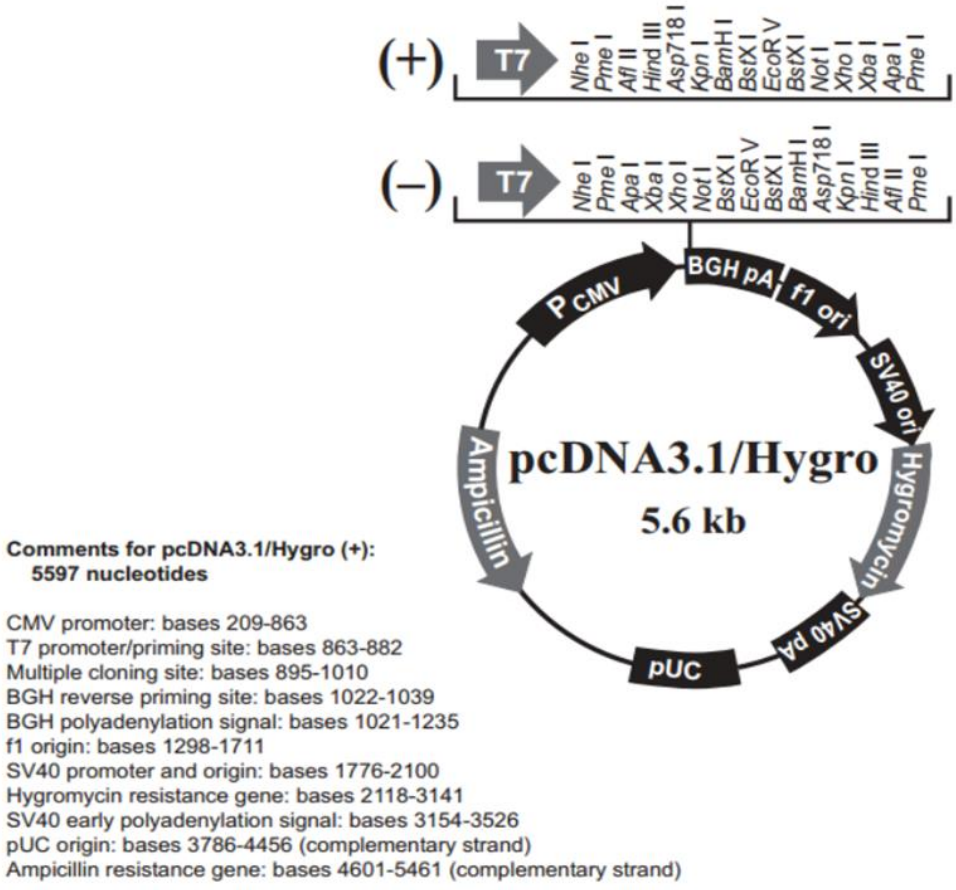

Figure 11: The pcDNA3.1/Hyg+ backbone was engineered for the expression of d2EGFP and a sponge construct. A destabilised EGFP variant was used and ligated using NotI and BamHI. The spare MCS was removed and a new MCS containing SanDI sites was integrated for the rapid ligation of miRNA binding sites downstream the reporter.

3.2 DNA based methods

3.2.1 DNA isolation

Genomic DNA was extracted using Qiagen DNA Mini Kit (Catalog number 51304) following the manufacturer's protocol. Cells growing in a monolayer were trypsinised and the reaction was stopped with basal media containing 5% foetal bovine serum. Cells were counted using Trypan Blue exclusion method and 2-3x10^6 cells were spun down and washed with PBS. The cell pellet was resuspended in 200 µl of PBS. The same amount of lysis buffer as added as well as 20 µL Proteinase K (1 mg/mL) and incubated for 10 minutes at 56°C. For enabling binding to the silica membrane 200 µL 100% EtOH was added and the lysed sample was transferred to a column proved in the kit and spun down at 6,000 g. Two wash steps were included using the buffers provided in the kit. Genomic DNA was eluted using nuclease free H_2O.

3.2.2 RNA isolation using TRIzol® reagent

TRIzol® (Life technologies) was used for the extraction of RNA following the manufacturer's protocol. Cells grown in adherence were trypsinised and counted using Trypan Blue exclusion method. All centrifugation steps were performed at 4°C. For the RNA isolation 2-3 x 10^6 cells were spun down at 200 g for 5 minutes and excess media was discarded. Cells were resuspended in 1 mL TRIzol® reagent as well as transferred into a 1.7 mL Eppendorf tube and incubated for 2-3 minutes at room temperature. The lysed sample was either stored at -80°C or immediately processed by adding 200 µL Chloroform (Sigma-Aldrich) and the sample was mixed for 15 seconds. The TRIzol®/Chloroform mix was spun down at > 16000 g for 10 minutes and the upper aqueous phase was carefully removed and transferred into a new 1.7 mL Eppendorf tube. Per mL of TRIzol® 500 µL of isopropanol was added and incubated for 10 minutes at room temperature. The sample was spun down at > 16000 g for 10 minutes and the supernatant was carefully removed. To remove residual isopropanol 1 mL of 75 % EtOH was added and the sample was centrifuged again for 5 minutes at > 8000 g. The EtOH was removed and the pellet was dried for 10 minutes before RNase-free H_2O was added and the sample was incubated for 10 minutes at 55°C. RNA was in general stored at -80°C to prevent degradation.

3.2.2.1 Qualitative and quantitative determination of DNA and RNA using NanoDrop® 1000

For the validation of DNA and RNA concentrations the NanoDrop™1000 (Thermo Scientific) spectrophotometer was used. The NanoDrop™1000 was first calibrated using a 2 µL H_2O sample and it was blanked using 2 µL of sample diluent. For the actual measurement 2 µL of the sample was dropped directly on the optical measurement surface of the NanoDrop™1000. The spectrophotometer can be used for evaluation of DNA and RNA concentrations at an absorbance of λ260 nm. Furthermore, information about the purity of a sample is provided by absorbance ratios of 280/260 nm and 260/230 nm.

3.2.3 High capacity cDNA reverse transcription

To assess mRNA expression extracted total RNA had to be reverse transcribed into complementary DNA (cDNA). Therefore, a reverse transcriptase is commonly used with viral origin. For the reaction 1 or 2 µg of total RNA with high quality in a volume of 20 µL was used (280/260 nm between 1.8 and 2.0; 260/230 nm > 1.8). The kit used was purchased from Applied Biosystems (Applied Biosystems, High-Capacity cDNA Reverse Transcription Kit, Catalog number 4368814). Depending on the reaction volume 10 x RT buffer, 25 x dNTPs (100 nM), 1 µL MultiScribe™ reverse transcriptase (50 U/ml) and 10x random primers were mixed as well as added to the total RNA. To reach a reaction volume of 20 µL the volume was increased with nuclease free H_2O. For the first strand synthesis primers were annealed at 25°C for 10 minutes. The reverse transcription was performed at 37°C for 120 minutes and the reaction was stopped at 85°C for 5 minutes in a Thermo cycler system (G-STORM). The cDNA was stored at -20°C till usage.

3.2.4 Fast SYBR® green based real time quantitative qPCR

For real-time PCR (RT-qPCR) MicroAmp optical 96-well plates (Applied Biosystems, Cat. No. 4346906) with corresponding Fast SYBR® green 2x master mix (Applied Biosystems, Fast SYBR® Green Master Mix, Cat. No. 4385612) was used. The prior reverse transcribed cDNA was diluted 1 to 5 to obtain a concentration of 20 ng/µL. The master mix was prepared using 10 µL 2x Fast® SYBR green master mix, 10 nM of each

primer targeting the gene of interest and 20 ng cDNA. Additional nuclease free water was added to reach a reaction volume of 20 µL and samples were measured as triplicate. The reaction was carried out with an Applied Biosystems 7500 Fast Real-Time PCR system using 40 cycles. Cycles contained a denaturation step at 95°C for 30 seconds and a annealing/elongation step at 60°C for 15 seconds.

3.2.5 TaqMan® small RNA assays

For TaqMan® small RNA assays total RNA was isolated as described in 3.2.2 and same High-Capacity cDNA Reverse Transcription Kit was used for reverse transcription. However, the TaqMan® assay provided looped primers which specifically bind mature miRNAs. The principle of the assay is displayed in Figure 12.

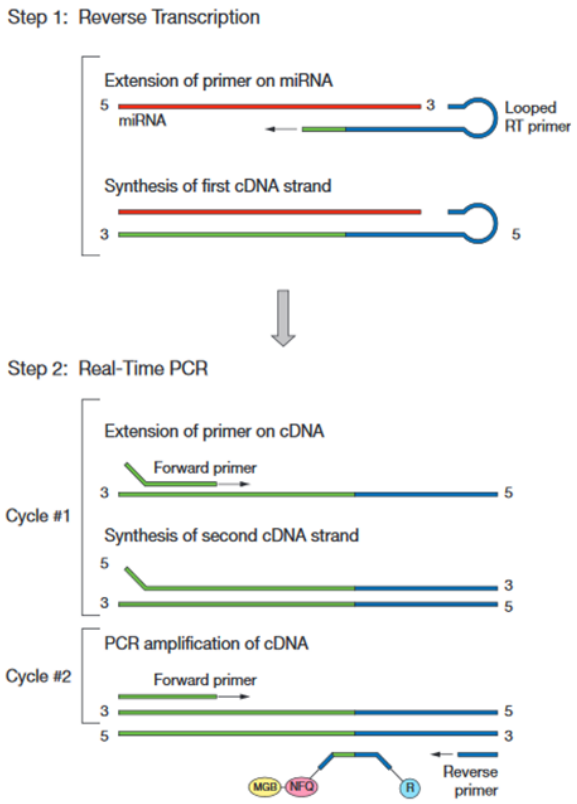

Figure 12: Principle of the TaqMan® small RNA assay. A looped primer binds to the mature miRNA and is extended by a reverse transcriptase which catalyses the first strand synthesis into cDNA. The second step is the binding of primers and amplification as well as the binding of a specific probe which contains a fluorophore and a quencher. Due to amplification the fluorophore is released and the signal can read. Picture was sourced from Life technologies TaqMan® miRNA assays protocol handbook.

A total amount of 100 ng RNA was reverse transcribed using specific looped primers. Primer annealing was performed at 16°C for 30 minutes. The reverse transcription was performed at 37°C for 30 minutes and the reaction was stopped at 85°C for 5 minutes in a Thermo cycler system (G-STORM). The cDNA was stored at -20°C till usage.

For the RT-qPCR step 6.67 ng cDNA (1 µL) was used for the amplification. The total reaction was 20 µL using 2x TaqMan Universal PCR Master Mix (Applied Biosystems, catalog number 4304437) and 20x TaqMan® probe provide in the TaqMan® assay. The reaction was carried out with an Applied Biosystems 7500 Fast Real-Time PCR system using 40 cycles in MicroAmp optical 96-well plates (Applied Biosystems, Cat. No. 4346906). To activate the enzyme a hold step was comprises at 95°C for 10 minutes. Cycles comprised a denaturation step at 95°C for 15 seconds and a annealing/elongation step at 60°C for 60 seconds.

3.2.6 General Polymerase Chain Reaction (PCR)

For the amplification of specific sequences out of genomic DNA, plasmid DNA or cDNA several different PCR kits were used. For a general purpose the MyTaq™ DNA polymerase (Bioline, catalog number BIO-21105) was used. If high-fidelity with proofreading was required the Phusion® kit (New England BioLabs Inc. catalog number M0530S) or Platinum® high fidelity DNA Polymerase (Thermo Fisher Scientific, catalog number 11304011) were used. The master mixes (2 x) contained all required ingredients e.g. $MgCl_2$, dNTPs and reaction buffer. The reaction volume was set usually between 20-50 µL and a primer concentration of 10 nM for forward and reverse primer was used. If plasmid DNA was used as template an amount of 10 pg was used. For the amplification of cDNA and genomic DNA 10-100 ng of template was used. Furthermore, the template and expected abundance dictated the number of cycles used which was 28 to 35. Depending on the kit a single denaturation step was performed at 95-98°C for 2-3 minutes followed by cycles. One cycle consists of a denaturation step (95-98°C for 0.5 to 2 minutes), a annealing step (Tm-3°C for 30 seconds) followed by the elongation (68-72°C, 0.5-1 minute/kb). A final elongation for 5 minutes at 68-72°C was applied.

3.2.6.1 PCR purification

If the PCR product is used for cloning or other enzymatic reactions the reaction mix had to be purified to ensure correct buffer conditions and the removal of primers as well as enzymes. Therefore, the QIAquick PCR Purification Kit (Qiagen, catalog number 28104) was used. Binding buffer was added containing a pH indicator. If the buffer/PCR mix was orange or purple 10 µL of 3 M sodium acetate was added to ensure correct binding conditions. The mix was added into provided columns and spun down at 12000 g for one minute. Bound DNA was washed using PE buffer contained in the kit and the column was spun down again at 12000 g for one minute. DNA was eluted using water and the DNA concentration was measured using Nanodrop™ 1000 (3.2.2.1).

3.2.6.2 Generation of standard curves for copy number investigations

For the investigation of copy numbers MyTaq™ DNA polymerase (Bioline, catalog number BIO-21105) was used. DNA was isolated as described in 3.2.1 and DNA concentrations were measured as triplicate. For the generation of the standard curve the corresponding plasmid concentration was measured as triplicate and diluted. The plasmid DNA was diluted to 10 ng/µL and serial dilutions were used to obtain plasmid concentrations between 10 ng/µL and 10^{-8} ng/µL. The diluent thereby was nuclease free H_2O spiked with 30 ng genomic wild type DNA and 1 µL of the diluted plasmid was used. One serial dilution should hereby statistically result in a difference in Ct values of 3.3. The reaction volume for the samples was 20 µL using MicroAmp optical 96-well plates (Applied Biosystems, Cat. No. 4346906) with corresponding Fast SYBR® green 2x master mix (Applied Biosystems, Fast SYBR® Green Master Mix, Cat. No. 4385612) and 10 nM of forward and reverse primer. The sample concentration was 20 ng total genomic DNA and samples were amplified as quadruplicate. For the purpose of normalisation the β-actin gene was amplified with specific primers. The reaction was carried out with an Applied Biosystems 7500 Fast Real-Time PCR system using 40 cycles. Cycles contained a denaturation step at 95°C for 30 seconds and a annealing/elongation step at 60°C for 15 seconds. Obtained Ct values for the standard curve were displayed over the calculated copies in the sample using knowledge about the size of the plasmid and the amount which was used for RT-qPCR. The resulting logarithmic graph was linearised and the function was used to calculate the copies which were in the analysed sample. The copies per genome were calculated using the amount

of copies which are statistically in the sample with 20 ng total DNA (4075.39 genomes) assuming diploidy. The Chinese hamster genome size of 2,447,154,408 base pairs is resulting in a theoretical weight of 4.9075 pg.

3.2.7 Cloning methods

3.2.7.1 LB-media and agar plates

For the preparation of LB media (10 g/L tryptone, 5 g/L yeast extract, 5 g/L NaCl, Sigma-Aldrich, catalog number L3022) 20 g of powder was solved in H_2O and autoclaved for 20 minutes at 121°C and 1 bar with saturated steam.

For the preparation of LB Agar plates (15 g/L Agar, 10 g/L tryptone, 5 g/L yeast extract, 5 g/L NaCl, Sigma-Aldrich, catalog number L2897) 35 g of powder was solved in H_2O and autoclaved for 20 minutes at 121°C and 1 bar with saturated steam. After reaching a temperature of 50°C heat sensitive ampicillin or kanamycin was added and liquid agar was poured into 90 cm petri dishes (Corning®). After solidification plates were stored at 4°C.

3.2.7.2 Restriction enzyme digest

Restriction enzymes were purchased from New England BioLabs or Thermo Fisher Scientific and most of the enzymes use their own buffer system for the optimal reaction conditions. Usually 1 µg of plasmid DNA was digested using 10x reaction buffer and the appropriate amount of nuclease free H_2O. The mix was incubated for the suggested amount of time with the optimal temperature which depends on the origin of the restriction enzyme. Many enzymes can be heat inactivated. If the enzyme could not be inactivated the mix was purified using gel electrophoresis and gel extraction.

3.2.7.3 Gel electrophoresis

For the visualisation of the prior amplified DNA an agarose gel used in combination with Ethidium bromide (EtBr) or SafeView nucleic acid stain (NBS Biologicals, catalog number NBS-SV1) was used. The amount of agarose used depends on the expected length of

the DNA sample. For fragments longer than 2 kilo bases 0.8 % (w/v) agarose and for smaller fragments 2 % (w/v) agarose was used. The agarose was diluted in 1x TAE (50x TAE: 242 g Tris base, 57.1 mL acetic acid and 100 mL EDTA (0.5 M, in 1 L and pH 8.5) and brought into solution by heating in a microwave. After the solution was cooled down to approximately 50°C EtBr (0.5 µg/mL) was added. For the analysis of the fragments 10x loading dye (25 mg bromophenol blue, 30 % glycerol, 25 mg xylene cyanol in 6.25 mL H_2O) was added to the sample and transferred into a pocket in the agarose gel. The samples were separated by running the gel for 30 minutes at 90 volts.

Gel extraction and purification

Gel extraction was performed using QIAquick® Gel extraction kit (Qiagen, catalog number 28704). The expected band was visualised as well as cut out and transferred into a 1.7 mL Eppendorf tube. Depending on the weight of the agarose piece, dissolving buffer was added and incubated at 55°C for 10 minutes until the agarose was dissolved. Isopropanol (0.2 volumes) was added and the mix was transferred into a provided column and spun down for 1 minute at 12000 g. The DNA was washed using 750 µL PE buffer and spun down again for 1 minute at 12000 g. The DNA was eluted using H_2O and quantified using Nanodrop™ 1000 as well as used for following approaches.

3.2.7.4 Alkaline phosphatase treatment

Alkaline phosphatase was purchased from Roche (1 U/µL, catalog number 10713023001) and was used for the removal of the 5'-phosphate of digested plasmid DNA. The removal prevents the re-ligation of plasmid DNA after enzymatic digestion and the bacterial repair machinery from ligating the double strand as well. One unit per µg of plasmid DNA was used with 10 x reaction buffer in an appropriate volume topped up with nuclease free H_2O. The enzyme was heat inactivated at 65°C for 10 minutes with addition of 1/10 volume of 200 mM EGTA. For further applications the DNA was purified using PCR Purification Kit described in 3.2.6.1.

3.2.7.5 Polynucleotide kinase treatment

Ordered oligo nucleotide sequences usually exhibit no 5'-phosphate. However, for the ligation of annealed oligo sequences the 5'-phosphate group is essential and had to be added. The annealing and addition was performed simultaneously. Therefore, 100 µM of top and bottom strand were mixed together and 1U T4 Polynucleotide kinase was added using provided 10 x reaction buffer (New England BioLabs, catalog number M0201S). Nuclease free H_2O was added to a total volume of 10 µL and the reaction was incubated for 30 minutes at 37°C in a Thermo cycler system (G-STORM). For the inactivation and annealing, the reaction mix was heated up to 95°C for 5 minutes and the temperature as step wise decreased to 25°C. The annealed oligo was diluted and was used for ligation or stored at -20°C.

3.2.7.6 Ligation

For the ligation of 10-50 ng dephosphorylated plasmid was added into the reaction with 10x reaction buffer in a total volume of 20. Insert was added in a standard ratio of 1 to 3 for large inserts. For the ligation of sgRNAs 1 µM annealed oligo sequences were added for 100 ng digested vector. For the ligation 1U of T4 DNA ligase (Rapid DNA ligation kit Roche, catalog number 11635379001) was used and incubated for 1 hour at room temperature. For the transformation into chemically competent cells 2-5 µL ligation mix were used.

3.2.7.7 TOPO®-TA cloning

TOPO®-TA cloning kits can be used for the ligation of blunt end and sticky end fragments into pCR™2.1 TOPO® vector (Thermo Fisher Scientific, catalog number 450641). The principle is based on a topoisomerase I isolated from *Vaccinia* virus which is covalently bound to the broken phosphodiester backbone of the vector. The covalent binding can be attacked by a 5'-hydroxyl group of a PCR amplified fragment or a previously digested DNA fragment and the topoisomerase is released resulting in ligation of the DNA fragment into the vector. For the ligation of PCR fragments containing an A'-overhang 4 µL purified PCR product was used and 1 µL topoisomerase I as well as 1 µL salt solution was added. The salt solution prevents topoisomerase from attacking the previously

ligated site as the binding motif (5'-CCCTT-3') is still exhibited. The mix was incubated for 5-30 minutes and transformed into chemically competent cells.

3.2.8 Transformation of competent cells

For the transformation of cells two different methods were used: Heat shock and electroporation. Heat shock is hereby based on the pre-treatment of *Escherichia coli* cells with a series of salts which disrupt the membrane. A temperature change to 42°C allows the DNA to enter the cell and the immediate incubation on ice closes the pores again. Electroporation is used to increase the permeability of the bacterial cell wall with the following uptake of exogenous DNA.

3.2.8.1 Heat shock based transformation

For the heat shock of chemically competent cells (Thermo Fisher Scientific, Subcloning Efficiency™ DH5α™ Competent cells, catalog number 18265017) the cells were thawed on ice and 10 pg of plasmid DNA was added and incubated for 30 minutes in ice. The heat shock was performed in a water bath at 42°C for 40 seconds and cells were incubated on ice again for 2 minutes. For the recovery pre-warmed S.O.C media (2 % (w/v) tryptone, 0.5 % (w/v) yeast extract, 10 mM NaCl, 2.5 mM KCl, 20 mM glucose, 10 mM $MgCl_2$, 10 mM $MgSO_4$) was added cells were incubated for 1 hour at 37°C at 300 rpm in an incubator. Cells were spun down at 3000 g for 5 minutes and the pellet was resuspended in 200 µL LB broth and plates on agar plates containing 100 µg/mL ampicillin or kanamycin.

3.2.8.2 Electroporation based transformation

For the efficient transfer and amplification of plasmid DNA ElectroMAX™ DH-5α-E™ *Escherichia coli* cells (Thermo Fisher Scientific, catalog number 11319019) were used. The cells were stored at -80°C and were thawed on ice before usage. For the transformation 10 pg plasmid DNA was added to 25 µL of electro competent cells and the suspension was transferred into pre-chilled cuvettes for electroporation (BioRad GenPulser® 0.1 cm, catalog number 1652083). For the validation of the transformation

efficiency 10 pg pUC19 vector was used. The settings for the electroporation were 2.0 kV, 200 Ω and 25 µF. After electroporation the cells where immediately transferred into 1 mL of pre-warmed S.O.C. media and recovered for 1 hour at 37°C before plated on ampicillin/kanamycin (100 µg/mL) containing agar plates.

3.2.8.3 Amplification procedure for the sgRNA-library

For the amplification of the sgRNA-library (3.1.12) it was necessary to ensure high transformation efficiencies. Therefore, ElectroMAX™ DH-5α-E™ *Escherichia coli* cells (Thermo Fisher Scientific, catalog number 11319019) were used. The cells were stored at -80°C and were thawed on ice before usage. For the transformation 10 ng of the sgRNA-library plasmid was added to 25 µL of electro competent cells and the suspension was transferred into pre-chilled cuvettes for electroporation (BioRad GenPulser® 0.1 cm, catalog number 1652083). For the validation of the transformation efficiency 10 pg pUC19 vector was used. The settings for the electroporation were 2.0 kV, 200 Ω and 25 µF. After electroporation the cells where immediately transferred into 1ml of pre-warmed S.O.C. media and recovered for 1h at 37°C. For the cultivation 2 mL of recovered cells were directly transferred into 500 mL 2x TY media (1.6% (w/v) peptone, 1% (w/v) yeast extract, 0.5% (w/v) NaCl, containing 100 µg/mL ampicillin) and cultivated over night at 30°C. The plasmid was isolated using the Qiagen Maxi Prep Plasmid Isolation Kit (Qiagen, catalog number 12162). For the transformation efficiency the cell suspension was diluted 1:10, 1:100 and 1:200 in S.O.C. media and 100 µL of the dilutions was plated on pre-warmed LB-Agar plates containing 50 µg/mL Ampicillin. The efficiency was calculated by following formula:

$$\frac{CFU\ control\ plate}{pg\ pUC19\ DNA} * \frac{1 * 10^6 pg}{\mu g} * \frac{volume\ transformants}{volume\ plated} * dilution\ factor$$

To ensure the amplification of the whole library a transformation efficiency of > 1 x 10^{10} CFU/µg DNA is recommended.

3.2.8.4 Plasmid mini and maxi preparation

For mini preps (Qiagen, catalog number 27104) single colonies of agar plates were inoculated in 5 mL LB media containing selection agent. For maxi preps (Qiagen, catalog number 12162) the culture volume was 50 mL. Both methods are based on the same principles with the exception that plasmids prepped using maxi kits are endotoxin free and can be used for transfections. Firstly, cells are harvested and resuspended in RNase containing buffer. The cells are lysed using alkaline lysis and protein as well as cell debris are separated using centrifugation. The DNA is bound to positively charged silica membranes and washed to remove endotoxins, lipids and polysaccharides before elution. The DNA was isolated following the manufacturer's protocol.

3.2.8.5 Sanger sequencing

For analysing InDel frequencies and the conformation of positive inserts after ligation samples were sent for sequencing. Therefore, miniprep cultures were prepped and the DNA was quantified. One µg was transferred into a 1.7 mL Eppendorf tube and the volume was increased to 15 µL if necessary. For the sequencing reaction 20 nM primer was added and the reaction was sent to Eurofins Genomics.

3.2.9 Surveyor® assay

The Surveyor® assay uses a nuclease which recognises mismatches between wild type strands and mutated strands which can be used for the assessment of InDels. The genomic region was first amplified using PCR and purified using PCR purification kit. It was essential that no unspecific bands were exhibited and otherwise the PCR product was purified using gel extraction. The hetero-duplex formation was performed in a Thermo cycler system (G-STORM) using 400 ng purified PCR product. If the PCR product was gel extracted 10x PCR reaction buffer (Phusion® High Fidelity buffer) was added as the Surveyor® nuclease which uses $MgCl_2$ as essential cofactor. The reaction was denatured at 95°C for 10 minutes and the temperature was decreased step wise using a programme displayed in

Table 2: Hetero-duplex formation for Surveyor® nuclease assay and ramping temperatures

Temperature	Time (s)	Ramp
95°C	600	
95°C to 85°C		-2°C/s
85°C	60	
85°C to 75°C		-0.3°C/s
75°C	60	
75°C to 65°C		-0.3°C/s
65°C	60	
65°C to 55°C		-0.3°C/s
55°C	60	
55°C to 45°C		-0.3°C/s
45°C	60	
45°C to 35°C		-0.3°C/s
35°C	60	
35°C to 25°C		-0.3°C/s
25°C	60	
4°C	Hold ∞	

After hetero-duplex formation 1 µL Surveyor Nuclease S as well 1 µL Surveyor Enhancer S was added and the reaction mix was incubated at 60°C for 60 minutes. Stop solution (1 µL) containing EDTA was added and 10x loading buffer. For the visualisation a 2% (w/v) agarose gel was used to achieve high resolution.

3.2.10 High throughput DNA and RNA sequencing using NGS

3.2.10.1 Indel sequencing using NGS for the analysis of CRISPR/Cas9 targeting efficiency

Indel sequencing was used for the assessment of Cas9 function as well as investigation of indel frequency after targeting each member of the miR-23 cluster. Furthermore, it was used to assess if clones showed targeting as well as off-targeting on both clusters. For preparation of sequencing, genomic DNA was isolated from clones and mixed populations (3.2.1). Primers were designed to target 100 bp up- and downstream of each targeted region. Additionally, primers had linkers added which were used for library preparation. After amplification the PCR product was analysed on an agarose gel for unspecific products. As no unspecific bands occurred the PCR amplicon was purified using a PCR purification kit (3.2.6.1) and sent for sequencing with our collaboration

partner (Helene Faustrup Kildegard and Thomas Amann at the The Novo Nordisk Foundation Center for Biosustainability, Technical University of Denmark, Kgs. Lyngby, Denmark).

Table 3: Primers including linkers for indel sequencing after targeting miRNAs with CRISPR/Cas9

Name	Linker and sequence	Amplicon length (bp)
miR-23a fwd_NGS	TCGTCGGCAGCGTCAGATGTGTATAAGAGACAGAGGTGCTACACTCCGATCCT	235
miR-23a rev_NGS	GTCTCGTGGGCTCGGAGATGTGTATAAGAGACAGCTCACAAGCAGCTAAGCCCT	235
miR-23b fwd_NGS	TCGTCGGCAGCGTCAGATGTGTATAAGAGACAGGGACAGGAGTGGTAGGGCAT	225
miR-23b rev_NGS	GTCTCGTGGGCTCGGAGATGTGTATAAGAGACAGCATCTTCGAAGGTTGCTGGC	225
miR-27a fwd_NGS	TCGTCGGCAGCGTCAGATGTGTATAAGAGACAGACTGGGTGAGAGAGAAGCCC	270
miR-27a rev_NGS	GTCTCGTGGGCTCGGAGATGTGTATAAGAGACAGTGGACTCCTGTTCCTGCTGA	270
miR-27b fwd_NGS	TCGTCGGCAGCGTCAGATGTGTATAAGAGACAGTGCAGATCCGTGGCTACTTT	245
miR-27b rev_NGS	GTCTCGTGGGCTCGGAGATGTGTATAAGAGACAGGCTGCAACTTAACTGTCCCC	245
miR-24-1-fwd_NGS	TCGTCGGCAGCGTCAGATGTGTATAAGAGACAGTCTCTTGTGTTTGCAGCCCA	184
miR-24-1-rev_NGS	GTCTCGTGGGCTCGGAGATGTGTATAAGAGACAGACTACAGGTGGGTAGGCGTT	184
miR-24-2-fwd_NGS	TCGTCGGCAGCGTCAGATGTGTATAAGAGACAGCACAGTGGCTAAGTTCCGCT	172

3.2.10.2 Sample preparation and RNA sequencing for transcripromic analysis

For studying transcriptomic data whole RNA sequencing is a common method. Therefore, total RNA was isolated with samples taken during exponential growth phase in biological triplicates. For extraction of total RNA Direct-zol (Zymo research) was used to ensure high sample quality. Sample quality and concentration was measures on a Nanodrop1000 (Thermo) and send for sequencing on dry ice (Genewiz RNA-Seq). RNAseq using poly-A enrichment was used to allow the removal of ribosomal RNA. After fragmentation and addition of linkers the sample were run on an Illumina HiSeq 2500 instrument with $47x10^6$-$66x10^6$ reads. For differential expression analysis DESeq2 was used and Wald test to generate p-values as well as log2-fold changes. Raw dispersion values were fitted to a common mean to improve testing accuracy. Fitting was performed using dispersion information for all genes (black dots). For analysis of statistical significance, a p-value <0.05 was applied and a log2 fold change of 0.58/-0.58. Only genes with a base mean of >100 were considered true.

3.2.10.3 Amplicon sequencing for the analysis of enriched or depleted sgRNAs regarding the CRISPR library

For the investigation of which sgRNAs were enriched or depleted after the mixed CRISPR/Cas9 library mixed population was exposed to hyperosmotic conditions or selected for high productivity clones, NGS was used. As the library is very complex it was important to ensure coverage. Genomic DNA was isolated using Midiprep Plus Kits (Zymo research, Catalogue number D4075) to obtain high yields and good quality DNA. One mg of genomic DNA was used for PCR reactions to ensure ~200-fold coverage using primers (forward AAAGTATTTCGATTTCTTGG, reverse ACTCGGTGCCACTTTTTCAA) amplifying the sgRNA region of the CRISPR library plasmid. The PCR product was assessed for quality, unspecific amplification and subsequently purified. Samples were shipped on dryice for further processing by Genewiz in terms of library preparation, HiSeq sequencing (Illumina) and bioinformatical analysis. Illumina HiSeq was used to reach sequencing depths between 10^7-10^8 reads as enrichment/depletion of sgRNAs might be very subtle. To identify sgRNAs the constant region was excluded to highlight unique sequences and abundance was analysed.

3.3 Protein based methods

3.3.1 Enzyme-linked immunosorbent assay (ELISA)

Sandwich ELISA method was used for the evaluation of product titres in conditioned media and specific productivity. Media was taken from batch or fed-batch cultures and spun down at 200 g for 5 minutes to remove cells. The supernatant was carefully removed without disturbing the pellet and stored at -80°C. For ELISA the conditioned media was diluted with corresponding to expected concentrations of product in the conditioned media. Solutions for ELISA were prepared as suggested by the manufacturer's protocol (Bethyl Laboratories, Inc. catalog number E80-104). Nunc MaxiSorp C bottom well microtiter plates (Bethyl Laboratories, Inc. catalog number E105) were used and 1 µg coating antibody was used per well in coating buffer. The coating antibody was incubated for 1 hour at room temperature. The plate was rinsed five times with washing buffer and 200 µL blocking buffer was added as well as incubated for at least 30 minutes. The plate was washed again and dilutes sample was added. The

sample dilutions were made in diluent buffer shortly before adding the sample. For the standard curve human reference serum of Fc receptor fusion proved by Biogen was used. Concentrations for the standard curve ranged between 500 ng/mL to 7.8 ng/ml using serial dilutions in a 1 to 1 ratio. A volume of 100 µL was added to the wells whereas the standard curve was added as duplicate and the samples were added as triplicates. The sample was incubated for one hour and wells were rinsed for five times again using washing buffer. Secondary antibody was diluted in diluent buffer with a dilution of 1:100,000 and 100 µL were added and incubated for 1 hour. The wells were washed again for five times and 100 µL 3'3,5'5-tetramethylbezidine (TMB) was added and incubated for 15 minutes. The solution turned into a blue colour and 100 µL 0.18 M H_3PO_4 was added to stop the solution which resulted into a yellow colour. Immediately after stopping the reaction the plate was assessed using Multiskan™ GO Microplate Spectrometer (Thermo Fisher Scientific, catalog number 51119280) at λ 450 nm. The standard curve as well as values were calculating using a four-parameter curve and obtained concentrations were multiplied by the dilution factor.

3.3.2 Protein A Antibody Affinity Chromatography

Protein A was originally found and isolated from *Staphylococcus aureus* as a protein incorporated in the cell wall which is able to specifically bind the Fc-part of immunoglobulins. The binding properties of protein A is commonly used as first step in industry to purify conditioned media containing a therapeutic protein e.g. mAbs or Fc-fusions. The stationary phase is usually based on spherical agarose beads which are conjugated to protein A.

For the investigation of posttranslational modifications conditioned media was spun down for 5 minutes at 200 g to remove cells. To further remove cell debris the conditioned media was spun down for 10 minutes at 2500 g. To ensure perfect binding conditions and a small sample volume the conditioned media was concentrated using Amicon® ultra centrifugal filter units (Merck KGaA, catalog number UFC905024) with a 10 kDa molecular weight cut off. The conditioned media was concentrated to a volume of 5 mL at 2500 g and 4°C. The buffer was exchanged to the corresponding binding buffer (20 nM Sodium hydrogen phosphate, pH 7.00) at 2500 g and 4°C using Amicon® ultra centrifugal filter units.

Before the application of the conditioned media the column (HiTrap MabSelect 1 mL, catalog number 28-4082-53) was equilibrated with 5 column volumes of binding buffer to ensure correct binding conditions with a flowrate of 1 mL/minute using a 5 mL syringe. The sample was applied and the column was washed with 10 volumes of binding buffer. The product was eluted using 3 column volumes 10 % acetic acid (pH 4.00). To avoid degradation of the product due to exposure of low pH 1 mL 1 M Tris (pH 8.00) was added. To ensure no unspecific binding all fractions were analysed using denatured polyacrylamide gel electrophoresis. For the further investigation of the glycosylation pattern the buffer was exchanged to PBS using Amicon® ultra centrifugal filter units and the sample was concentrated to a volume of 1 mL.

3.3.3 Investigation of changes in glycosylation pattern

A process can have dramatic effect on the glycosylation of the therapeutic product. Therefore, depletion of a miRNA may have a crucial impact on glycosylation as well and the function/efficacy of the product. Therefore, product quality had to be assessed after knockdown of miRNAs. Conditioned media (~50 mL) was taken from control cultures as well as knockdown cultures. The conditioned media was prepared and purified using protein A chromatography as described in 3.3.2. For the analysis of changes in glycosylation species, LC/LFR-MS/MS was used according to Carillo and colleagues (Carillo et al., 2017). The work was carried out by Jonathan Bones and Sara Carillo in the National Institute for Bioprocessing Research and Training (NIBRT) as part of a collaboration.

3.3.4 Analysis of oxygen uptake rate and extracellular acidification rate

For the investigation of oxygen uptake rates (OCR) and extracellular acidification rates (EACR) the Seahorse XFe96 Analyser (Agilent) was used. OCR and EACR can give indication for energy phenotypes by measuring indicators for increased glycolysis or oxidative phosphorylation. EACR hereby is the indicator for glycolysis which results in the production of lactic acid and protons without consumption of oxygen. For mitochondiral respiration oxygen is used and OCR can therefore give indications for increased mitochondrial function. For measuring OCR and EACR the Agilent Seahorse

XFp Cell Energy Phenotype Test Kit (Cat No 103275-100) was used according to the manufacturer's recommendations.

3.3.5 Sodium dodecyl sulphate - Polyacrylamide gel electrophoresis

The sodium dodecyl sulphate – Polyacrylamide gel electrophoresis (SDS-PAGE) is a method used in biochemistry to separate proteins corresponding to their molecular weight. For the separation 4-12% Bis-Tris protein gels (NuPAGE™ Novex™, Thermo Fisher catalog number NP0322BOX) under denaturing condition in an XCell SureLock™ Minicell electrophoresis chamber (Thermo Fisher, catalog number EI0001) for the optimal separation of medium to small sized proteins. The sample was prepared using 10 µg of total protein by adding 2x laemmli buffer (Sigma, catalog number 3401) to a final 1x concentration. To equalize final sample volumes PBS was added. The sample was incubated at 95°C for 5 minutes and allowed to cool down before being centrifuged. A maximum of 30 µL sample was loaded and the gel was run for 45 minutes at 200 V using 1x MOPS running buffer (Sigma, catalog number M1245). To maintain denaturing conditions NuPAGE® antioxidant (Thermo Fisher, catalog number NP0005) was added in the upper chamber.

3.3.6 Staining and detaining of protein gels

Staining for proteins after SDS-PAGE was performed using 50% Methanol, 40% H_2O, 10% acetic acid as well as 0.25% Coomassie Brilliant Blue G250. The gel was incubated for one hour at RT following detaining in H_2O overnight.

3.3.7 Bradford protein assay

The Bradford assay is an accurate colorimetric measurement to determine protein concentrations in a sample. The assay is based on Coomassie Brilliant Blue G250, a dye which binds protein due to hydrophobic and electrostatic interactions. The shift in absorbance is directly proportional to the amount of protein in the sample. For the measurement of protein concentrations 5 µL of each standard (Bovine serum albumin, 1 mg/mL, 0.75 mg/mL, 0.5 mg/mL, 0.25 mg/mL and 0.125 mg/mL, Thermo Scientific

catalog number 23208) was prepared and transferred as triplicate into a 96-well plate. The sample was diluted corresponding to the expected amount of protein in the range of the standard curve and 5 µL were transferred into the same plate. A total volume of 250 µL Coomassie Brilliant Blue G250 (Quick StartTM Bradford Protein Assay, Bio-Rad catalog number 5000201) was added to each standard as well as sample and incubated for 10 minutes. The absorbance was read using Multiskan™ GO Microplate Spectrometer at λ 595 nm.

3.3.8 Filter-aided sample preparation for label free LC/MS

For the analysis of DE protein abundance due to the knockdown of different miRNAs quantitative label-free LC-MS/MS profiling was used. The samples were lysed, digested and prepared using filter-aided sample preparation (FASP) according to a protocol published by Coleman and colleagues (Coleman et al., 2017).

3.3.9 Label free quantitative LC/MS

Peptides were initially separated using a reverse-phased capillary High-pressure Liquid Chromatography on an UltiMate 3000 nano system (Thermo Scientific) coupled directly in-line with the Thermo Orbitrap Fusion Tribrid Mass Spectrometer (Thermo Scientific). 4 µL of digested sample was loaded onto the trapping column (PepMap100, C18, 300 µm × 5 mm) at a flow rate of 25 µL/min with 2% (v/v) ACN, 0.1% (v/v) TFA for 3 minutes before being resolved onto an analytical column (Easy-Spray C18 75 µm × 500 mm, 2 µm bead diameter column) using a binary gradient of 98% A (0.1% (v/v) formic acid (FA)): 2% B (80% (v/v) ACN, 0.08% (v/v) FA) to 27.5% B over 110 min at a flow rate of 300 nL/min.

For peptide ionization, 1900 V was applied and a 320 °C capillary temperature was used. For the Orbitrap Fusion MS detection, a precursor scan was performed in the Orbitrap by scanning from *m/z* 375–1500 with a resolution of 120,000 (at *m/z* 200), a targeted automatic gain control (AGC) value of 4e5 and a maximum injection time of 50 ms. The ions selected under top-speed mode were isolated in the Quadrupole with an isolation width of 1.6 Da, and they were fragmented by higher energy collision-induced dissociation (HCD) with a normalized collision energy of 28%, then measured in the

linear ion trap. The typical MS/MS scan conditions were as follows: a targeted AGC value of 2e4, a maximum fill time of 35 ms, included charge states of 2+ to 6+ and the dynamic exclusion was employed for 60 s. The resulting files were analysed using Progenesis QI for Proteomics version 4.1 for label-free LC-MS/MS analysis as recommended from the manufacturer (Nonlinear Dynamics). The LC retention times were aligned to the reference run and samples were set up into two experimental groups. Peptide features were filtered for an ANOVA value ≤ 0.05 between experimental groups, mass peaks with charge states between +1 and +3 and greater thanone isotope per peptide. Spectra were exported as a MASCOT generic file (.mgf) and identified within Proteome Discover 2.1 using Sequest HT (Thermo Fisher Scientific), MASCOT and percolator. Data was searched against the NCBI Cricetulus griseus database containing 44,065 sequences (fasta file downloaded November 2016). Identified peptides were imported into Progensis QI and filtered applying the following criteria: an ANOVA value < 0.05, a fold change of ≥ 1.25 between experimental groups and ≥ 2 peptides contributing to protein identifications.

3.3.10 Selection for high-producing CHO cell subpopulations using FACS

For enrichment of high producing clones, FACS has been shown to be a reliant tool in cell line development. The principle is based on staining an IgG producing cell line with an antibody-FITC conjugate. For our purpose, CHO-K1 mAb was used which was transfected with a sgRNA library. Knockout of certain genes was proposed to increase productivity and clones can be isolated applying several rounds of sorting whilst isolating the highest 10-15% cells in intensity (Figure 13). Cells were washed, treated with staining antibody (anti-human IgG Fab specific-FITC antibody, goat) and sorted as described by (Gallagher & Kelly, 2017). Cells were hereby kept at 4°C to decrease secretion kinetics and ensure stable labelling with the antibody. Obtained subpopulations were then recovered in 6-well plates until high confluency was reached.

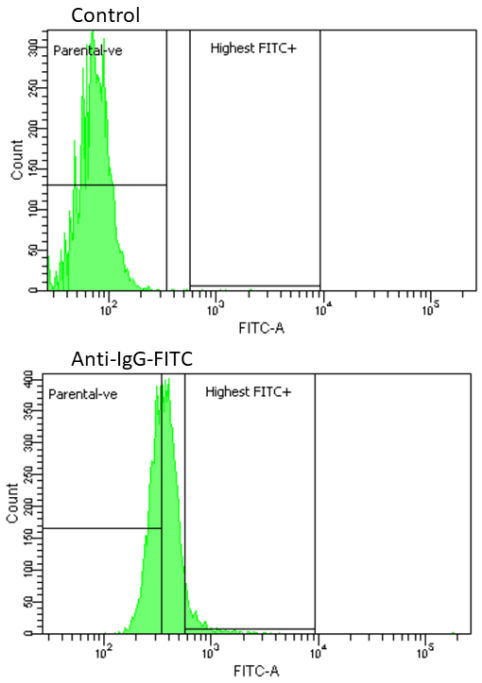

Figure 13: Enrichment of high-producing clones using FACS combined with low temperature stain of an IgG. Using an antibody labelled with FITC in combination with a low temperature setting high producing cells can be selected. Due to low temperature secretion is slowed down and IgGs can be stained using an anti-IgG/FITC conjugate. Isolating cells showing high FITC intensities can then be sorted and should show higher producitivity or secretion properties.

Antibody concentration was tested prior sorting using a range of dilutions from 1:10 to 1:100. The ideal concentration for sorting for high producing subpopulations was found to be 1:50.

3.3.11 Statistical analysis

For analysis of statistical significance, an unpaired two tailed student's t-test was applied unless otherwise stated (*P ≤ 0.05, **P ≤ 0.01 and ***P ≤ 0.001) on biological triplicates between two independent sets of samples.

4.0 Results

4 Results

4.1 Stable depletion of the miR-23 cluster and single miRNA members in industrial relevant cell lines

4.1.1 MicroRNA expression of each indicidual member of the miR-23 cluster across a panel of cell lines

The first task was to establish the endogenous levels of each miR in each cell line. The levels of each mature miRNA of each parental producer cell line was assessed by qPCR. Total RNA was extracted and miRNA expression was analysed using TaqMan® small RNA assays**.** Seven different cell lines were assessed using CHO-K1 parental cells as the native miRNA expression control. The expression of each miRNA was normalised to an endogenous control (U6 snRNA) and relative expression was quantified using the ΔΔCt method. Cell lines chosen expressed different industrially relevant molecules i.e. an Fc receptor fusion (Fc) and monoclonal antibodies (mAbs). Samples for RNA extraction were taken in exponential growth phase and Figure 14 shows the relative expression when compared to the CHO-K1 parental cell line.

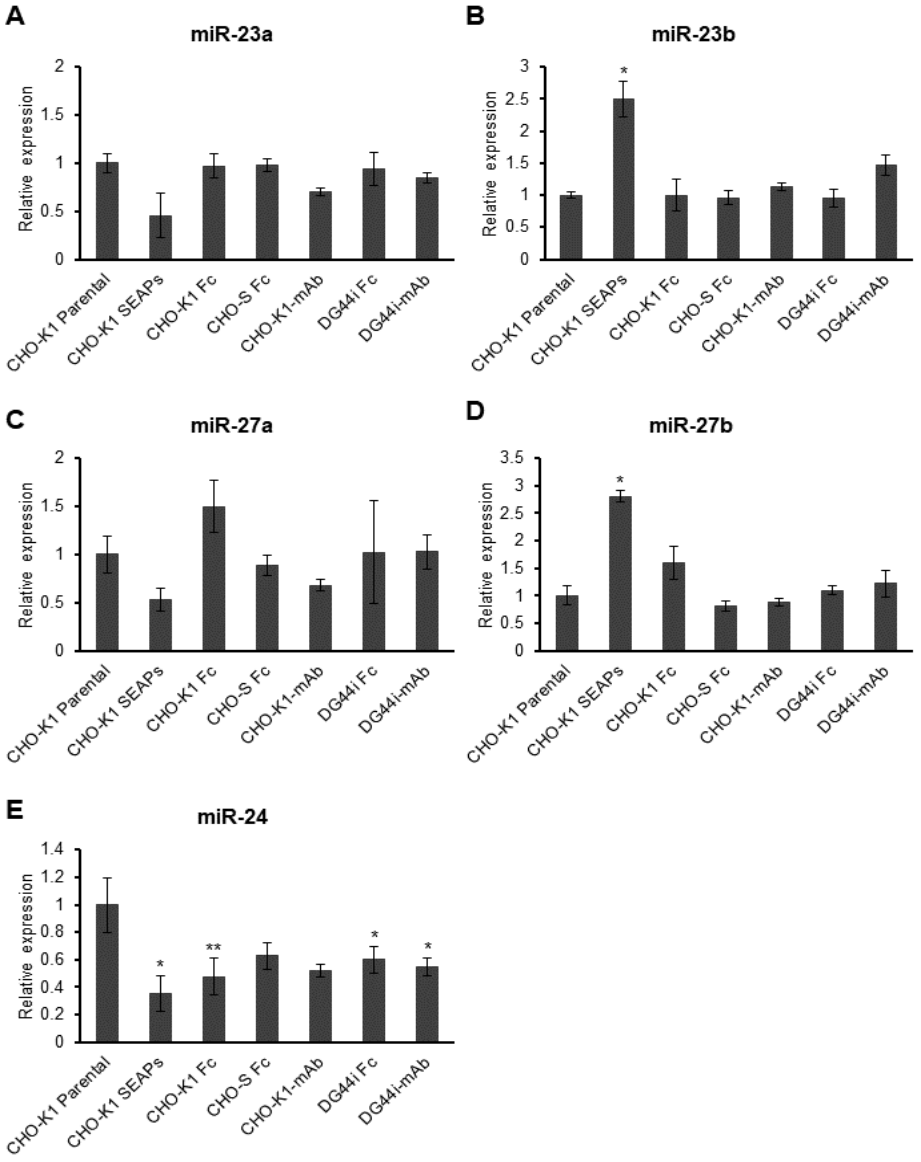

	MicroRNA				
Cell line (Ct values)	miR-23a	miR-23b	miR-24	miR-27a	miR-27b
CHO-K1 parental	23.03	25.99	18.53	20.45	23.58
CHO-K1 SEAPs	24.17	24.67	20.03	21.36	22.09
CHO-K1 Fc	23.08	25.99	19.60	19.87	22.89
CHO-S Fc	23.06	26.05	19.20	20.62	23.87
CHO-mAb	23.55	25.81	19.48	21.00	23.77
DG44i Fc	23.12	26.06	19.27	20.42	23.44
DG44i mAb	23.27	25.44	19.39	20.41	23.29

Figure 14: Endogenous miRNA expression of mature miR-23a/b, miR-27a/b and miR-24 in a panel of CHO cell lines. A to E) MiRNA expression was compared to a CHO-K1 non-producing cell line. The overall miRNA expression was very similar over the panel of cell lines. However, miR-24 was significantly lower expressed in CHO-K1 SEAPs, CHO-K1 Fc, DG44i Fc and DG44i mAb. MiR-23b and miR-27b was more abundant in CHO-K1 SEAPs compared to parental CHO-K1. (* $p < 0.05$ vs parental, ** $p < 0.01$ vs parental; n=3).

Expression of mature miR-23a, miR-23b, miR-24, miR-27a and miR-27b did not vary hugely across all tested cell lines was similar (Figure 14 A to D). However, miR-24 was significantly lower expressed in all the cell lines compared to the parental CHO-K1 cell line (Figure 14 E). However, miR-24 is the highest expressed miRNA amongst all member with Ct-values of ~18 compared to the lowest expressed miRNA (miR-23b) with Ct-values of ~26. Furthermore, it was found, that miR-23b and miR-27b were significantly upregulated in CHO-K1 SEAP expressing cells when compared to the CHO-K1 parental cell line (Figure 14 B to D). In contrast miR-23a was decreased in CHO-K1 SEAP expressing cells (Figure 14 A).

4.1.2 Sponge design considerations for the depletion of the miR-23 cluster as well as single miRNA members

The sponge sequences were designed to be complementary to their miRNA targets except for a four-base pair mismatch between nucleotides 10 to 14 to create an imperfect binding site. The introduced mismatches create a bulged sponge which should protect against endonucleolytic cleavage mediated by Ago2 in the RISC (Ebert et al., 2007; Kluiver et al., 2012a). The same study showed that miRNAs sharing the same seed family can be targeted effectively. The miRNA binding sites (MBS) are located downstream of a destabilised EGFP reporter (d2EGFP) in the 3'UTR which allows estimation of the binding efficiency of endogenous target miRNAs based on a decrease in GFP intensity and the percentage of total GFP positive cells. The vector is based on pcDNA3.1-hyg and the d2EGFP with the 3'UTR including SanDI restriction sites were cloned by Dr. Nga Lao. The control sponge was similar with the exception that the MBS were designed not to target any known expressed sequence (Figure 15 A to D).

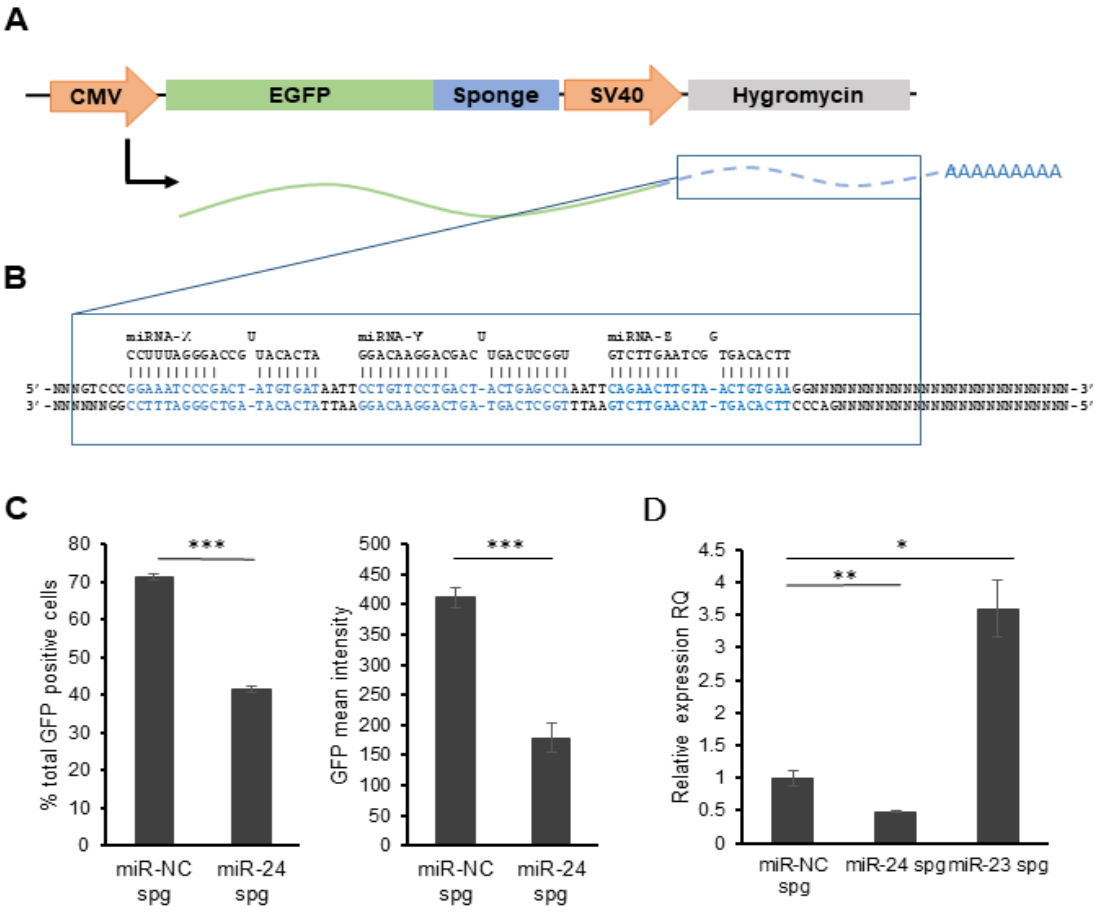

Figure 15: Construction of sponge decoy constructs for the depletion of miRNAs in CHO-K1 cells. Schematic overview of the sponge expression plasmid used. A) The d2EGFP reporter is expressed under control of a CMV promoter together with the sponge in the 3'UTR and a poly-A tail. B) The MBS were cloned into the vector using SanDI sites which are located between the poly-A tail and the d2EGFP reporter. The sponge sequence (highlighted in blue) has a four-nucleotide mismatch which introduces a bulge after binding of the miRNA target and increases the stability of the mRNA due to protection against cleavage by AGO2 comprised in the RISC complex. To create a stable expressing CHO population the vector has an additional mammalian selection marker (hygromycin resistance gene). C) GFP mean intensity as well as GFP positive population compared beween control and sponge construct (miR-NC spg). D) Expression of miR-24 in CHO-K1 cell transfected with the sponge (* $p < 0.05$ vs NC, ** $p < 0.01$ vs NC, *** $p < 0.001$ vs NC; n=3).

To assess their impact on cell growth and productivity, the previously tested panel of cell lines was transfected with decoys for the depletion of the miR-23 cluster. The transfection was performed using electroporation or a PEI based transfection reagent (Mirus TransIT®-X2) depending on the cell line. To ensure stable integration of the sponge constructs the selection pressure was maintained for four weeks using hygromycin B. The transfection efficiency was assessed using Guava® easyCyte flow cytometer using ExpressPlus programme for measuring GFP intensity 24 hours post-transfection on a Guava^{TM} benchtop cytometer. To assess the functionality of binding miRNAs to the sponge construct the same programme was used after selection. Successful binding should result in lower GFP signals due to the translational inhibition or degradation of GFP mRNA (Figure 15 C). Besides using GFP as an indication of miRNA binding, TaqMan® small RNA assays (section 3.2.5) were used (Figure 15 D). Lower miRNA abundance would indicate a depletion of the endogenous miRNA. This apparent increase in miRNA levels has been observed by others previously and has been attributed to the miRNA accumulating on the sponge transcript and not being turned over. Upon cell lysis for qPCR the bound (and protected) miRNA is then released and appears to be elevated - though it has been sequestered away from it's endogenous targets and therefore functionally depleted (see section 5.2.3). Both observations ultimately indicate a reduction of miRNAs being available to bind endogenous targets.

Phenotyping was first performed in four different industrially relevant cell lines which were provided by Biogen (Cambridge MA). The initial screen showed that depletion of miR-23-24-27 led to increased productivity in CHO-S Fc. Other cell lines did not show any phenotype after stable depletion. Reducing endogenous levels of miR-23 had no effect in all four cell lines (compare Figure S 1, Figure S 2 and Figure S 3).

4.1.2.1 Stable depletion of the miR-23 cluster in CHO-S Fc leads to increased productivity

As mentioned depletion of miR-23-24-27 led to increased productivity in a mixed population of Fc fusion expressing CHO-S. Initial screens for an impact on the phenotype upon stable depletion of the miR-23 cluster was performed in 5 mL batch cultures using TPP 50 mL TubeSpin® bioreactor tubes. Media was supplied by Biogen (Cambridge MA) for all cell lines and cells were grown at 35°C, 170 rpm and 80% humidity. Cells were cultivated in a Kuhner Clima-shaker incubator (ISF1-X). Cells were seeded at $2x10^5$ cells/mL and samples were taken every second day for ELISA, GFP and viable cell

density. Depletion of miR-23-24-27 led to no observed change in growth nor viability (Figure 16 A and B). However, Fc fusion levels were significantly elevated (n=4, * p<0.05) on day 6 and 9 of the batch culture (Figure 16 C) Elevated productivity led to 1.5-fold increase (n=4, * p<0.05) in titre on day 8. This increase in product level was due to a significant increase in productivity on day 8 of the culture (Figure 16 D). GFP mean intensity as well as percentage of GFP positive population was decreased in the miR-23-24-27 sponge compared to the control indicating successful depletion of targeted miRNAs (Figure 16 E). Lower miRNA abundance would indicate a depletion of the endogenous miRNA. Expression of miR-23 and miR-27 was reduced and miR-24 was slightly enriched when compared to the control (Figure 16 F). This apparent increase in miRNA levels has been observed by others previously and has been attributed to the miRNA accumulating on the sponge transcript and not being turned over (see section 5.2.3).

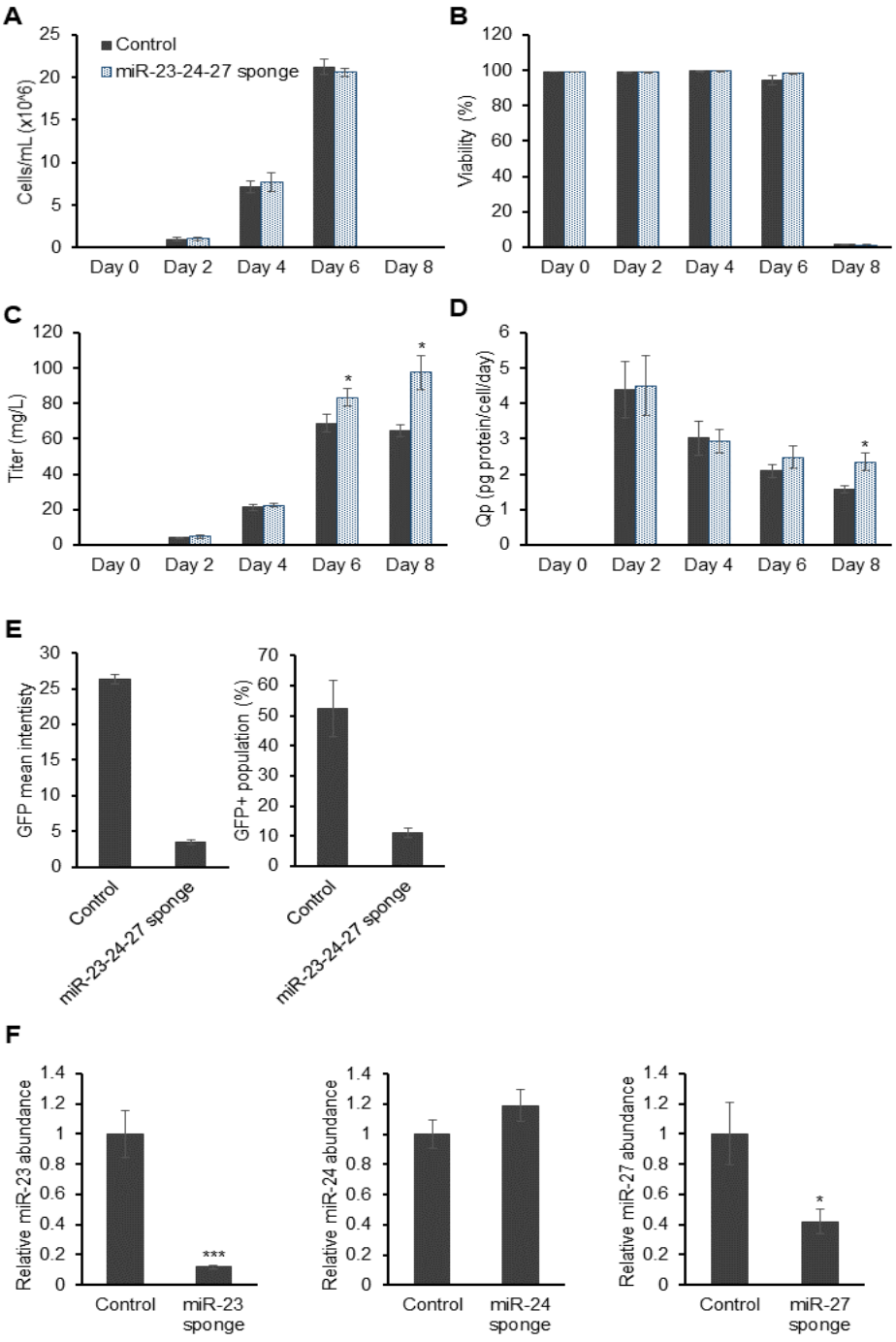

Figure 16: Impact of stable depletion of miR-23-24-27 in CHO-S Fc. Growth, viability and productivity was compared to a control sponge containing a scrambled sequence instead of MBS. A) Viable cell density on day 2, day 4, day 6 and day 8. B) Cellular viability on day 2, day 4, day 6 and day 8. C and D) Titre of Fc receptor fusion and specific productivity on all days of the batch culture. E) GFP positive population as well as mean intensity. F) Expression of miR-23, miR-24 and miR-27 compared to the control sponge (miR-NC spg) in CHO-S cells (* $p < 0.05$ vs control; *** $p < 0.001$ vs control: n=4).

4.1.2.1.1 Performance of CHO-S Fc-fusion cells stably expressing a miR-23-24-27 sponge in fed-batch mode

Most biopharmaceutical manufacturing processes nowadays are based on fed-batch cultures, whereby a standard basal medium supports initial growth and a concentrated feed is added in exponential phase to boost cell growth and prevent depletion of nutrients during stationary phase. Fed-batch cultivation has several benefits as it increases maximum cell densities, productivity and prolongs cultivation times due to increased viability in late culture stages. Fed-batch experiments cells were seeded with an initial cell density of $4x10^5$ cells/mL in 30 mL using 250 mL Erlenmeyer shake flasks. Media and feed was supplied by Biogen and culture conditions were set to 160 rpm, 35°C and 80% humidity in a Kuhner Clima-shaker incubator (ISF1-X). Samples were taken on a daily basis for the assessment of viable cell density and media was taken every 48 hours for investigation of product titres using ELISA. A 14-day extrapolated feeding strategy was provided by Biogen but had never been used for CHO-S Fc. Optimisation was necessary to prolong culture times to 14 days. However, initial optimisation increased the cultivation time up to 11 days. The CHO-S Fc cell line reached a peak cell density of approximately ~$38x10^6$ cells/mL on day 8 (n=2) (Figure 17 A). The viability declined from day 8 on but no difference in viability were observed between control and miR-23-24-27 sponge in the early or late stages of the culture (Figure 17 B). However, product titres were increased compared to batch cultivations. In batch mode Fc-fusion titre reached a peak of 97 mg/L from cells expressing the miR-23-24-27 sponge on day 8. In fed-batch cultivation, a product titre of about 750 mg/L on day 11 in CHO-S Fc was observed. Furthermore, the titre was higher compared to the control on day 10 and day 11 (Figure 17 C). However, the fed-batch culture was not as reproducible as desired and further optimisation would be necessary. Nevertheless, the same trend in higher productivity was seen in fed-batch culture as well as in batch cultures.

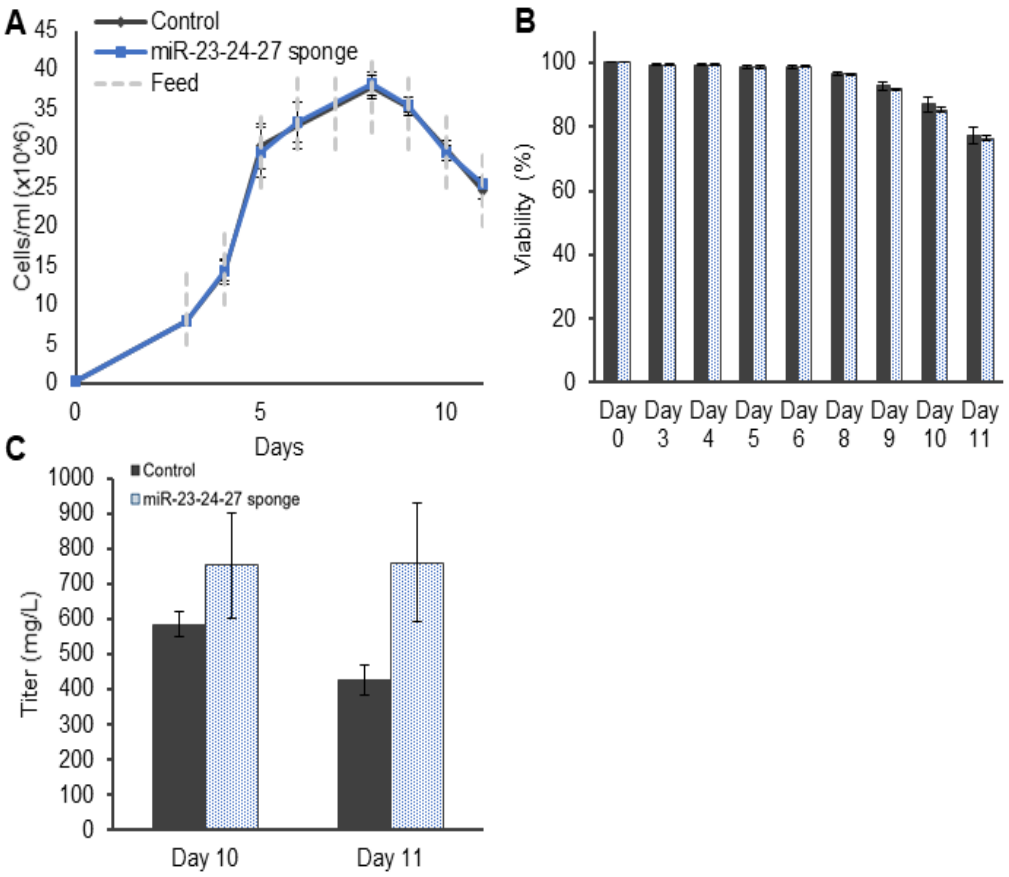

Figure 17: Impact of stable depletion of miR-23-24-27 in CHO-S Fc cultivated in fed-batch mode. Feed (highlighted in broken gray line) was added on daily basis beginning from day 3. A and B) Assessment of viable cell density and viability over a period of 11 days. C) Fc receptor fusion for day 10 and day 11 in miR-23-24-27 depleted CHO-S Fc cells in fed-batch cultivation (n=2).

Higher productivity was exhibited in batch as well as in fed-batch cultures using the miR-23-24-27 sponge compared to the control. However, the fed-batch was only repeated twice as variations in feed occurred which may have led to different growth behaviours. Furthermore, the feed was never optimised for the CHO-S Fc-fusion cell line and further adaption of feed volumes would be necessary to repeat results and prolong culture times. Optimisation efforts might be very beneficial and can even result in higher titres. However, the observed increase in productivity was very encouraging, prompting us to investigate whether this phenotype was reflected, and to what extent, at the clonal level.

4.1.2.2 Generation of single cell clones expressing miR-23-24-27 sponge

Limited dilution cloning was used to generate a panel of single cell clones expressing either a control sponge or miR-23-24-27 sponge. Cells were grown in 96-well format using 10 % conditioned media to improve cloning efficiency and positive colonies resulting from only one cell were transferred into 24-well plates under maintenance of selection pressure using hygromycin B. Clones were analysed for GFP expression and nine clones expressing the control sponge or miR-23-24-27 sponge were selected based on GFP intensities to ensure an excess of sponge mRNA. Clones were further assessed for growth behaviour and productivity. The GFP intensity was assessed using Guava easyCyte with ExpressPlus programme on the Guava^{TM} benchtop cytometer. It was shown that the GFP expression in all nine control clones was significantly higher compared to miR-23-24-27 sponge clones. The miR-NC sponge showed an average GFP mean intensity of 223 (Figure 18 E) and the percentage of GFP positive cells was ~90 % of the total population, respectively (Figure 18 F). In comparison, the GFP mean intensity of all nine miR-23-24-27 sponge clones was 16.97 (Figure 18 E) and ~30 % of the total population was shown to be GFP positive (Figure 18 F) which indicates further that the GFP sponge is working by translational inhibition or degradation of GFP mRNA. Similar results were obtained for the mixed populations in previous results. However, the average GFP mean intensities were higher in all selected clones compared to mixed populations.

After selecting clones, the growth behaviour was analysed in batch mode over a period of six days. Cells were seeded in 24-well suspension plates in a culture volume of 1 mL. The initial cell density was 1 x 10^5 cells/mL and samples for assessment of viable cell density as well as for ELISA were taken every 48 hours (Figure 18 C and D). Across the panel all clones grew differently and reached different viable cell densities on day 4 and day 6. No significant difference in cell densities in control clones compared to cells expressing the miR-23-24-27 sponge was observed but a great variation in the panel was shown.

To investigate the impact of miR-23-24-27 sponge on productivity ELISA was performed for all 18 clones with samples taken every 48 hours. Average titre between miR-NC cultures compared to miR-23-24-27 did not show any significant difference (miR-NC sponge: 101 mg/L ± 44 mg/L and miR-23-24-27 sponge: 82 mg/L ± 41 mg/L) on day 6. Furthermore, clones expressing the miR-23-24-27 sponge did not show higher specific

productivity unlike the phenotype obtained in batch and fed-batch mode with mixed populations would suggest (Figure 18 C and D).

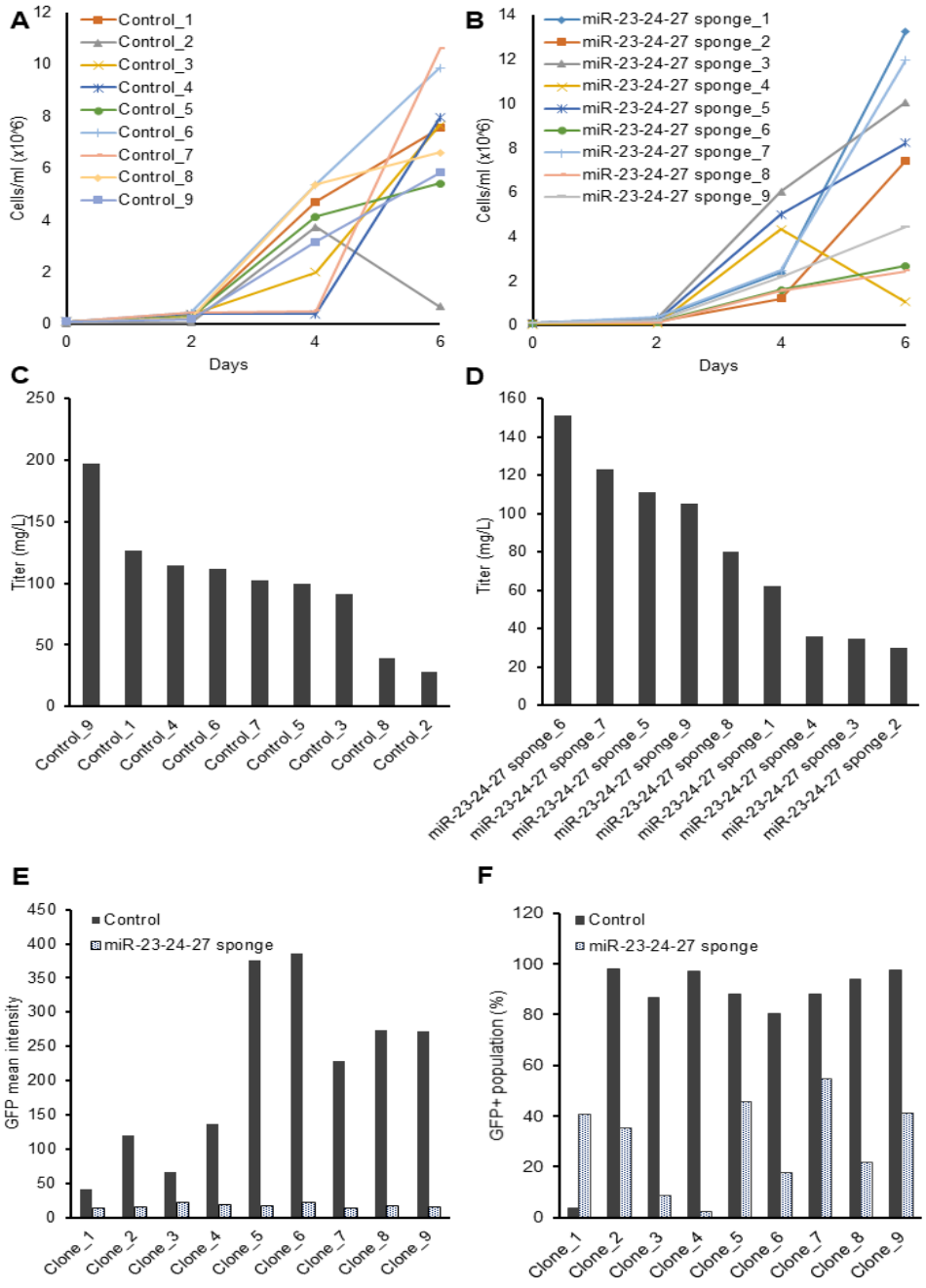

Figure 18: Assessment of individual clones derived from control and miR-23-24-27 sponge expressing mixed populations (CHO-S Fc). A and B) Viable cell density for each clone on day 2, 4 and 6. C and D) Titres for every individual clone from both panels assessed on day 6. E and F) GFP intensity and positive population of all nine clones selected for control and miR-23-24-27 sponge (n=3, technicals).

The impact on productivity using a sponge depleting miR-23-24-27 in CHO-S Fc resulted in a ~1.5-fold increase in titres in a mixed population. However, the productivity phenotype in a mixed population was not reflected in the clonal panel. Average Fc-fusion levels reached 101 mg/L on day 6 for the negative control and 82 mg/L for miR-23-24-27 sponge. Analysing growth compared with productivity showed however, that high productivity in clones seemed to be at the expense of growth which is a commonly observed phenomenon. Highest specific productivity (in pg/cell/day) were exhibited with clones showing reduced proliferation. Clones 6, 8 and 9 expressing miR-23-24-27 sponge showed high specific productivities however, these clones only grew to low cell densities of about $2x10^6$ to $4x10^6$ cells/mL on day 6. These clones also exhibited low GFP mean intensities but showed a high percentage of GFP positive cells in the total population. The possible reasons for this outcome will be discussed later. At this point we decided to revert to the mixed population where the productivity gains were observed to investigate whether the depletion of the three miRNAs had any impact on another important aspect of a recombinant protein - glycosylation.

4.1.2.3 Impact on glycosylation due to the depletion of miR-23-24-27

To investigate if the depletion of the miR-23 cluster had an impact on glycosylation species, 50 mL of cell culture supernatant was taken and the product was purified using protein-A chromatography as described in 3.3.2 (Figure 19 A and B). Samples were analysed for changes in glycosylation pattern using LC/LFR-MS/MS as described in 3.3.3. This work was performed by Dr. Sara Carillo (NIBRT) as part of a collaboration. Depletion of miR-23-24-27 was shown to have some minor effects on glycosylation pattern of the Fc-fusion product (Figure 19 C).

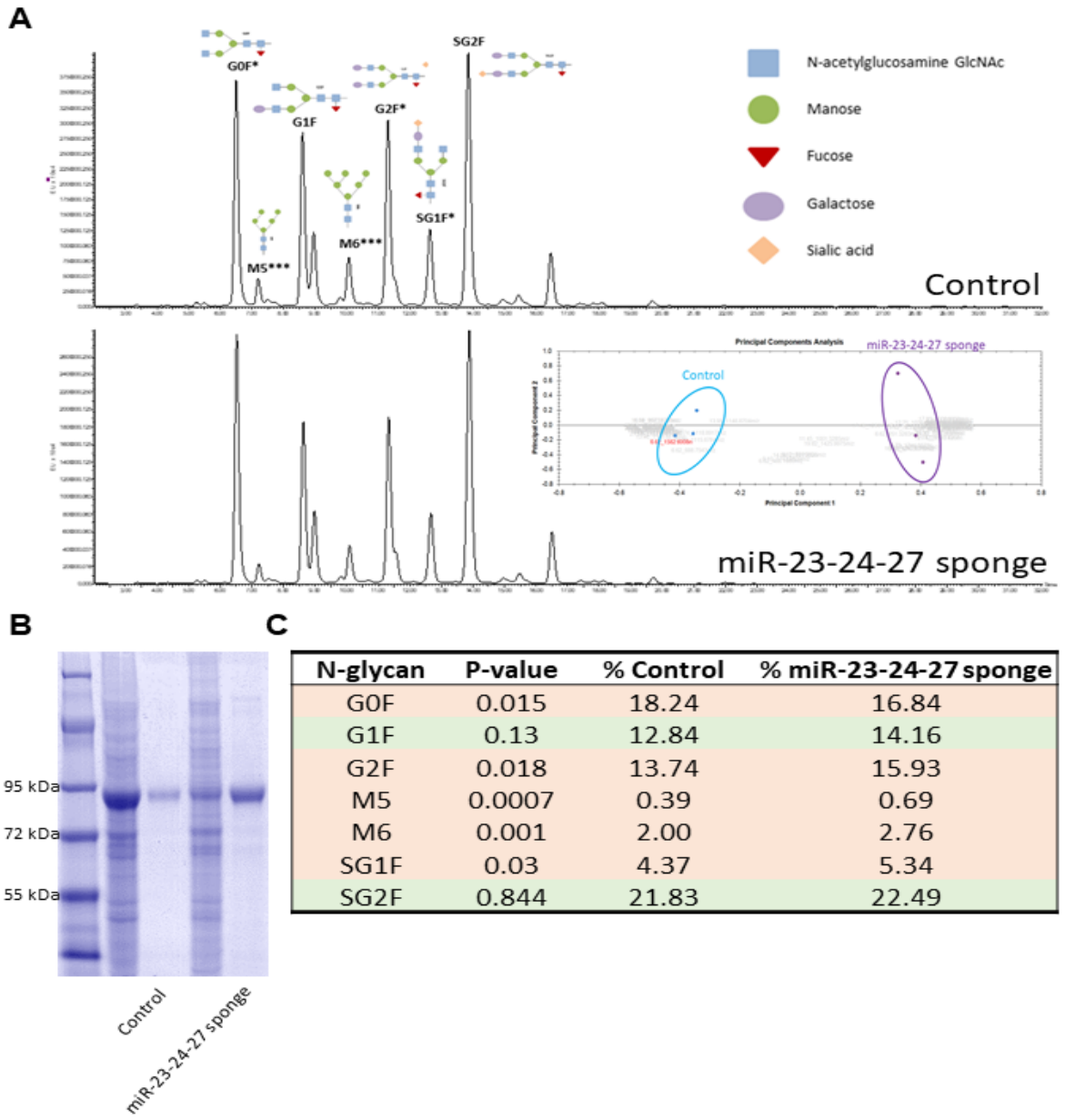

N-glycan	P-value	% Control	% miR-23-24-27 sponge
G0F	0.015	18.24	16.84
G1F	0.13	12.84	14.16
G2F	0.018	13.74	15.93
M5	0.0007	0.39	0.69
M6	0.001	2.00	2.76
SG1F	0.03	4.37	5.34
SG2F	0.844	21.83	22.49

Figure 19: Changes in glycosylation pattern on expressed Fc fusion protein after depletion of miR-23-24-27. A) Chromatogramm for control and miR-23-24-27 sponge obtained by LC/LFR-MS/MS. B) Protein-A chromatography and SDS-PAGE for Fc fusion which was purified out of conditioned media. Sucessful purification was confirmed by SDS-PAGE. C) Abundance of key glycosylations which were differential after depletion of miR-23-24-27 (n=3, technicals).

Stable depletion of miR-23-24-27 had a very slight affect on the glycosylation pattern of the Fc-fusion protein. Increased levels of mannose-5 and mannose-6 can potentially have a drastic impact on antibody-dependent cell-mediated cytotoxicity (ADCC) of mAbs due to accompanying reduction of A-fucosylation. Therefore, increased mannose species may reduce ADCC. Higher levels of galactosylation has no impact on ADCC but can have significant impacts on complement-dependent cytotoxicity (CDC) as G2F as well as SG1F were significantly elevated in miR-23-24-27 depleted cells compared to the control. The impact of glycosylation on the therapeutic protein are discussed later.

Summary of impact of miR-23-24-27 on CHO-S Fc-fusion expressing cells

A CHO-S cell line expressing an Fc receptor fusion with stable depletion of miR-23-24-27 using a sponge resulted in a ~1.5-fold increase in productivity compared to the negative control in batch culture. In a fed-batch process preliminary data showed that an increase in productivity was obtained as well. The same effect was observed in CHO-K1 SEAP expressing cells as well as higher proliferation (Noèlia Sanchez, 2013). Single cell clones were generated using limited dilution cloning and selected by GFP intensity to ensure an excess of sponge mRNA. The clonal panel showed a significant difference in GFP intensity indicating that the sponge was working as expected.

Both clonal panels were analysed for growth behaviour in 1 mL suspension cultures in 24-well plates. All clones differed in proliferation and growth rates as well as productivity. However, the productivity phenotype observed in mixed population in batch and fed-batch culture was not reproduced.

Analysis of the product glycosylation pattern revealed changes in galactose content as well as mannose content which could possibly impact ADCC as well as CDC.

The results achieved with the mixed population cluster depletion prompted us to investigate whether the effect was due to synergistic activities of the cluster members or whether one miRNA in particular was responsible. We designed individual sponges for miR-24 as well as miR-27. The action of miR-23 depletion was already tested at this point and did not show any impact (shown in Figure S 1, Figure S 2 and Figure S 3).

4.1.3 Impact of miR-24 and miR-27 sponge overexpression on the bioprocess phenotype of CHO-S Fc

To investigate which miRNA was responsible for higher titres and specific productivities observed, individual sponges for miR-24 and miR-27 were designed. Once again, the miR-24 and miR-27 sponge sequences were designed to be complementary to their miRNA targets (see Figure 15) except for four base pair mismatches between nucleotides 10 to 14 to create an imperfect binding site. The control sponge was designed similarly with the exception that the sequence was designed not to target any known miRNA. Oligo sequences containing MBS were annealed and ligated into the sponge expression vector (engineered pcDNA3.1/Hyg+). Due to SanDI restriction sites several inserts can be directionally ligated into the expression vector. The ligation mix was transformed and clones were picked. The insert size was assessed using PCR and confirmed by Sanger sequencing (Figure S 4). For the miR-NC sponge a plasmid containing ten scrambled MBS was picked. For the miR-24 and miR-27 sponge both plasmids contained twelve MBS which has been shown to be sufficient for high efficacy (Kluiver et al., 2012a). The CHO-S Fc-fusion expressing cell line was transfected with each sponge construct and selected using hygromycin B over a period of four weeks before being assessed in batch culture. Over a period of eight days samples were taken every 48 hours for assessment of viable cell density and for ELISA. Cells were seeded with at a cell density of $2x10^5$ cells/mL in a culture volume of 5 mL with media provided by Biogen without using antibiotics or selection markers.

No difference in proliferation was observed due to stable depletion of miR-24 or miR-27 compared to the negative control. Furthermore, no difference in viability was observed (Figure 20 A and B). The depletion of miR-24 led to slightly increased levels of Fc-fusion on day 4. Titres on day 6 and 8 were significantly increased compared to the control sponge with increased of 1,3-fold to 2-fold respectively. The depletion of miR-27 had a similar effect resulting in a 2-fold increase of Fc-fusion on day 6 and 8 (Figure 20 C). This increase was due to significantly increased specific productivity (Qp) on day 4 (1.5-fold), 6 (1.2-fold) and 8 (3-fold) of the batch culture with depletion of miR-24 (Figure 20 D). For the depletion of miR-27 the increase in specific productivity (Qp) was even higher on day 4 (3-fold), 6 (2-fold) and 8 (3-fold) of the batch culture (Figure 20 D).

The decrease in GFP mean intensity compared to the control suggested that both sponges bound endogenous miR-24 or miR-27 effectively (Figure 20 E and F). MiRNA

abundance was also measured using TaqMan® assays. Surprisingly, miR-24 levels appeared slightly higher, compared to the control despite suppression of GFP expression. Possible reasons for this will be discussed later. The abundance of miR-27 was significantly reduced compared to the control (Figure 20 G) which is what would be expected when using sponges for a knockdown.

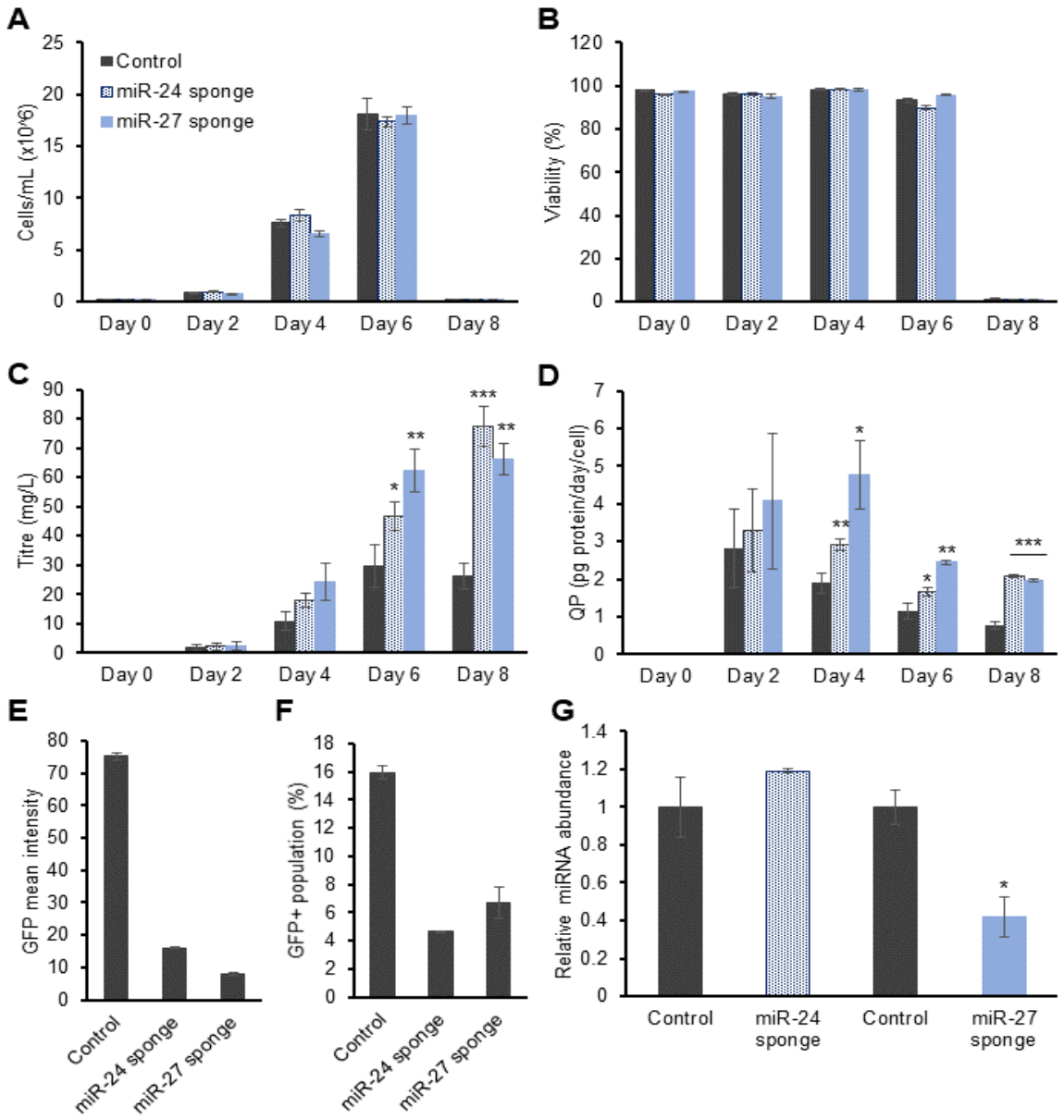

Figure 20: Impact of stable depletion of miR-24 and miR-27 on CHO-S Fc in batch cultures. A) Viable cell density on day 2, day 4, day 6 and day 8. B) Viability assessed on day 2, day 4, day 6 and day 8. C) Fc fusion levels compared to the control after depletion of miR-24 and miR-27 in CHO-S. D) Specific productivity on day 4, 6 and 8 for both depleted miRNAs. E and F) Reduced levels of GFP positive population as well as mean G) MicroRNA abundance for the depletion of miR-24 and miR-27. Statistical significance was calculated using standard student's t-test (* $p < 0.05$ vs control, ** $p < 0.01$ vs control, *** $p < 0.001$ vs control; n=3).

As in the case of the overexpression of the miR-23-24-27 sponge we then analysed the Fc-fusion protein for changes in glycosylation.

4.1.3.1 Investigation of impact on glycosylation due to the depletion of miR-23, miR-24 or miR-27.

To investigate the potential effects on glycosylation of each individual miRNA depletion, 50 mL of cell culture supernatant was taken and the Fc-protein was purified using protein-A chromatography as described in 3.3.2 (Figure 21 A). Samples were analysed for changes in glycosylation pattern using LC/LFR-MS/MS as described in 3.3.3 and the work was performed by Dr. Sara Carillo (NIBRT). Even though no phenotype was observed for the depletion of miR-23 we wanted to include it in our approach to get a bigger picture of the impact of the cluster depletion on glycoslation.

The depletion of all three miRNAs had significant effects on glycosylation patterns on the Fc-fusion (Figure 21 B, C and D). Each point on the graphs represent a different species which was compared to the control. A different species for mannose are for example M3. M3F, M5 etc. All differential glycosylation species are represented in Figure S 5. The control sponge was additionally assessed to investigate if GFP expression alone might have an impact on glycosylation.

Reduced levels of miR-23 led to higher levels of mannose as well as non-sialylated complex N-glycans. Depletion of miR-24 led to an increase in terminal sialic acid, mannose as well as non-sialylated complex N-glycans. Lower endogenous levels of miR-27 led to slightly elevated levels of mannose as well as non-sialylated complex N-glycans. Interestingly depletion of the whole cluster increased levels in mannose species and terminal sialic acid species as well (see 4.1.2.3). Each miRNA might be involved in a different aspect of changed glycosylation and will be further discussed later.

Increased levels of mannose and terminal sialic acid can influence ADCC and target binding efficacy negatively. Taken together results from depleting the miR-23 cluster as well as each individual miRNA indicates that the dysregulation of transcriptional networks using miRNAs can impact the glycosylation pattern of the Fc-fusion protein.

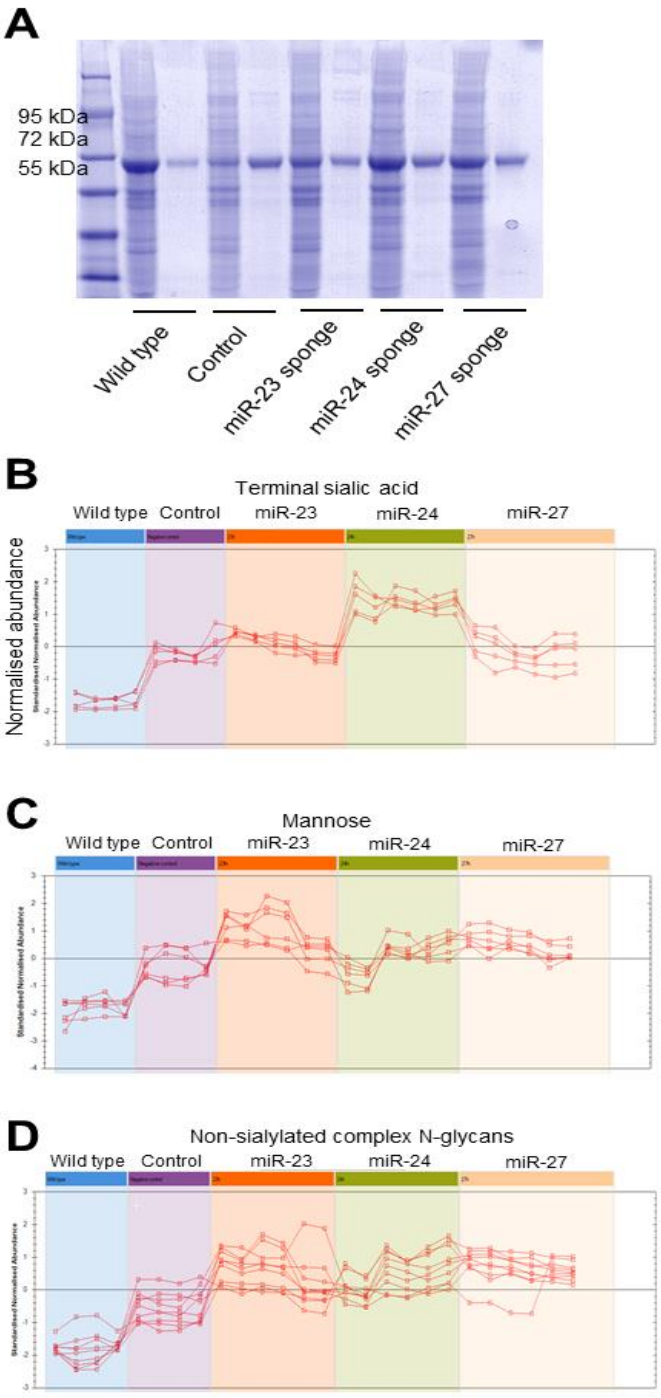

Figure 21: Assessment of glycosylation pattern after depletion of miR-23, miR-24 and miR-27 on expressed Fc fusion. Each point on graphs represent a different glycosylation species i.e. for mannose M3, FM3, M5 etc. A) SDS-PAGE of whole cell lysate after and before protein-A purification. B) Species of terminal sialic acid which were shown to be differential for each member of the miR-23 cluster. C) Mannose species demonstrated to be differential for each member of the miR-23 cluster. D) Non-sialylated glycans which were differential for each member of the miR-23 cluster (n=3, technicals).

As mentioned earlier miRNAs can have multiple mRNA targets in a cell. Perturbing the levels of three miRNAs would therefore be likely to impact even more genes. Given the phenotypic impact we had seen so far and the potential cross talk between miRs from the same genomic cluster, we decided it would be really interesting to investigate proteins being differentially expressed in response to the various sponge decoys. We chose proteomic analysis for this purpose due to the inherent challenge of interpreting transcriptomic data after dysregulation of miRNAs.

4.1.4 Identification of potential targets of miR-23-24-27, miR-23, miR-24 and miR-27 using proteomic profiling and pathway analysis

As miRNAs mainly act at the post-transcriptional level, we sought to find differentially expressed (DE) proteins due to the knockdown of a miRNA with the aim to identify potential direct targets. For the study we compared the knockdown of miR-23-24-27, miR-23, miR-24 as well as miR-27 to control sponge. There is evidence in the literature that each individual member of a miRNA cluster is potentially involved in similar pathways which will be discussed later. Therefore, we included miR-23 even though no phenotype was observed in this particular CHO-S Fc cell line. Samples for label-free proteomic profiling using HPLC-MS/MS were taken in exponential growth phase and prepared as described in 3.3.9. Using mass spectrometry, we identifed 3893 to 4010 proteins with an overlap of 74.3% between samples (Figure 22). Due to the fundamental mechanism of miRNA action we focused on proteins which showed higher abundance compared to the control sponge. Depletion of the whole cluster led to 49 (17 with >1.5-fold change) proteins with higher abundance and 100 which showed reduced levels. Depletion of miR-23, miR-24 and miR-27 individually showed generally higher numbers of DE proteins. One posibble explanation for this could be the difference in MBS in the miR-23-24-27 sponge which only had two binding-sites per miRNA compared to the individual sponges which had 10-12 MBS. Depletion of miR-23 resulted in 385 more abundant proteins with 135 >1.5-fold change. Reduced levels of miR-24 led to increased levels of 219 proteins (72 with >1.5-fold change). Lastly miR-27 depletion increased levels of 210 proteins with 146 having a fold-change of >1.5.

Comparing all the DE proteins (>1.5-fold change) due to miR-23, miR-24 and miR-27 depletion showed that 17 proteins were upregulated in all three sample sets indicating some overlap in target mRNAs between the cluster members.

	Depleted miRNA			
CHO-S Fc	Cluster	miR-23	miR-24	miR-27
Total DE	149	845	434	819
Upregulated	49	385	291	356
> 1.25 fold change	32	253	219	210
> 1.5 fold change	17	135	72	146
Total IDs	3978	3900	4010	3893

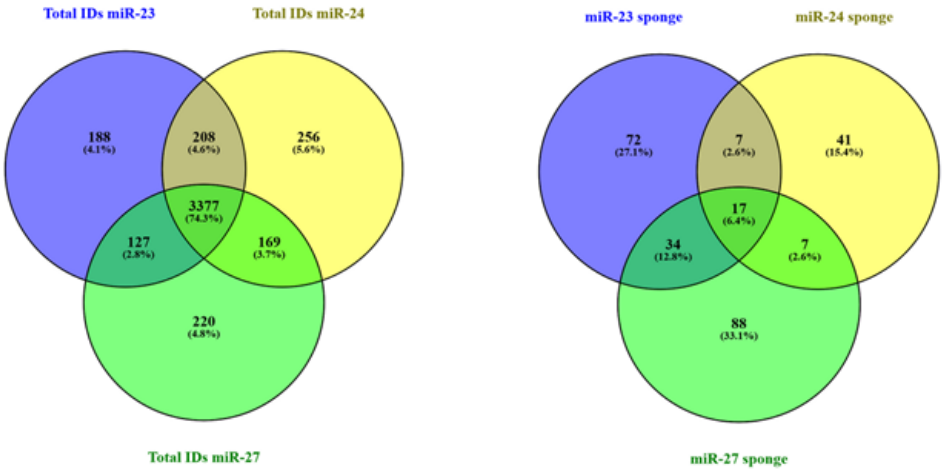

Figure 22: Overlap of proteins identified using Label-free proteomic profiling after depletion of miR-23-24-27, miR-23, miR-24 and miR-27 in CHO-S Fc. A range of 3893 to 4010 total proteins was identified with a coverage of 74.3% between the samples, respectively. Proteins having a fold-change of >1.25, an Anova value <0.05 with 2 peptides were included in analysis of differential expression. Depletion of miR-23-24-27 depletion showed a total of 149 DE proteins.

To try to understand which DE proteins were potentially contributing to the observed higher productivity phenotype, we looked at what pathways were overrepresented based on the known function of the proteins identified. We used the Database for Annotation, Visualization and Integrated Discovery (DAVID 6.7) to identify enriched biological processes (BP) after knockdown of each individual miRNA and cluster (Table 4).

Table 4: Pathway analysis of DE proteins after knockdown of miR-23-24-27 simoultaneously or miR-23, miR-24 and miR-27 individually.

	Depletion of miR-23		
BP	Proteins	P-value	False discovery rate
Translation	63	9,0E-42	1,3E-38
tRNA aminoacylation for protein translation	9	5,7E-6	4,1E-3
Amino acid activation	9	5,7E-6	4,1E-3
tRNA aminoacylation	9	5,7E-6	4,1E-3
Generation of precursor metabolites and energy	19	1,6E-5	7,6E-3
Cellular respiration	9	3,8E-5	1,4E-2
Energy derivation by oxidation of organic compounds	11	5,2E-5	1,5E-2
Oxidation reduction	32	6,1E-5	1,5E-2
Coenzyme metabolic process	13	6,6E-5	1,3E-2
tRNA metabolic process	11	1,7E-4	3,0E-2
Aerobic respiration	6	2,5E-4	4,0E-2
Protein folding	11	4,5E-4	6,2E-2
Acetyl-CoA metabolic process	6	5,0E-4	6,3E-2
Cellular response to reactive oxygen species	5	5,2E-4	6,1E-2
	Depletion of miR-24		
BP	Proteins	P-value	False discovery rate
Translation	40	7,3E-22	8,9E-19
Translational elongation	21	4,2E-16	2,7E-13
RNA processing	40	3,0E-14	1,2E-11
ncRNA metabolic process	22	4,6E-10	8,0E-8
tRNA aminoacylation	10	7,2E-8	9,8E-6
Amino acid activation	10	7,2E-8	9,8E-6
tRNA aminoacylation for protein translation	10	7,2E-8	9,8E-6
Ribonucleoprotein complex biogenesis	17	8,6E-8	1,0E-5
Ribosome biogenesis	14	1,8E-7	1,9E-5
Protein folding	16	4,1E-7	4,1E-5
RNA transport	12	8,5E-7	7,9E-5
Establishment of RNA localization	12	8,5E-7	7,9E-5
Nucleic acid transport	12	8,5E-7	7,9E-5
tRNA metabolic process	12	5,9E-6	3,4E-4
	Depletion of miR-27		
BP	Proteins	P-value	False discovery rate
Cellular response to oxidative stress	4	2,1E-3	8,7E-1
Homeostatic process	12	4,5E-3	8,9E-1
Response to oxidative stress	5	1,6E-2	9,9E-1
Nucleotide biosynthetic process	5	2,4E-2	9,9E-1
Cofactor metabolic process	5	2,8E-2	9,8E-1
Anti-apoptosis	5	3,4E-2	9,7E-1
Regulation of cell proliferation	10	4,2E-2	9,7E-1
Deoxyribonucleotide biosynthetic process	2	4,6E-2	9,6E-1
Regulation of apoptosis	10	4,7E-2	9,6E-1
Regulation of programmed cell death	10	5,0E-2	9,5E-1
Regulation of cell death	10	5,1E-2	9,5E-1
Negative regulation of apoptosis	6	5,8E-2	9,5E-1
Negative regulation of programmed cell death	6	6,1E-2	9,5E-1
Negative regulation of cell death	6	6,2E-2	9,4E-1
	Depletion of miR-23-24-27		
BP	Proteins	P-value	False discovery rate
Protein folding	4	4,4E-3	5,3E-1
Chaperone mediated protein folding	2	2,5E-2	7,6E-1
Protein peptidyl-prolyl isomerization	2	7,5E-2	9,3E-1
Regulation of translational initiation	2	7,8E-2	9,0E-1
Translational initiation	2	8,6E-2	8,9E-1
Chaperone-mediated protein folding	2	8,6E-2	8,9E-1

In our analysis we focused on the most significant pathways with low false discovery rates (Benjamini-Hochberg procedure) and all proteins in our DE lists with a fold change of >1.25. Depletion of miR-23-24-27, miR-23 and miR-24 resulted in an enrichment of biological processes involved in translational initiation, elongation and protein folding were enriched. Interestingly processes involved in activation of amino acids as well as tRNA biosynthesis were enriched, indicating potential upregulation of the translational machinery. For miR-23 depletion alone (no phenotype observed in CHO-S), higher levels of proteins involved in cellular respiration, oxidation and generation of precursors for metabolites and energy were enriched. Depletion of miR-24 resulted in enrichment of pathways involved in rRNA biogenesis, ribosome assembly, translation and protein folding as well as tRNA aminoacylation, which are consistent with what might be expected in a high productivity phenotype.

Reduced levels of miR-27 seem to result in activation of stress response pathways. No pathways associated with a high productivity phenotype were observed for miR-27. Interestingly an increase in proteins involved in apoptotic regulation were observed.

4.1.4.1 Identification of differential expressed proteins involved in glycosylation

As described in 4.1.2.3 and 4.1.3.1, depletion of miR-23, miR-24, miR-27 or the complete cluster, impacted the glycosylation pattern of the Fc-fusion protein. Generating lists of DE proteins also allowed the analysis of potential proteins involved in glycosylation (Figure 23). Depletion of miR-23 led to upregulation of Glucosidase 2 (PRKCSH), Phosphomannomutase 2 (PMM2) and Neutral alpha-glucosidase AB (GANAB). PRKCSH and GANAB are both involved in N-glycan metabolism. Furthermore, PMM2 is important for catalysing the transfer of mannosyl groups to proteins in the early stages of N-glycan maturation.

	Glycosylation related proteins			
ID	miRNA	Fold change	P-value	Peptides
Phosphomannomutase 2 [PMM2]	miR-23	1.52	0.001157	2
Glucosidase 2 subunit beta [PRKCSH]	miR-23	1.37	0.005921	6
Neutral alpha-glucosidase AB [GANAB]	miR-23	1.33	0.001029	9
Glucosidase 2 subunit beta [PRKCSH]	miR-24	1.31	0.024168	2
Phosphomannomutase 2 [PMM2]	miR-27	1.41	0.016579	2

	Glycosylation related proteins
ID	Gene function
Phosphomannomutase 2 [PMM2]	Mannosyl transfer reactions
Glucosidase 2 subunit beta [PRKCSH]	N-glycan metabolism
Neutral alpha-glucosidase AB [GANAB]	N-glycan metabolism

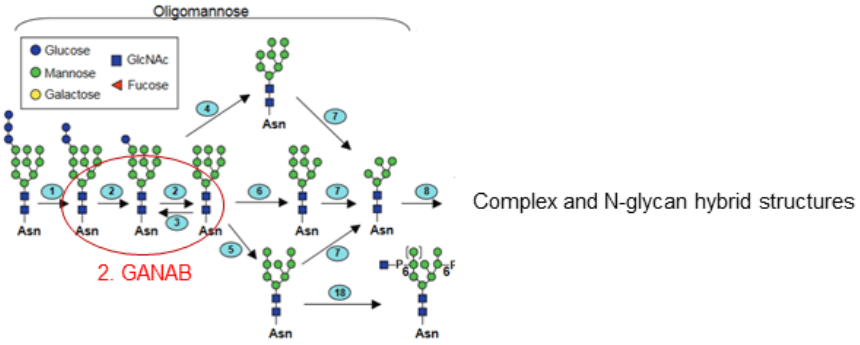

Figure 23: Differential proteins identified by proteomic profiling which can be related to changes in glycosylation after depletion of individual miRNA members of the miR-23 cluster. Three genes involved in processing of glycosylation were identified. These three proteins were Glucosidase 2 (PRKCSH), Phosphomannomutase 2 (PMM2) and Neutral alpha-glucosidase AB (GANAB). GANAB is important for the conversion of ER localised glycans into high-mannose N-glycans. PMM2 is responsible for providing mannose precurosers ffor the addition of mannose to N-glycans.

Depletion of miR-23 led to increased mannose content on the expressed Fc-fusion which correlates with the observation of upregulation of GANAB, PRKCSH and PMM2. Knockdown of miR-24 increased terminal sialic acid as well as non-sialylated complex N-glycans however, none of the detected DE protein are involved in these modifications. Furthermore, miR-27 led to slightly increased mannose and non-sialylated complex N-glycans content. PMM2 is more abundant in miR-27 depleted cells which might potentially explain the increase in mannose species.

4.1.4.2 *Depletion of miR-24 in CHO-S Fc leads to an upregulation of ribosomal RNA biogenesis and the translational machinery resulting in a high productivity phenotype*

Reduced levels of miR-23-24-27 led to increased productivity in one of four tested cell lines (CHO-S Fc). To get a better insight into which miRNA was responsible for the increase in productivity, individual sponges were designed and tested. Depletion of either miR-24 as well as miR-27 led to significantly elevated Fc-fusion protein titre compared to the control sponge. To analyse further which proteins were dysregulated and potentially involved in the observed phenotype, we performed proteomic profiling combined with pathway analysis. This comparison showed that for miR-27 no obvious pathway involved in increased productivity was identifiable. In contrast, depletion of miR-24 resulted in 72 (Anova value < 0.05, fold-change >1.5) more abundant proteins which are involved in several biological processes which could be associated with increased Fc-fusion levels (Figure 24 A to E). Several more proteins are involved in pre-rRNA and rRNA-processing including the members of the PeBoW complex (Figure 24 A). Interestingly, proteins involved in the assembly of ribosomal subunits were upregulated including RACK1 and EIF6 as well as proteins building the ribosomal subunits itself (Figure 24 B). Furthermore, TUFM and GFM1, critical proteins involved in recruiting of aminoacyl-tRNAs and removal of deacetylated tRNAs, were more abundant (Figure 24 C). Upregulation of TUFM and GFM1 is accompanied by synthetases of aminoacyl-tRNAs i.e. AARS, WARS, IARS, NARS and YARS (Figure 24 E). Perhaps, as a result of increased productivity other proteins involved in unfolded protein response (UPR) were upregulated as well e.g. RUVBL2, LONP1 and CCT8 (Figure 24 D).

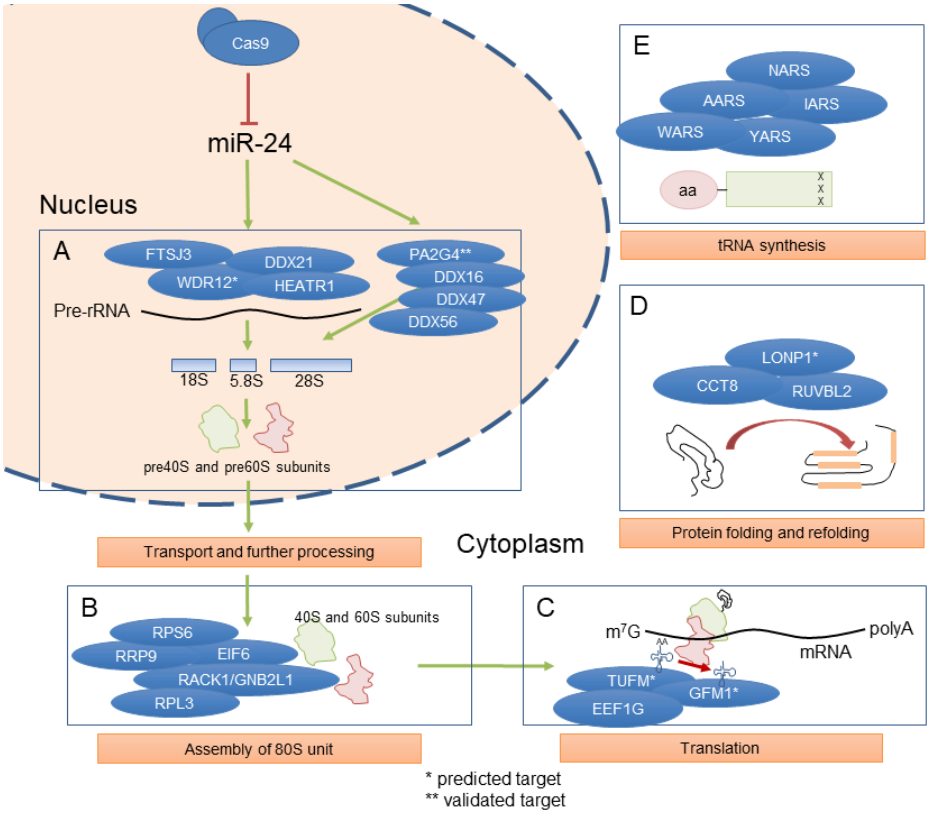

Figure 24: Schematic diagram of how various proteins dysregulated by miR-24 depletion could impact translation in the cell. A and B) Several proteins showed elevated levels involved in pre-rRNA processing, rRNA processing as well as assembly of ribosomal subunits. C) Proteins involved in recruiting and removal of aminoacyl-tRNAs was observed. D) Accompanied by increased levels of translation, UPR seems to be more abundant in miR-24 depleted cells. E) An increase in translational machinery, aminoacyl-tRNA synthases showed elevated levels as well.

Pathway analysis revealed the potential mechanisms leading to increased productivity in response to miR-24 depletion in CHO-S Fc cells. In order to investigate whether this phenomenon was cell line specific or more broadly applicable we engineered several other CHO cell lines to reduce mir-24 expression and measured the impact on the productivity.

4.1.5 Depletion of miR-24 improved productivityof CHO-K1 mAb expressing an IgG

To test if reduced miR-24 levels could impact positively on other cell lines we transfected a CHO-K1 mAb producer cell line. For completeness we also generated stable CHO-K1 mAb pools overexpressing a miR-27 and miR-23-24-27 sponge. The impact of miR-23 individually was assessed by Dr. Paul Kelly (Paul S. Kelly, 2014b) in the same cell line and is therefore not displayed in this thesis. After transfection we performed experiments in 5 mL batch cultures using TPP 50 mL TubeSpin® bioreactor tubes. Cells were grown CHO-SFM II media using CHO-SFM II in a Kuhner Clima-shaker incubator (ISF1-X) at 37°C, 170 rpm and 80 % humidity.

Depletion of miR-23-24-27 or miR-27 individually had no impact in CHO-K1 mAb expressing cells (Figure S 6). However, depletion of miR-24 resulted in slight but significantly elevated levels of IgG (Figure 25 A to E). Viable cell density as well as viability on day 7 was slightly reduced for miR-24 depleted cells compared to the control (Figure 25 A and B). However, IgG titre was elevated on day 2, day 4, day 6 and significantly on day 7 (Figure 25 C). The increase in yield was due to an increase in specific productivity on day 7 of the culture (Figure 25 D). The GFP positive population as well as GFP mean intensity was reduced which indicated binding of endogenous miR-24 to the sponge sequence compared to the control.

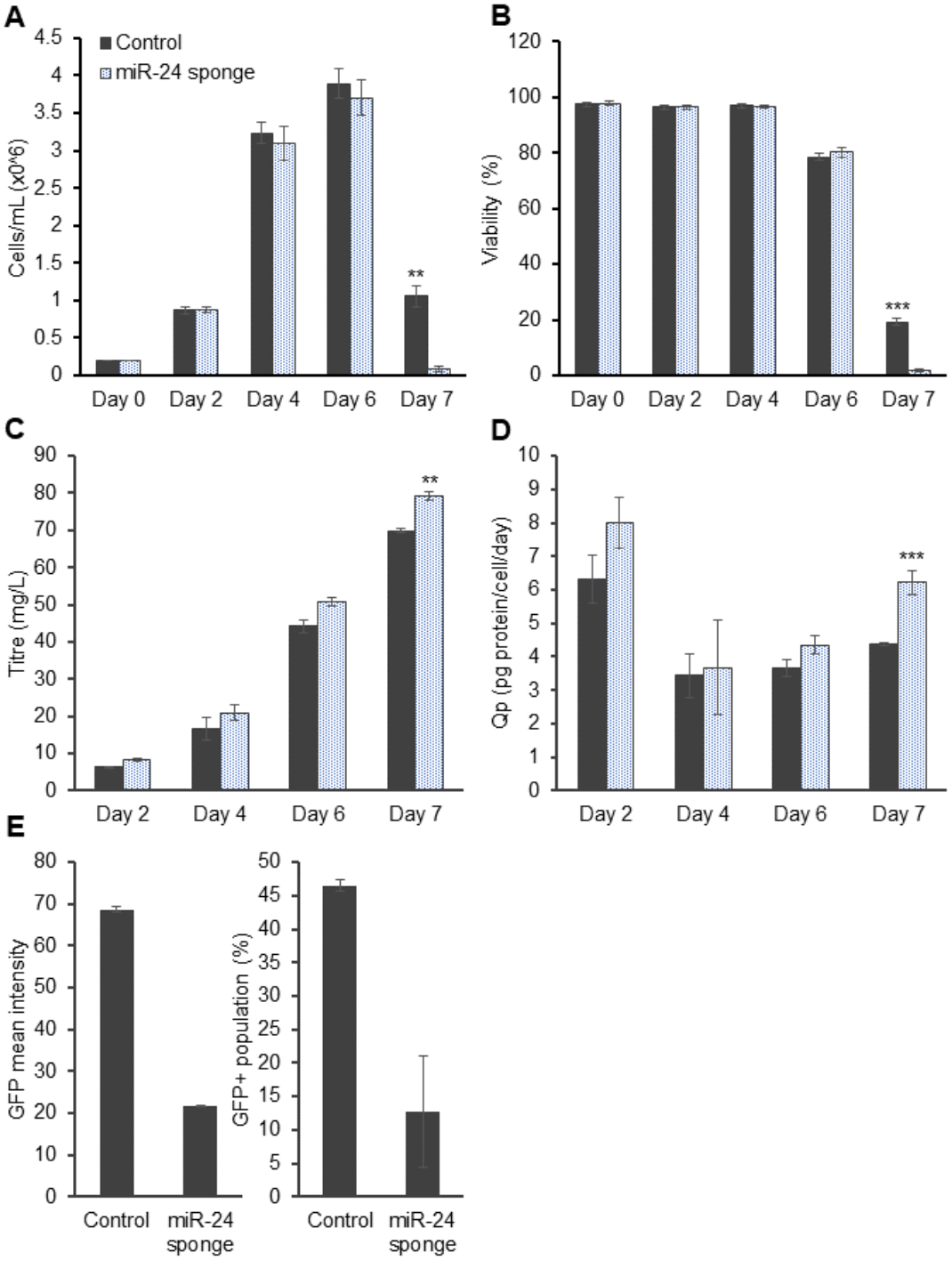

Figure 25: Depletion of miR-24 in CHO-K1 mAb expressing a miR-24 sponge. A and B) Viable cell density and viability compared to the control. C) IgG levels of miR-24 depleted cells compared to the control. D) Specific specific productivity after depletion of miR-24. E and F) GFP positive population and mean intensity. (** $p < 0.01$ vs control, *** $p < 0.001$ vs control; n=3).

In summary, the depletion of miR-24 led to an increase of product level as well as specific productivity in two different CHO cell lineages producing two different therapeutic proteins (CHO-S Fc and CHO-K1 mAb). Next, we expanded our investigation to assess miR-24 depletion on a panel of industrially relevant CHO cell lines expressing different therapeutic proteins. Sponges were transfected in other industrially relevant cell lines including CHO-K1 Fc, DG44i Fc and DG44i mAb. These three cell lines were provided by Biogen. CHO-K1 DP12 (IgG) was purchased from ATCC and CHO-K1 EPO was generated in house by Dr. Srinivas Suda. All functional assessments of these cell lines are summarized in Table 5.

Table 5: Summary of all cell lines tested with sponges for miR-23-24-27 and single members of the cluster.

	Depleted microRNA			
Cell line	miR-23-24-27	miR-23	miR-24	miR-27
CHO-K1 SEAPs	Growth, Qp	Qp	n/a	n/a
CHO-K1 Fc	No	No	Qp	n/a
CHO-S Fc	Qp	No	Qp	Qp
CHO-K1 mAb	No	Longevity	Qp	No
DG44i Fc	No	No	No	n/a
DG44i mAb	No	No	Qp	n/a
CHO-K1 DP12	n/a	n/a	Qp	n/a
CHO-K1 EPO	n/a	n/a	Qp	n/a

Depletion of miR-23 in CHO-K1 SEAP as well as CHO-K1 mAb were performed previously by Dr. Paul Kelly which led to positive effects on longevity as well as productivity. Dr. Noelia Sanchez used a miR-23-24-27 sponge in CHO-K1 SEAP expressing cells which resulted in elevated SEAP levels while compromising cell growth.

As in the CHO-S Fc and CHO-K1 mAb cell lines, the depletion of miR-24 led to increased levels of expressed therapeutic product. An increase was observed in CHO-K1 Fc, CHO-K1 EPO, CHO-K1 DP12 as well as DG44i mAb (experiments performed by Dr. Srinivas Suda). This broadly observed beneficial impact on specific productivity demonstrated the potential of miR-24 depletion as cell line engineering tool.

One drawback of using sponge decoys is the introduction of a reporter/transgene. Furthermore, the specificity of a sponge is not guaranteed as many miRNAs with a similar “seed” family could potentially bind to the MBS. Therefore, we decided to target the genomic locus using the recently developed CRISPR/Cas9 system. As we did see beneficial phenotypes regarding the knockdown of individual members of the miR-23

cluster we selected them as targets for establishing CRISPR/Cas9 in our laboratory. Additionally, we proposed that a knockout of a miRNA may enhance the phenotype observed.

4.2 CRISPR/Cas9 as genome engineering tool to target miRNAs

Previous results had shown that stable depletion of individual members of the miR-23 cluster (miR-23, miR-24 and miR-27) can have an influence on proliferation, viability and productivity. These phenotypes make the miR-23 cluster and each member a potential target for cell line engineering. The sponge approach has been proven to be an efficient method to deplete mature miRNAs in CHO cells. However, for an eventual application in industry it would be beneficial to avoid the introduction of transgenes. Rather than depleting the target miRNA we decided to attempt a complete knockout of the target miRNA. Therefore, the CRISPR/Cas9 system for rapid generation of knockout cell lines was chosen. CRISPR/Cas9 is not only an efficient tool to knockout proteins but it has been shown to be efficient in knocking out miRNAs as well (Chang et al., 2016a; Q. Jiang, Meng, Meng, Chang, Xiong, Cao, & Liang, 2014b). Efficiency was an important factor for us given the existence of cluster paralogues in the genome as well as the possibility of there being >2 or more alleles due to the aneyploid nature of the CHO genome. The organisation of the miR-23a and miR-23b cluster are shown in Figure 26 A.

To knockdown or completely knockout miRNAs, single guide RNAs (sgRNAs) were designed to target the seed sequence of the target miRNAs if possible. The selection of the target genomic locus depends on the presence of a protospacer adjacent motif (PAM) which must be located proximally. The specific PAM sequence is dependent on the Cas9 endonuclease species of origin (NGG for S. *pyogenes*). SgRNAs were delivered as single stranded oligos and were first annealed and then ligated into pSpCas9 (BB)-2A-puro (further referred as PX459) which was digested with BbsI. The sgRNA was expressed off a U6 RNA polymerase III promoter and Cas9/puromycin was under the control of a CMV promoter (Figure 26 B).

To investigate if nucleotide sequence changes proximal to the seed region could potentially alter the stem loop sequence we used RNAfold (http://rna.tbi.univie.ac.at/cgi-bin/RNAWebSuite/RNAfold.cgi) to predict the secondary structure of the wildtype as well as with insertions and deletions (indels) of ± 2bp (Figure 26 C). This demonstrated that both deletions and insertions can have a considerable effect on the secondary structure of the non-processed miRNA precursor which might lead to impairement of processing or inability to recognise its native mRNA target.

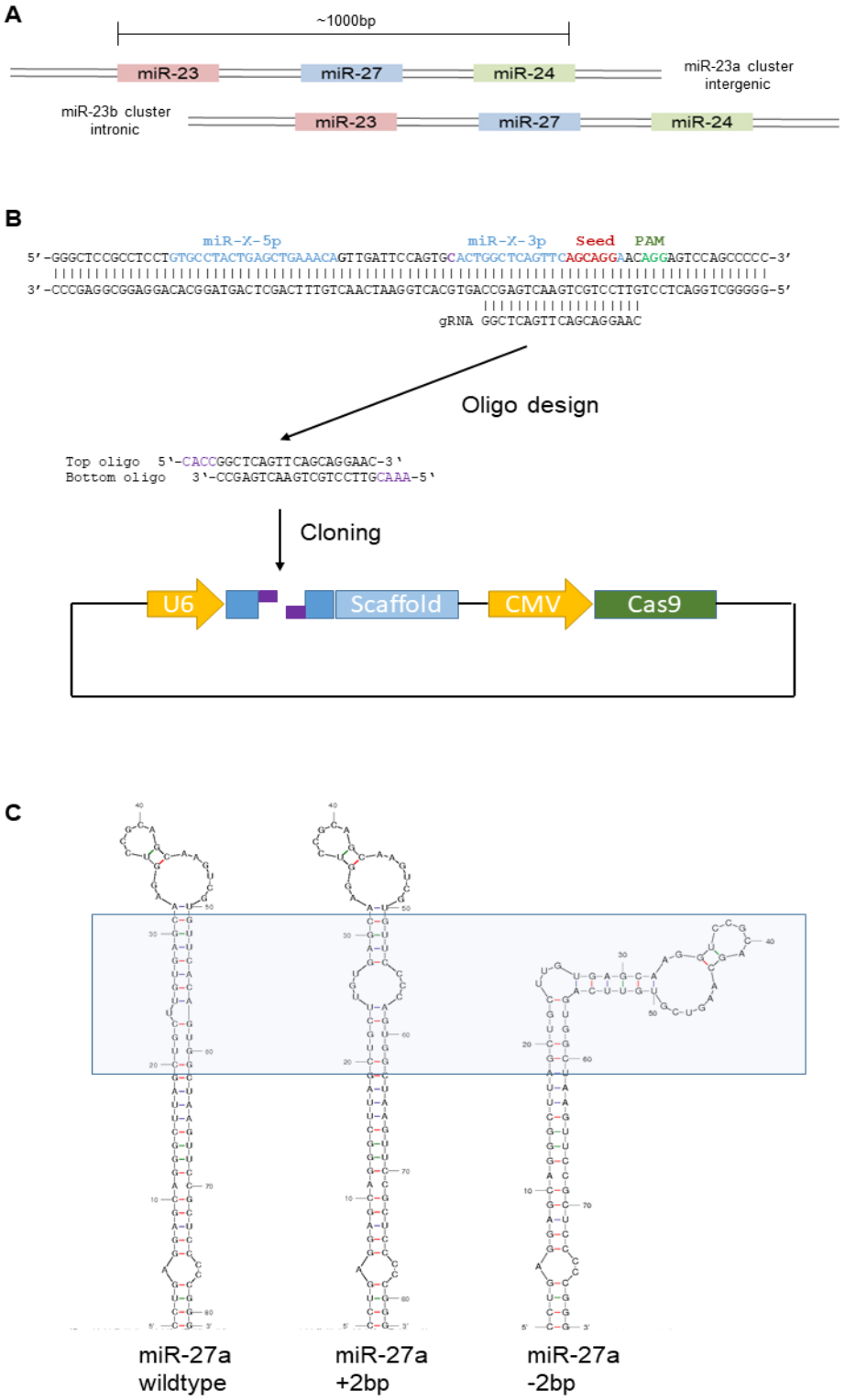

Figure 26: Design and ligation of sgRNAs for targeting miRNAs in CHO cells. A) Organisation of the miR-23a and miR-23b cluster. B) Oligos were designed to target the seed region of the miRNA where possible. Oligos were annealed and ligated upstream the scaffold which enables the co-expression as sgRNA instead of a separate transfection of a guideRNA. C) RNA stability analysis showed that deletions proximal to the seed region could change the structure of the miRNA hairpin.

The Cas9 used was a fusion protein with the puromycin resistance gene enabling selection using puromycin after transfection. The ligation mixes were transformed into DH5-α competent cells and clones were picked and sent for sequencing to confirm successful ligation. Verified plasmids were amplified in DH5-α and midi-prepped to isolate the plasmid DNA and to remove endotoxins. Several gRNAs were used for targeting every single member of the miR-23 cluster including the paralogues (Table 6).

Table 6: Guide RNAs used for targeting each miRNA member of the miR-23-24-27 cluster.

miRNA targeted	Sequence	PAM
miR-23a	5'-CACCGAGTCACAAATCACATTGCC-3' 3'-CTCAGTGTTTAGTGTAACGGCAAA-5'	AGG
miR-23b	5'-CACCGAGATTAAAATCACATTGCC-3' 3'-CTCTAATTTTAGTGTAACGGCAAA-5´	AGG
miR-27a	5'-CACCGCAGCAAGTCGTGTTCACAGC-3' 3'-GTCGTTCAGCACAAGTGTCCAAA-5´	TGG
miR-27b	5'-CACCGGTTTCCGCTTTGTTCACAGC-3' 3'-CCAAAGGCGAAACAAGTGTCCAAA-5´	TGG
miR-24	5'-CACCGGGCTCAGTTCAGCAGGAAC-3' 3'-CCCGAGTCAAGTCGTCCTTGCAAA-5´	AGG

For miR-24 we were able to use a single sgRNA to target both paralogues as miR-24-1 and miR-24-2 are identical in their sequence. As a control we utilised PX459 only expressing the scaffold construct containing a non-specific gRNA sequence. CHO-K1 mAb expressing cells were transfected with each plasmid and selected for two weeks. DNA was isolated and the miR-23a-27a-24-2 and the miR-23b-27b-24-1 cluster were amplified using standard PCR. Analysis of indels was performed using either the T7E1 endonuclase assay, Sanger sequencing or NGS. After selection, mixed populations and clones were analysed using TaqMan® miRNA assays. For each assay primers were designed to target up- and downstream of each miRNA. A general workflow for the generation of stable cell lines and analysis of indels as well as phenotypic analysis using growth curves and ELISAs is displayed in Figure 27.

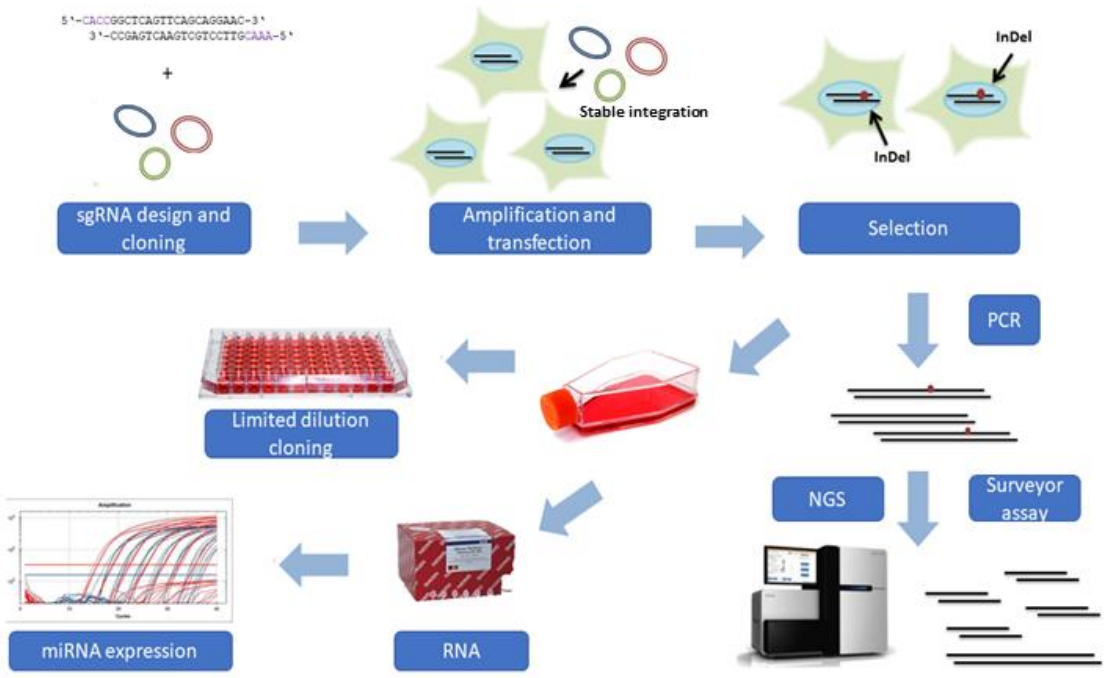

Figure 27: General workflow used for the generation of stable cell lines with CRISPR/Cas9 targeting miRNAs. After design and amplification of the plasmid a CHO-K1 mAb expressing cell line was transfected with and selected using puromycin to ensure stable integration of the plasmid into the hosts genome. Plasmids were generated with sgRNAs targeting each miRNA. However, to avoid co-transfections we targeted only one miRNA at a time. Genomic DNA was extracted and each cluster was amplified using standard PCR with high fidelity polymerases to ensure no unspecific mismatches. Analysis of indels was performed using NGS, Surveyor® assay or standard Sanger sequencing after TOPO-TA® cloning. MiRNA expression was analysed in mixed populations as well as in single cell clones. After a successful knockdown was obtained the phenotype was analysed using growth curves and ELISA.

As mentioned above we used three different methods for the analysis of indels generated:

Firstly, the PCR product was cloned into TOPO-TA® and positive colonies were amplified and sequenced using standard Sanger sequencing (Figure 28). We found that for every targeted miRNA insertions and deletions were detectable. Most common indels were between ±3 bps. However, larger deletions were found for miR-27a (-62 bps) and miR-24 (-40 bps), respectively.

Another method to analyse indels is the use of Surveyor® assays which utilise a T7 endonuclease. The PCR product was purified and mixed with wt amplicon. The mix was then denatured and re-annealed as well as treated with Surveyor® nuclease which is an enzyme that cuts DNA at mismatches. Mismatches will occur where amplicons with indels re-aneal with wt amplicons. The cleavage of the PCR product was analysed on a 2 % agarose gel for higher resolution. To calculate indel frequencies the intensity of the digested product was compared to wildtype PCR amplicon. By comparing the intensity of each band the amount of cleaved PCR product was calculated by following formula:

$$f_{cut} = (b+c)/(a+b+c)$$

With *b* and *c* being the integrated intensities of each cleaved product and *a* being the undigested PCR product. To calculate the indel percentage the following formula was used:

$$\text{Indel (\%)} = 100 \times (1 - \sqrt{(1 - f_{cut})})$$

All sgRNAs except for miR-23a were shown to target their corresponding miRNA target loci and induce indels. At this point it was necessary to re-clone and prove targeting for the sgRNA which was used to target miR-23a. However, the Surveyor® assay was not repeated for miR-23a but NGS was used instead. The Surveyor® assay showed that the sgRNA for miR-23b induced an indel occurance of 64 %. Mir-24-1 and miR-24-2 induced indels at 40 % and 34 % efficiency, respectively. Furthermore, miR-27a and miR-27b were targeted with an efficiency of 48 % and 41 % (Figure 28 B).

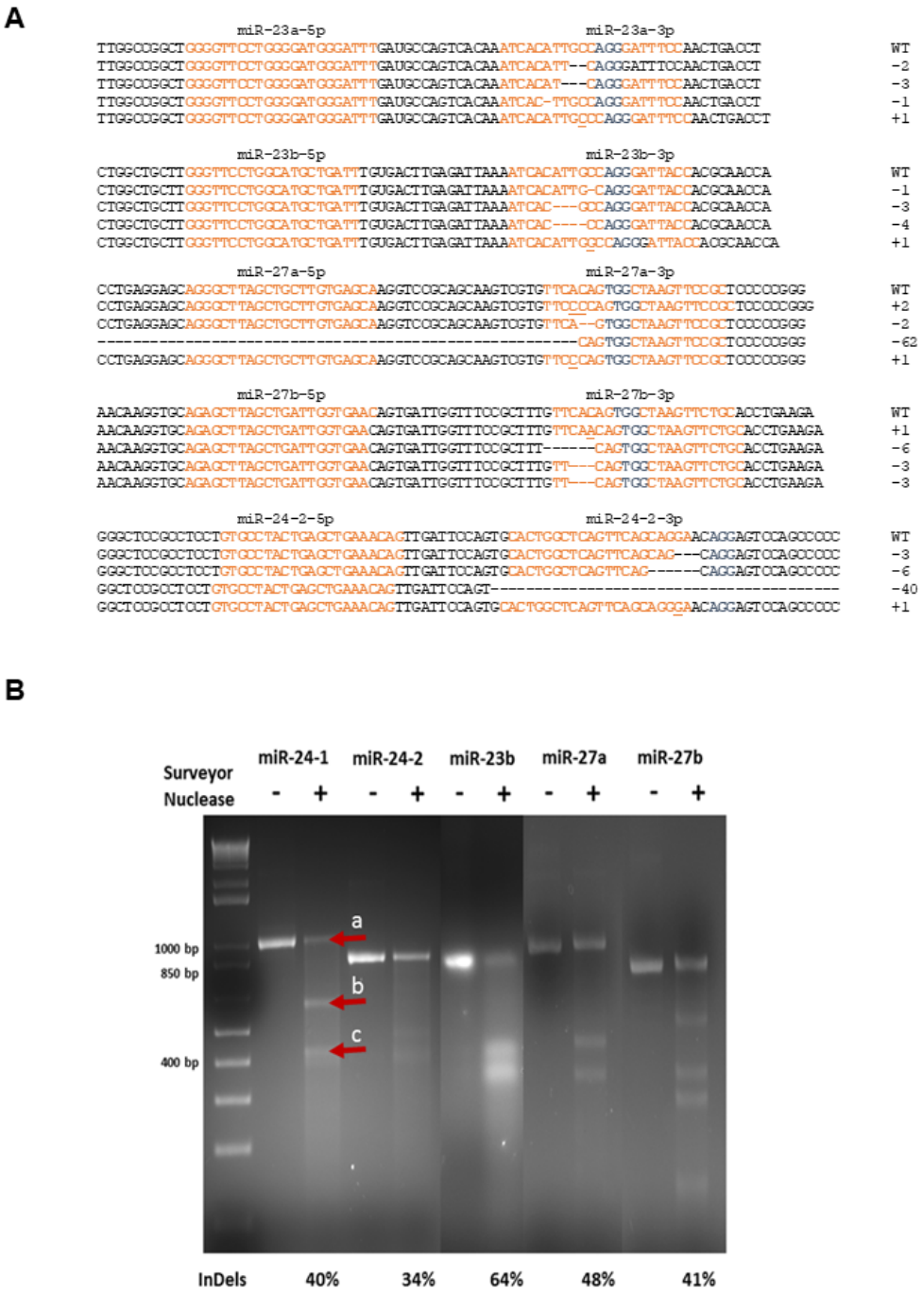

Figure 28: Analysis of indels generated by CRISPR/Cas9 using Sanger sequencing and Surveryor® assays. A) Targeted region was amplified using PCR and cloned into TOPO plasmids. Subsequent Sanger sequencing showed a wide range of deletions and insertions ranging from ±1 to ±3 bps. The mature miRNA sequence is displayed in orange and the PAM is shown in blue. B) After targeting with CRISPR the genomic DNA for each miRNA was amplified and Surveyor® assay was used to visualise indel induction. *A* represented the undigested product, *b* and *c* were the cleaved products.

Having established that we can target all members of the miR-23 cluster with high efficacy we wanted to observe the influence on mature miRNA expression.

4.2.1 MicroRNA expression in mixed populations targeted with CRISPR/Cas9

Both Sanger sequencing after TOPO-TA cloning and the Surveyor® assay showed that the loci of interest could be successfully targeted, obtaining high percentages of indels. To investigate the effect of these indels on mature miRNA expression, total RNA of selected mixed populations was isolated and first strand cDNA synthesis was performed with specific looped primers contained in the TaqMan® small RNA assay kit. The cDNA was amplified using specific forward and reverse primers and a TaqMan® probe labelled with a fluorophore was included in the kit for specific detection of miRNAs. To normalise expression U6 snRNA was used as an endogenous control. Expression was calibrated to the control (PX459) which was also transfected into CHO cells (CHO-K1 mAb control).

The expression of each mature miRNA was significantly reduced in all mixed populations (Figure 29 A). MiR-27a showed a 65% reduction (* $p < 0.05$ vs control) and miR-27b showed an 90% reduction (** $p < 0.01$) compared to the control. The greatest reduction was observed for miR-24 with a 98% (*** $p < 0.01$ vs control). However, the TaqMan® assay does not distinguish between miR-24-1 and miR-24-2 as both mature miRNA sequences are completely identical. Furthermore, miR-24 is in general highly expressed which was observed by testing a panel of cell lines for individual expression of all miRNAs located in the miR-23 cluster and paralog. The highest fold change in a mixed CHO population was observed when targeting miR-23a with 98% less mature miRNA compared to a control population (*** $p < 0.001$ vs control). Targeting miR-23b also led to respective reduction of mature miRNA of 95% (*** $p < 0.001$ vs control).

When investigating the full range of deletions or insertions obtained in mixed populations, the Surveyor® assay and Sanger sequencing only give information on a small sample of events. Therefore, we decided to use Next-generation sequencing to investigate which insertions or deletions are most common. For indel sequencing it was necessary to design primers ±100 bps up- and downstream of the presumed mutated site. Furthermore, linker sequences were added to the primers and a high-fidelity polymerase with proofreading function was used. Figure 29 B shows the targeting efficiencies and most common deletions/insertions observed.

A

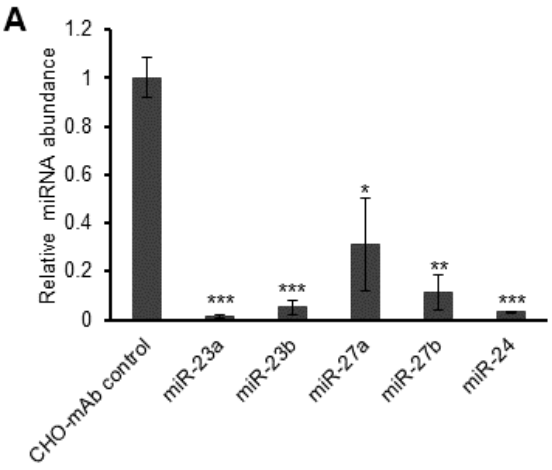

Ct value	Control	sgRNA
miR-23a	22.51	30.18
miR-23b	24.76	29.16
miR-27a	19.59	20.91
miR-27b	24.31	26.87
miR-24	19.45	29.16

B

Sample	%WT	%Indel	Indels				
miR-23a	35.89%	64.11%	-2	-1	1		
miR-23b	13.04%	86.96%	-1	1			
miR-27a	16.29%	83.71%	1				
miR-27b	10.46%	89.54%	1				
miR-24-1	4.21%	95.79%	1				
miR-24-2	3.70%	96.30%	-9	-6	-2	-1	22

C

CHO-mAb	miR-23a	miR-23b	miR-27a	miR-27b	miR-24
Phenotype	Longevity	Longevity	Reduced growth	Longevity	Growth, Qp

Figure 29: CRISPR/Cas9 mediated targeting of miRNA led to reduced mature miRNA levels. A) Mature miRNA expression was assessed and abundance of miRNAs was significantly reduced for each targeted miRNA compared to the control. B) NGS was used to analyse indels and a variety of indels was observed. C) Summary of phenotypes obtained in mixed population for each miRNA targeted with CRISPR/Cas9. Phenotypes correlated with experiments performed using sponge decoys in the same cell line. (* $p < 0.05$ vs control, ** $p < 0.01$ vs control, *** $p < 0.001$ vs control; n=3).

This demonstrates that miR-24-1 and miR-24-2 were most effectively targeted with a %indel of ~95-96 in mixed population. Interestingly, miR-24-2 showed a high variety of common deletions up to -22 bps. At the miR-24-1 locus an insertion of +1bp was more common. Both guides for miR-27a and miR-27b seemed to induce insertions of +1bp with relatively high indel percentage of 83-89%. For miR-23a, 64% of all reads showed indels with -2, -1 and +1bp being the most common. Targeting miR-23b resulted in 87% indels in a mixed population with insertions and deletions of ±1bp, respectively.

Having shown that we can effectively induce a variety of indels we wanted to investigate if these indels result in similar phenotypes to these observed during the earlier sponge decoy work. Therefore, we analysed the phenotype of mixed populations and it demonstrated that targeting miRs by CRISPR/Cas9 led to similar phenotypes when compared to sponge decoy approach (Figure 29 C).

As the miR-23 cluster consists of two genomic paralogues (miR-23a and miR-23b) and the sgRNAs used were very similar we wanted to investigate if the sgRNA for miR-23a targeted miR-23b and vice versa. Similarly, we wanted to assess this for miR-27a and miR-27b. We assessed the mature expression of miR-23a in two mixed populations: firstly, the mixed population in which miR-23a was targeted and secondarly the mixed population in which miR-23b was targeted. We followed the same approach for miR-23b, miR-27a and miR-27b (Figure 30 A and B). In mixed populations where miR-23a was targeted, both paralogues were downregulated. This was also demonstrated for miR-23b. The sgRNAs used for targeting miR-23a and miR-23b showed a high level of similarity especially in the 3' region close to the PAM. When miR-27a was targeted the expression of both paralogues was downregulated. The same result was observed for miR-27b and again both sgRNAs showed similarity in the 3' region. However, the sgRNAs for miR-27a and miR-27b showed only a 50% sequence overlap. As mentioned before we have no way in differenciating between the levels of miR-24-1 and miR-24-2.

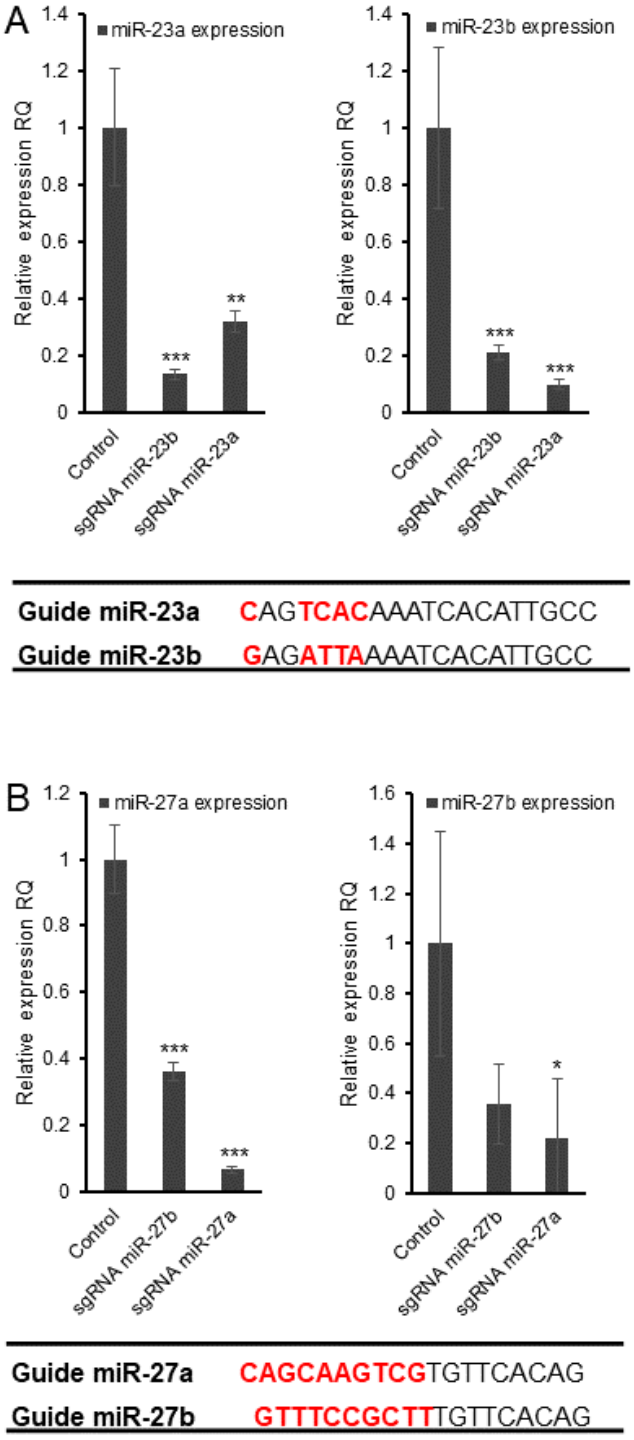

Figure 30: Investigation of off-targeting between similar sgRNAs used for targeting paralogues and analysis of mature miRNA expression. A) Analysis of mature expression of miR-23a and miR-23b after using sgRNAs for miR-23a and miR-23b in mixed population. Furthermore, the sequence of both sgRNAs was compared. B) Analysis of mature expression of miR-27a and miR-27b after using sgRNAs for both in mixed population. Furthermore, the sequence of both sgRNAs was compared ((* p< 0.05 vs control, ** p < 0.01 vs control, *** p < 0.001 vs control; n=3).

To investigate the cross-targeting of the genomic paralogues further and to ensure the accuracy of the Taqman® assays, we performed NGS on mixed populations where miR-23a, miR-23b, miR-27a and miR-27b were targeted (Table 7).

Table 7: Investigation of cross-targeting using NGS.

Sample	Primer	%WT	%Indel	Indels		
miR-23a	miR-23a	35.89%	64.11%	-2	-1	1
miR-23a	miR-23b	93.49%	6.51%	-1		
miR-23b	miR-23a	83.55%	16.45%	-1		
miR-23b	miR-23b	13.04%	86.96%	-1	1	
miR-27a	miR-27a	16.29%	83.71%	1		
miR-27a	miR-27b	88.84%	11.16%	-1		
miR-27b	miR-27a	78.40%	21.60%	-2	-1	
miR-27b	miR-27b	10.46%	89.54%	1		

When we investigated cross-targeting by the sgRNA used for targeting miR-23a we amplified the region where miR-23a was located in the genome as well as miR-23b. We used the same approach for the miR-27a and miR-27b loci. It was observed that when miR-23a was targeted, miR-23b was targeted also. However, frequencies of targeting were much lower with only 6.51% showing indels of -1bp. For miR-23b it was demonstrated that miR-23a was targeted as well with 16.45% showing mutations of -1bp. When miR-27a was targeted, miR-27b was also affected with 11.16% of reads showing a mutation. When targeting miR-27b the miR-27a locus showed the highest indel frequency of 21.60% with -1 and -2 bp being observed most frequently. Therefore, cross targeting effects must be considered and it confirmed the assessment of mature miRNA expression using Taqman® assays.

Having proved that we can target miRNAs effectively we wanted to investigate the impact on the phenotype after depletion of each individual miRNA member of the miR-23 cluster further.

4.2.1.1 Bioprocess phenotype on mixed populations after targeting miRNA members of the miR-23 cluster using CRISPR/Cas9

Our experiments demonstrated that CRISPR/Cas9 can be successfully used to knockdown miRNAs in mixed populations. It is known that the targeting efficiency is dependent on individual sgRNAs. The high efficiencies observed would suggest that there should be many clones within the population that have a complete knockout of the miRNA target. Before exploring clones, the mixed populations were assessed in batch culture (Figure 31 A to C) in a culture volume of 5 mL with an initial cell density of 2 x 10^5 cells/mL using TPP 50 mL TubeSpin® bioreactor tubes. Cells were grown BalanCD CHO Growth A media and samples were taken every 48 hours to assess viable cell density and for ELISA to assess productivity. Targeting miR-23a, miR-23b and miR-27b had no or neglectable effect on cell growth (Figure 31 A). However, for all three miRNAs a significant increase in viability was observed on day 10 of the culture (Figure 31 B). The same phenotype was observed as depletion of miR-23a and miR-23b in the sponge experiments. Targeting of miR-27a led to a decrease in growth which also had been observed in the same cell line using antagomiRs. Depletion of miR-24 on the other hand led to a significant increase in growth on day 2, day 4 and day 6. However, elevated proliferation presumably led to the decrease in viability on day 10 due to higher nutrient demands. Interestingly, titres were significantly elevated as well at all stages of the culture (Figure 31 C). Targeting of miR-27b and miR-23a similarly led to increased (not significant) IgG levels.

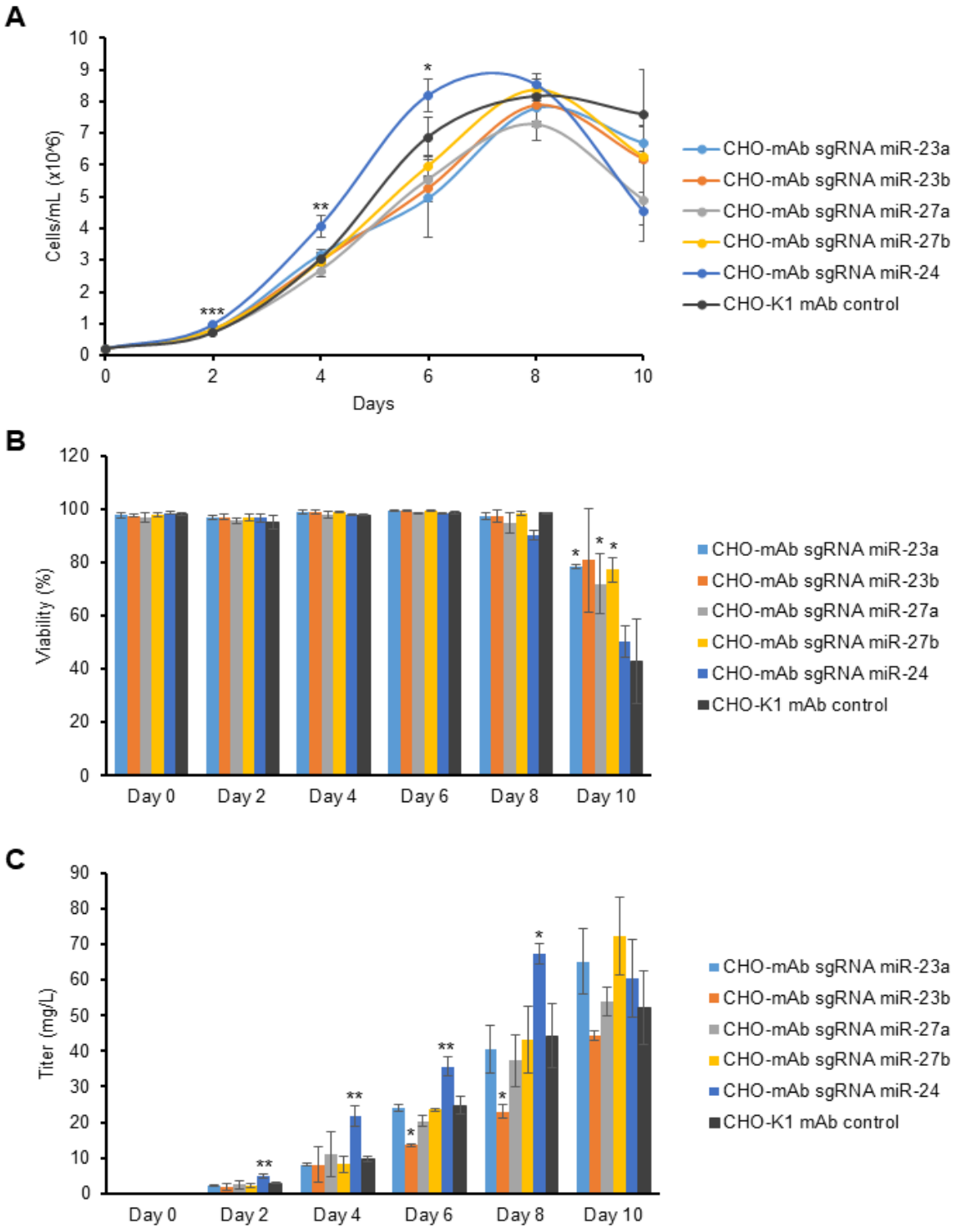

Figure 31: Impact of targeting each miRNA of the miR-23 cluster with CRISPR on phenotype in mixed population in batch cultures. A) Viable cell density for the depletion of miR-23a, miR-23b, miR-27a, miR-27b and miR-24. B) Viability for the depletion of miR-23a, miR-23b, miR-27a, miR-27b and miR-24. C) Impact on titre IgG density for the depletion of miR-23a, miR-23b, miR-27a, miR-27b and miR-24. (* $p < 0.05$ vs control, ** $p < 0.01$ vs control, *** $p < 0.001$ vs control; n=3).

Previous work in our lab using miRNAs mimics or antagomiRs has shown that up- or downregulation of individual members of the miRNA cluster can influence the bioprocess phenotype of CHO-K1 cells. Transfection of mimics for miR-23a and miR-24 inhibited proliferation in CHO-K1 mAb. However, knockdown of miR-24 resulted in enhanced growth rates. Transient depletion of miR-27a resulted in a decrease of growth in CHO-K1 mAb but increased proliferation in a different cell line CHO2B6 showing a cell type specific phenotype (Noèlia Sanchez, 2013). To further investigate the impact of a complete knockout of a miRNA in a clonal population we used limited dilution cloning to generate single cell clones from each mixed population.

4.2.1.2 Identification of clones with complete miRNA knockouts induced by CRISPR/Cas9

Targeting each miRNA member of the miR-23 cluster was possible using CRISPR/Cas9. To investigate if it is possible to identify single cell clones exhibiting a complete knockout, limited dilution cloning was used. After two weeks clones were picked, expanded and total RNA was isolated. Mature miRNA levels were analysed using TaqMan® microRNA assays. For each targeted microRNA a lower abundance was observed. For miR-23a and miR-23b a reduction similar to the mixed populations was exhibited (Figure 32 A and B). Targeting miR-27a was less effective compared to targeting each other miRNA member. This was also observed for isolated single cell clones (Figure 32 C). Furthermore, clones derived from the miR-27b targeted mixed population showed either very low mature levels or moderate depletion (Figure 32 D). Targeting of miR-24 using CRISPR/Cas9 was very effective with all clones showing minimal levels of expression (Figure 32 E). We demonstrated that we could find clones with low levels of expression of each miRNA member. Some clones showed residual miRNA expression which could mean that e.g. expression is not inhibited if only an indel of ±1 bp occurs. Furthermore, it remains questionable if an assay for miR-23a will also recognize miR-23b and vice versa.

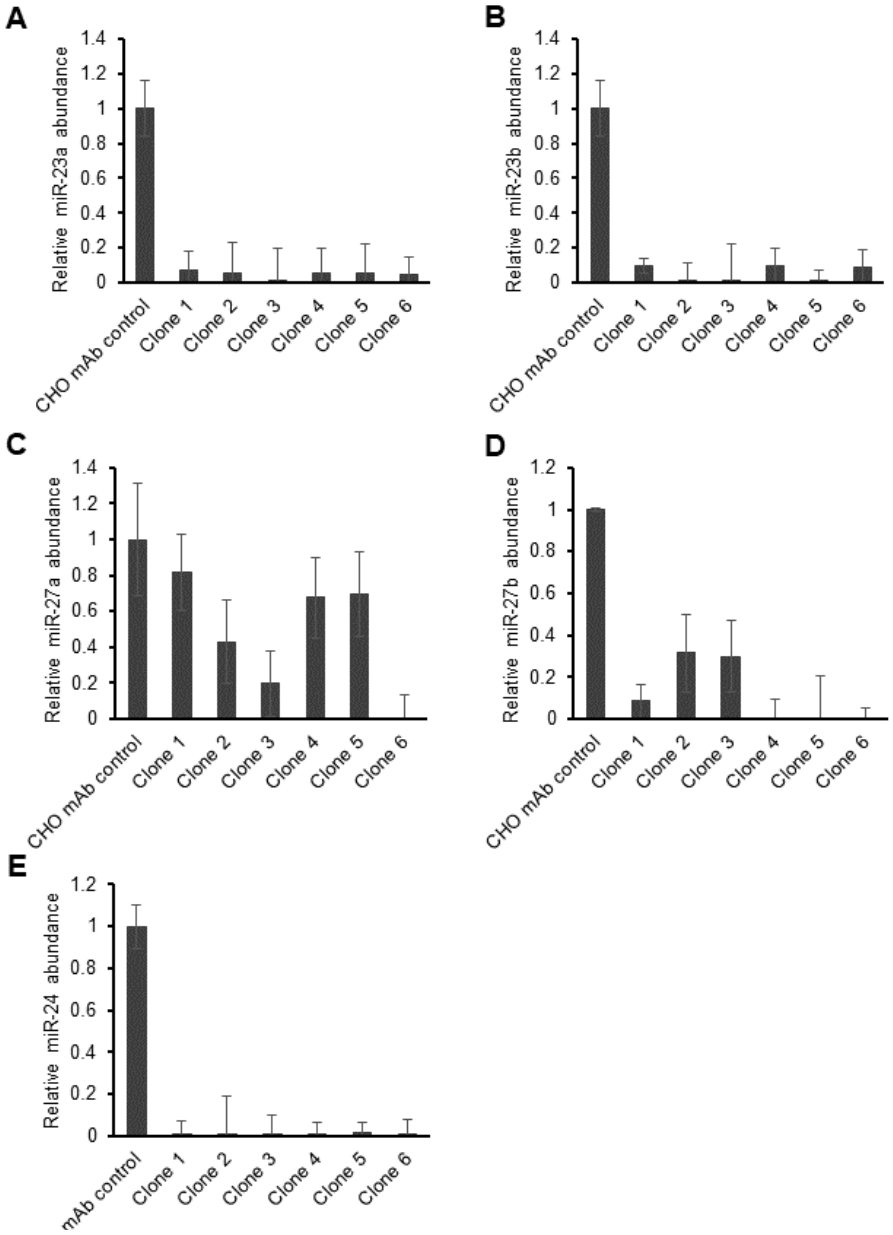

Figure 32: Single cell clones derived from CRISPR targeted mixed populations and assessment of miRNA expression. A and B) Derived single cell clones from miR-23a and miR-23b targeted mixed populations and assessment of mature miRNA expression. C and D) Derived single cell clones from miR-27a and miR-27b targeted mixed populations and analysis of mature miRNA expression for each clone compared to the control. E) Single cell clones derived from a mixed population where miR-24-1 and miR-24-2 was targeted. Mature miR-24 expresseion was compared to the control. No differentiation between miR-24-1 and miR-24-2 was possible. (n=3, technicals)

Having demonstrated that the isolation of clones exhibiting a significant reduction or elimination of mature miRNA is possible, we focused our future experiments on investigating the beneficial phenotypesreported in section 4.2.1.1. Most interesting was the increase of productivity and growth after targeting miR-24 as the same phenotype was exhibited in the sponge decoy experiments as well. Identifying the pathways involved might reveal other cell line engineering targets. Furthermore, depletion of miR-27b led to increased viable cell densities in later stages of the culture. Therefore, depletion of miR-27b could be a valuable strategy to improve longevity and improve therapeutic protein production.

4.2.2 CRISPR mediated depletion of miR-27b increased viability in late stages of batch and fed-batch cultures

As described in 4.2.1.1, depletion of miR-27b led to increased viability in late stages of the culture. The phenotype was assessed in batch as well as fed-batch cultures in a culture volume of 5 mL with an initial cell density of $2x10^5$ cells/mL using TPP 50 mL TubeSpin® bioreactor tubes or 250 mL Erlenmeyer flasks. Cells were grown BalanCD CHO Growth A media and samples were taken every 48 hours to assess viable cell density for ELISA to assess productivity. For experiments in fed-batch cultures BalanCD CHO Feed1 was used with 10% bolus feeds on day 1, day 5 and day 7. The results for both culture formats is shown in Figure 33 A to F. Reduced mature miR-27b levels led to an increase in viable cell density in late stages of batch and fed-batch cultures of ~50% (Figure 33 A and D). This was also reflected in percentage viability in late stages for day 10 (batch) as well as on day 12 and 13 (fed-batch) was significantly higher compared to the control (~50%) (Figure 33 B and E). The general observation was that miR-27b depletion led to slightly reduced IgG titre. However, with extended culture times final titres were slightly but not significantly elevated compared to the control for both culture formats (Figure 33 C and F).

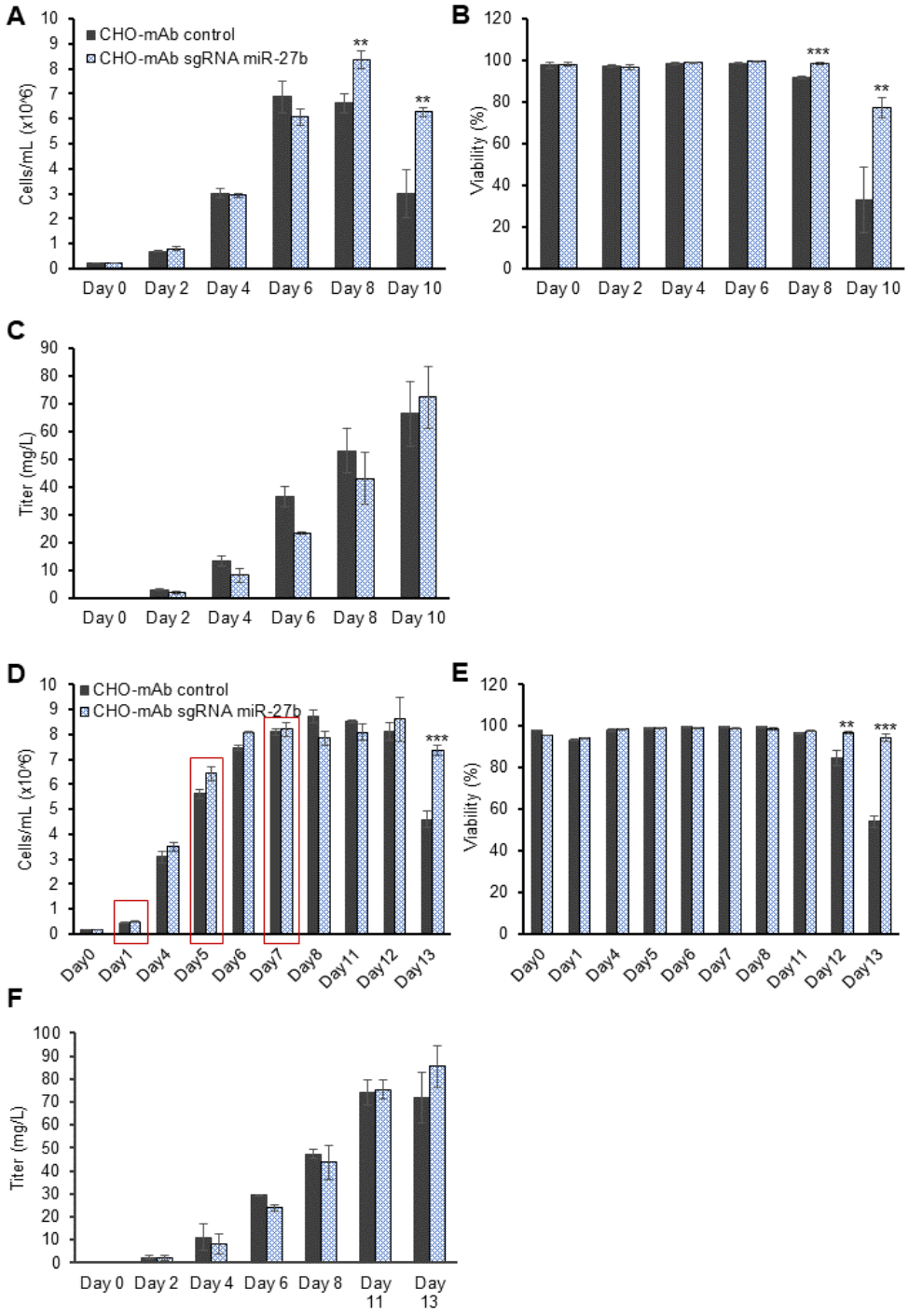

Figure 33: Batch and fed-batch experiments for miR-27b depleted cells led to prolonged cultivation times in batch and fed-batch cultures. A and B) Viable cell density as well as viability compared to the control. C) MiR-27b depletion resulted in lower IgG levels. However, due to increased longevity final titre on day 10 was elevated compared to control. D and E) Viable cell density and viability after depletion of miR-27b in fed-batch cultures. F) Levels of expressed mAb compared to the control. (** $p < 0.01$ vs control, *** $p < 0.001$ vs control; n=3).

In this study it was demonstrated that the extension of longevity can elevate levels of expressed therapeutic protein and makes the depletion of miR-27b potential tool for cell line engineering. MiR-27 was first identified as more abundant during hypothermic conditions. RNA was extracted and mature miRNA expression was assessed. As targeting efficiency of miR-27b was low (4.2.1) in the mixed population (CRISPR) we wanted to investigate if the expression remains constant over time. Furthermore, we wanted to assess if the passenger strand was targeted as well. Therefore, the expression of miR-27b* (miR-27b-5p) was analysed as well in exponential phase (Figure 34 A and B).

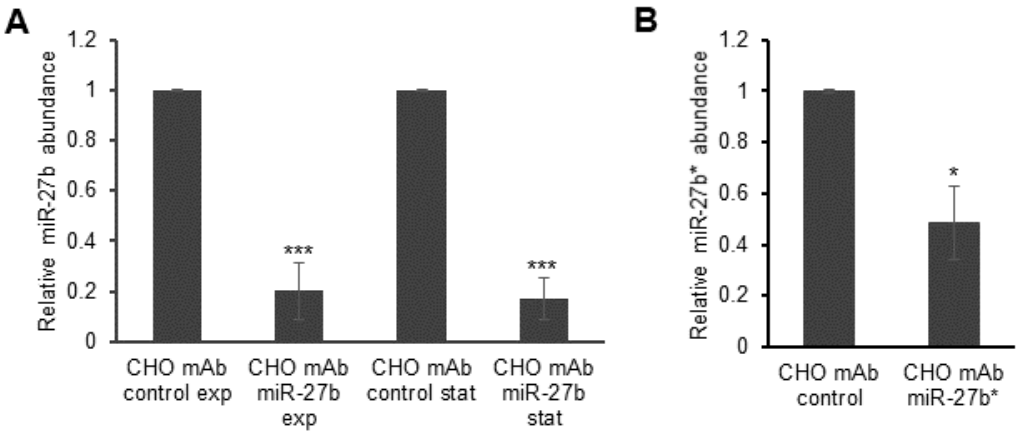

Figure 34: Expression of miR-27b in exponential/stationary growth phases and miR-27b* expression. A) Expression of miR-27b in exponential (day 3) and stationary phase (day 5) of batch cultures. B) Expression of miR-27b* in exponential phase (day 3) after targeting with CRISPR. (* $p < 0.05$ vs control, *** $p < 0.001$ vs control; n=3).

Significant depletion of miR-27b was observed in exponential growth (day 3) as well as stationary phase (day 5) compared to the control on the same days.

The passenger strand (miR-27b-5p) exhibited lower abundance as well. Due to changes in confirmation of the precursor processing might be impaired after targeting with CRISPR/Cas9. As increasing productivity was generally the more interesting phenotype the depletion of miR-24 was further investigated.

Extended viability in this cell line is accompanied by the observation, that targets of miR-27 in CHO-S Fc (see section 4.1.4) seem to be involved in apoptosis. Therefore, a study for DE proteins using mass spectrometry could give further insight in how depletion of miR-27 increases viability in late culture stages.

4.2.3 CRISPR mediated depletion of miR-24 boosts specific productivity and mAb titre in mixed populations of CHO-K1 cells

As described in 4.2.1.1, depletion of miR-24 led to increased IgG titre on each day of the culture due to increased specific productivity. Growth was increased which led to reduced culture duration presumably due to higher nutrient demands or waste accumulation. It was indicated in the literature that the passenger strand might be targeted as well when CRISPR/Cas9 is used. To investigate whether this was the case for our cells, we analysed the expression of miR-24-3p and its passenger strand miR-24-5p using TaqMan® small miRNA assays (Figure 35 A and B). We found, that both mature miR-24-3p levels and miR-24-5p were significantly downregulated. The original sgRNA was designed to target the seed region of miR-24-3p. This demonstrated that even when targeting miR-24-3p the cellular levels of the passenger strand miR-24-5p, was affected similarly. To assess if incorrect processing of the precursor was the cause of this simultaneous decrease of both miRNAs, the expression of pre-miR-24 was measured using specific primers by RT-qPCR. Pre-miR-24 was significantly more abundant compared to the control suggesting an inhibition of its processing due to changes in Drosha or Dicer recognition sequences (Figure 35 C). MiR-24 is located proximal to its cluster members and we were concerned about possible effects on the other miRNAs. As a result, we analysed the expression of miR-23a, miR-23b, miR-27a and miR-27b in cells where miR-24 was targeted. Targeting miR-24 had no effect on the abundance of other members of the cluster (Figure 35 D) which was evident based on comparable Ct values. However, the Ct of miR-24 was higher compared to the control which indicated lower expression. To analyse the effect of miR-24 depletion, cells were seeded with with an initial cell density of $2x10^5$ cells/mL using TPP 50 mL TubeSpin® bioreactor tubes and a culture volume of 5 mL. Cells were grown BalanCD CHO Growth A media and samples were taken every 48 hours to assess viable cell density and for ELISA to assess productivity. Depletion of miR-24 led to a significant increase in growth on day 2, day 4 and day 6 (Figure 35 E). On day 8 significantly reduced viable cell density was observed compared to the control. This was reflected in viability (%) which started to decline earlier (day 8) when compared to the control (Figure 35 F). This reduction in viability could presumably be related to increased nutrient demands or faster waste accumulation in cultures with faster growth/enhanced productivity. And as before the titre appears to be negatively impacted perhaps due to the low viability on day 10 and an eventual release of proteases into the media.

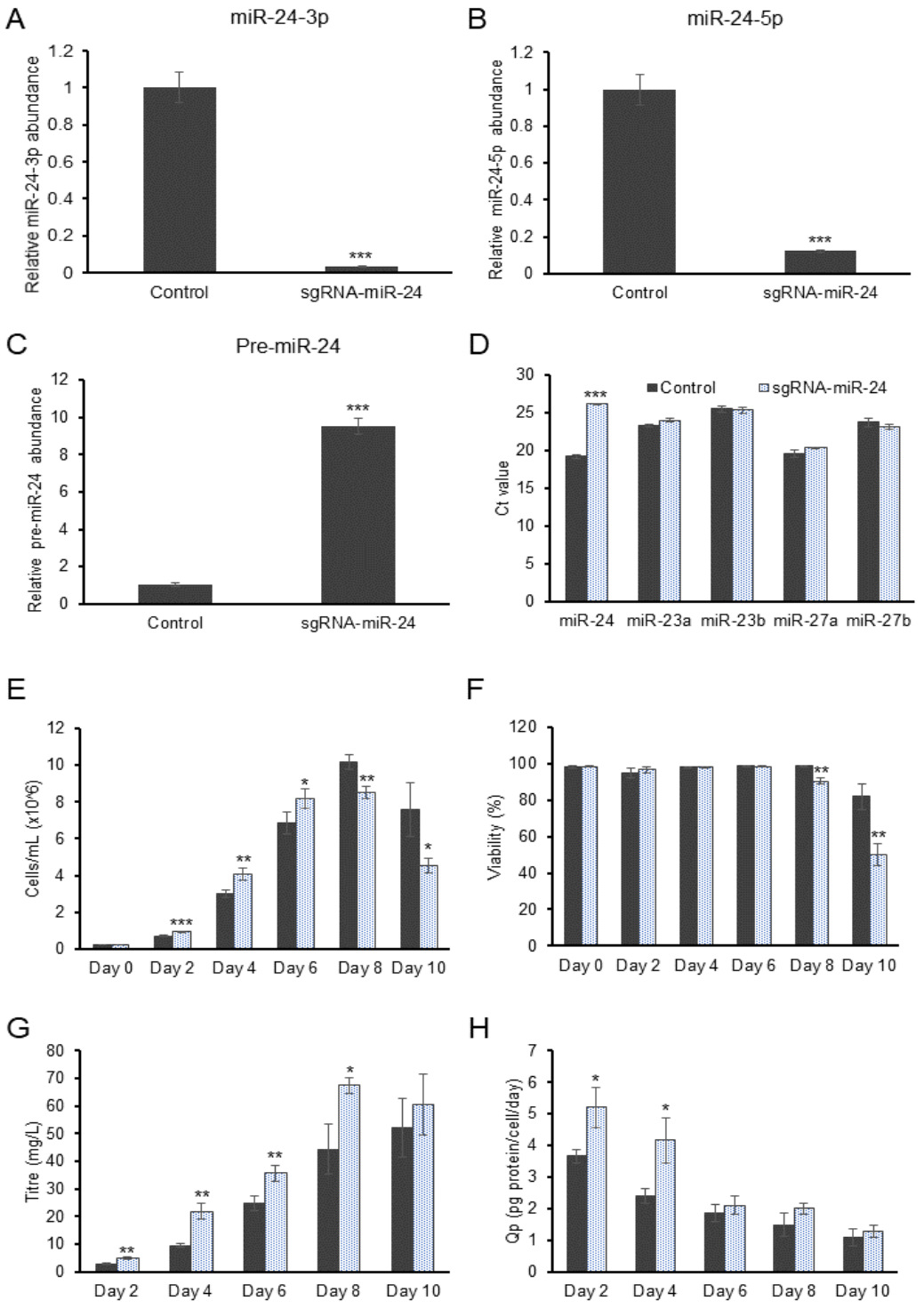

Figure 35: Depletion of miR-24 using CRISPR/Cas9 led to increased producitivity and growth in batch cultures. A and B) Expression of miR-24-3p and miR-24-5p after targeting. C) Pre-miR-24 expression compared to control. D) Expression of proximal located members of the miR-23 cluster. E) Viable cell density after knockout of miR=24 compared to control F) Viability compared to control population. G and H) IgG levels and specific productivity after depletion of miR-24. (* $p < 0.05$ vs control, *** $p < 0.001$ vs control; n=3

IgG levels were significantly elevated from day 2 onwards to day 8. Day 10 also exhibited increased titre but not significantly. The increase was due to also increased specific productivity on day 2 and day 4 compared to the control culture (Figure 35 G and H).

Reduced levels of mature miRNA as well as passenger strand led us to question which miRNA was responsible for the observed effects. Therefore, miRNA mimics for miR-24-3p, miR-24-5p and a control mimic were transiently transfected into the parental CHO-K1 mAb expressing cell line (Figure 36 A to C). After transfection no effect on day 2 was observed for all mimics. However, four days post-transfection, growth of cells transfected with miR-24-3p mimic was significantly reduced compared to the control. An effect on cell growth was also observed on day 4 for control and miR-24-5p overexpression compared to transfection reagent only (Figure 36 A). Overexpression of miR-24-3p and miR-24-5p was quantified and an increase of ~60 fold for miR-24-3p and ~650 fold for miR-24-5p was seen. The general abundance of miR-24-5p is very low (Ct ~28) compared to miR-24-3p (Ct ~18) which explained the large fold change after transfection of mimics (Figure 36 A).

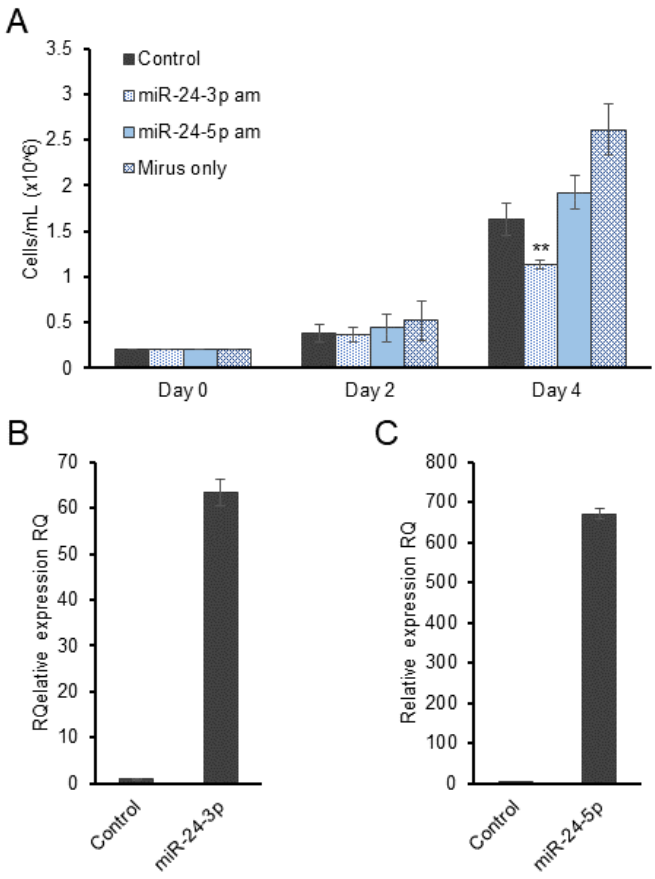

Figure 36: Transient transfection of miR-24 mimics and resulting phenotype in CHO-K1 mAb. A) **Growth compared to control for o**verexpression of miR-24-3p and miR-24-5p on day 2 and 4 after transfection. B and C) Overexpression of miR-24-3p as well as miR-24-5p using miRNA mimics (** $p < 0.01$ vs control; n=3)

To investigate further if the phenotype is observed at the clonal level as well, clones were isolated and assessed in batch cultures. Six clones were selected out of 31 screened for miR-24 and which exhibited low miR-24 expression as well as showed fast proliferation rates (Figure S 9). All 6 clones showed increased growth behaviour compared to the control population (mixed population) and reached the peak cell density approximately two days earlier (Figure 37 A). Similar, to miR-24 depletion in a mixed population the culture duration and viability on day 8 and day 10 were reduced (Figure 37 B).

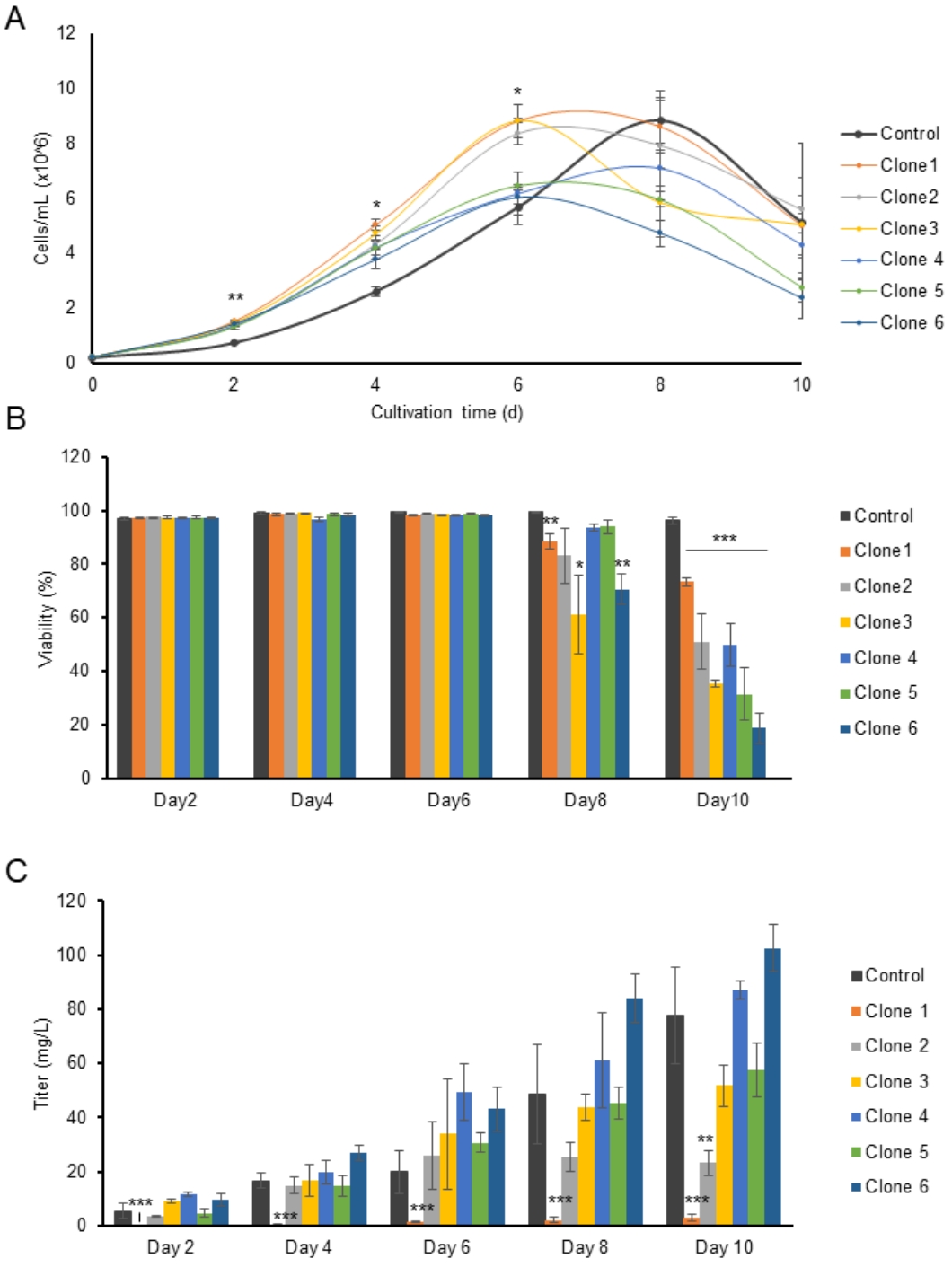

Figure 37: MiR-24 depleted single cell clones showed increased growthrates at the expense of productivity. A and B) Viable cell density and compared to the control mixed population. Viability was reduced on late stages of the culture. C) IgG levels for each clone compared to the control population. (* $p < 0.05$ vs control, ** $p < 0.01$ vs control; *** $p < 0.001$ vs control: n=3)

The titres achieved showed no improvement but a considerable variation for all six clones. As clones were selected based on growth profiles the selection was biased purely on growth and not on productivity. Furthermore, it could come down to clonal effects as six clones represent a very limited panel.

To investigate clones further for expression of miR-24-3p, miR-24-5p and pre-miR-24 we isolated total RNA from each clone. Expression of both mature miRNAs was quantified using TaqMan® miRNA assays. The ΔCt levels were higher compared to the control which indicates lower abundance of miR-24-3p as well as miR-24-5p (Figure 38 A). Furthermore, levels of miR-24-5p seemed to be lower as part of targeting of miR-24-3p by CRISPR.

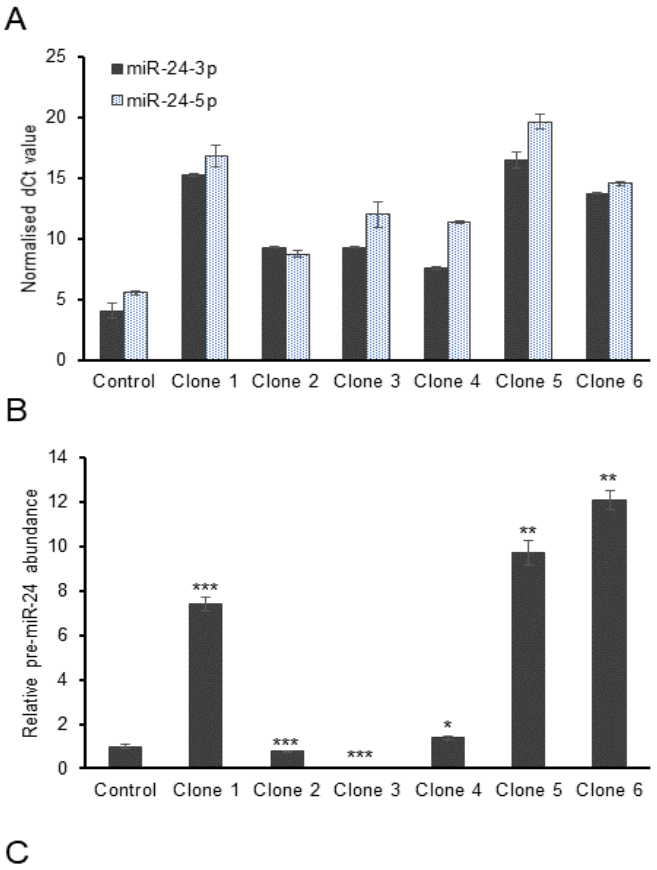

C

Sample	Primer	%WT	%Indel
Clone 4	miR-24-1	0.35%	99.65%
Clone 4	miR-24-2	77.61%	22.39%
Clone 5	miR-24-1	0.28%	99.72%
Clone 5	miR-24-2	0.00%	100%
Clone 6	miR-24-1	0.41%	99.59%
Clone 6	miR-24-2	0.13%	99.87%

Figure 38: Expression of miR-24-3p, miR-24-5p and pre-miR-24 in all single cell clones. A) Expression of miR-24-3p as well as miR-24-5p was displayed in ΔCt values. Higher values indicate a lower abundance. B) Pre-miR-24 abundance for clones 1, 4, 5 and 6. Clone 2 and 3. C) NGS for indels for clones 4, 5 and 6. (* $p < 0.05$ vs control, ** $p < 0.01$ vs control, *** $p < 0.001$ vs control; n=3).

To investigate if pre-miR-24 was also accumulated in clones as previously observed for the mixed population (section 4.2.3), its levels were analysed using RT-qPCR. It was shown, that the expression in Clone 2 and 3 was significantly lower compared to the control (Figure 38 B). Clone 1, 5 and 6 showed an accumulation of pre-miR-24. Clone 4 showed only a mild increase in the miR-24 precursor. Clone 4,5 and 6 were analysed by indel sequencing and it was shown that for clone 5 and 6 no wildtype sequence was

detectable for miR-24-1 and miR-24-2 which indicates a clonal origin (Figure 38 C). For clone 4 no wildtype sequence was detectable for miR-24-1 however, only 22% of miR-24-2 reads showed insertions or deletions. This could mean that clone 4 did not originate from a single cell clone. Furthermore, the observation that pre-miR-24 is only slightly enriched, showed that pre-miR-24 processing is only partially impaired and that at laeast one allele of each paralogue is still fully functional and expressed.

Due to the mechanism of a miRNA action, targets of miR-24 should be upregulated after depletion. To investigate if target mRNAs were upregulated we assessed the expression of c-Myc and CDKN1B in mixed depleted population as well as in three isolated clones (Clones 1, 2 and 3). Both were shown to be direct targets of miR-24 and are important regulator genes in terms of cell cycle progression, growth and showed important roles in cancer progression (Figure 39). The expression c-Myc as well as CDKN1b was signifcanlty higher in mixed population which indicates reduced levels of miR-24. For all three assessed clones the expression of c-Myc seemed inconclusive but CDKN1b was more abundant.

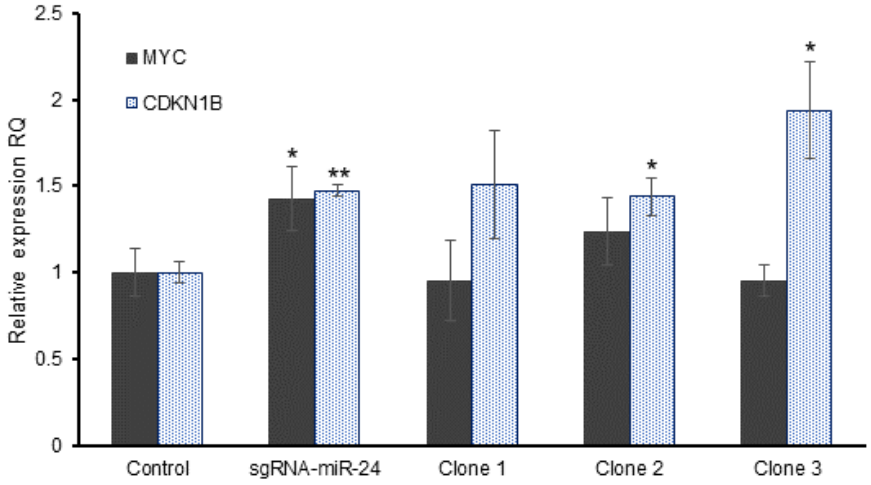

Figure 39: Expression of validated mRNA targets of miR-24 after CRISPR/Cas9 mediated depletion in CHO-K1 mAb mixed population. As validated targets c-Myc as well as CDKN1B were chosen and assessed for expression using RT-qPCR. Total RNA was extracted in exponential growth phase for mixed population and clone 1,2 and 3, reverse transcribed and specific primers of c-Myc and CDKN1B were used to assess expression. Expression was compares to beta-actin which served as endogenous control. (* $p < 0.05$ vs control, ** $p < 0.01$ vs control; n=3).

It is a commonly observed phenomenon that mammalian cells in cell culture including cancer cells use aerobic glycolysis instead of the more efficient mitochondrial based oxidative phosphorylation for energy production. Glycolysis and subsequent conversion of pyruvate to lactic acid decreases the pH of the media and measuring the extracellular acidification rate (EACR) is a good indicator for the assessment for cells undergoing enriched glycolysis. EACR can also be an indicator for higher CO_2 production due to increased citric acid cycle activity. Anaerobic glycolysis does not require oxygen for the conversion. Oxidative phosphorylation however, uses electron acceptors such as oxygen for the synthesis of ATP. Therefore, measurement of the oxygen consumption rate (OCR) and EACR can provide information of the preferred metabolic process utilised by cells. As the phenotype of miR-24 depleted cells demonstrated enriched growth and increased specific productivity it could be assumed that energy demands are increased leading to higher rates of EACR or OCR.

Assessing OCR and EACR for miR-24 depleted mixed population and all six derived clones showed that OCR and EACR were reduced compared to the non-targeted control (Figure 40). On the contrary the control showed higher OCR and EACR compared to miR-24 depleted mixed population and all six clones. Having observed a higher productivity or enhanced growth would indicated higher demands for nutrients and

eventually an increase in OCR/EACR. In fact, the production of lactic acid or CO_2 (EACR) remained low compared to the control. The metabolic potential which describes the ability to meet an energy demant using glycolosis or oxidative phosphorylation however, seemed similar for EACR.

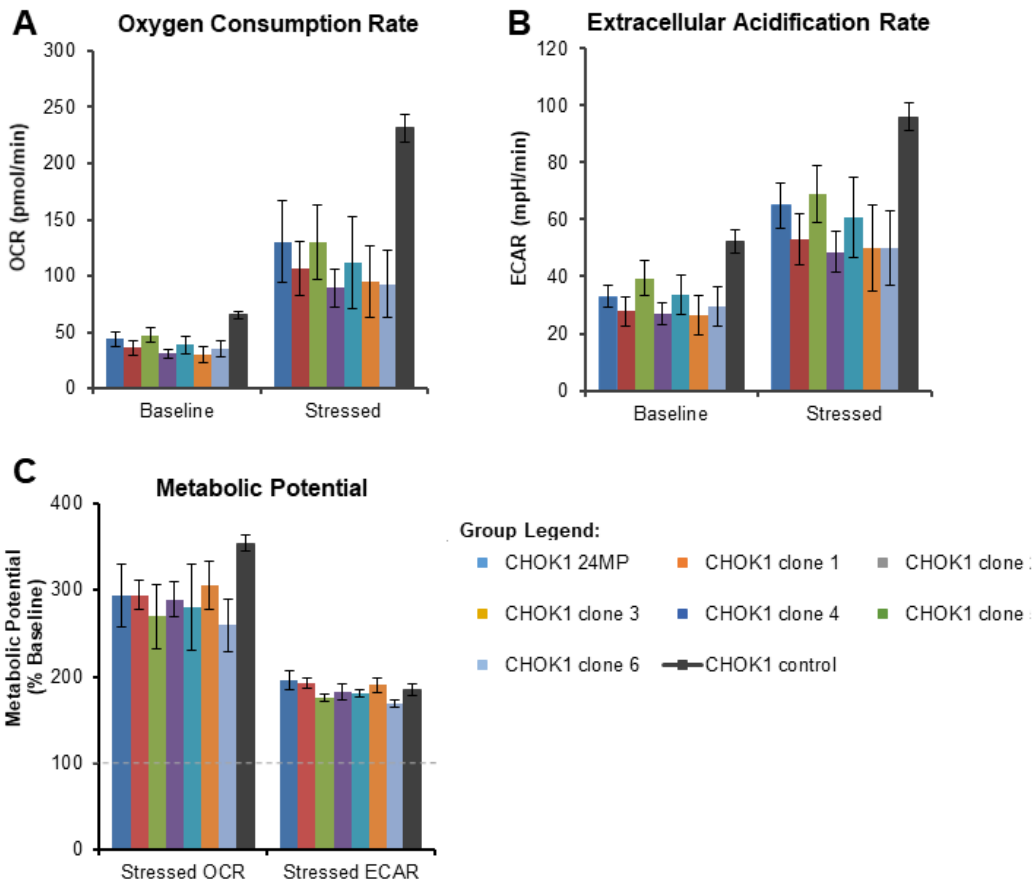

Figure 40: Impact of depletion of miR-24 on oxygen consumption rate as well as extracellular acidification rate. Both were measured using Seahorse FX analyser using a cell energy phenotype test. Stress was induced by small molecule-based blocking of either glycolysis or oxidatative phosphorylation. A) OCR baseline and stressed conditions for miR-24 depleted mixed population and clones. B) Extracellular acidification rate baseline and stressed conditions for miR-24 depleted mixed population and clones. C) Metabolic potential for stressed OCR and EACR of miR-24 depleted mixed population and clones.

Depletion of miR-24 using sponge decoys in CHO-S Fc showed significant changes on glycosylation of the recombinant expressed protein. Hence, we wished to investigate if CRISPR/Cas9 mediated depletion of miR-24 resulted in changes in glycosylation on the expressed mAb.

4.2.3.1 *Impact on glycosylation due to the depletion of miR-24 using CRISPR/Cas9*

To investigate if the depletion of miR-24 had an impact on glycosylation, 50 mL of cell culture supernatant was taken and purified using protein-A chromatography as described in 3.3.2 (Figure 41 A). Samples were analysed for changes in glycosylation pattern using LC/LFR-MS/MS as described in 3.3.3 and the work was performed by Dr. Sara Carillo (NIBRT). Figure 41 B shows all identified glycoforms regarding their intensity and retention time in the chromatogram. Figure 41 C and D shows differential abundance of glycosylation. Each dot on the line represents a different species e.g. M3, FM3 etc. It was observed that all mannose species were downregulated due to CRISPR mediated depletion of miR-24. When compared to the Fc fusion depletion of miR-24 using sponges resulted in higher abundance of mannose species with several genes being associated with it (compare 4.1.4.1). Proteomic profiling for CRISPR mediated depletion of miR-24 (4.2.3.2) showed that several genes involved in conversion of high mannose species to complex N-glycans were downregulated. These genes were alpha-mannosidase 2 (MAN2A1), alpha-mannosidase 2C1 (MAN2C1) and GDP-mannose 4,6 dehydratase (GMDS). Terminal sialic acid species was inconclusive with a trend to be less abundant with no obvious related genes being differential expressed.

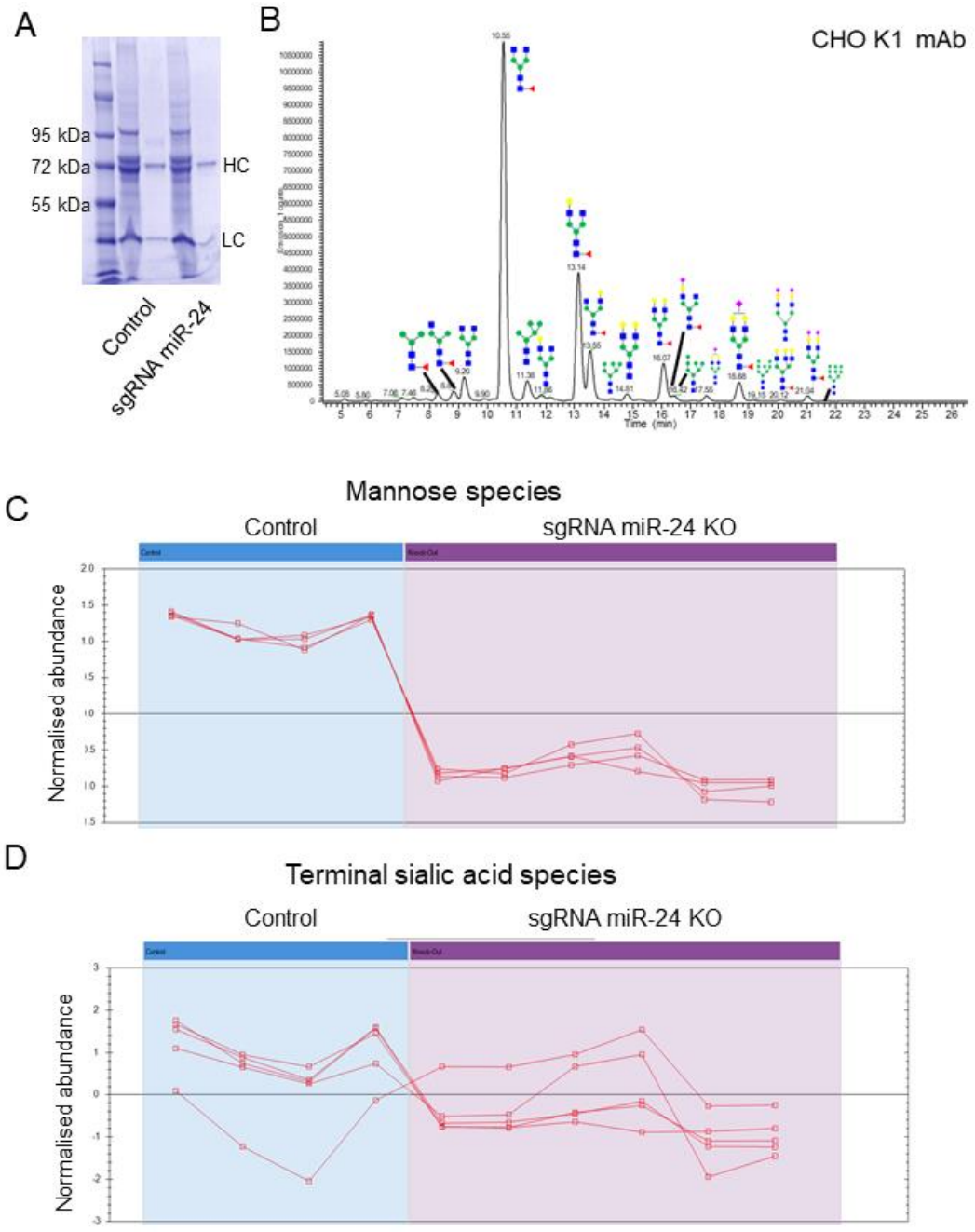

Figure 41: Impact on glycosylation after CRISPR/Cas9 mediated depletion of miR-24 on expressed mAb. A) The expressed IgG was protein A purified out of conditioned media and analysed using SDS-PAGE. B) Chromatogram for retention time and intensity of glycospecies. C and D) Each point represented a different species of glycosylation for mannose and terminal sialic acid e.g. M5, FM3 etc.

Lower levels of mannose species could potentially have a beneficial effect on the IgG function as lower levels might be associated with increased ADCC. To furthermore investigate the proteins involved in the phenotype observed after targeting miR-24 using CRISPR/Cas9, proteomic profiling was the method chosen. As mentioned earlier we identified proteins which were potentially involved in lower abundance of mannose species.

4.2.3.2 Depletion of miR-24 in CHO-K1 mAb leads to an upregulation of ribosomal RNA biogenesis and the translational machinery resulting in a high productivity phenotype

After targeting miR-24 using CRISPR/Cas9, increased productivity and growth was observed as it was after sponge mediated depletion of miR-24 in several other cell lines. Consequently, we wanted to investigate which proteins were dysregulated and were potentially involved indriving this phenotype. Depletion of miR-24 using CRISPR resulted in 352 (Anova value < 0.05, fold-change >1.20, 2 or more peptides) more abundant proteins. Moreover, 119 had a fold-change higher 1.25 and only 15 showed a fold-change higher than 1.5. For pathway analysis we used proteins with a fold-change of over 1.25. A total of 5098/5093 proteins (control/sgRNA-miR24) was identified before applying filters for DE and statistical analysis (Figure 42 A).

To identify which proteins were potential targets of miR-24, predictive mRNA:miRNA analysis was used (miRWalk2.0). It was demonstrated that out of 119 more abundant proteins 77 were predicted targets of either miR-24-3p or miR-24-5p. Furthermore, 5 proteins were also validated targets (Figure 42 B). Out of 77 predicted targets, 63 were targets of miR-24-3p and 24 being targets of miR-24-5p (10 are shared between both). This makes miR-24-3p the more prominent miRNA but showed that miR-24-5p plays its role as well. With over ~60% being predicted targets of miR-24 we were confident in the lists generated.

A

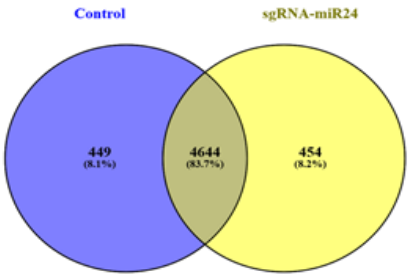

CHO-K1 mAb	miR-24
Total DE	355
More abundant	192
> 1.25	119
> 1.5	15
Total IDs	5098/5093

B

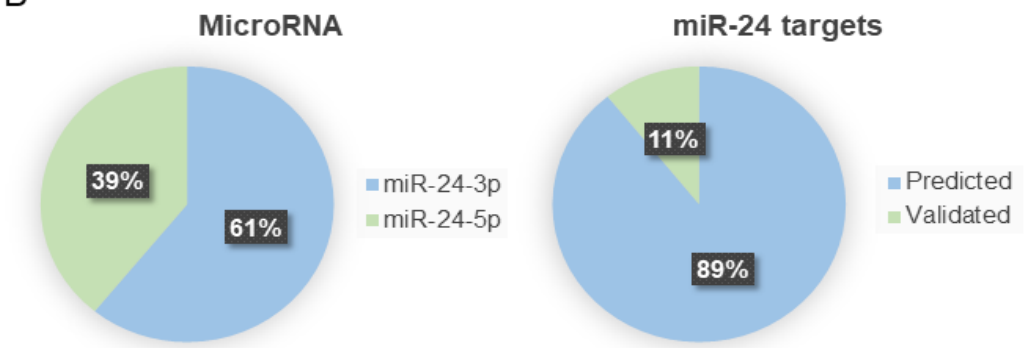

Figure 42: Summary of proteomic profiling for targeting miR-24 using CRISPR/Cas9. A) A total of 5098 and 5093 unique IDs were identified for both groups. A total of 355 proteins were DE with 119 over 1.25-fold and 15 >1.5-fold. B) Out of all 355 DE proteins 67% were predicted or validated targets of miR-24-3p or miR-24-5p.

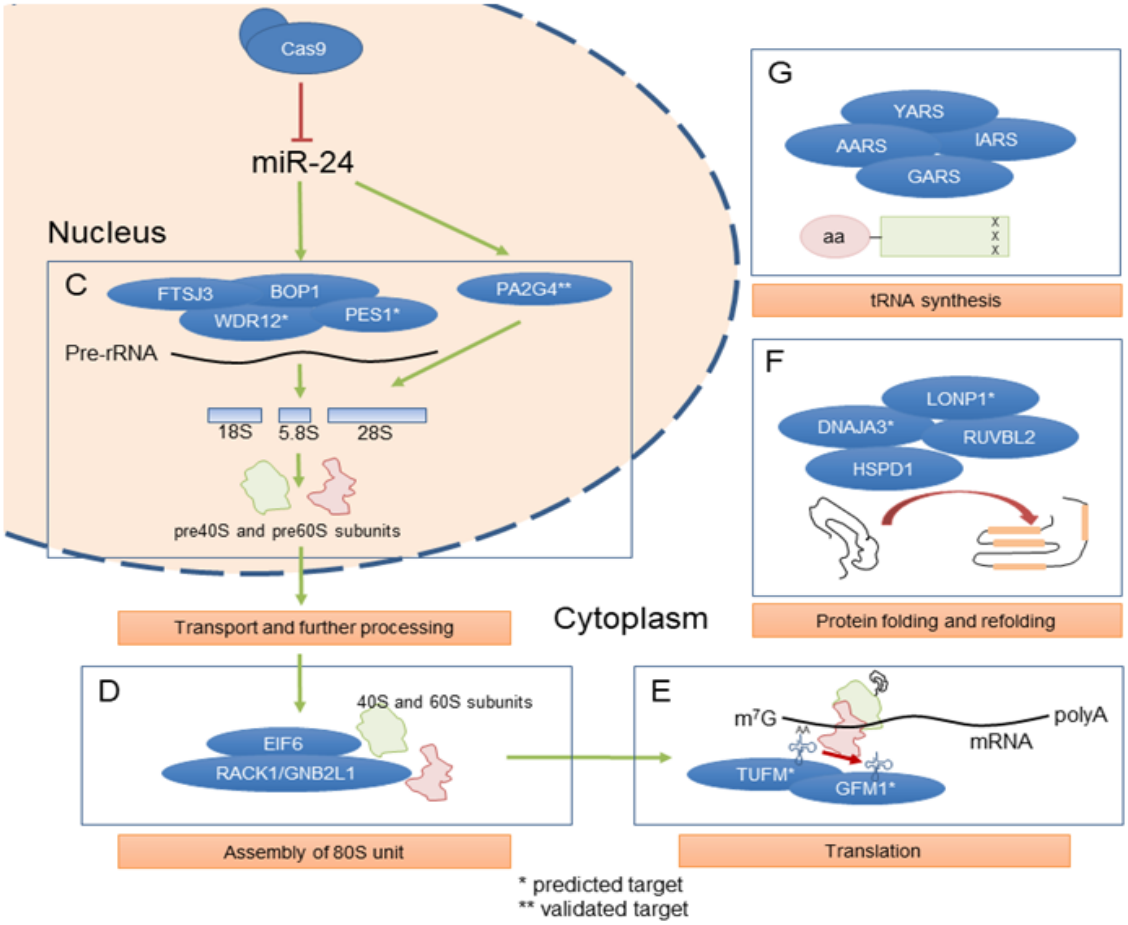

Figure 43: Proteomic profiling combined with pathway analysis for the depletion of miR-24 using CRISPR/Cas9. A) Qualitative and differential expression data after depletion of miR-24 using an Anova-value < 0.05, fold-change >1.20 fold and identification of more than 2 peptides. B) Analysis of predicted and validated targets for miR-24-3p and miR-24-5p. Approximately 60% of all upregulated proteins were targets of either miR-24-3 or miR-24-5p. C to G) Proteins upregulated seemed to be involved in translation, protein folding, rRNA processing and assembly of ribosomal subunits.

To investigate which pathways were overrepresented in the list of DE proteins, pathway analysis was used (Figure 43 C to G). Several more abundant proteins are involved in pre-rRNA and rRNA-processing including BOP1, WDR12 and PES1 which are members of the PeBoW complex (Figure 43 C). Interestingly, proteins involved in the assembly of ribosomal subunits were also upregulated as well including RACK1 and EIF6 (Figure 43 D). Furthermore, TUFM and GFM1, critical proteins involved in recruiting of aminoacyl-tRNAs and removal of deacetylated tRNAs, were more abundant (Figure 43 E). Upregulation of TUFM and GFM1 is accompanied by several tRNA synthetases of i.e. AARS, GARS, IARS and YARS (Figure 43 G). Increased productivity may also activate the unfolded protein response (UPR) which was upregulated. Several proteins were upregulated including RUVBL2, LONP1, HSPD1 and DNAJ3A (Figure 43 F). Interestingly, similar pathways were upregulated in CHO-S Fc expressing cells which were miR-24 depleted using sponges (section 4.1.4.2).

The enrichment of particular biological processes is shown in Table 8.

Table 8: Pathway analysis for depletion of miR-24 using CRISPR/Cas9.

	Depletion of miR-24		
BP	Proteins	P-value	False discovery rate
Translation	20	8,5E-19	2,6E-16
Ribosome biogenesis	13	8,9E-15	1,4E-12
Ribonucleoprotein complex biogenesis	14	3,4E-14	3,5E-12
RNA processing	19	1,5E-13	1,2E-11
ncRNA metabolic process	12	3,5E-10	2,2E-8
RNA splicing	11	4,6E-8	2,4E-6
Translational elongation	8	6,0E-8	2,7E-6
ncRNA processing	9	2,7E-7	1,0E-5
rRNA processing	7	8,2E-7	2,8E-5
rRNA metabolic process	7	1,1E-6	3,0E-5
mRNA processing	10	1,6E-6	4,1E-5
mRNA metabolic process	10	5,1E-6	1,2E-4
tRNA metabolic process	6	5,9E-5	1,3E-3
Response to unfolded protein	5	1,1E-4	2,4E-3
Protein folding	6	3,9E-4	7,6E-3
Response to protein stimulus	5	5,5E-4	1,0E-2
tRNA aminoacylation for protein translation	4	5,7E-4	9,8E-3
Amino acid activation	4	5,7E-4	9,8E-3
tRNA aminoacylation	4	5,7E-4	9,8E-3
tRNA processing	3	3,0E-2	3,9E-1

To create a study which not only involved proteomic profiling but also transcriptomics, RNA sequencing was used. The purpose was to investigate further which genes and proteins are influenced by depletion of miR-24 and to increase the confidence in our lists generated by proteomics. Increased confidence might also help in the selection of cell line engineering targets. Therefore, total RNA was isolated with samples taken during exponential growth phase in biological triplicates. RNAseq using poly-A enrichment was used to allow the removal of ribosomal RNA. After fragmentation and addition of linkers the sample were run on an Illumina HiSeq 2500 instrument. For differential expression analysis DESeq2 was used and Wald test to generate p-values as well as log2-fold changes. Library preparation, sequencing and analysis was performed by Genewiz.

On average samples showed total reads between 46,948,472 and 55,899,929 with good quality scores (>28). For all reads, ~71-78% were mapped to the reference genome (Figure 44 A). Raw dispersion values were fitted to a common mean to improve testing accuracy.

Overall, 9810 genes were differentially expressed using no statistical restrictions. Using a p-value <0.05 showed 525 genes which are significantly differential expressed without applying log2 fold change. Out of 525 DE genes, 200 showed a higher abundance and 325 showed lower expression compared to the control. The corresponding heatmap showed a good distribution of abundances between the genes and samples (Figure 44 C). Applying a log2 fold change of 0.58/-0.58 showed that 32 genes were upregulated by 1.5-fold and 92 were 1.5-fold less abundant.

A

Sample	Depletion of miR-24		
	Total reads	Mapped reads	% total/mapped
CHO-K1 mAb control-1	44871600	32134545	71.61
CHO-K1 mAb control-2	48636683	35419222	72.82
CHO-K1 mAb control-3	52526403	38128962	72.59
CHO-K1 mAb sgRNA-24-1	53237081	40720559	76.49
CHO-K1 mAb sgRNA-24-2	45411015	33865177	74.57
CHO-K1 mAb sgRNA-24-3	53943216	41980769	77.82

B

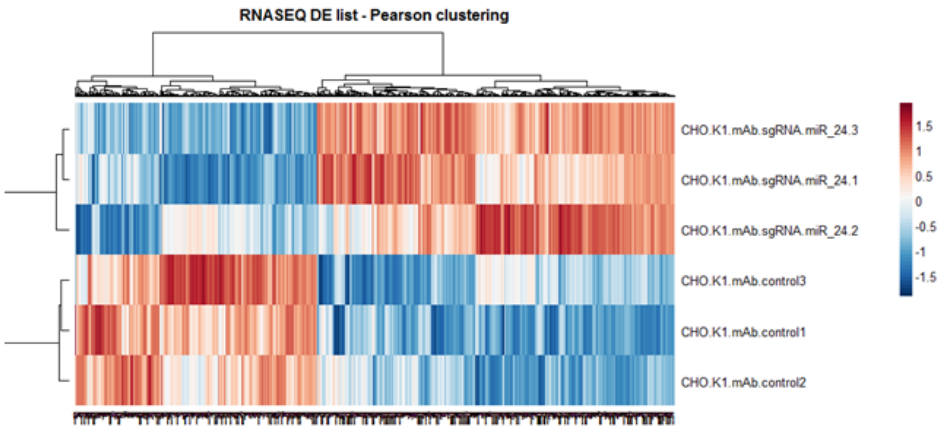

C

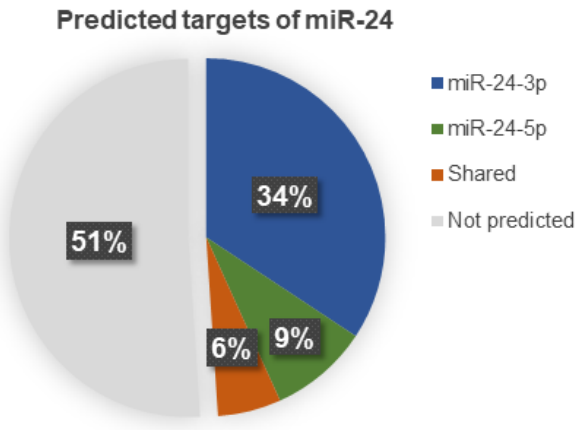

Figure 44: RNAseq data summary for the depletion of miR-24 using CRISPR/Cas9 in CHO-K1 mAb and predicted targets. A) Total and mapped reads in comparison with the CHO reference sequence. B) Heatmap of abundances of all 525 DE genes showed clear distribution for most genes. C) Predicted targets of miR-24-3p and miR-24-5p as well as shared genes. As DE was considered every gene with a fold change > ±1.50 and anova > 0.05.

We compared both lists obtained from proteomic profiling and RNAseq to investigate if we could relate same pathways previously identified (4.2.3.2), keeping in mind that transcription may or may not be reflected in protein expression. Comparing all 525 DE genes with 355 DE proteins showed that only 17 genes are common between our proteomics and transcriptomics data (Figure 45).

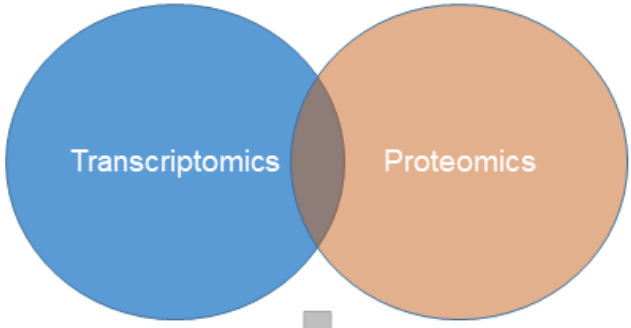

	Depletion of miR-24		
BP	Proteins	P-value	False discovery rate
ncRNA metabolic process	4	4,3E-2	9,5E-1
tRNA aminoacylation for protein translation	2	4,3E-2	9,5E-1
amino acid activation	2	4,3E-2	9,5E-1
tRNA aminoacylation	2	8,5E-2	9,8E-1
rRNA processing	2	8,8E-2	9,6E-1
rRNA metabolic process	2	4,3E-2	9,5E-1

Figure 45: Comparison of lists for DE proteins generated using proteomic profiling and RNAseq for CRISPR/Cas9 mediated depletion of miR-24 showed only a limited overlap. Overlap of DE genes and DE proteins showed that only 17 matched. Pathway analysis of 17 matched proteins/genes showed strong evidence for regulation of rRNA processing, tRNA processing and amino acid activation indicating involvement in translation.

However, the 17 common targets showed that miR-24 is involved in regulating genes in pathways for rRNA processing, tRNA processing and amino acid activation. The same pathways were upregulated in CHO-S Fc as well as CHO-K1 mAb (sponge mediated depletion of miR-24) providing a strong evidence that miR-24 is involved in regulation of ribosomal biogenesis as well as translational regulation (Figure 45 B).

Three genes which were demonstrated higher abundance in all our lists were highlighted as potential engineering targets: TUFM, GFM1 and HSPD1. TUFM and GFM1 were also predicted miR-24 targets.

4.2.4 Multiplex genome engineering of miRNAs using CRISPR/Cas9 to target two miRNAs simultaneously

To investigate if it is possible to target two miRNAs at the same time or to delete a specific sequence within the miR-23 cluster we designed our vector to express two different sgRNAs which has been used by other laboratories to delete larger genomic sequences. Previous results demonstrated that the deletion of the whole miR-23 cluster may lead to a beneficial phenotype. We proposed the deletion of the whole cluster by using CRISPR to target up- and downstream of the cluster (compare section 1.3.3). To clone a second sgRNA into the same vector we designed primers to amplify the region which includes the U6 promoter, the integration site for the gRNA as well as the scaffold, including termination site. As a vector we chose our already proven plasmid which expressed sgRNA-miR-24 to target miR-24. To clone the second sgRNA we amplified the U6 promoter, sgRNA, scaffold and terminator sequence for either miR-23a or miR-23b which were already cloned and proven to be functional into PX459. Primers including restriction enzyme sites for XbaI as well as KpnI were used to ensure directional ligation of the PCR product. Insertion was confirmed using standard Sanger sequencing. Figure 46 A shows the cloning strategy for the expression of two sgRNAs simultaneously. After successful ligation was confirmed the plasmids were amplified and transfected together with the control into CHO-K1 mAb expressing cells. It was demonstrated that miR-23a as well as miR-24 levels were significantly reduced upon targeting both with one plasmid (Figure 46 B). Furthermore, mature miRNA expression of miR-23b and miR-24 was significantly reduced compared to the control (Figure 46 C).

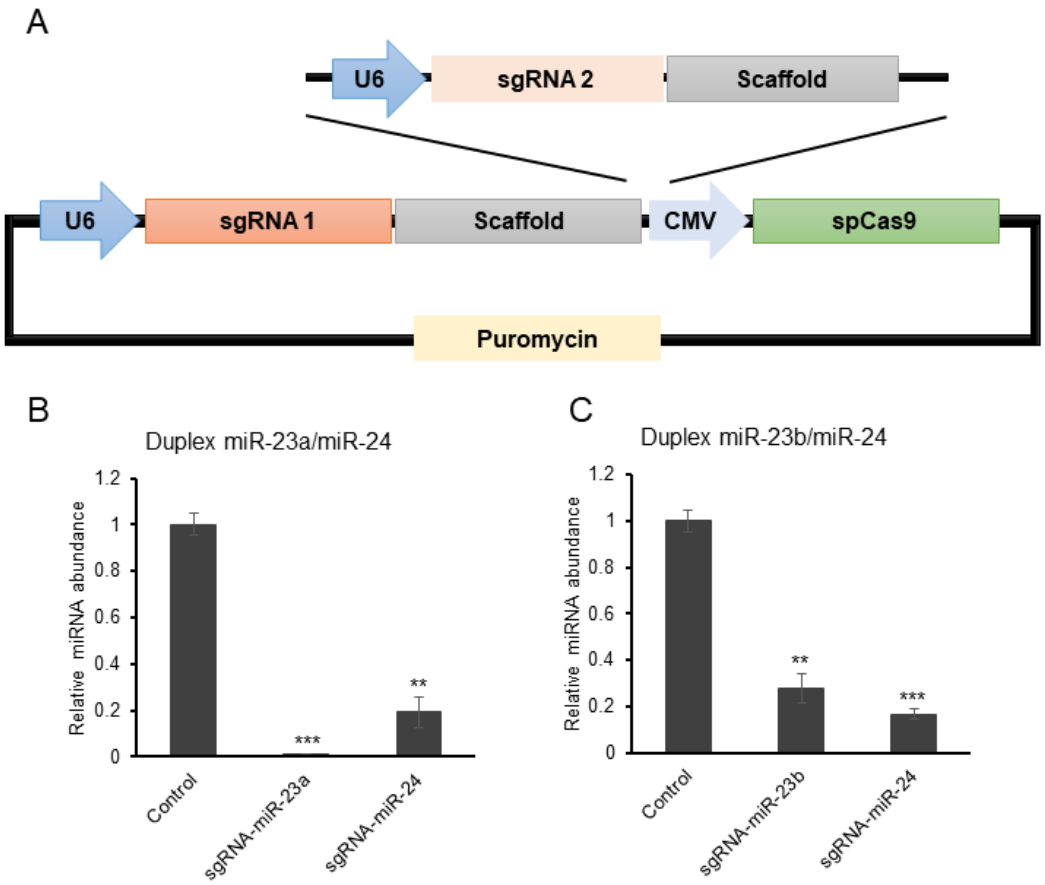

Figure 46: Cloning strategy for targeting more than one miRNA at the same time. A) A second sgRNA was cloned into the same vector including U6 promoter, sgRNA scaffold as well as termination sequence. B and C) The sgRNA for miR-23a as well as miR-23b were cloned into the vector already expressing the sgRNA for miR-24. Mature miRNA expression was analysed using TaqMan® miRNA assays. (** $p < 0.01$ vs control, *** $p < 0.001$ vs control; n=3).

By targeting miR-23 and miR-24 we assumed miR-27 located in the middle would be deleted. Mature levels of miR-27a and miR-27b were analysed however no changes in mature levels were evident.

Targeting miRNAs using CRISPR/Cas9

Sponge decoy technology has been demonstrated to be a viable tool for miRNA engineering. However, certain drawbacks i.e. the necessity for a reporter gene led us to another strategy using the CRISPR/Cas9 system. Advantages are for example the ease of use and the possibility for transient use without integration of plasmids into the host genome. In CHO cells it has not been published that CRISPR can be used to target miRNAs and therefore we needed to demonstrate its utility. We designed sgRNAs to target the seed region of the functional miRNA (-3p) for each member of the miR-23 cluster. It was also possible to target miR-24 with only one sgRNA. The reduction of each miRNA member of the cluster was observed compared to the control (Figure 29). Furthermore, NGS data as well as data generated from Sanger sequencing and Surveyor® assays indicated successful targeting and generation of indels in the seed sequence of every miRNA member (Figure 28). We additionally screened single cell clones to investigate if it was possible to obtain clones with complete knockouts of the miRNA target. We found clones for every miRNA target that showed a significant reduction of mature miRNA expression compared to the control (Figure 32). As a comparison to previous work in the same cell line performed by Dr. Paul Kelly and Dr. Noelia Sanchez, we analysed the phenotype which was shown to be very comparable to the sponge decoy approach (Figure 31). In addition, we found another interesting phenotype which has not been demonstrated using sponge decoy technology: depletion of miR-27b led to prolonged culture lengths in batch as well as fed-batch cultures. However, titres were compromised but due to longer cultures, elevated IgG levels were observed.

Similarly, to the depletion of miR-24 using sponge decoy technology in CHO-K1 mAb a significant increase in IgG levels was observed when miR-24 was targeted with CRISPR/Cas9. Additionally, growth was boosted which has not been demonstrated using a decoy for miR-24. This phenotype was especially interesting and we followed up with several methods to investigate the molecular impact of the miR-24 depletion. We performed label-free HPLC-MS/MS for proteomic profiling as well as transcriptomic profiling using RNAseq. We demonstrated that several genes and proteins involved in pre-rRNA biogenesis, ribosome maturation, translation, tRNA activation as well as unfolded protein response showed higher abundance.

Lastly, we investigated if two miRNAs can be simultaneously targeted using a multiplex approach to investigate if we can delete larger sequences in the genome. We used a strategy by expressing two sgRNAs which were designed to target up- and downstream the miR-23 cluster. It was demonstrated that miR-23 and miR-24 could be targeted but miR-27 seemed to be unaffected. Local indels might inhibit miR-23 and miR-24 and another strategy to delete the whole cluster should be discovered in the future.

4.3 Establishing a platform for genome-wide “loss of gene function” studies in Chinese Hamster Ovary cells using a CRISPR/Cas9 library

CRISPR/Cas9 can be used efficiently to target genes and miRNAs to generate gene/miRNA deficient cell lines. A further application of CRISPR/Cas9 is the implementation of genome wide “loss of gene function” studies as previously reported by several research groups (Agrotis & Ketteler, 2015; Shalem et al., 2015; T. Wang et al., 2014). Based on using a library of sgRNA this approach allows the targeting of all genes in the genome which enables the screen for gene-function. Our library contained 87,897 different sgRNAs, targeting 19,150 mouse genes, which can be purchased as a lentiviral delivery system. For the library we chose to transduce a CHO-K1 cell line expressing a mAb and human codon optimised spCas9. The most critical step for this approach is to guarantee maximum coverage of the library but also to ensure a low number of integration events - ideally one copy per cell. However, one beneficial feature of CHO-K1 cells as recombinant protein production hosts is their resistance to viral infections. The aim of this project was to attempt to identify genes which are responsible for beneficial phenotypes created after exposure of bioprocess relevant conditions i.e. high osmolality, ammonia, lactate. Furthermore, a screen for genes linked to a high producing phenotype was conceived. The basic premise of the approach is that under certain environmental conditions certain genes can confer a survival advantage and others may compromise survival – essentially the Darwinian theory of “Survival of the fittest”. By sequencing the “surviving” cells in a given stress we expect to find some sgRNAs enriched (loss of their target gene is beneficial) and others depleted or lost (loss of the target gene is detramental). Many more sgRNAs would be expected to remain unchanged compared to the original library.

Preliminary data showed, that it is possible to reduce integration events to three per cell using diluted lentiviral particles which would be sufficient to use the library. Nevertheless, the transduction efficiency was shown to be very low and would not ensure a multiple fold coverage of the library. To overcome that problem different transfection methods were considered and applied to investigate the effect on integration events. Nucleofection seemed to be the most suitable method to ensure high efficiency combined with low copy numbers of the plasmid. Figure 47 summarises the workflow for the CRISPR library.

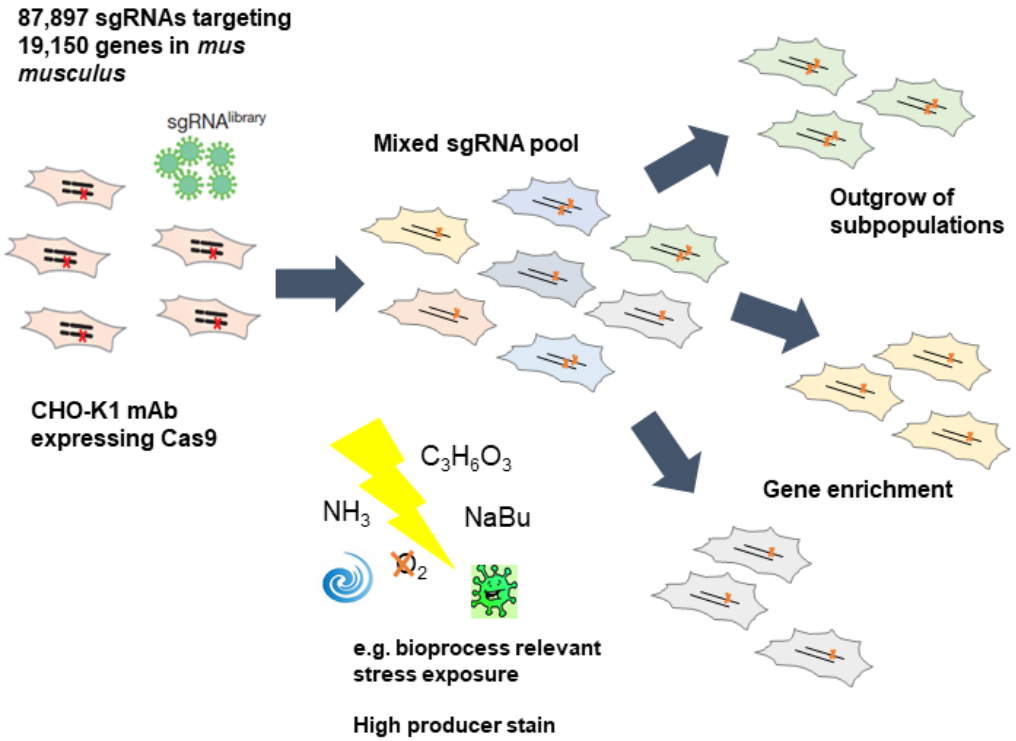

Figure 47: Workflow for the introduction of the CRISPR/Cas9 sgRNA library in CHO. Plasmids of the sgRNA library are packed into a lentiviral system which allows the integration of only 1-2 copies per cell. The libray did not express Cas9 which required the generation of a Cas9 expressing cell line before the introduction of the pooled library. After integration of the library, the mixed population was exposed to stress conditions to enrich for subpopulations in which the knocout of a gene led to survival or better adaption. Guide RNAs which were enriched or depleted were identified using NGS.

The first step was to test whether the library can be delivered using a lentiviral delivery system.

4.3.1 Amplification of the CRISPR/Cas9 library and determination of the optimal delivery method

To ensure a sufficient level of amplification and coverage of every sgRNA, the plasmid library was transformed into highly electro-competent E. coli DH5α-E cells. As theoretically not every plasmid is amplified with the same efficiency the cells were grown for 16 hours in 2xTY rich nutrient media at 30°C under ampicillin selection. The transformation efficiency was calculated using pUC19 and was shown to be $1.43x10^{10}$ cfu/µg DNA. The amplified sgRNA-library was isolated and HEK293T cells were co-transfected with the sgRNA-library as well as two lentiviral packaging plasmids containing gag, pol and env genes using Lipofectamine®2000. An EGFP construct was also co-transfected into HEK293T cells to create a second set of lentiviral particles as a control. The lentivirus containing media was harvested 48/72 hours post transfection, filtered and concentrated by centrifugation of the supernatant for 2.5 hours at 20,000 g. For the introduction of the sgRNA-library in CHO-K1 mAb expressing cells it was necessary to determine the optimal multiplicity of infection for lentiviral transduction of the library. This is essential to ensure an optimal ratio between coverage of the library but also to integrate only one or two sgRNA per cell.

CHO-K1 mAb expressing cells were transduced with both the EGFP and sgRNA-library lentiviral particles using serial dilutions (0, 2, 4, 6, 8, 10). Cells transduced with the sgRNA-library were analysed for BFP expression using flow cytometry 48 hours post-transduction. Cells transduced with the EGFP-lenti were analysed using Guava easyCyte with ExpressPlus programme on the Guava™ benchtop cytometer. As a control the sgRNA library control was transfected and cells were selected using 10 µg/ml puromycin (Figure 48 A and B).

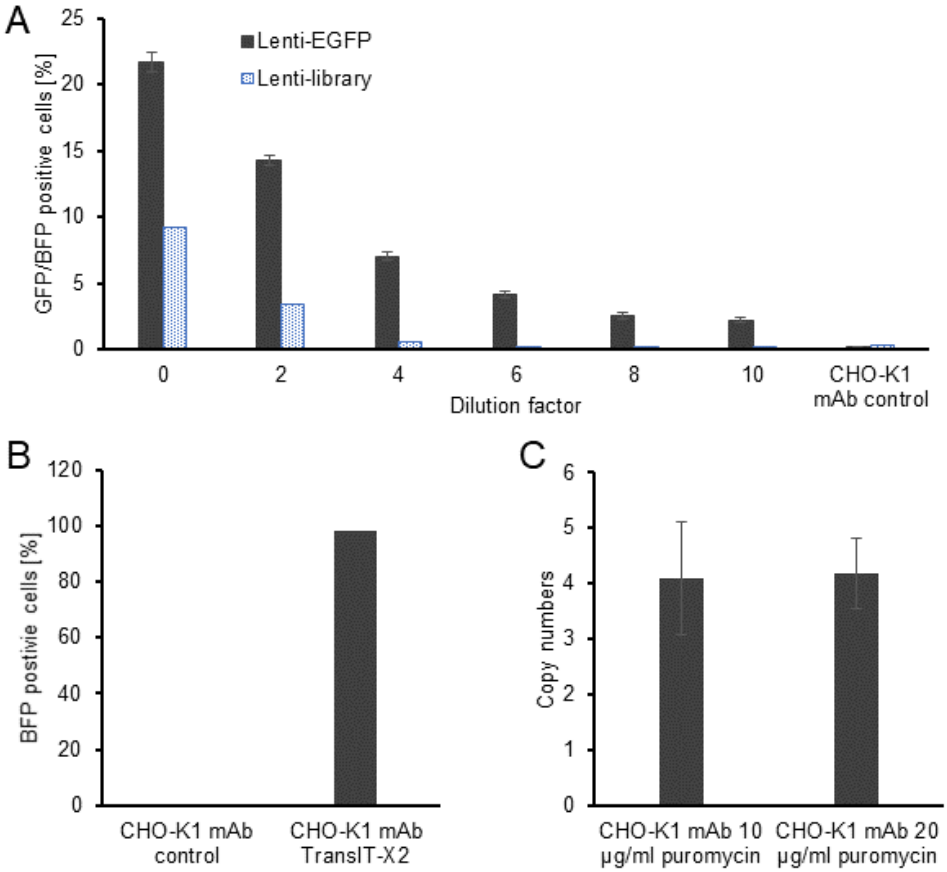

Figure 48: Lentiviral transduction of sgRNA library showed low transduction efficiency and high number integration events. A) The sgRNA library as well as a GFP control plasmid were packed into a lentiviral delivery system and CHO-K1 mAb was transduced with different dilutions. GFP or BFP intensity were analysed using FACS B) Postive BFP control generated by PEI based transfection. C) CHO-K1 mAb was transduced and selected with either 10 µg/mL or 20 µg/mL puromycin. Number of intergrated copies was analysed using PCR.

Transduction using the EGFP construct containing lentiviral particles was more efficient (~22%) compared to the sgRNA-library lentivirus (~14%) using no dilution of the lentivirus containing supernatant. The transduction efficiency decreased as the supernatant was diluted. Higher dilution of the sgRNA-library lentivirus (6, 8 and 10) led to almost no BFP signal. Given that no dilution led to the highest amount of BFP signal, CHO-K1 mAb cells were transduced again with the sgRNA library and selected with two different concentrations of puromycin (10 µg/mL and 20 µg/mL) over a period of two weeks. Genomic DNA was isolated and a standard curve was generated using different dilutions of sgRNA-library plasmid spiked with genomic DNA imitating actual sample

conditions for qPCR. The puromycin resistance gene was amplified which is a fusion with BFP. Using the standard curve, the copy number was calculated assuming diploidy and 4.9075 pg of DNA per cell (Xu et al., 2011). It was shown that no dilution of the sgRNA-library lentivirus led to ~4 integration events per cell regardless of the amount of puromycin used for selection (Figure 48 C).

To knockout only one gene at a time it is crucial that only one or two sgRNAs are integrated per cell. This ideally goes along with a several fold coverage of the library. To investigate if lower integration events could be achieved, the same cells were transduced with different dilutions of the virus and assessed for integration events using qPCR after selection with 5 µg/mL puromycin. Cells were transduced using the following dilutions of sgRNA-library lentivirus: 3. 6, 9, 12, 16 and 20. To investigate further if other transfection methods would be suitable we used a PEI based transfection reagent TransIT-X2® (Mirus Bio LCC) as well as electroporation. For PEI-based transfections a ratio between plasmid DNA/transfection reagent of 1:1 was used. The following amounts of DNA were used to transfect $1x10^6$ cells: 5, 2.5, 1, 0.5, 0.25 and 0.1 µg. For Nucleofection the following amounts were used to transfect $1x10^6$ cells: 2, 1 and 0.5 µg. After selection the DNA was isolated and amplified using primers targeting puromycin and compared to a standard curve (Figure 49 A to C). The results indicated that dilution of the lentivirus following selection for 2 weeks had no effect on the number of integrations per cell suggesting that there may be subpopulations which are susceptible to transduction by lentiviral particles and others are resistant. Furthermore, the small number of cells surviving selection indicated that the library coverage would be severly compromised

(Figure 49 A). PEI based transfection resulted in a high number of copies per cell depending on the amount of DNA used (Figure 49 B). The most promising results for amount of integrations per cell were achieved using Nucleofection. Using 0.5 µg resulted in two copies per cell whereas 1 and 2 µg showed about 7 copies per cell (Figure 49 C).

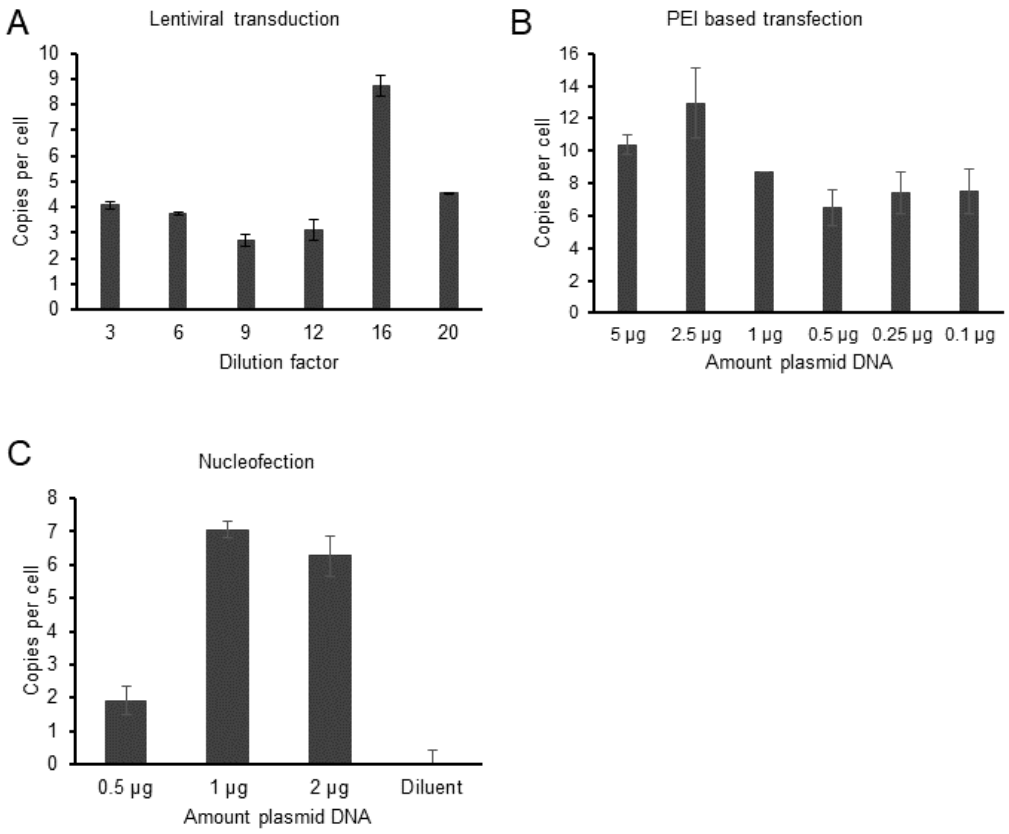

Figure 49: Delivery of the sgRNA library using lentivirus, PEI-based transfection and Nucleofection as well as resulting integrations per genome and cell. Cells were selected using 10 µg/mL puromycin over a period of two weeks. A) Lentivirus containing supernatant was diluted before added to the culture. D) PEI based transfection reagent and different concentrations of library plasmid. C) Nucleofection combined with low concentrations of plasmid DNA and a high viability program (n=2).

Lentiviral transduction as well as PEI based transfection were demonstrated to be unsuitable for the delivery of the sgRNA library. We aimed for one to two copies per cell which can be achieved using 0.5 µg plasmid DNA for electroporation.

A further challenge for the integration of the library was that most commonly used Cas9 plasmids use the puromycin resistance gene for selection of transfected populations. The sgRNA library contained a puromycin resistance marker as well and did not encode Cas9. Therefore, the puromycin resistance gene had to be exchanged on our vector to another resistance gene before generating a cell line stably expressing Cas9.

For our experiments we wanted to use the same plasmid which was used for experiments used in section 4.2.1 for depletion of miRNAs. Exchange of the hygromycin b phosphotransferase (*hph*) gene was our preferred option as a selection marker. The cloning strategy for the exchange of the *pac* gene to *hph* is displayed in Figure 50 A. A plasmid with correct orientation of the hph gene was chosen and transfected into CHO-K1 mAb then selected using 800 µg/mL hygromycin b. Optimal selection conditions were established in a separate experiment. Besides Sanger sequencing, Cas9 function was confirmed by transfecting a test sgRNA and confirmation of targeting by Cas9. The sgRNA library is based on a plasmid called pklv-U6gRNA(BbsI)-PGKpuro2ABFP (short pklv). This vector was utilised as our control plasmid and furthermore, can be used to express a sgRNA without Cas9. To investigate the function of our Cas9-2A-hyg plasmid, a sgRNA targeting miR-24 was cloned into pklv. Targeting miR-24 with this sgRNA sequence was very effective in section 4.2.1. The pklv-sgRNA-miR-24 plasmid was transfected into CHO-K1 mAb stably expressing Cas9-2A-hyg and selected using 10 µg/mL puromycin over a period of two weeks. The abundance of miR-24 was significantly reduced compared to the control (pklv only) proving Cas9 function (Figure 50 B).

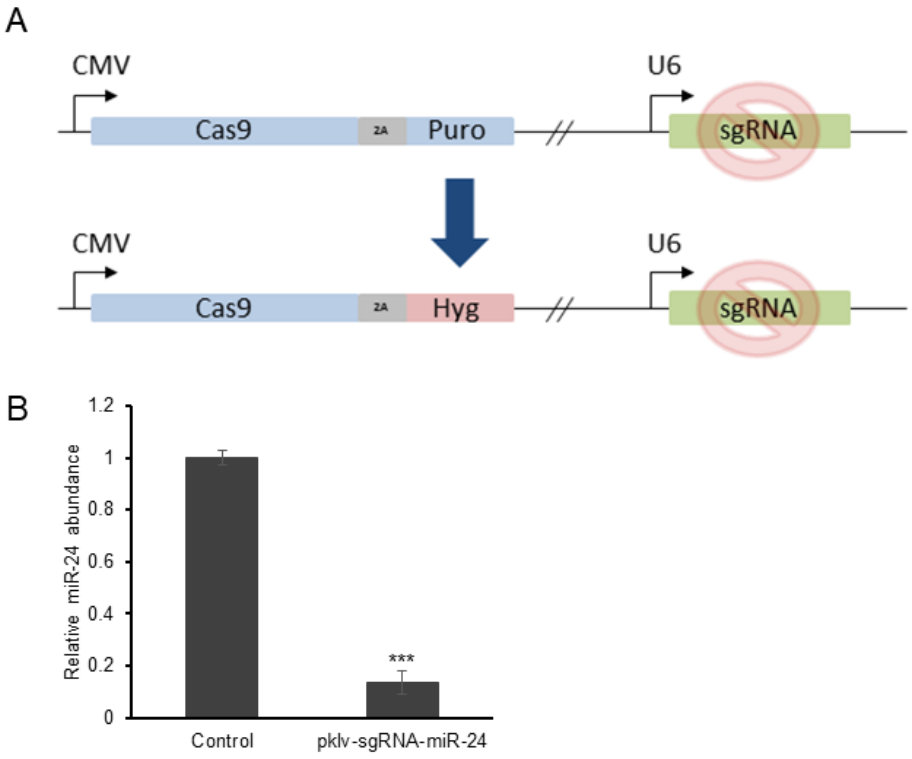

Figure 50: Cloning strategy for exchanging the puromycin resistance gene to hygromycin in PX459 and test for function. A) Exchange of the *pac* gene to *hph* was performed using specific primers for hph under addition of EcoRI restriction sites including the 2A self-cleavage sequence. Correct ligation and if sequence was in frame was analysed using Sanger sequencing. B) Function of Cas9-2A-hyg was confirmed using a sgRNA expression vector (pklv). A sgRNA for miR-24 was cloned into pklv and transfected as well as selected. Expression of miR-24 was subsequently analysed to prove Cas9-2A-Hyg function. Statistical significance was calculated using standard student's t-test (*** $p < 0.001$ vs control; n=3).

After Cas9-2A-hyg function was confirmed, limited dilution cloning was used to isolate single cell clones which were consequently assessed for growth and productivity. This step was important to select a clone which was properly performing i.e. similar to the parental CHO-K1 mAb and to generate a baseline for future experiments.

4.3.1.1 Generation and characterisation of a CHO-K1 mAb cell line stably expressing Cas9

Limited dilution cloning was used to isolate single cell clones from the CHO-K1 mAb Cas9-2A-hyg expressing stable pool. The characterisation of single cell clones was necessary to start with a baseline cell population which performed similar to the parental cell line before introducing the CRISPR library. A total of ten clones were isolated and cultivated in CHO-SFM II media. Clone performance was assessed in batch cultures in a culture volume of 5 mL with an initial cell density of 2 x 10^5 cells/Ml and samples were taken every 48 hours to assess viable cell density as well as for ELISA to assess productivity.

As expected various growth patterns were exhibited by all ten clones in batch cultures (Figure 51 A and B). Clone 2, 4 and 7 performed worst compared to other clones. Growth behaviour of all other clones was quite comparable with the original mixed population. Different growth pattern was also reflected in viability where clone 2, 4, 7 and 9 demonstrated lower percentages. Furthermore, IgG titres showed differences on day 4 and 6 for most clones (Figure 51 C). With an average IgG level of 10 mg/L to 20 mg/L the productivity was quite low compared to prior experiments with that cell line. Clone 4, 6 and 8 performed best overall and were further expanded as well as cryopreserved for further experiments. Besides growth, Cas9-2A-hyg function was also important. The same control plasmid expressing a sgRNA for miR-24 (pklv-sgRNA-miR-24) was used to investigate targeting efficiency and successful indel generation. All clones were transfected with pklv-sgRNA-miR-24 and selected using puromycin over a period of two weeks. Mature miR-24 expression was analysed using TaqMan® miRNA assays and compared to the control vector (pklv only) (Figure 51 D).

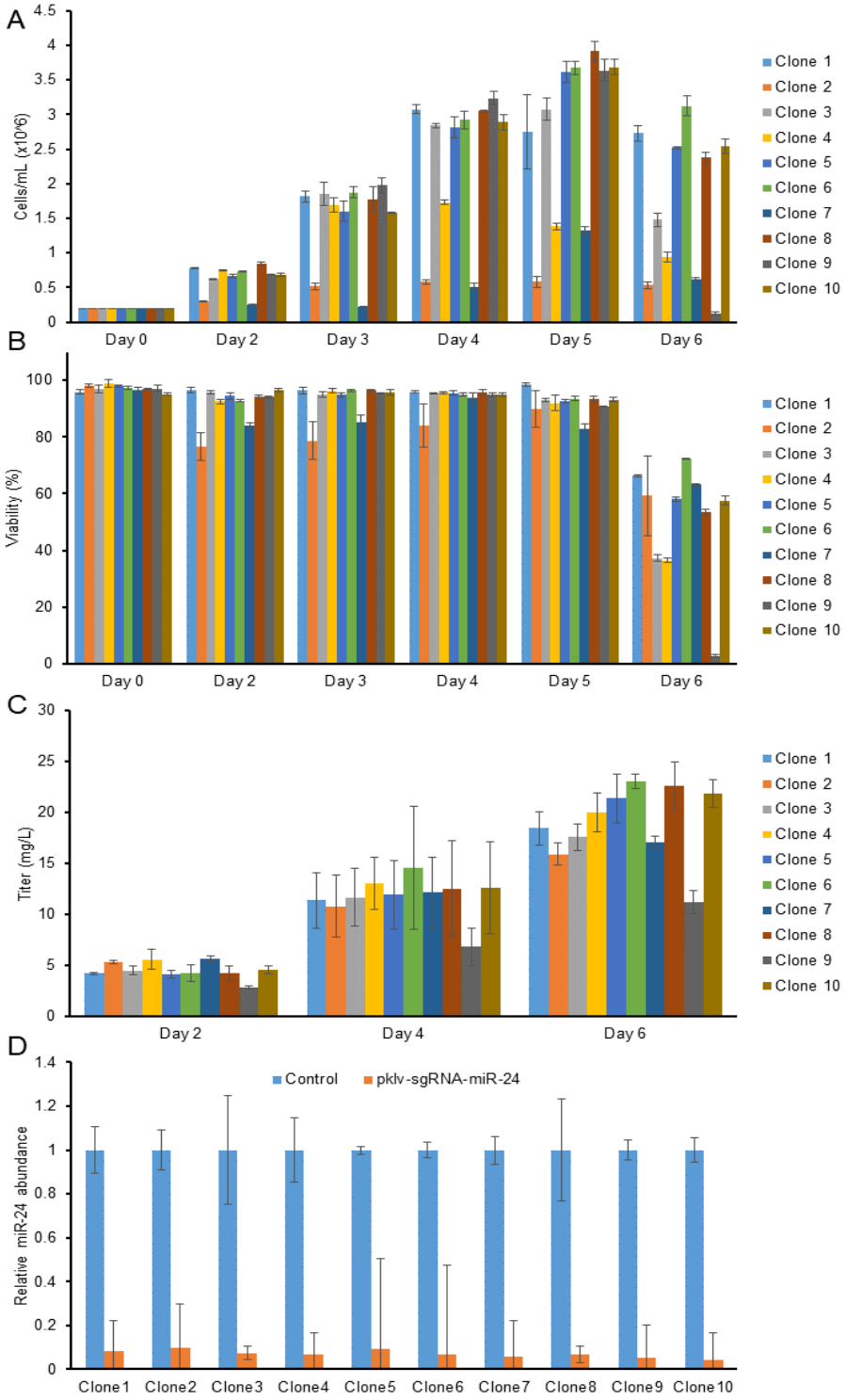

Figure 51: Characterisation of clones expressing Cas9-2A-hyg for growth and titre as well as Cas9 function. A and B) Viable cell density and viability for all ten derived clones showed differences in growth behaviour. C) IgG expression on day 4 and day 6. IgG levels averaged between 10mg/L to 20 mg/L. D) Cas9-2A-hyg function was analysed and showed that Cas9 is targeting miR-24 effectively in all clones (n=1).

Cas9 was fully functional in all ten clones and miR-24 expression was significantly reduced compared to the control. After assessing Cas9 function and performance we decided to use CLONE 8 for all further experiments regarding the CRISPR library. Clone 8 was chosen as performing best of the panel of clones and closest to the parental mixed population.

To progress with the sgRNA library, clone 8 was transfected using optimised conditions for Nucleofection (4.3.1) using 0.5 µg plasmid. To ensure high coverage of the library $15x10^6$ cells were transfected and cells were selected using 5 µg/mL puromycin for two weeks in CHO-SFM II supplemented with 5% FBS in T175 flasks. In addition, to the library plasmid the control plasmid (pklv) was also transfected. Media and dead cells were removed every 3 to 4 days. Once the T175 flasks reached 80% confluency, cells were readapted back to suspension conditions for two passages in CHO-SFM II media (Kuhner Clima-shaker incubator (ISF1-X) at 37°C, 170 rpm and 80 % humidity).

To ensure that, for example, slower growing cells (after a knockout of a functionally important gene) were maintained in the population we followed a strategy to expand cells into larger volumes (250 mL Erlenmeyer flasks). For generating a master cell bank, media was only added without discarding cells. Once a cell density of $5x10^6$ cells/ml was reached a cell bank was created by freezing $1x10^7$ cells per vial. The same procedure was applied twice to ensure a sufficient number of cells and coverage of the sgRNA pool.

To investigate the number of integration events per cell, genomic DNA was isolated and a standard curve was generated using different dilutions of sgRNA-library plasmid spiked with wildtype genomic DNA. The puromycin resistance gene was amplified and copy numbers were calculated assuming diploidy and 4.9075 pg of DNA per cell (Xu et al., 2011). For the sgRNA library as well as the control ~1-2 copies per cell were observed (Figure 52).

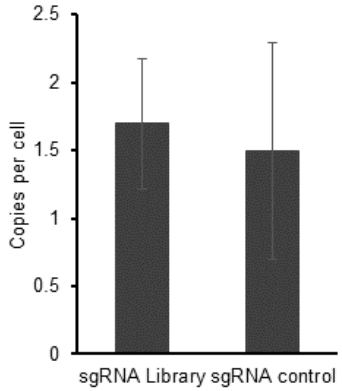

Figure 52: Integration events after transfection of the sgRNA library and control plasmid. It was shown, that transfection the sgRNA library under same conditions led to ~ 1-2 copies per cell. Amount of copies is similar for the control plasmid as well (n=3).

Having established that cell expansion was sucessful and copy numbers per cell were low for our CRISPR library we wanted to use the pooled library for “loss-of-gene” function studies. Therefore, certain stress conditions to test the library were further explored.

4.3.2 Investigation of genes involved in programmed cell death by induction of apoptosis

Programmed cell death and its key regulators are well studied. Therefore, an obvious strategy to explore “loss-of-gene” function was to induce apoptosis and select for sub-populations which are more resistant to programmed cell death due to a loss in gene function. Sodium butyrate (NaBu) is a Histone deacetylase inhibitor (HDAC) and is not only used for the improvement of productivity but can also induce apoptosis. Furthermore, hyperosmotic conditions are a potential stress condition in a bioreactor and it is known that high osmotic pressure can induce growth inhibition and programmed cell death. As a result, we wanted to explore both strategies as potential stress conditions for enrichment of sub populations showing a level of resistance. Firstly, we tested conditions suitable for induction of apoptosis by NaBu as well as for high salt conditions (Figure 53 A and B). Conditions were assessed in batch cultures for several concentrations of NaBu and NaCl in a culture volume of 5 mL with an initial cell density

of 2 x 10^5 cells/mL. Samples were taken every 48 hours to assess viable cell density. After 3 days the media was completely exchanged and either NaBu or NaCl was added.

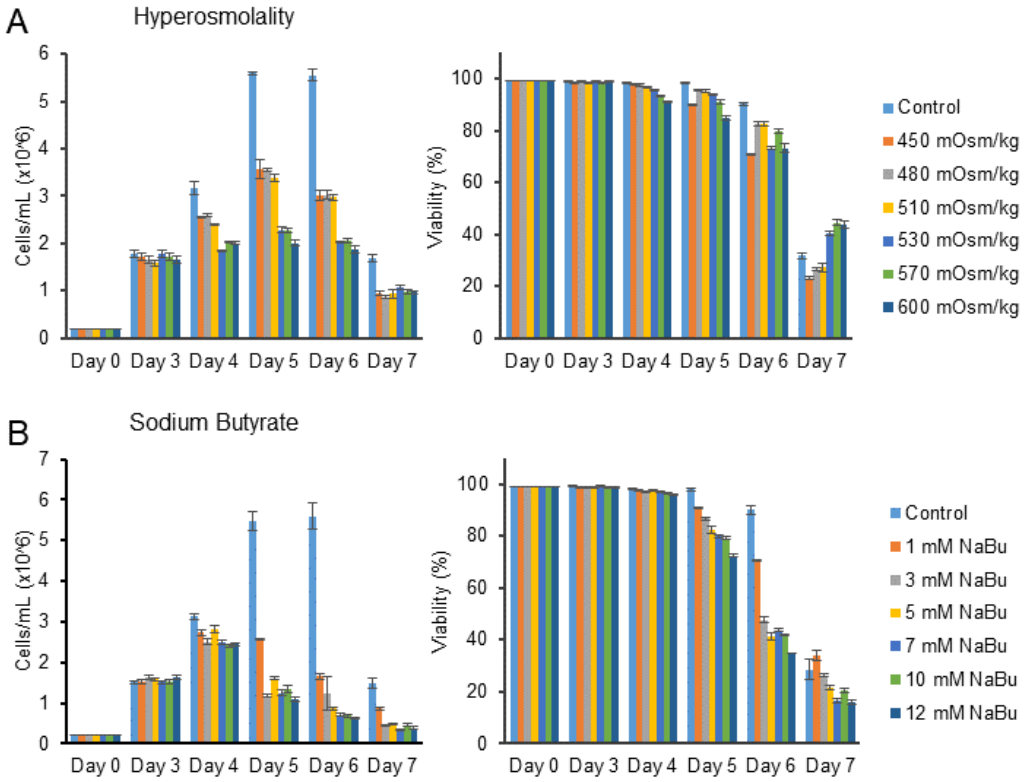

Figure 53: Optimisation of NaBu and NaCl concentration for induction of apoptosis. A) Cells were seeded with a cell density of 2x10^5 cells/mL and media was exchanged after 3 days. With the media exchange, NaCl was added to reach an osmolality between 450 to 600 mOsm/Kg. Viable cell density and viability was monitored daily until day 7. B) Like NaCl a range from 1 mM to 12 mM NaBu was tested. Viable cell density and viability was monitored daily until day 7 (n=1).

To change the osmolality, 5 M stock NaCl was added to reach conditions between 325 mOsm/Kg to 600 mOsm/Kg (Figure 53 A). Growth was already inhibited by conditions of 450-510 mOsm/Kg on day 4 and growth was inhibited until the end of the culture. Inhibition was more pronounced on higher salt concentrations. The effect on viability was very mild compared to the control. For NaBu all concentrations showed effects on both growth and viability from day 5 to the end of the culture compared to the control. For further exploration of genes involved in induction of apopotosis hypersomolality was the more controlable condition and was chosen for our further experiments

4.3.2.1 *Exposure of CHO cells to high osmolality conditions*

High salt conditions between 500-600 mOsm/Kg had a considerable affect on proliferation and viability. However, mild hyperosmotic conditions between 410-450 mOsm/Kg decreased proliferation and viability but still permitted cells growth. Based on our preliminary experiment we cultured cells at 400 mOsm/Kg, batch cultures in a volume of 30 mL with an initial cell density of 2 x 10^5 cells/mL using 250 mL Erlenmeyer flasks (Corning). After 3 days the media was refreshed and NaCl was added to reach set osmolality. Samples were taken every 24 hours to assess viable cell density (Figure 54).

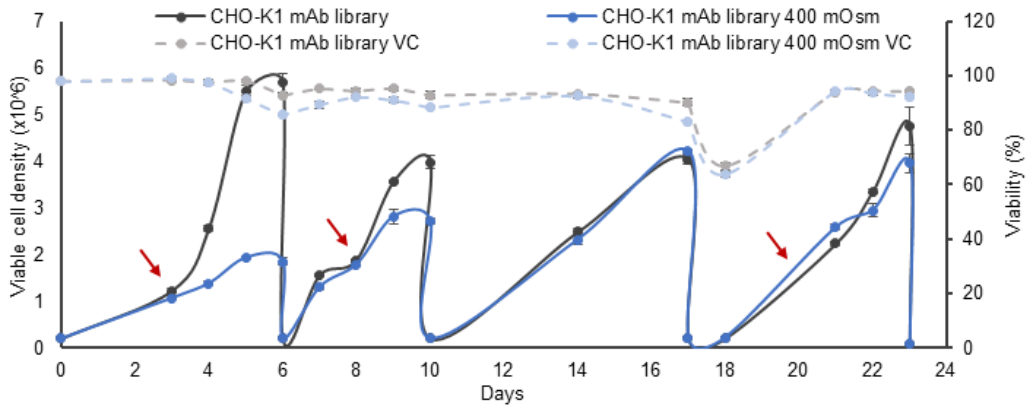

Figure 54: Exposure of CHO-K1 mAb transfected with sgRNA library to hyperosmotic conditions. Addition of 5M NaCl to reach 400 mOsm/kg is indicated by a red arrow. Untreated cells transfected with the CRISPR/Cas9 library were used as a control. To permit recovery and promote growth a recovery phase between day 10 and 17 was applied. Further NaCl was added on day 20 and cultures were harvested on day 23 for DNA extraction (VC = viability).

Over a period of 23 days at 400 mOsm/kg a stepwise adaption of the treated culture was observed. Viability was generally reduced compared to the control. To investigate which genes were knocked out and which are potentially involved in adaption to hypersomotic stress we prepared samples for NGS.

4.3.3 Efficient enrichment of CHO cell subpopulations with enhanced productivity

One possible application of the library is to find cell line engineering targets or pathways which are associated with increased productivity or secretion. The hypothesis behind it is that after knockout of certain genes, productivity may be enriched and these clones

could be enriched using cell sorting. After transfection of the library into CHO-K1 mAb cells were selected over a period of two weeks. To enrich for clones and to maintain a good coverage of sgRNAs, $8x10^6$ cells were collected, washed with PBS and immediately put on ice to slow down secretion of produced IgG. The membrane transiting IgG can then be stained with a FITC labelled anti-IgG using a “cold-capture” technique. All steps were performed at 4°C to prevent full secretion of the mAb and maintain staining (compare 3.3.10). As a negative control a parental CHO-K1 non-producing cell line was used to account for unspecific binding. Furthermore, a positive control population of CHO-K1 mAb (pklv negative control) was stained and analysed. Gating was performed using an unstained population as well as using the negative control to exclude FITC signals resulting from unspecific binding (Figure 55 A and B). The pklv control showed a shift towards higher fluorescence compared to nonproducing and unstained cells and was comparable to the library transfected population in intensity (Figure 55 C and D). For sgRNA library transfected cells, the highest 10-15% in intensity were selected and sorted into 6 well plates. Sorted populations were then further expanded and transferred into suspension when the appropriate cell density was reached. The obtained population (Sort I) was then resorted and cells showing the highest intensity (10-15%) were then again sorted (Sort II) and expanded (Figure 55 E). Compared to Sort I a distinct shift in intensity was observed in Sort II indicating a successful selection of high producing clones or subpopulations.

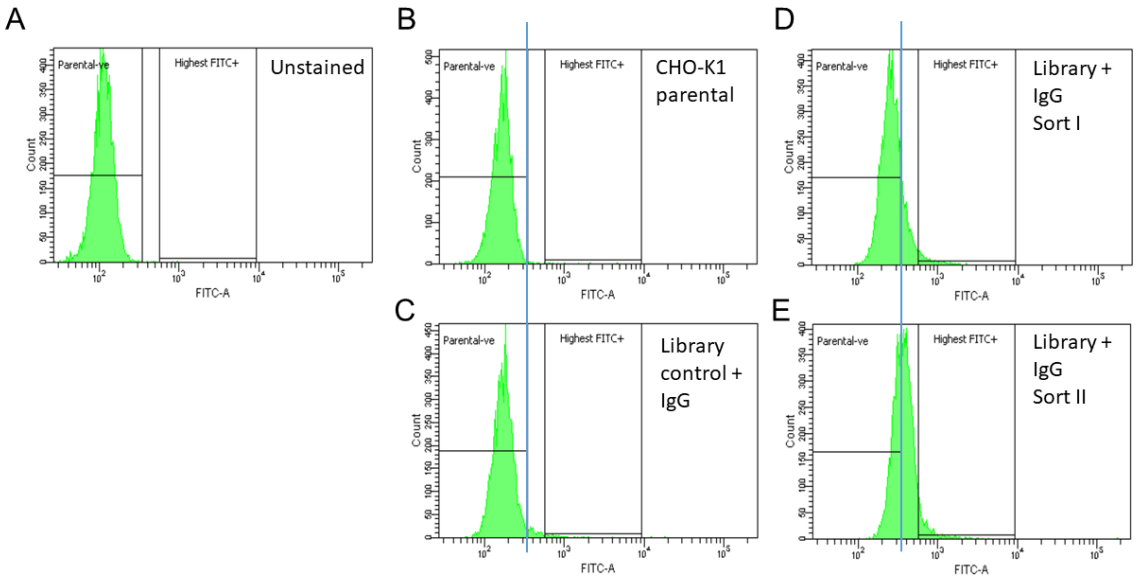

Figure 55: Selection of high producing subpopulations using FACS and low temperature antibody stains. A and B) An unstained (CHO-K1 mAb) and a nonproducing CHO-K1 cell line were used for selection of gates. The non-producing CHO-K1 cell line was treated with anti-IgG FITC to exclude unspecific binding. C) CHO-K1 mAb transfected with pklv negative. D) Cells transfected with the library were sorted corresponding to the gating to obtain the highest 10-15% in intensity (Sort I). E) SgRNA library transfected cells were re-sorted for the highest 10-15% in intensity (Sort II).

Sub-populations sorted for higher staining should theoretically show increased titres in batch cultures compared to the unsorted population. All three populations (Library unsorted, Sort I and Sort II) were cultivated in batch cultures in a volume of 30 mL with an initial cell density of 2 x 10^5 cells/mL using 250 mL Erlenmeyer flasks. Cells were grown CHO-SFM II media and samples were taken on a daily basis to assess viable cell density and IgG titre. No effect on growth nor viability was observed between the unsorted and sorted populations (Figure 56 A and B). Furthermore, elevated IgG levels were observed compared to the unsorted population indicating a successful selection of high producing cells using this method (Figure 56 C). From day 2 on IgG levels were elevated for Sort I and Sort II. Titres of 35 ± 5 mg/L were reached for the unsorted population and 45 ± 2 mg/L (Sort I). Sort II reached 52 ± 1.5 mg/L respectively. The increase in IgG levels was observed due to increased specific productivity Qp for all timepoints when compared to the unsorted populations (Figure 56 D) which is not unexpected given the staining method used.

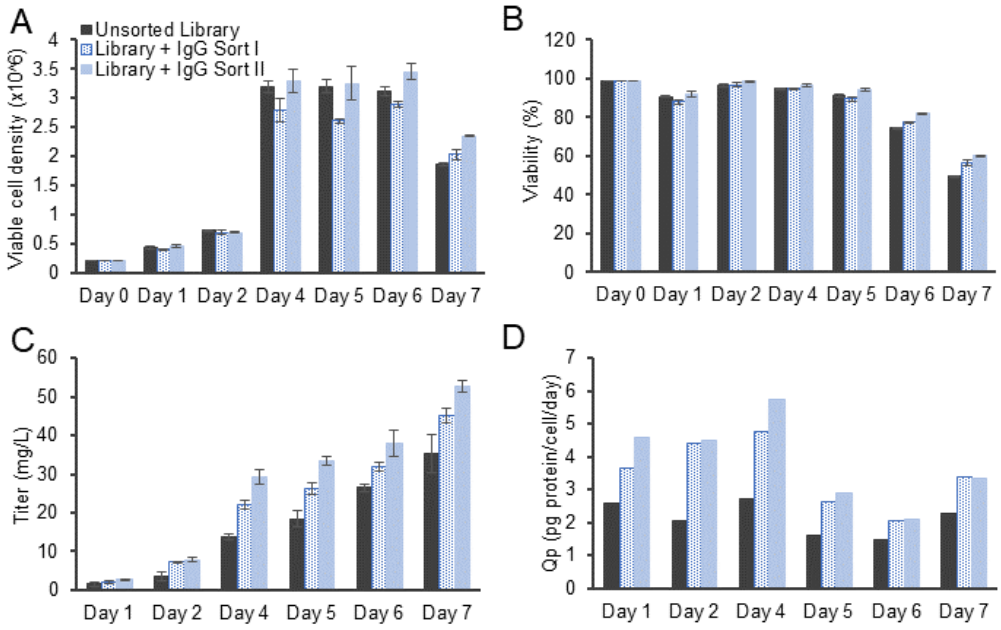

Figure 56: Growth, viability and productivity of cells sorted using a low temperature antibody stain. A and B) Viable cell density as well as viability low temperature sorted populations (Sort I and Sort II) compared to the control (unsorted sgRNA library). C) IgG levels for unsorted and populations sorted for higher productivity. Titres reached 45 ± 2 for first sort and 52 ± 1.5 for the resorted population, respectively. D) Increase in IgG levels was presumably due to elevated specific productivity at each day compared to the control (n=1).

As the sort for high-producing cells was successful, the next step was to isolate genomic DNA to amplify the region containing the sgRNA. It was hypothesised that gene knockouts which led to increased productivity or secretion would be enriched in high producing cells. The genes can be then identified using NGS.

Summary CRISPR/Cas9 library for genome wide “loss of gene function” studies in Chinese Hamster Ovary cells

The results showed that the sgRNA-library consisting of 87,897 different sgRNAs can be successfully packed into a lentiviral delivery system. However, transduction efficiencies using a CHO cell line expressing a mAb and human codon optimised spCas9 showed low (~10 %) transduction efficiency. Copy numbers were investigated and were shown be to average four integration events when selected with 10 µg/ml and 20 µg/ml puromycin using no dilution of the lentiviral supernatant. This number of integrations per genome was too high for our purpose. To reduce copy number the same cell line was transduced using several different dilutions of the lentiviral stock. The number of integration events was not dependent on the dilution used and averaged at three to four copies per genome suggesting that some cells in a population are susceptible to viral infection and integration and some are resistant. Furthermore, varying the amount of selective agent had no effect on the number of integration events. The conclusion was that the lentiviral delivery system was not suitable for this purpose in CHO cells.

To investigate if other transfection based methods can be used, PEI-based TransIT-X2® was used with different amounts of plasmid concentrations. High amount of plasmid showed high transfection efficiencies but also high copy numbers of approximately ~11 integrations. Lower amounts of plasmid showed a considerably low transfection efficiency and a reduction of integration events to approximately seven per genome as well.

Nucleofection has been demonstrated to be an efficient transfection tool in the literature. It is an electroporation based method and low integration events can be achieved with high transfection efficiencies. As the sgRNA library was based on selection with puromycin our stable cell line had to be generated using Cas9-2A-Hyg (based on PX459). Therefore, the hygromycin resistance gene had to be cloned into corresponding vector. Function of the new fusion was confirmed by targeting miR-24-3p. Clones were isolated and characterised for growth and productivity. The clone performing most similar to the parental cell line (clone 8) was used for stable transfection of the sgRNA library. The library was transfected, selected and analysed for copy numbers. It was shown, that -2 copies were integrated. Adaption to hyperosmolality was used to induce apoptosis and to enrich for gene knockouts resulting in survival. Apoptosis is well investigated and hyperosmotic conditions were hypothesised to enrich for sgRNAs targeting pro-apoptotic

or stress related genes. Furthermore, we wanted to identify gene knockouts resulting in a high productivity phenotype. Therefore, selection of high producing clones using FACS combined with a surface cold stain was performed. Populations could be enriched which exhibited higher titres and specific productivity.

5.0 Discussion

5 Discussion

5.1 Stable depletion of the miR-23-24-27 cluster and individual cluster members in industrially relevant cell lines

5.1.1 MicroRNAs as tools for CHO cell engineering

Recent advances in genetic engineering as well as improved tools and techniques using different integrated omic' approaches have been used to better understand regulatory networks in CHO cells and became a trending research field to improve the performance of CHO cells in recombinant protein production processes (Fischer et al., 2015). Integrated omic' approaches include for example the transcriptome, proteome, glycome, and the phospho-proteome. MicroRNAs with their ability to regulate a whole network of target genes have been identified as novel targets for cell line engineering to improve numerous aspects of CHO cell performance in a production bioreactor.

Recent studies have demonstrated the beneficial use of miRNA engineering to improve productivity (Barron et al., 2011; Fischer et al., 2015a; Fischer et al., 2015b; P. S. Kelly et al., 2015a), enhance longevity by preventing apoptosis (Druz et al., 2011) and improvement of growth (Jadhav et al., 2012b) to mention only a few. Numerous differential expression studies exist with the aim to identify more miRNAs which can be used as potential engineering tools to improve bioprocess relevant phenotype (reviewed by (Jadhav et al., 2013b).

5.1.2 Selection of the miR-23-24-27 cluster and individual members for CHO cell engineering

Previous results in our group demonstrated that the depletion of miR-23 resulted in increased productivity in CHO-K1 SEAP expressing cells (Kelly et al., 2015). MiR-23 was originally identified as differentially expressed together with other miRNAs in a temperature shift study by Gammell and colleagues (Gammell, 2007). Biphasic processes are commonly used in industry with cells maintained in growth promoting conditions to boost proliferation in the first stage of the culture. After reaching high cell densities the reduction of temperature leads to growth inhibition and promotes productivity. Due to reduced growth rates and lower nutrient consumption the longevity of the culture is often increased. Other miRNAs identified in the study were miR-21, let-

7, miR-25/26 and several members of the miR-17 cluster. Interestingly, miR-27a and miR-24 were identified as being more abundant during hypothermic conditions. MiR-27 and miR-24 are part of the miR-23 cluster. This cluster comprises two genomic paralogues, miR-23a-27a-24-2 and miR-23b-27b-24-1, and its members are quite well studied in terms of their function in certain diseases. The miR-23a cluster consists of miR-23a, miR-27a and miR-24-2, whereas the miR-23b cluster accompanies miR-23b miR-27b and miR-24-1 (Chhabra et al., 2010a). The two paralogues most likely resulted from gene duplications during evolution in mammals (Wang et al., 2016). The miR-23a cluster is intergenic and its paralog is intronic in human and reside on two different chromosomes. In Chinese hamster the miR-23b cluster is located in an intron of the Aminopeptidase O-like gene (AMPO). The mature sequences of the paralogues differ in only one base pair. The mature sequence of miR-24-1 and miR-24-2 are identical which makes their distinction during analysis of mature miRNA expression impossible. Furthermore, several multi-alignment studies have shown that all three miRNAs in the cluster are conserved in mammals (Chhabra et al., 2010a). Table 9 shows a sequence comparison of all miRNA members of the cluster between human (hsa), Chinese hamster (cgr) and mouse (mmu).

Table 9: Comparison of the mature microRNA -3p sequence across different mammalian species

MicroRNA	Mature miRNA sequence (-3p)
cgr-miR-23a-3p	A**UCACAU**UGCCAGGGAUU**U**CC
hsa-miR-23a-3p	A**UCACAU**UGCCAGGGAUU**U**CC
mmu-miR-23a-3p	A**UCACAU**UGCCAGGGAUU**U**CC
cgr-miR-23b-3p	A**UCACAU**UGCCAGGGAUU**A**CC
hsa-miR-23b-3p	A**UCACAU**UGCCAGGGAUU**A**CC
mmu-miR-23b-3p	A**UCACAU**UGCCAGGGAUU**A**CC
cgr-miR-27a-3p	U**UCACAG**UGGCUAAGUUC**C**GC
hsa-miR-27a-3p	U**UCACAG**UGGCUAAGUUC**C**GC
mmu-miR-27a-3p	U**UCACAG**UGGCUAAGUUC**C**GC
cgr-miR-27b-3p	U**UCACAG**UGGCUAAGUUC**U**GC
hsa-miR-27b-3p	U**UCACAG**UGGCUAAGUUC**U**GC
mmu-miR-27b-3p	U**UCACAG**UGGCUAAGUUC**U**GC
cgr-miR-24-1-3p	U**GGCUCAG**UUCAGCAGGAACAG**G**
hsa-miR-24-1-3p	U**GGCUCAG**UUCAGCAGGAACAG
mmu-miR-24-1-3p	U**GGCUCAG**UUCAGCAGGAACAG
cgr-miR-24-2-3p	U**GGCUCAG**UUCAGCAGGAACAG**G**
hsa-miR-24-2-3p	U**GGCUCAG**UUCAGCAGGAACAG
mmu-miR-24-2-3p	U**GGCUCAG**UUCAGCAGGAACAG

The seed regions of the miR-23 paralogues are almost identical to the seed region of miR-27 with only one base is exchanged from U to A in mouse, human and Chinese hamster. Similarly, a C to U is exchanged for miR-27a and miR-27b. The sequences of miR-24-1 and miR-24-2 are completely identical except for the mature microRNA in Chinese hamster. An addition of one guanine base is exhibited for miR-24 in Chinese hamster.

The first step before using sponges for the depletion of the whole cluster or individual members, was to investigate the expression of each microRNA in a panel of different cell lines. In our study, expression seemed similar in all cell lines when compared to a parental CHO-K1 cell line (Figure S 7).

A lower Ct value corresponds to a higher abundance and vice versa. The expression of miR-24 was in general the highest in all tested cell lines. However, the TaqMan® assay does not differentiate between miR-24-1 and miR-24-2. MiR-23a and miR-27a seemed to be higher expressed than their genomic paralogs. Comparing same members of the cluster it seemed that miR-27a was higher expressed compared to miR-23a suggesting an independent regulation of the members of the cluster. This was supported by comparison of the expression of miR-23b and miR-27b. Using TaqMan® assays may give a good indication of the miRNA abundance in a simple experiment e.g. knockdown of a particular miRNA at a given point in one cell line. When it comes to more complex approaches like comparing expression levels of several miRNAs in a miRNA cluster or a comparison over cell lines, NGS may be a more efficient method to use.

MicroRNAs can be transcribed within their host genes. Prevoius work has demonstrated that the intergenic miR-23a-27a-24 cluster was RNA-Polymerase II dependent but shows a lack of common promoter core elements such as a TATA box or TFIIB recognition element yet exhibited evidence of expressed sequence tags which are a physical indication of a gene (Saini et al., 2007). However, given the observation that the cluster is initially transcribed as a single primary transcript sequencing indicated that abundances of the single members of the miR-23 cluster showed great differences (Hackl et al., 2011). This may indicate a differential processing of each member of the cluster.

Depletion of miR-23-24-27 using a sponge decoy led to increased productivity in a CHO-S Fc fusion expressing cell line (Figure 16). This prompted us to explore how much each individual miRNA contributed to this effect or whether depletion of all three miRNAs was

necessary. Therefore, sponges for all individual miRNA were designed, transfected and phenotype analysed. Depletion of miR-24 as well as miR-27 led to increased productivity and pathway analysis to identify cell line engineering targets was performed (see section 4.1.3). The method of choice was proteomic profiling using HPLC-MS/MS to identify differentially expressed proteins. Besides the phenotype it was interesting to explore shared and individual targets of all three miRNAs.

It was demonstrated that 88 protein targets seemed to be shared between miR-23 and miR-24 which was unexpected given that the seed region of miR-24 and miR-23 are very different. It has been previously reported that different miRNA seed families can target the same mRNA. MiR-23 and miR-27 seemed to have 13 shared targets and miR-27 and miR-24 showed 31 overlapping proteins (Figure S 8). Between all three miRNAs, eight were common targets. Given that the seed region of miR-24 and miR-27 is very different it was unexpected to see overlapping targets.

The seed region of a miRNA is crucial for mRNA target identification, binding of the RISC and subsequent translational inhibition. With the seed region of miR-23 and miR-27 being very similar it could be that targets might be shared between the two microRNAs. In fact, prediction tools e.g. TargetScan suggest that shared binding of mRNA targets is likely and that similar pathways are targeted. Clustered microRNAs or miRNA families often share functionally related targets according to several studies (T. Liang et al., 2014; Ventura et al., 2008; J. Wang et al., 2011). Interestingly, Liang and colleagues explored predicted targets of the miR-23a and miR-23b cluster in silico. All six members possibly target genes involved in the same pathways as hypothesized. This co-targeting is observed in different regions of the target mRNAs (T. Liang et al., 2014).This is accompanied by the observation that entire miRNA families are conserved over mammals and vertebrates (Bartel, 2009). As one single miRNA can target several genes and evidence of involvement of whole miRNA families in pathways it is not a surprise that the defects in a miRNA regulation or expression can have tremendous effects on phenotype and development (Ambros, 2003; Bartel, 2009). Therefore, the hypothesis that miRNAs are clustered and conserved over species to avoid detrimental errors was topic of investigation by several research groups. Clustering of miRNAs might be important for the development of new miRNAs in many ways described by the functional co-adapting model (Y. Wang et al., 2016).

When we investigated which pathways and biological processes are commonly targeted between all three members of the cluster it was demonstrated that 9 shared pathways were over-represented including nucleotide biosynthesis, oxidation reduction and biosynthesis of nucleotide as well as nucleoside precursors. Interestingly, 46 biological processes were impacted in common between miR-24 and miR-23 depleted cells. These were all translation, translational regulation, tRNA metabolism or RNA processing related which supports the observed productivity phenotype. When comparing shared protein targets of miR-23 and miR-27 as well as miR-27 and miR-24, only a limited number of pathways were identified, with the major ones involved in response to oxidative stress and protein complex assembly. The formation of disulphide bonds during protein folding and processing in the ER leads to the formation of reactive oxygen species (ROS) (Schröder & Kaufman, 2005). Due to increased demands in protein folding and a resulting increase in ROS the oxidative stress response in the form of upregulating genes encoding antioxidant enzymes and cytokines might be observed. Interestingly, miR-27 had individual pathways targeted which seemed to be involved in regulation of apoptosis. ER stress has been demonstrated to trigger intrinsic apoptosis pathways which are controlled by a balance of pro- and antipoptotic proteins. With depletion of miR-24 being involved in an upregulation of translation and lower levels of miR-27 showing an increase in antiapoptotic proteins, observed productivity phenotype could be resulting of a synergetic effect of both. However, it is mentioned in the literature that miR-24 alone can target pro- or antiapoptotic genes (Agrawal et al., 2014; Singh & Saini, 2012b) and is further discussed in section 5.1.2.1.

With many pathways being common, our data agrees with many studies that support the co-targeting theory (T. Liang et al., 2014). Besides co-targeting of a miRNA cluster, each single member may have a role of its own which is suggested by different expression pattern which is especially evident for the miR-23 cluster. Therefore, we wanted to investigate individual functions of each miRNA further.

5.1.2.1 Role of individual miRNA members of the miR-23 cluster

Each cluster member has been shown to be involved in different as well as common biological processes and pathways by our study and several others. Previous results for transient up- or downregulation as well as sponge mediated stable depletion of the miR-23 cluster or individual members showed beneficial impact on growth, viability or productivity in several cell lines. The investigation of phenotypes after depletion of the miR-23 cluster or each individual member is discussed in the next section.

5.1.2.1.1 Impact of miR-23-24-27 depletion on the phenotypes of CHO cells and their resulting bioprocess performance

Transient upregulation of the miR-23-24-27 cluster led to enhanced productivity and viability at the expense of proliferation which was decreased in previous results generated in our lab. Normalised productivity was enriched by 1.35-fold and 1.7-fold in late stages of the culture in CHO-K1 SEAP expressing cells whereas viability was decreased by approximately 2-fold. Stable depletion of the cluster showed opposite effects leading a ~2.9-fold increase in cell density in mixed population and a 1.4-fold increase in a clonal panel of CHO-K1 SEAPs. The viability was improved in late stages of the culture by 12.5 %. To investigate the possible beneficial impact in other producer cell lines the cluster was depleted using a stable expressed sponge for miR-23-24-27. GFP intensity for all cell lines was reduced for sponge constructs indicating a successful binding if miRNAs.

Only one cell line showed a beneficial phenotype after depletion of the miR-23 cluster which led to increased levels of fusion protein on day 6 (1.26-fold) and day 8 (1.56-fold) of batch cultures in CHO-S Fc due to increased specific productivity. The same productivity phenotype (1.86-fold increase, day 11) was observed in fed-batch cultures but experiments could not be reproduced due a non-ideal feed strategy and not enough data could be collected for calculation of statistical significance. Optimisation of feed strategies in biopharmaceutical industry is a critical process and is usually performed in high throughput studies using DoE with defined media compositions. However, it is time consuming and dependent on the balance of multiple factors like components, time points and volumes. Changing only one component at a time implies very long optimisation times and the usage of high amount of resources. DoE uses a statistical

approach to “predict” cellular behaviour based on preliminary experiments and delivers the optimal feeding strategy which can be verified by only one final experiment (Horowitz et al., 2009). However, our resources in the laboratory were limited and the fed-batch strategy was never optimised. To investigate if the observed phenotype in CHO-S Fc can be increased by isolation of single cell clones, limited dilution cloning was used. Nine clones were chosen for miR-23-24-27 depleted clones and control expressing clones each. The GFP intensity exhibited an average of 223 (control sponge) in comparison to miR-23-24-27 sponge with an average of 16.97. This indicates again that miRNAs are successfully binding to the sponge construct and GFP translation is inhibited. The assessment of clones in batch cultures showed to our surprise no increase in productivity. However, growth behaviour of all clones varied in comparison to the mixed population which is expected due to clonal variations of CHO cells. The genetic instability of CHO cells leads to chromosomal aberrations like rearrangements or deletions (M. F. Wurm, 2013). Those effects can lead to loss of transgenes but also to multiple copy numbers of the transgene (Osterlehner et al., 2011). This amplification effect is desirable for the establishment of producer cell lines and is used for DHFR and GS expression systems (Kito et al., 2002). However, the same effect is also involved in the appearance of many different phenotypes due to clonal stability (M. Kim et al., 2011b).

For the generation of stable cell lines different systems are commonly used including lentiviral delivery or undirected random integration of plasmids. These systems do not give the possibility for a site directed integration of the transgene. Lentiviral delivery usually occurs in transcriptionally active regions (Bushman et al., 2005) running the risk of interupting gene function leading to a variety of phenotypes. Similarly transfecting our sponge constructs and random integration i.e. could lead to gene loss or integration in transcriptional active regions to increase the translational burden on cells. The consequence is a genotype which could result in different phenotypes i.e. slower or faster growth resulting in different subpopulations in a transfected mixed population. As a result, a great attention is focused on clone stability in biopharmaceutical industry (F. M. Wurm & Wurm, 2017).

Davies and colleagues analysed a subpopulation of 199 clones from a parental CHO-K1SV cell line (Davies et al., 2013). It was shown that over 100 generations specific growth rates vary and even increase towards later generations. It was concluded that subpopulations acquire traits due to mutations as well epigenetic events and are selected by for example by standard culture procedures like subcultivation or cryopreservation.

In biopharma industry a great effort is invested in for the selection of high producing clones ranging of up to over 1000 clones (F. Li et al., 2010). To find clones which show high productivity, a larger scale screen of clones would presumably be more appropriate and would give a view of the range of phenotypes in batch cultures. It is a commonly observed phenomenon that the expression of transgenes declines over time in culture and despite exhibiting multiple genomic copies (S. J. Kim et al., 1998; Strutzenberger et al., 1999). Kim and colleagues selected a high producing clone which was subsequently cultivated for 18 months and routinely sub-cultivated. It was demonstrated that the transgene expression steadily declined over a period of 18-month. The effect was investigated by several groups and it was shown that the commonly used CMV promoter is exposed to DNA methylation in the 5' and 3' end of the promoter sequence which eventually leads to a decrease in expression (M. Kim et al., 2011b; Moritz et al., 2015; Osterlehner et al., 2011). To target declining transgene expression promoter engineering is an extensive research field and it was observed that the induction of mutations in the promoter can prolong expression and counteract declining titres over cultivation time. As our sponge construct uses a CMV promoter the decline of sponge expression could be one reason why no phenotype in clones was observed. Furthermore, various copy numbers of sponge transcript for each clone might affect the phenotype where low sponge expression may not lead to increased productivity.

Small scale cultures allow higher throughput and avoid the extensive use of recourses i.e. expensive media. It furthermore allows the prediction of growth and transgene expression even before upscaling experiments. However, the evaporation of media in outer wells (referred as "edge effect") is a common drawback using 96- or 24-well plates (Patel et al., 2005). Sealing plates would solve the evaporation but allows insufficient exchange of oxygen between media and environment ultimately leading to reduced growth and changes in growth behaviour. All our single cell clones were cultivated in 24-well suspension plates, however the plates were sealed to avoid evaporation and prevent bacterial or fungal contaminations. Limited oxygen and the different culture format could also potentially impact the phenotype. Therefore, clones should also be assessed in bigger scales for our experiment in order to get a true comparison with mixed population and hence a better appreciation of the range of productivity changes within the pools.

To investigate which microRNA was responsible for the impact on productivity, individual sponges for miR-23, miR-24 as well as miR-27 were designed and tested in the same CHO-S Fc cell line.

5.1.2.1.2 Impact of miR-23 depletion on phenotype of CHO cells and bioprocess performance

Transfection with miRNA mimics or antagomiR has shown that up- or downregulation of individual members of the miRNA cluster can impact the bioprocess phenotype of CHO cells. Overexpression of miR-23a for example inhibited proliferation in transient experiments in CHO-K1 SEAP expressing cells. Stable depletion of miR-23 led to an increase of SEAP productivity bu 50% in batch and fed-batch cultures due to an increase in mitochondrial capacity in terms of oxidative phosphorylation (Kelly et al., 2014; Kelly et al., 2015). In a range of tested cell lines including CHO-K1 Fc, CHO-S Fc, DG44i Fc and DG44i mAb no change in behaviour was observed. This could indicate that the phenotype observed for CHO-S Fc for the depletion of the miR-23-24-27 cluster is resulting from reduced levels of miR-24 and miR-27 only.

5.1.2.1.3 Impact of miR-24 depletion on phenotype of CHO cells and bioprocess performance

Overexpression of miR-24 using mimics inhibited proliferation in CHO-K1 mAb and transient knockdown with antagomiRs resulted in enhanced cell growth performance (Noèlia Sanchez, 2013). Stable depletion of miR-24 in CHO-S Fc led to an increase in productivity of 1.3-fold on day 6 and 1.8-fold on day 8 (Figure 20). This was also observed in CHO-K1 mAb however the increase in IgG was very mild with only 10% on day 6 and day 7 of the batch culture (Figure 25).

To identify targets which are potentially involved in productivity due to the depletion of miR-24, we used proteomic profiling to investigate differential protein abundance. This approach has been shown to be very successful in CHO cells for the identification of potential targets of miR-7 (Meleady et al., 2012), miR-23 (Kelly et al., 2015) and other potentially growth related miRNAs including members of the miR-17-92 cluster (Clarke et al., 2012a).

Using label-free LC-MS/MS we obtained two datasets for the depletion of miR-24: CHO-S Fc using a sponge for miR-24 (see 4.1.4.2) and CHO-K1 mAb using CRISPR to target miR-24 (see 4.2.3.2). Although we used two different technologies for the depletion of miR-24, the phenotype was very comparable and therefore, we focused primarily on

genes which showed differential expression in both DE lists. Furthermore, we wanted to compare shared pathways and DE genes which may not be affected in CHO-S Fc but in CHO-K1 and vice versa as there is evidence that different CHO cell linages might not be as related as previously expected (M. F. Wurm, 2013). For the functional annotation DAVID as well as STRING® was used to identify pathways as well as protein interactions. Using that information, we were able to identify functions of dysregulated proteins and relate them back to the phenotype observed. For the depletion of miR-24 it was shown, that especially pathways related to translation, rRNA processing, tRNA processing as well as protein folding were upregulated (Figure 24 A to E).

PES1, BOP1 and WDR12 were identified in our study as upregulated due to knockdown of miR-24. PES1 and WDR12 were predicted as being targeted by miR-24. Interestingly, PES1 and WDR12 together with BOP1 are associated in a protein complex, the so called PeBoW (Holzel et al., 2005; Rohrmoser et al., 2007). The PeBoW is crucial in ribosome maturation by processing parts of the pre-rRNA to generate pre40S and pre60S subunits which will be further processed and transported into the cytoplasm (reviewed by (Lafontaine, 2015). Consequently, it has been shown that the PeBoW complex is crucial for translation and proliferation. As additional part of the rRNA processing machinery, PA2G4 has been upregulated as well and was related to growth (Squatrito et al., 2004; Squatrito et al., 2006). Two other significantly upregulated proteins in our study are EIF6 and RACK1/GNB2L1. EIF6 is responsible together with RACK1/GNB2L1 for the assembly and recycling of 40S and 60S ribosome subunits into the mature 80S translation initiation complex in the cytoplasm (Miluzio et al., 2009). Furthermore, 60S ribosomal protein L3 (RPL3), 60S ribosomal protein L7 (RPL7L1) and 40S ribosomal protein S15a (RPS15A) have shown to be upregulated as well. RPL3 and RPS15A are hereby interacting with each other in a structural context and have shown to be involved in translation (Ghanem et al., 2011; Lopez et al., 2012; Rosen et al., 2010). Further evidence that depletion of miR-24 results in upregulation of parts of the translational machinery is the higher abundance of TUFM and GFM1. Both are involved in recruitment of aminoacyl-tRNAs and release of deacetylated-tRNAs in the mitochondria (Christian & Spremulli, 2012; Simon et al., 2017). Upregulation of TUFM and GFM1 could presumably open a bottleneck as tRNAs are usually highly abundant and not a limiting factor. Interestingly, seven aminoacyl-transferases (EPRS, IARS, AARS, YARS, WARS, GARS and NARS) responsible for loading amino acids to its cognate tRNA were upregulated as well in our study. This strengthens that parts of the translational machinery are

upregulated eventually leading to higher specific productivity after knockdown of miR-24. Not only parts of the translational machinery were upregulated but also proteins associated with response to UPR and ER stress response. One member is HSPD1 which interestingly previously described as associated with a high productivity phenotype (Meleady et al., 2011; Sommeregger et al., 2016). Besides, productivity HSPD1 overexpression seems also to be associated with increased proliferation in tumour cell lines (W. Liang, Yang, Peng, Qian, & Wang, 2015) and CHO cells (Clarke et al., 2012c). Furthermore, Meleady and colleagues identified RUVBL which was also higher expressed in miR-24 depleted cells and is potentially associated with higher Qp.

Agrawal and colleagues showed that miR-24 is involved in apoptosis through targeting pro-apoptotic genes like Bim, FAF-1, Caspase-9 and Apaf-1. On the other hand, studies showed targeting of antiapoptotic genes like BCL-2 (Singh & Saini, 2012b). It seems that the action of miR-24 in a pro- or antiapoptotic manner is cell type specific or that regulation is involved in keeping the sensitive balance of apoptotic mediators. Overexpression of miR-24 using mimics inhibits cell proliferation of six different human cancer cell lines by inducing the expression of p53 and p21 (Mishra et al., 2009a). The same study showed that miR-24 overexpression also targets DHFR which catalyses the conversion of dihydrofolate into tetrahydrofolate. Tetrahydrofolate is required for purine and pyrimidine synthesis and therefore plays an essential role in cell growth and proliferation. Consequently, down regulation of miR-24 causes an increase of proliferation in human epithelial cells (Cheng et al., 2005). In our DE protein lists after the depletion of miR-24, DHFR was more abundant (1.35-fold, ** $p = 0.01$) suggesting that proliferation could be influenced. However, in our sponge experiments no change in proliferation was observed in CHO-S Fc nor CHO-K1 mAb. Interestingly, growth was enhanced when miR-24 was either targeted using CRISPR/Cas9 and overexpression of miR-24-3p using mimics resulted in inhibited proliferation (Figure 35 and Figure 36).

Therefore, targeting miR-24 is a valid strategy for the improvement of productivity for CHO cell lines. Due to the amount of genes targeted by miRNAs changes in the transcriptome as well as on the therapeutic protein quality should be explored further.

To establish whether these effects were cell line or product dependent, five more cell lines were transfected including CHO-K1 Fc, CHO-K1 EPO, CHO-K1 DP12, DG44i Fc and DG44i mAb. All chosen cell lines originated from different CHO lineages and

expressed different recombinant therapeutics. The depletion of miR-24 in following cell lines was performed by Dr. Srinivas Suda and

Depletion of miR-24 resulted in a high productivity for all tested cell line except DG44i Fc making miR-24 a broadly applicable tool for cell line engineering and the improvement of productivity in CHO.

5.1.2.1.4 Impact of miR-27 depletion on phenotype of CHO cells and bioprocess performance

Overexpression of miR-27a resulted in a decrease in growth (CHO-K1 mAb) but increased proliferation in a different cell line (CHO2B6) showing evidence for cell type specific effects (Noèlia Sanchez, 2013). Depletion of miR-27 in CHO-S Fc resulted in a 2-fold (day 6) to 2.5-fold (day 8) increase in productivity. However, this productivity phenotype was only observed in CHO-S Fc and not in any other cell line tested. Comparing data from proteomic profiling no relation to the phenotype could be made when looking for DE proteins. When comparing with the literature miR-27 seemed to be involved in mediation of apoptosis. In fact, our pathway analysis of DE proteins showed a connection to oxidative stress as well as apoptosis in over-represented pathways. However, no increase in culture length was observed upon miR-27 depletion in CHO-S Fc (Figure 20) whereas an effect can not be excluded as samples were taken every 48h and anti-apoptotic effects might not be as long lasting. To overcome this growth curves with samples taken every 4-6 hours could be performed. However, when miR-27b was targeted in CHO-K1 mAb using CRISPR/Cas9, cultures were prolonged (further discussed in 5.2.2.2) indicating its involvement in apoptosis. Furthermore, it could be a cell line specific phenotype.

5.1.2.2 Impact on the glycosylation pattern of a Fc fusion protein and a mAb after depletion of miR-23-24-27, miR-23, miR-24 and miR-27

With their ability to regulate whole transcriptional networks, targeting miRNAs could be a route to impact complex phenotypes towards productivity, viability and growth as shown by our study. For this same reason, it is important to also check for any changes in product quality as a result of intervention. Culture conditions, media components, the

cell type and the bioprocess itself can have a significant influence on the glycosylation pattern of a therapeutic protein. Furthermore, the glycosylation pattern of a therapeutic protein must be investigated extensively to meet FDA regulations and to ensure that product quality is consistent at all times. It has been shown that different glycosylation patterns can influence the circulation half-life of IgGs, ADCC and biological activity. Changing product attributes have also been demonstrated to be a potential strategy for cell line engineering to improve recombinant protein quality (Bork et al., 2009; Hossler et al., 2009a). Depletion of miR-23, miR-24 and miR-27 resulted in significant changes in the glycosylation pattern on the Fc fusion product expressed by CHO-S (Figure 19). When miR-24 was depleted in CHO-K1 mAb significant changes were also observed on glycosylation of the IgG (Figure 23). This led us to investigate if the proteomic profiling datacould give more insight into differentially expressed proteins influencing glycosylation.

In fact, it was shown that depletion of miR-23 led to increased levels of Phosphomannomutase 2 (PMM2), Glucosidase 2 subunit beta (PRKCSH) and Neutral alpha-glucosidase AB (GANAB) in CHO-S Fc. Depletion of miR-24 led also to increased levels of PRKCSH and reduced levels of miR-27 led to an increase in PMM2 in CHO-S Fc. PMM2 which is a predicted target of miR-24-3p is well studied in glycosylation disorders like congenital disorder of glycosylation (CDG). It is an enzyme responsible for catalyzing the reaction from 6-mannose phosphate to 1-mannose phosphate, a key metabolite in the generation of N-glycans. Defects in PMM2 often result in unoccupied N-glycosylation sites on proteins as PMM2 is involved in early stages of glycosyation (Sharma et al., 2011). GANAB is the catalytic active alpha subunit of Glucosidase II and forms together with the noncatalytic beta subunit PRKCSH, Glucosidase II. It is a crucial enzyme involved in correct folding of glycoproteins and processing of N-glycans (D'Alessio & Dahms, 2015; Pelletier et al., 2000). High mannose content on mAbs usually is accompanied by afucosylation impacting biological activity. High levels of sialylation has been shown to negatively impact ADCC as well as CDC for IgGs (CMC Biotech Working Group, 2009). As relatively new therapeutics Fc fusions are not as thoroughly studied as mAbs. However, similar to mAbs the efficacy depends heavily on glycosylation of the Fc fusion. Increased levels of sialylation could lead to increased sucess rates in terms of efficacy and serum half-life (Czajkowsky et al., 2012). Therefore, it seems that miRNAs of the miR-23 cluster are involved in the fine-tuning of protein glycosylation.

5.1.3 CHO cell lines, clonal variation and cell line specific behaviour

Members of the miR-23 cluster were chosen because of a beneficial impact on the phenotype after their depletion or overexpression of such. For example, miR-23 has been shown to increase longevity in CHO-K1 mAb and productivity in CHO-K1 SEAP expressing cells (Kelly et al., 2014). Depletion of the miR-23 cluster resulted in higher productivity in CHO-K1 SEAP also (Sanchez et al., 2014). When we tested a panel of industrial relevant cell lines of CHO-K1, CHO-S and DG44i, only CHO-S showed increased productivity after depletion of miR-23-24-27 and no effect after depletion of miR-23 alone was observed at all. This cell line dependent behaviour may be a consequence of the origin and linage of CHO cells as well as evolutionary adaption in miRNA targets which will be discussed later.

The original CHO cell line was first isolated in 1957 by Dr. Theodore Puck (Puck et al., 1958) and CHO cells were used for intensive studies of chromosome aberrations and mutations due to their ease in culturing and large chromosomes. Furthermore, CHO cell populations were easy to select for metabolic mutations using selective media. The original fibroblast like cell type was isolated from 0.1 g of tissue and further cultivated for several passages. The original CHO cell line was diploid and had 22 chromosomes (11 pairs). The morphology of the cells changed after ten months in culture and cells became spontaneously immortalised. Therefore, the genetic instability of CHO cell lines was well studied over the last decades.

In the last 50 to 60 years several cell lines have been created and non-standardised culture conditions and the high genetic modulation of the CHO genome led to many different cell types. Each generated sub cell line from CHO-K1 e.g. CHO-S, DG44 to mention only a few can be more likely described as its own cell line with exhibiting different phenotypes and behaviours (M. F. Wurm, 2013). This genetic instability is a useful feature which is commonly exploited in the biopharmaceutical industry to amplify transgenes and ultimately increase copy numbers as well as the resulting higher expression (e.g. DHFR, GS systems). The variation inherent in a genetically unstable population also means that individual clones can be found, during screening, with a wide range of phenotypes including faster growth and/or high productivity. Hence clone screening is a very successful way in finding good performing clones. However, loss of expression is a common problem that can occur despite maintenance of selection pressure (M. Kim et al., 2011b). It has been shown that the generation of many

recombinant CHO cell lines led to several chromosome aberrations, deletions and rearrangements (Derouazi et al., 2006). Genetic instability and a loss or an increase in copy numbers could also influence miRNA target regulation. It is known that miRNA regulation is a “fine-tuning” process and can be easily dysregulated with dramatic impact on development or cell survival.

In addition to genetic instability, the evolution of miRNA targeting as well as clustering of miRNAs may influence cell line specific behaviour observed. The efficiency with which a miRNAs to binds to its target and the regulation of miRNAs seem to have alternative modes which are cell line and tissue dependent (Kulkarni et al., 2016). Kulkarni and colleagues showed that after co-transfection of ten cell lines with let-7a and a plasmid containing the luciferase reporter gene renilla with binding sites for let-7a that differences in miRNA regulation can occur depending on the cell line. All tested cell lines showed a significant reduction in luminescence after binding and inhibition due to let-7a. However, the level of suppression was highly cell line dependent suggesting a difference in mediated mRNA stability due to regulation by let-7a. Five cell lines stabilised the mRNA transcript, three cell lines did not show any effect and two cell lines showed translational inhibition due to degradation. This suggests a cell line dependent regulation of genes by any particular miRNA regulator.

A further reason why the depletion dependent impact of miRNAs could be cell line specific is the usage of 3’UTR isoforms which can change the number of binding sites in this highly regulatory region. The mRNA:miRNA interaction is usually located in the 3’UTR of the mRNA resulting in translational inhibition or degradation. The 3’UTR is furthermore a regulatory region. However, alternative long and short UTR isoforms have been reported in the same ORF due to different poly-A signals which can occur distal or proximal (Decker & Parker, 1995; Miyamoto et al., 1996). Longer or shorter isoforms can have a different number of binding sites and a cell line dependent shift in using longer or shorter isoforms can weaken or enhance the miRNA regulation and seems to be dependent on the cellular context (Nam et al., 2014). In addition, one messenger of a gene can have multiple miRNA binding sites. The difference in the 3’UTR can strongly effect gene regulation in this context by adding or deleting miRNA binding sites due to the cell line specific and preferred isoform usage. As we accumulate a better understanding regarding the use of different 3’UTRs in CHO this may help explain some of the cell line differences observed.

Another element playing a role in miRNA binding to its target mRNA could be the variation of copy numbers occurring in the genome compared to the reference genome (e.g. a CHO-S cell line compared the original CHO-K1 tissue). This could involve copies of miRNAs itself or copies of the target gene. Higher abundance of mRNAs could possibly alter the gene expression significantly and could influence the phenotype and diversity (Veerappa et al., 2014). Furthermore, there is a strong evidence that multiple gene numbers increase the level of gene expression (Schuster-Bockler et al., 2010; Stranger et al., 2007). However, an increase in expression could unbalance to the normal gene regulation by its miRNA binding partner resulting in only partial silencing of the target gene. A dosage-dependent target selection for miRNAs has been reported for several miRNAs and their target mRNAs (Shu et al., 2012). This effect is suggested to be based on the miRNA expression level itself and mRNA levels in the cell triggering feedback loops as endogenous mRNAs can act as a “sponge” reducing miRNA availability in the cell and therefore dysregulates othe mRNAs. Let-7a-7f were co-transfected with reporter plasmids containing DICER and c-MYC as reporter genes with MBS in the 3’UTR. Overexpression of let-7a downregulated the expression of DICER but downregulated the c-MYC reporter at even higher levels suggesting a selective behaviour of the miRNA itself supporting their role in “fine-tuning” gene expression and evolutionary development. Leading to genetic variability and an exploration of new functions due to gene overexpression as well as ultimately into a phenotype - desirable or not.

5.2 CRISPR/Cas9 as a genome engineering tool to target miRNAs in CHO cells

Recent studies have demonstrated the beneficial use of miRNA engineering to improve productivity, enhance cultivation times and improved growth rates (Barron et al., 2011; Druz et al., 2011; Jadhav et al., 2012b; P. S. Kelly et al., 2015a). Besides transient depletion of miRNAs using antagomiRs, sponge decoy technology for the stable depletion of miRNAs is a commonly used tool to study miRNA function (Kluiver et al., 2012a). However, the usage of sponges is a challenge due to the necessity for a reporter gene which will eventually siplay a translational burden and may decrease therapeutic protein production. Further challenges are for example generation of a stable cell line using plasmids leading to random integrations and the fact that it is rather a depletion than a knockout. We wanted to investigate as well if a complete knockout can be tolerated. This goes along with the observation that gene expression varies a lot during different growth phases making sponges susceptible to changes in expression consequently also allowing miRNA abundances to be differential. Previous results have shown depletion of mature miRNA but on the contrary enrichment was observed as well. The enrichment is most likely a result of miRNA mediated target protection (TMMP) whereby miRNA binds to a mRNA causing translational inhibition. In case of introducing sponges with aritifical MBS, miRNA binds to its target as well. However, after lysing of cells miRNA is released and appears to be “overexpressed”. This effect led to inconclusive results about miRNA expression in cell lines tested. It was demonstrated that whole miRNA families with similar seed sequence can bind to the sponge which can potentially lead to phenotypes not resulting from the miRNA studied (Kluiver et al., 2012a).

Consequently, we wanted to implement CRISPR/Cas9 as a tool to knockout miRNAs and to overcome these challenges. The miR-23 cluster has been demonstrated to be an interesting cluster for miRNA engineering which we wanted to target with CRISPR. It was demonstrated that miRNAs can be successfully targeted using CRISPR/Cas9 in human cell lines by Chang and colleagues (Chang et al., 2016) and coding genes have been targeted in CHO before FUT-8 (Ronda et al., 2014). However, miRNAs have not been targeted. To compare CRISPR/Cas9 to sponge decoy technology we chose CHO-K1 mAb. We used this cell line for stable and transient miRNA depletion experiments as well as for overexpression.

5.2.1 Functionality of CRISPR/Cas9 in CHO cells

Targeting coding genes with CRISPR/Cas9 is relatively easy and straight forward as even a small indel of ±1 bp will generate a frame shift resulting in premature stop codons and error prone mediated degradation of the amino acid chain. Targeting of miRNAs could therefore represent a special challenge as miRNAs are non-coding and a small indel close to the seed region may not affect function nor processing. The seed region is most crucial for target recognition (Lewis et al., 2003) but it was demonstrated that a complete pairing of the seed region to a mRNA might not be necessary (Didiano & Hobert, 2006). We designed sgRNAs to target either the seed region or proximal to the seed region. Physical and statistical analysis using RNA-fold predicted that small indels in the stem-loop sequence or the seed region of a miRNA has strong effects on the structure of the miRNA (Figure 26) precursor and might influence processing or target recognition of the mature miRNA. With ~22 nucleotides in length miRNAs are very small molecules and targeting the seed region can be a challenge due to the limiting factor of the PAM. The PAM must be located immediately downstream of the sgRNA binding site in the genomic locus and to allow Cas9 efficient function of endonucleolytic domains. The PAM is dependent on the species origin of Cas9. *S. Pyogenes* (spCas9) for example uses NGG as a PAM. Different Cas9 variants have been recently discovered which use different PAM like *N. meningitides* (NNNNGATT) or *T. denticola* (NAAAAC). CRISPR/Cas9 has been proven to be an efficient tool for genome engineering but the PAM limits the range of possible binding sites. However, the PAM used for *S. pyogenes* Cas9 (NGG) can be found approximately every eight base pairs in the human genome (Cong et al., 2013). In our case a PAM site was located upstream of the seed region for miR-23a, miR-23b, miR-27a and miR-27b. For miR-24 a PAM was located in the seed region of the miRNA itself.

In our experiments we demonstrated by Sanger sequencing, Surveyor® assay and NGS that we can effectively target miRNAs proving that CRISPR/Cas9 can be used in CHO cells without the need of codon optimisation. We also observed a reduction in mature miRNA expression. Comparing targeting efficacy showed that not every miRNA is targeted with the same efficiency which was evident by the amount of indels generated and miRNA expression (Figure 28 and Figure 29). Targeting efficiency seems to be highly dependent on the nature of the locus or the sgRNA (Ronda et al., 2014). The sgRNA is critical for the specificity and binding efficiency of Cas9 to the genomic target locus. However, studies have shown that not every position of the 20-nucleotide long

sequence is equally important. 5'-truncated forms of the sgRNA did not reduce the cleavage efficiency. However, deletions at the 3'-end prevented cleavage of the target DNA (Fu et al., 2013b; Hsu et al., 2013; Jinek et al., 2012). Functional analysis of Cas9 orthologues showed that the 3'- region works as a "seed" region and is indispensable for target binding and efficient cleavage of the target DNA. In addition, the amount and the position of mismatches which are tolerated is dependent on the sgRNA used and is highly variable but reasons for this effect remain unclear (Fu et al., 2013b; Hsu et al., 2013). When we targeted miR-23a the expression of miR-23b was affected and vice versa. The same was observed for miR-27a and miR-27b (Figure 30). When the sgRNAs were compared it was apparent that the 3' of the guide which is located close to the PAM had a high sequence similarity. Cross-targeting was also observed when indels were analysed using NGS (Table 7) supporting the observation that the 5' region of the sgRNA is not as important for targeting.

It has been suggested that the binding efficiency of Cas9 is dependent on DNA methylation and chromatin modifications. Wu and colleagues showed that DNA methylation of CpG target sites is related to a lower binding efficacy of Cas9 (X. Wu et al., 2014). Furthermore, they proposed that histone modifications, which affect the chromatin accessibility, could hinder sgRNA binding but it has yet to be proven.

Our results demonstrated that targeting efficiency was either sgRNA or locus dependent with the highest efficacy observed for miR-23a, miR-23b and miR-24 with up to 98% indel frequency in mixed populations. For miR-27a and miR-27b lower targeting efficacy was observed which was also reflected in mature miRNA expression data which showed a range between ~3 and ~10-fold reduction in abundance for both. As we successfully proved that miRNAs could be targeted and miRNA expression could be reduced we wanted to explore whether the passenger strand or the processing of the precursor was affected.

Both, miR-24-3p and miR-24-5p were shown to be less abundant in CHO-K1 mAb after targeting the seed region of miR-24-3p. Levels of miR-24-3p as well as miR-24-5p showed a comparable level of reduction. We also observed the same reduction for miR-27b-3p and miR-27b-5p after targeting miR-27b-3p. The same reduction in mature levels of both miRNA strands was observed by Chang and colleagues after targeting miR-17, miR-200c and miR-141 in human HCT116 cells (Chang et al., 2016a). In contrast to

reduced expression levels of individual mature miRNA members, an increase in primary (pri-miR) microRNA levels were observed for miR-17-92, miR-200c and miR-144.

To investigate whether this was also the fact in our cells, expression levels of the miR-24 precursor was analysed. In fact, an accumulation of ~9-fold was observed for pre-miR-24 in the mixed population (Figure 35). The same strong accumulation was observed in 3 out of 6 clones (clone 1, 5, 6) isolated from a mixed population where miR-24 was targeted. Clone 4 showed a slight enrichment of pre-miR-24, however it was confirmed using NGS that this could be due to a non-clonal origin or reduced efficiency of targeting (22% indels in miR-24-2). Clone 5 and 6 on the other hand showed a high accumulation of precursor as well as complete targeting of miR-24-1/2 confirmed by NGS with >99% indels. Therefore, impaired processing is most likely the cause of accumulation after targeting of a microRNA. Upregulation of pre-miR-24 or the primary construct could also be the cells reaction of reduced mature miR-24 levels. However, when mature levels of all other members of the cluster was assessed no difference was observed.

The first step after transcription of the primary construct is the cleavage by Drosha RNase III which processes the pri-miRNA into a ~70 nucleotide long precursor miRNA (pre-miRNA). If the miRNA is located in an intron, mRNA splicing can alternatively lead to formation of pre-miRNAs (Y. Lee et al., 2003). The pre-miRNA exhibits a 5´-phosphate and a 2 nucleotide 3`-overhang resulting from the RNase III cleavage. The second step is the export of the pre-miRNA into the cytoplasm mediated by exportin-5 which binds dsRNA and uses RanGTP as a cofactor (Lund et al., 2004). In the cytoplasm the pre-miRNA is further processed by Dicer RNase III multi protein complex into a 22-nucleotide miRNA-miRNA* duplex with a two nucleotide 3`-overhang (Y. Lee et al., 2003) and the duplex is incorporated into a pre-RISC. Pre-miR maturation can alternatively be conducted by AGO2 (Y. P. Liu, Schopman, & Berkhout, 2013). The increase in accumulated pre-miR suggests an inhibition of maturation due to the loss of specific sequence features or structures (Starega-Roslan et al., 2015). The two main drivers for processing are the RNases Drosha and Dicer which recognise different sequence motifs. In the case of Dicer and Drosha, a bias towards uracil was observed at processing sites and a lack of guanine (Gu et al., 2012; Starega-Roslan et al., 2015). Loop positioning has been shown to be a determining factor of dsRNA recognition and processing for Dicer activity (Starega-Roslan et al., 2015). However, mutating Drosha recognition sites has shown, that structural changes may only cause alternative processing of the pri-

miRNA (Ma et al., 2013). Targeting structural important regions of the miRNA i.e. the stem-loop or the seed region may be therefore the most effective strategy for miRNA engineering to impair miRNA processing and mature function.

Keeping in mind that using CRISPR or other targeted genome engineering tools like ZNFs or TALENs (Jiang et al., 2014), may also inhibit the passenger strand it is important to remember that the phenotype potentially is a result of the miRNA partner. For a long time, the idea was that after recruitment and processing of miRNA/miRNA* duplex the passenger strand which usually shows a lower stability is degraded. However, several studies have shown that the miR* strand also has a role in transcriptional repression under certain circumstances. The miR* strand is usually found in much lower abundance than the mature counterpart (Lagos-Quintana et al., 2002). Studies have shown that the miRNA and miRNA* can function both in regulation of related pathways or independent roles (Shan et al., 2013; Yang et al., 2013).

To establish whether the phenotype after depletion of miR-24 in CHO-K1 mAb was a result of miR-24-3p or miR-24-5p, mimics for miR-24-3p and miR-24-5p were transfected in expectation of opposing phenotypes. It was indeed the case that miR-24-3p inhibited proliferation significantly. Growth inhibition after overexpression of miR-24-3p was also observed by other groups in several cell lines (Mishra et al., 2007). MiR-24-5p however, had no effect on growth in this particular cell line.

5.2.2 Assessment of phenotypes after CRISPR/Cas9 mediated targeting of individual members of the miR-23 cluster

5.2.2.1 Targeting of miR-23a and miR-23b using CRISPR/Cas9 leads to prolonged culture length

Depletion of miR-23a and miR-23b led to increased viable cell densities in late stages of batch cultures at the expense of productivity. Sponge mediated depletion of miR-23 in the same cell line showed the same phenotype (Kelly et al., 2014). The involvement of miR-23 in regulation of apoptosis is well studied. The X-linked inhibitor of apoptosis (XIAP) is a direct target of miR-23a and was shown to increase viable cell densities upon overexpression in CHO-K1 and HEK293T cells (Sauerwald et al., 2002). Inhibition of programmed cell death is regulated by binding of XIAP to caspase-3, -7 and -9. Additionally, there is evidence that miR-23a/b can prevent apoptosis during hypoxia by targeting important key components like Bax-like BH3 protein (BID), caspase-7 and BCL2/Adenovirus E1B 19kDa Interacting Protein 3-Like (BNIP3L) (Agrawal et al., 2014). MiR-23a has also been shown be involved in regulating the survival of embryonic stem cells due to inhibiting BMP-4 which normally drives apoptosis by activating PUMA and BAX (Musto et al., 2015). Besides, regulating direct targets for apoptosis, miR-23a and miR-23b were shown to be involved in regulation of cancer progression (Hu et al., 2017). It was demonstrated that miR-23 is involved in proliferation as well as glutamine metabolism in human B-lymphocytes as well as in CHO cells by targeting GLS and contributing to the Warburg effect (Kelly et al., 2015).

5.2.2.2 Targeting of miR-27a using CRISPR/Cas9 reduces growth and targeting of miR-27b leads to prolonged cultures

Targeting of miR-27a using CRISPR resulted in decreased growth rates compared to the control in CHO-K1 mAb. Transient depletion of miR-27a caused the same phenotype in the same cell line (Sanchez et al., 2014).

CRISPR mediated depletion of miR-27b resulted in an increase of culture duration in batch and fed-batch cultures with CHO-K1 mAb. Prolonged culture times were at the expense of specific cellular productivity however, increased viable cell density still led to

higher final titers. Sponge mediated depletion of miR-27 however showed no effect in CHO-K1 mAb.

Increased viability in late stages of the culture due to reduced levels of miR-27b could possibly be due to its role in regulation of apoptosis. Agrawal and colleagues showed that miR-27 targets APAF1 and consequently inhibits apoptosis in hypoxic conditions (Agrawal et al., 2014). Further studies proved that miR-27 negatively regulates FADD which interacts with caspase-8 and apoptotic signalling and prevents apoptosis in human cells (Chhabra et al., 2009). Studying the effects of miR-27 depletion in CHO-S Fc also showed upregulation of proteins which are involved in mediation of apoptosis (Figure S 10) including BAG3, BCL-2 and CIAPIN1.

BAG3 for example (Bcl-2 associated anthanogene 3) has been shown to be involved as co-chaperone together with Hsp70 in the regulation of several pro-apoptotic proteins i.e. Bim (Rosati et al., 2011) and is also involved in development of apoptosis resistance in lung cancer (Zhang et al., 2012). Another upregulated protein was CIAPIN1 (cytokine-induced apoptosis inhibitor-1) which was shown to be involved in developing drug resistance in several cancer cell lines due to its role in regulation of BCL-2 and BAX (Li et al., 2007) as well as Bcl-L and MDR-1 (Zhang et al., 2011). Overexpression of BCL-2 has been very well described as a cell line engineering tool to prevent apoptosis in many industrially relevant cell lines like CHO, NS0 myeloma and SF9 cells (Goswami et al., 1999; Mastrangelo et al., 2000; Mitchell-Logean & Murhammer, 1997). Increased resistance to apoptosis was assessed in various circumstances including shear stress, oxygen limitation, ammonia and nutrient depletion. However, it was also shown that the phenotype exhibited by the overexpression of both factors is cell line dependent. Furthermore, depletion of Bax using siRNAs or deletion using ZFNs resulted in increased cell viability in late stage CHO cell culture (Cost et al., 2010; Lim et al., 2006).

Therefore, depletion of miR-27 and the resulting extension of culture times could be interesting for cell line engineering. To understand the effect after depletion of miR-27b better, proteomic profiling combined with pathway analysis in CHO-K1 mAb was performed.

5.2.2.3 CRISPR/Cas9 mediated targeting of miR-24 enhances CHO cell growth rate and productivity

Depletion of miR-24 using CRISPR/Cas9 led to increased growth rates and productivity in CHO-K1 mAb. Overexpression of miR-24-3p inhibited growth (Figure 38). This was also observed by Mishra and colleagues where overexpression of miR-24 inhibited cell proliferation in six different human cancer cell lines by inducing the expression of p53 and p21 (Mishra et al., 2009a). E2F2 and MYC are proteins which are involved in rapid cell cycle progression and Lal and colleagues showed that miR-24 targets both mRNAs and blocks uncontrolled proliferation. However, E2F2 and MYC do not have predicted binding sites for miR-24 in the 3'UTR (Lal et al., 2009). Mishra and colleagues also showed that miR-24 targets the DHFR gene which catalyses the reaction of dihydrofolate into tetrahydrofolate. Tetrahydrofolate is required for purine and pyrimidine synthesis and therefore plays an essential role in cell growth and proliferation. Consequently, down regulation of miR-24 caused an increase of proliferation in human epithelial cells. For our DE protein lists generated by proteomic profiling an upregulation of DHFR (1.27-fold, *** p = 0.00083) was also observed upon targeting miR-24 using CRISPR.

Besides growth, IgG productivity was signficanlty higher in miR-24 depleted CHO-K1 mAb cells. The same was observed for sponge mediated depletion in both CHO-K1 mAb and in CHO-S Fc. Proteomic profiling of cells where miR-24 was targeted using CRISPR/Cas9 demonstrated that same proteins upregulated in CHO-S Fc after sponge depletion were also upregulated in a different CHO cell linage (CHO-K1 mAb) producing a different protein product (see section 5.1.2.1.3). These were involved in translation, rRNA processing, tRNA processing and protein folding and have been extensively discussed in this section.

To investigate the effect of miR-24 depletion on the transcriptome, RNAseq was performed. This revealed that 700 DE genes after targeting of miR-24. However, only 17 genes were actually to common when proteomic and transcriptomic data were compared. It is not an uncommon phenomenon to observe that transcriptomic data does not correlate with proteomic data (Ghazalpour et al., 2011; Schwanhausser et al., 2011). Noncorrelation can have several reasons i.e. when stability of mRNA is compared to protein stability. With a typical half life of 15-20h for mRNAs their stability is significantly less than protein stability with a half-life of up to 72h (Hargrove & Schmidt, 1989; Schwanhausser et al., 2011). Schwanhausser and colleagues also stated that mRNA

abundance was significantly less compared to protein. Furthermore, the half-life depends on the state of the protein including phosphorylation, localisation or other PTMs as well as N-terminal residues (Maier, Guell, & Serrano, 2009). Besides, considerably lower stability of mRNAs, it is also important to mention that if the mRNA is detectable it does not mean the mRNA is translated. Binding to the ribosome, the number of bound ribosomes and processing factors may influence the translation as well as accessibility (Ingolia, Ghaemmaghami, Newman, & Weissman, 2009). In addition, the phase of the cell cycle influences the correlation between mRNA expression and proteomic data (Cho et al., 1998). Therefore, a correlation between our proteomic data and transcriptomic data might not be as evident. Furthermore, as mRNA abundance is comparably lower slight changes may not be recognized by applying stringent statistics but still can have a considerably high effect on protein levels.

Interestingly, miR-23b was significantly upregulated (*** p = 0.0000017, log2 fold change 6.09) compared to the control. Although statistically significant the base mean was low and would be considered “noise” from sequencing. Chhabra and collegues showed that the miR-23b cluster has a RNA-polymerase II promoter and all core elements needed for initiation of transcription (Chhabra, Dubey, & Saini, 2010c). Transcription by RNA-polymerase II will result in a poly-A tail which will be enriched in common RNASeq approaches. As an enrichment of pre-miR-24 was demonstrated after targeting of miR-24 using CRISPR, it is possible that the pri-miR-23-24-27 transcript is enriched as well. An increase in primary transcript has been shown by Chang and colleagues for targeting the miR-17-92 cluster (Chang et al., 2016b). For these reasons it could be possible that miR-23b is more present or is eventually upregulated as a compensation for less levels of miR-24. We showed that miR-24 and miR-23 have a coorporate function in regulating similar pathways (Figure S 8) which has also been predicted by Liang and colleagues (T. Liang et al., 2014). To investigate this further the expression of the primary construct could be assessed.

5.2.2.3.1 Role of miR-24 in cell cycle progression, increased proliferation and metabolism

The function of miR-24 in proliferation, cell cycle, metabolism and apoptosis has been intensively studied by several research groups (Agrawal et al., 2014; Lal et al., 2009; Mishra et al., 2007; Mishra et al., 2009b; Qin et al., 2010). We showed that downregulation of miR-24 increased proliferation and furthermore boosted productivity. To ensure that the phenotype was a result of miR-24 depletion and upregulation of known targets we assessed the expression of c-MYC and CDKN1b in clones and mixed populations. Expression of c-Myc showed some inconsistency in three clones assessed but was upregulated in mixed population. As an oncogene c-Myc plays a crucial role in cell cycle progression and proliferation through the transcriptional control of important cell cycle regulators including cyclin-dependent protein kinases (cdks) and E2F transcription factors (Bretones, Delgado, & Leon, 2015). Furthermore, it antagonises the expression or function of proliferation inhibitors including p21, p27 or RAS (Born et al., 1994; Obaya et al., 2002; Perez-Roger et al., 1999). Besides the regulation of cell cycle progression, c-Myc is involved in boosting ribosomal biogenesis and translation but is also regulated itself tightly by miR-24. Together with ribosomal proteins, miR-24 is recruited to the 3'UTR of the c-Myc mRNA to regulate its translation when ribosomal stress is induced by treatment with actomycin D (Challagundla et al., 2011). Other ribosome related targets of c-Myc are for example RPL3, RPL6 and RPS15a (J. Kim et al., 2010). RPL3 (* p = 0.03, 1.20-fold) and RPS15a (* p = 0.03, 1.22-fold) were upregulated in our DE protein lists after targeting miR-24. Our observations that c-Myc is increased after depletion of miR-24 and that ribosomal processing as well as translation is increased could be part of the mechanism of driving both growth and productivity.

CDKN1b or p27 is a cyclin-dependent kinase (CDK) and is a cell cycle inhibitor important for progression through G1 to S phase. Interestingly CDKN1b is a target of miR-24 (Lynch et al. 2016) and was more abundant when miR-24 was depleted in mixed population as well as in all assessed clones (Figure 39). Being more abundant it could be argued that cell cycle progression might be arrested. Besides being a target of miR-24 however, it was demonstrated that c-Myc is involved in regulating p27 and therefore may rescue cell cycle arrest and drive progression into the next phase (Vlach et al., 1996) Even though CDKN1b is higher expressed, growth was increased for our miR-24

depleted CHO-K1 mAb cell line which might be due to antagonising effects of c-Myc. The active form of p27 is dephosphorylated and located in the nucleus. Deactivation occurs due to phosphorylation and subsequent relocation into the cytosol triggered by c-Myc. Cyclin E-cdk2 which is responsible for the phosphorylation is presumably recruited and causes deactivation of CDKN1b.

The role of c-Myc in metabolism was first described in the 1920's by Otto Warburg and coworkers hypothesising the change of cancer cells from using more efficient oxidative phosphorylation to aerobic glycolysis. Glycolysis is preferred in low oxygen conditions such as hypoxia where the universal energy source is converted to lactic acid rather than entering the TCA cycle (Warburg et al., 1956). This goes along with the observation that glucose transporters as well as glycolytic enzymes were upregulated (Osthus et al., 2000). One of these enzymes is ENO1 which was also upregulated upon depletion of miR-24 in our study. However, an increase or shift towards glycolysis was not observed in our study (Figure 40). On the contrary oxidative phosphorylation and lactic acid production remained low upon the depletion of miR-24. This was a surprise as the production of lactic acid in exponential phase of fast growing cells is usually very high (Zagari et al., 2013). The same study observed a correlation of increased EACR combined with a reduction in oxidative phosphorylation. Surprisingly our observed increase in growth combined with increased productivity did not lead to increased mitochondrial function or acidification. Rapid consumption of glutamine and upregulation of glutaminolysis has been demonstrated to be another characteristic of fast growing cells (Deberardinis et al., 2008). This process is driven by overexpression of c-Myc which consequently drives the expression of the mitochondrial glutamine synthetase (GLS) (Dang, 2011). Upregulation of GLS and the resulting drive of glutamate and α-ketoglutarate into the TCA-cycle is usually accompanied by increased pyruvate levels as well as increased lactic acid production which was not observed. However, anabolic reactions can also be driven by glutaminolysis such as fatty acid production which is necessary for rapid cell proliferation (Figure 57).

Besides metabolism, c-Myc has also been demonstrated to be directly involved in nucleotide synthesis which ultimately drives proliferation and translation (Liu et al., 2008; Mannava et al., 2008) as well as UPR/chaperone activation through LONP1, HSPD1, DNAJ3 and RUVBL2. The activation of UPR can also be independent of c-Myc but be in response to higher oxidative stress caused by higher translational demands. ROS are a side product of formation of disulphide bonds – and their formation would be increased

in a high productivity phenotype and could ultimately trigger the UPR (Schröder & Kaufman, 2005) which was also supported by our findings. UPR upregulation and ER stress are tighly co-regulated and it has been demonstrated that both can mediate intrinsic apoptosis pathway activation. Furthermore, it was shown that miR-24 is involved in targeting pro-apoptotic proteins like Bim, FAF-1, Caspase-9 and Apaf-1 (Agrawal et al., 2014; Cheng et al., 2005; Qin et al., 2010) or targets which are responsible for cell survival e.g. Bcl-2 (Singh & Saini, 2012a). Depletion of miR-24 resulted in an upregulation of NADH dehydrogenases which are associated with cell survival in instances of increased cellular stress (Ghosh & Girigoswami, 2008). However, increase in NADH dehydrogenase could also be a result of increased ROS and might be miR-24 and c-Myc independent.

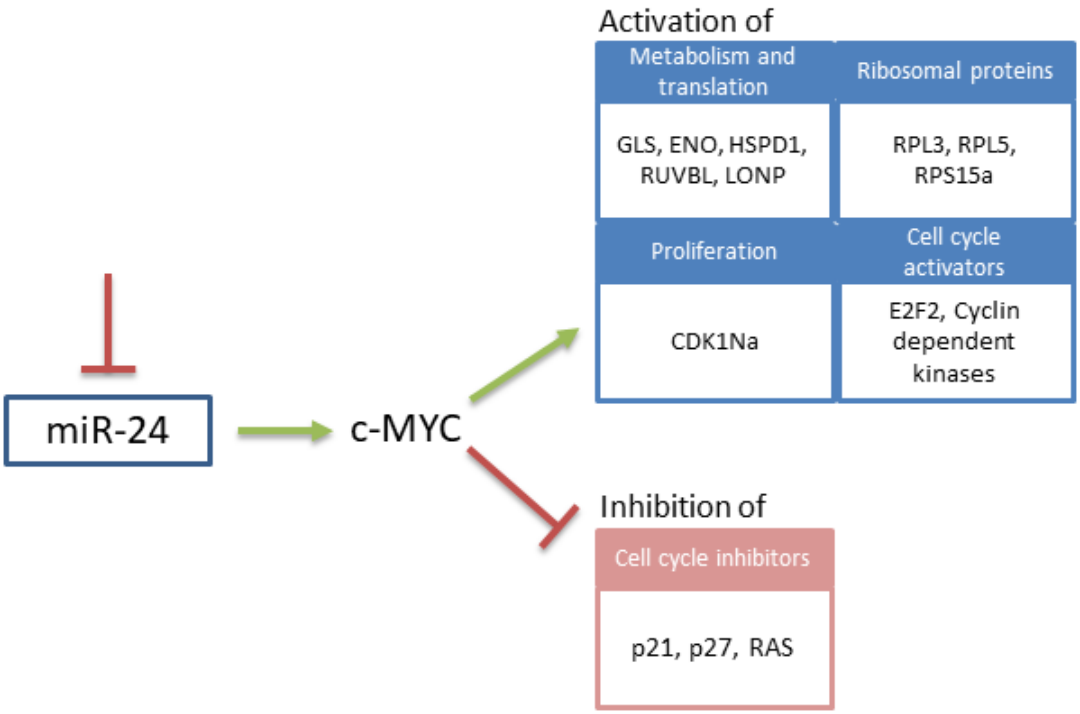

Figure 57: Depletion of miR-24 abolishes the regulation of c-Myc. As oncogene c-Myc inhibits cell cycle regulators and activates the expression of cell cycle activators, ribosomal proteins, proliferation associated proteins as well as proteins involved in metabolism and translation.

Rather than promoting glycolysis, depletion of miR-24 and subsequent upregulation of c-Myc seem to preferably promote translation, ribosomal processing as well as nucleotide synthesis based on our results and findings by other groups. C-Myc and miR-24 could also act cooperatively function as many targets seem to be targeted by c-Myc as transcription factor and miR-24 as transcriptional repressor.

Taken together all results for targeting individual members of the miR-23 cluster shows that the phenotype obtained by transient upregulation or stable depletion are very comparable to our CRISPR experiments. However, it remains questionable if CRISPR/Cas9 is beneficial over sponge technology which is further discussed in 5.2.3.

5.2.3 Comparison of sponge and CRISPR/Cas9 approaches for the knockdown of miRNAs

Experiments performed by stable depletion using sponges correlate with our findings when targeting with CRISPR/Cas9 in the same cell line. Depletion of miR-23 with a sponge showed the same phenotype as when miR-23a/miR-23b was targeted with CRISPR. In the case of targeting miR-24 the productivity phenotype was stronger using CRISPR/Cas9 compared to sponge mediated depletion and growth was additionally enhanced. In this section the features of sponge decoy and CRISPR technology are compared to discuss which tool might be better for targeting miRNAs.

One way to investigate if the sponge for a miRNA is working is the comparison of reporter presence compared to the control. In our case reduced GFP levels indicated the successful depletion of a miRNA target. Additionally, miRNA abundance can be measured using i.e. TaqMan® assays. Lower abundance of the miRNA would indicate successful depletion of miRNA presumably due to binding of miRNA:RISC to sponge mRNA (Chekulaeva & Filipowicz, 2009). However, for the depletion of miR-24 in CHO-S Fc an increase in abundance was observed. This effect could be due to translational inhibition. Our sponges were designed with imperfect binding sites (Kluiver et al., 2012b). The degree of inhibition or cleavage is presumed to be determined by either imperfect binding or complete binding. Perfect complementarity in binding to the target mRNA will lead to cleavage (Chekulaeva & Filipowicz, 2009) whereas imperfect binding will most likely lead to inhibition and stabilisation of the miRNA:mRNA complex (Huntzinger & Izaurralde, 2011). Due to target mediated miRNA protection (TMMP) miRNA

expression/levels can appear to be increased possibly occur and consequently higher levels of mature miRNA despite translational inhibition of the mRNA target (Chatterjee et al., 2011).

We demonstrated that when targeting one miRNA that the passenger strand was affected as well due to impaired processing of the precursor. Effects on the phenotype can however be further investigated by performing complementary transient experiments to deplete or overexpress both miRNAs. In the case of sponge decoys, it is hypothesised that not only the targeted miRNA can bind to the sponge but also whole miRNA seed families could potentially be bound (Kluiver et al., 2012a). The seed region is important for mRNA recognition but a perfect match of each nucleotide of the seed region is not necessary (Didiano & Hobert, 2006; Lewis et al., 2003). This increases the target range of a miRNA itself but also enables the binding of several different miRNAs to for example a sponge. However, binding of multiple different miRNAs with a similar seed region to a sponge could potentially reflect a false phenotype and the CRISPR/Cas9 system might be more suitable for direct targeting.

One advantage of using the CRISPR/Cas9 system over sponge technology is that no transgene has to be expressed. This is an advantage as additional expression of a transgene may affect the expression of the therapeutic protein in industrially used cell lines. All our experiments were performed using CRISPR/Cas9 plasmids expressing Cas9 and a chimeric sgRNA however, the possibility of transfecting Cas9 as protein combined with a sgRNA exists. This could be an advantage when cytotoxicity of the reporter gene is a concern as demonstrated in neuronal cell lines (Detrait et al., 2002). Another concern could be changes in metabolome due to high expression of selection markers or reporter which was observed by Yang and collegues in mesenchymal stem cells (Yang et al., 2017). The same has been demonstrated in CHO cells where the usage of selection markers negatively influenced translation as well as metabolism (Yallop et al., 2003). For CHO cells clonal stability is an important concern (discussed in section 5.1.3) and random integrations in cell line development could be avoided using CRISPR/Cas9 and hence reduce clonal variability.

In conclusion, the CRISPR/Cas9 system might be the more beneficial tool than sponges for miRNA targeting. Furthermore, we found that phenotypes were reproducible or even enhanced compared to depletion with the sponge counterpart at least in the case of members of the miR-23 cluster.

5.2.4 CRISPR/Cas9 as tool for improving biopharmaceutical production

With CRISPR being an effective and easy to use tool for the generation of cell lines an industrial application to improve production or product attributes is conceivable. One main concern for the usage of CRISPR in therapeutic/cell therapy applications are off-target effects. In fact, two recent studies showed that off-targeting might occur more often than it was presumed (Fu et al., 2013; Mali et al., 2013). For the use of CRISPR to improve productivity of CHO cells or product attributes of an expressed recombinant protein off-targets may not be as detrimental as long-term studies are applied to ensure genetic stability of production clones as well as intensive clinical studies to ensure patient safety. Furthermore, using CRISPR to alter product attributes like glycosylation could reduce immunogenicity and enhance efficacy of therapeutic proteins. One example is the knockout of FUT8 to reduce fucose levels on mAbs which ultimately will lead to enhanced ADCC (Ronda et al. 2014). Therefore, using CRISPR in biopharmaceutical industry could be a reliable tool to improve phenotypes and therapeutic protein products.

5.3 Genome-wide "loss of gene function" studies in Chinese Hamster Ovary cells using a CRISPR/Cas9 library

CRISPR/Cas9 can be successfully and efficiently used to target genes as well as miRNAs and generate clones with complete knockouts of the target gene. As a further application we wanted to use CRISPR/Cas9 for the implementation of genome wide "loss of gene function" study as previously reported by several research groups (Agrotis & Ketteler, 2015; Shalem et al., 2015; T. Wang et al., 2014) in human cells. The principle is based in using a library containing 87,897 different sgRNAs, targeting 19,150 mouse genes, which can be packed into a lentiviral delivery system. The library was supposed to be transduced into a CHO-K1 cell line expressing a mAb and human codon optimised spCas9. However, many Cas9 expressing vectors are commercially available but the sgRNA-library used for this study expresses only the sgRNA scaffold under the control of U6 promoter. Consequently, the first step was the generation of a cell line and the selection of a clone which expressed Cas9 stably. The plasmid used for miRNA experiments had puromycin as the selection marker and was proven to be very effective in the same cell line. As the library was based on selection with puromycin as well, we had to exchange the Cas9-2A-puro version with Cas9-2A-hygromycin. After successful investigation if the Cas9-2A-hyg version was functional targeting (miR-24), it was transfected into CHO-K1 mAb and single cell clones were isolated. Ten clones were characterised and one final clone was selected for the introduction of the library. All analysed clones behaved differently in batch cultures which reflects discussed heterogenous populations of CHO cells (see section 5.1.3). For all ten isolated clones the Cas9-2A-hyg version was fully functional when tested on miR-24.

The library consisted of 87,978 different sgRNAs which target every gene in mouse at least four times to ensure an efficient knockout as not every sgRNA will exhibit the same efficiencies, as previously discussed. Sequencing of the CHO-K1 genome shows, that 20,612 genes in mouse are homologues to Chinese hamster genes (Xu et al., 2011). Therefore, the introduction of the mouse sgRNA-library should theoretically target most genes in CHO-K1 cells.

The most critical step for this approach was to guarantee that the coverage of the library was maintained but also to ensure a low number of integration events - ideally one copy per cell. Amplification of the library using electroporation of highly competent *E. coli* cells and low temperatures for cell growth showed a transformation efficiency of 1.43×10^{10}

cfu/µg DNA, which was sufficient enough to ensure a good coverage of sgRNAs after plasmid isolation. When CHO-K1 mAb was transduced with library containing lentivirus a very low efficiency was observed. The investigation was based on BFP which as a fusion protein shows low intensities. The EGFP lentiviral construct can be delivered more efficiently in comparison to the sgRNA-library (Figure 48) despite similar plasmid sizes. Therefore, the usage of lentivirus to deliver the library was not suitable for our approach. The ability to resist viral infections is one benefit of CHO cells and is desirable in a bioprocess environment. Transcriptome analysis and comparison of human genes which are important for viral entry and vesicular transport show a lack of expression in CHO-K1 cells (Xu et al., 2011). Many of these non-expressed genes encode for cell surface proteins like integrins, cadherins and selectins which are important for viral attachment and recognition. Furthermore, CHO-K1 cells are also resistant to the Herpes simplex virus, Hepatitis B virus and human immunodeficiency virus type-1 (HIV-1) due to a lack of expression of their membrane surface binding receptors (Conner et al., 2005; Xie et al., 2005). These cell adhesion molecules include CD2, CD4, CD48 and CD 48. Interestingly the lentivirus is a replication deficient HIV-derived and uses CD4 as the cell surface receptor which is recognised by gp120 glycoprotein on the surface of the virus itself. These findings could explain the low efficiency of transduction using a lentiviral delivery system for CHO-K1s. As previously discussed, chromosome rearrangements and aberrations lead heterogenous populations. Our experiments showed that only a small number of cells were transduced with the lentivirus leading to the conclusion that only a subpopulation was susceptible to viral attachment and integration. Even clonal selected cells which should theoretically form a homogenous population with similar gene expression patterns etc. can show distinct deviations into subgroups (Datta et al., 2013; Davies et al., 2013). This heterogeneity could be one reason why some cells show multiple integration events despite low viral titres.

Another reason resulting in a low level of viral transduction could be the efficiency of integration. Infection of human osteosarcoma cells with HIV showed that only 0.41 % of the virus input is reverse transcribed and integrated into the host's genome (Thomas, Ott, & Gorelick, 2007). If the viral genome is integrated into the host's genome it has been shown that it is preferentially integrated into transcriptionally active units e.g. CpG islands and transcriptional start sites (Bushman et al., 2005; Demeulemeester et al., 2015). However, a low level of transduction would be desirable for this project to ensure

single copy integrations but the coverage of the library has to be ensured for an efficient screen of all genes in the CHO genome.

The sgRNA-library contained a mammalian selection marker for puromycin and after selection using two different concentrations (10 µg/ml and 20 µg/ml of puromycin) ~50-60 % of all cells exhibited BFP positive signals. Nevertheless, FACS analysis showed that in comparison to the negative control, a shift of the whole cell population was visible. This indicates that cells were infected and successfully selected, however, the intensities of BFP signal were low. Low intensities could occur due to the BFP/Puromycin fusion which shows a weaker fluorescence signal as shown before in the transfection efficiency. To validate this result, a standard curve was generated to investigate the number of integrated copies using qPCR analysis. Using the CHO-K1 genome size of 2,447,154,408 base pairs, the number of chromosomes and weight of all DNA in a cell allows the calculation of integration events (Maccani et al., 2013; Xu et al., 2011). This calculation showed that four integration events per cell occurred without relation to the amount of Puromycin used for selection. The low MOI in combination with an unexpected higher number of viral integrations agrees with with the observation that CHO-K1 cells are relatively resistant to infections by viral systems and only a subpopulation exposed with an excessive number of lentiviral particles is able to uptake several particles. Four integrations and the low transduction efficiency suggested that the lentiviral system is not applicable for CHO-K1 cells. Several library approaches for genome “loss of gene” function studies have been reported (Shalem et al., 2015; Wang et al., 2014; Koike-Yusa et al., 2014; Gilbert et al., 2014) using a lentiviral delivery system for introduction of the sgRNA library. However, it was not demonstrated that transduction efficiency was an issue as human cell lines were primarly used including reporter genes which can be used to isolate positively transduced cells using FACS.

To investigate alternative delivery methods, PEI-based transfection as well as nucleofection was performed to transfect the sgRNA library. For both approaches different numbers of plasmids were used and copy numbers were investigated using qPCR (Figure 49). It was observed that copies per cell vary around six to eight and transfection efficiencies were reduced with lower amounts of plasmid DNA. The goal was to deliver one to two copies per cell suggesting that PEI-based transfection was like the lentiviral system not suitable for CHO cells. When nucleofection was used with 0.5µg of plasmid DNA, a high transfection efficiency was observed as and resulted in 1-2

integrations per cell. Higher amounts of plasmid DNA led to over 7 copies per cell. Therefore, nucleofection was chosen for the delivery of the sgRNA library.

5.3.1 Advantage of CRISPR/Cas9 sgRNA libraries over siRNA/shRNA libraries

For the identification of pathways and biological functions of proteins, RNA interference or short RNAi was used in the past. However, RNAi has several drawbacks as for example off target effects, cytotoxicity as well as cell line dependent effects (Mohr & Perrimon, 2012). Furthermore, RNAi is based on a very similar mechanism to miRNAs where short dsRNA is incorporated by Dicer, processed and the mature single strand plays its role in transcriptional regulation of mRNAs in the RISC. The approach usually depends on a knockdown and if transiently performed will only last for several days. Therefore, the delivery using lentiviral systems for a stable expression were developed and applied with success (Bassik et al., 2009; Root et al., 2006). However, even with the stable expression through a lentiviral system other disadvantages had to be overcome. A suggested method was hereby the generation of sgRNA libraries (Koike-Yusa et al., 2014). Combining the high specificity of Cas9 with high efficacy, sgRNA based screens can provide better and more reliant information about pathways and protein function through powerful “loss of gene function” studies. Here we proposed a way of using a sgRNA library for the identification of genes involved in survival of bioprocess related stress conditions as well as gene loss which may lead to higher productivity.

5.3.1.1 Investigation of stress conditions leading to an enrichment or depletion of subpopulations with enhanced stress resistance

To investigate if cells transfected with the library can be adapted to certain stress conditions and if exposure to these will lead to an outgrow of subpopulations, we decided to apply treatments with NaBu as well as high salt conditions (Figure 53). NaBu as well as hyperosmotic conditions have been described in the literature to increase productivity of CHO cells expressing recombinant proteins. Treatment with NaBu has been shown to increase productivity in CHO cells (Jiang & Sharfstein 2008; Sung et al., 2004) due to inhibition of HDAC and subsequent hyperacetylation. Less condensed DNA increases accessibility of transcription factors leading to increased gene expression (Vidali et al.,

1978). Furthermore, apoptosis is induced as well as an inhibition of proliferation due to upregulation of several cell cycle regulators i.e. c-Myc (Davie, 2003). Interestingly, NaBu was used for induction of apoptosis by overexpression of BCL-2 (Kim et al., 2002). It was demonstrated that BCL-2 overexpression can inhibit apoptosis induction using sodium butyrate. Therefore, we wanted to use NaBu to induce apoptosis after transfection of the library to enrich for subpopulations in which a “loss of gene function” led to resistance to apoptosis induction. Apoptosis is well studied and genes identified can be most likely related back to either anti- or proapopotic function. Genes can be related back through idenfication of which sgRNA was used: treatment in stress conditions will either lead to an enrichment or depletion of a subpopulation as the knockout was either beneficial or critical to cell survival. SgRNAs used can be then identified using NGS and related back to targeted gene. Using apoptosis was proposed to serve as “proof of concept” for our library in CHO cells. Concentrations for treatment were hereby between 1-5 mM however, treatment of our CHO-K1 mAb cell line led to decreased cell growth and low viability even at low concentrations. Consequently, further optimisation would be necessary to use NaBu as potential stress condition.

Another environmental stress that we chose was the adaption to high salt conditions. Hyperosmolality has been described as a tool to improve productivity of CHO cell lines (Zhang et al., 2010) presumably due to growth inhibition however, with possible effect on glycosylation of therapeutic product (Lee at al., 2017). Furthermore, it is well characterised that high salt conditions can induce apoptosis and autophagy in CHO cells (Han et al., 2010). We proposed that adaption to hyperosmolality could be used to proof that our library was working. A knockout of a gene which led to inhibition of apoptosis as well as an outgrowth of subpopulations should theoretically be identifed by an enrichment of sgRNAs targeting that gene. More or less abundant sgRNAs can then be identified using NGS.

We tested several salt concentrations by adding NaCl to the growth medium and monitoring proliferation and viability (Figure 53). High concentrations showed drastic effects on proliferation and viability. We used 450 mOsm/kg as a baseline for adaption to hyperosmotic conditions. However, after three passages no growth of treated cells was observed and as consequence we decreased the osmolality to 400 mOsm/kg. Adaption to these hyperosmotic conditions was reflected in a stepwise increase in proliferation. This was presumably due to outgrowth of resistant subpopulations (Figure 54). Besides induction of apoptosis, osmolality might be interesting for certain bioprocess

applications i.e. fed-batch cultures. High osmotic pressure due to addition of feed and pH regulation is the cause in fed-batch cultures. Genes involved in overcoming this stress could be used as cell line engineering targets. After adaption over three passages genomic DNA of untreated and treated sgRNA population was isolated and prepared for NGS.

5.3.2 Selection of high producing subpopulations using FACS based enrichment

One possible application of the library is the usage of FACS in combination with low temperature cell staining to select high producing clones. SgRNAs which lead to an increase in producitivity or secretion should be enriched and identified using NGS. The cells transfected with the sgRNA library were sorted twice and a distinct shift in intensity was observed for Sort I and Sort II compared to unsorted populations. Furthermore, productivity as well as IgG titres were elevated compared to the unsorted sgRNA library expressing cell population.

From the point of translation at the endoplasmic reticulum for secreted proteins, further processing as well as PTMs and secretion are limiting steps which can result in low productivity. Therefore, the identification of genes which lead to closing this bottleneck could be interesting for cell line engineering. As a FACS based method is used for the stain of a secreted therapeutic protein on the surface of the cell, cells showing a high secretion or productivity can be isolated easily (Brezinksy et al., 2003; Pichler et al., 2011). For cells where no amplification procedure (no MTX) was used an increase of 25-fold in specific productivity was observed. Using MTX for amplification resulted even into higher Qp of > 100-fold over several sortings (Pichler et al., 2011). In our study, sorting the sgRNA library resulted in an increase in Qp of ~1.5 fold. Although a 1.5-fold increase was considered to be successful, Qp could be further increased by applying more sorts as it was suggested by serval studies. However, applying several sorts may decrease the number of genes that can be identified by NGS as knockouts resulting in only a mild increase in productivity will be most likely neglected. Furthermore, high specific productivity may not be the result of a gene knockout but is the result of clonal variation. The amount of sgRNAs identified will most likely reduce with increasing number of sorts. After sorting genomic DNA of following populations was isolated and prepared for NGS: Unsorted, Sort I, Sort II.

6.0 Conclusions

6 Conclusions

6.1 Stable depletion of the miR-23 cluster and its individual miRNA members in a panel of industrially relevant cell lines.

- Depletion of the miR-23 cluster or individual members is cell line dependent.
- MiR-23b and miR-27b expression in CHO-K1 SEAP expressing cells was shown to be ~3-fold higher compared to the CHO-K1 parental cell line. Across the panel of cell lines miR-24 was lower expressed compared to a parental CHO-K1 cell line.
- Depletion of miR-23 and the resulting phenotype seems to be highly cell line/clone dependent as no cell line tested showed the same effects as in CHO-K1 SEAP expressing cells.
- Stable depletion of miR-23-24-27 led to increased Fc-fusion levels and specific productivity in CHO-S Fc in batch as well as fed-batch cultures. Viability or growth were not affected. This phenotype was only observed in mixed population but not in derived single cell clones.
- The impact of depletion of miR-23-24-27 is highly cell line dependent as no other cell line showed beneficial phenotypes.
- Depletion of miR-24 and miR-27 led to increased productivity in CHO-S Fc
- The depletion of miR-24 also showed beneficial effects on productivity in six out of seven tested cell lines including CHO-K1 Fc, CHO-K1 mAb, CHO-K15 EPO, CHO-K1 DP12 and DG44i mAb. Increase in productivity is not product dependent.
- Proteomic profiling and pathway analysis for CHO-K1 mAb and CHO-S Fc after depletion of miR-24 revealed that several proteins involved in ribosomal biogenesis, ribosome assembly, translation, tRNA synthesis and unfolded protein response were significantly upregulated.
- Depletion of miR-23-24-27 seems to have an impact on mannosylation, sialylation and non-sialylated species of Fc-fusion product. Depletion of miR-24 seems to increase terminal sialic acid, non-sialylated complex glycans as well as mannose species. Depletion of miR-23 increased non-sialylated complex glycans as well as mannose content and miR-27 depletion showed increased levels of non-sialylated complex glycans.

- Proteomic profiling combined with pathway analysis showed that the miR-23 cluster and individual members act cooperately by sharing targets but also have individual roles. Especially miR-24 as well as miR-23 showed high level of synergetic interactions.

6.2 CRISPR/Cas9 as a genome engineering tool to target miRNAs in CHO cells

- All designed sgRNAs targeting miR-23a, miR-23b, miR-27b, miR-27a and miR-24 were functional and induced indels in or close to the seed region of targeted miRNAs. The human codon optimised spCas9 variant was fully functional in CHO-K1 mAb expressing cells and the targeting efficiency of CRISPR/Cas9 led to a knockdown of 85-99% in mixed populations.
- Knockdown efficiency of miRNA expression seems to be highly sgRNA dependent.
- Targeting between paralogues was observed due to high sequence complementarity of miRNA targets.
- Single cell clones exhibiting a low expression of the miRNA target were identified.
- Multiplex targeting of miRNAs is possible
- Phenotype obtained during transient screens as well as for sponge mediated depletion seemed comparable to CRISPR/Cas9 knockdowns.
- Targeting one strand of a microRNA can reduce levels of passenger strand as well. This observation seems to be correlated to an increase in precursor and indicates impaired processing by Drosha or Dicer.
- CRISPR/Cas9 mediated depletion of miR-23a as well as miR-23b led to prolonged viability in batch mode at the expense of productivity. Depletion of miR-27a reduced growth rates in batch culture.
- Depletion of miR-27b led to a reduction in IgG titre or productivity however, it also led to prolonged viable cell densities in late stages of the cultures in batch and fed-batch. Prolonged culture times led to increased final titres. Extended cultivation times may be due to reduced targeting of anti-apoptotic genes which was shown by pathway analysis.
- Depletion of miR-24 using CRISPR/Cas9 in CHO-K1 mAb increased specific productivity as well as proliferation.

- Overexpression of miR-24-3p led to decreased proliferation reversing the effect observed by depletion. MiR-24-5p overexpression did not have any effect.
- Proteomic profiling revealed that upregulated proteins due to reduced levels in miR-24 are involved in ribosomal biogenesis, ribosome assembly, translation, tRNA synthesis and unfolded protein response. The same pathways and proteins were identified for sponge mediated depletion with subsequent proteomic profiling of CHO-S Fc.
- Over 60% of upregulated proteins were predicted targets of either miR-24-3p or miR-24-5p.
- Using NGS, 700 mRNAs were significantly DE however, only 17 correlated with our proteomics list. When DE mRNAs were analysed for impacted pathways, an involvement in ribosomal biogenesis, translation, tRNA synthesis and unfolded protein response was observed.
- Mannose species were negatively affected due to CRISPR mediated knockdown of miR-24.

6.3 Genome-wide "loss of gene function" studies in Chinese Hamster Ovary cells using a CRISPR/Cas9 library

- The sgRNA-library which consisted of 87,897 different sgRNAs targeting 19,150 protein coding genes was successfully amplified and packaged into a lentiviral delivery system.
- Transduction efficiency was very low presumably due to only subpopulations which were susceptible to viral integration. This led to a high number of integration events (~4) but low number of surviving cells during selection.
- The lentiviral delivery system does not seem to be suitable to achieve a sufficient coverage of the full set of sgRNAs in CHO cells.
- Transfection of the sgRNA-library using PEI-based TransIT®-X2 showed a high amount of integration events concluding it was not suitable to achieve a high coverage.
- Nucleofection led to approximately 2 integration events per cell making it the preferred method for delivery of the sgRNA-library.
- The cloned Cas9-2A-hyg version was fully functional. Integration of the sgRNA library led to ~1.5 copies per cell.

- High salt conditions and sodium butyrate were tested for the induction of apoptosis. Due to the drastic impact of NaBu, hyperosmolality was chosen to enrich for knockouts which may lead to outgrowth of resistant subpopulations.
- FACS based selection for high producing cell subpopulations was successful and after two enrichments higher specific productivity as well as IgG titre was observed.

7.0 Future Work

7 Future work

7.1 Stable depletion of miR-23-24-27 as well as individual miRNA members in industrially relevant cell lines and the impact on growth and productivity

Using a mixed population of a CHO-S cell line expressing an Fc-fusion showed that stable depletion of miR-23-24-27 led to a ~1.5-fold increased productivity compared to the negative control in batch culture. Same phenotype was observed in fed-batch mode but not on a clonal level. Depletion of miR-24 and miR-27 in CHO-S Fc led to a similar increase in productivity and titre. Similar effect of depletion of miR-24 resulting in increased specific productivity was observed in 6 out of 7 tested cell lines including CHO-K1 mAb. Reduced levels of miR-23 led to no impact at all. Following future experiments could be performed:

- Optimisation of fed-batch cultures for CHO-S Fc to further boost productivity after sponge mediated depletion.
- Isolation of more clones for the depletion of miR-23-24-27 as well as miR-24 and miR-27 to enhance the observed productivity phenotype if possible as well as investigation what led to it.
- Reduced levels of miR-24 seemed to have a beneficial effect in 7 out of 8 tested cell lines. As cell lines are highly variable, proteomic profiling of all 7 cell lines could be used to identify key players in resulting phenotype as well as targets for cell line engineering.
- Only CHO-K1 mAb as well as CHO-S Fc have been characterised for the depletion of miR-27 with inconclusive results. Impact of reduction of miR-27 could be tested in all other cell lines as well.
- CRISPR/Cas9 was so far only introduced into CHO-K1 mAb showing enhanced effects of phenotypes over targeting. Clones exhibiting a complete deletion of a miRNA target can be generated to possibly boost phenotype for i.e. miR-24 depletion.
- Depletion of the whole cluster as well as each member was investigated in CHO-S Fc to identify if synergetic effects may exist. Due to the high variability proteomic profiling together with RNA sequencing could be performed to investigate the molecular function of the miR-23 cluster over a panel of cell lines.

- Further studies on how the glycosylation pattern is affected by the usage of sponge decoy technology to deplete certain miRNAs and if the effect is detrimental on efficacy of the produced protein product.

7.2 CRISPR/Cas9 as genome engineering tool to target miRNAs in CHO cells

It was shown, that miRNAs can be successfully targeted using CRISPR/Cas9 in CHO cells. Beneficial and comparable phenotypes can also be obtained compared to sponge decoy technology. Future work will hereby be focused on investigating mentioned phenotypes in a range of other cell lines as well as the introduction of an RNP based targeting approach as well as off-target considerations.

CRISPR/Cas9 targeting miR-23

It was shown, that a knockdown of miR-23a and miR-23b showed significantly increased cultivation times on expense of IgG production. Therefore, miR-23 depletion can be a viable tool for miRNA engineering:

- CRISPR/Cas9 mediated targeting of miR-23a and miR-23b over a panel of cell lines.
- Optimisation of batch and fed-batch cultures to investigate if culture times can be prolonged further as well as if titres can be boosted.
- Characterisation of a clonal panel to investigate if culture length can be boosted or reduced productivity can be prevented.

CRISPR/Cas9 targeting miR-24

It was shown, that a knockdown of miR-24 showed significantly increased proliferation as well as productivity in mixed populations. Increased proliferation was also observed in a clonal panel. Increase in productivity was presumably due to upregulation of proteins involved in ribosomal biogenesis, ribosome assembly, translation, tRNA synthesis and unfolded protein response. Future work will aim on further investigation on the molecular impact of miR-24 as well as validation of possible cell line engineering targets.

- Unbiased isolation and characterisation of clones to investigate if productivity phenotype can be boosted.

- Overexpression of HSPD1, TUFM and GFM1. All three proteins were upregulated due to depletion of miR-24. TUFM as well as GFM1 are also predicted targets and can potentially play a role in translation. Therefore, an overexpression study will be performed using transfections and co-transfections to investigate a possible effect on phenotype.
- Depletion of miR-24 in a panel of cell lines to investigate of effect can be boosted as well as compared to sponge decoy results. If a phenotype is exhibited a proteomic profiling study over the panel of cell lines would be suitable to identify and also to strengthen confidence in selected targets.
- Implementation and transfection of RNP/crRNA/tracrRNA approach to generate a stable cell line without the integration of a Cas9 plasmid.

CRISPR/Cas9 targeting miR-27

Depletion of miR-27b led to prolonged batch and fed-batch cultures. This phenotype was hereby on expense of IgG production however, due to extended cultivation times the final product titre was elevated compared to the control. Therefore, future experiments will aim on an investigation of the phenotype on protein level as well as an improvement with the help of clones.

- CRISPR/Cas9 mediated targeting of miR-27a and miR-27b over a panel of cell lines.
- Optimisation of batch and fed-batch cultures to investigate if culture times can be prolonged further as well as if titres can be boosted.
- Characterisation of a clonal panel to investigate if culture length can be boosted or reduced productivity can be prevented.
- The molecular impact of the knockdown/knockout of miR-27a and miR-27b will be investigated using HPLC-MS/MS. Once differential expressed proteins were identified target validation can be performed using a targeted CRISPR/Cas9 approach.
- Impact on critical quality attributes due to the knockdown of miR-27b.

CRISPR/Cas9 strategy for targeting miR-23a and miR-23b cluster simultaneously

Besides using CRISPR/Cas9 as tool for only targeting one miRNA at one time another approach would be the co-transfection of two CRISPR plasmids with sgRNAs targeting up and downstream of each cluster to investigate the whole knockout of one cluster at a time. A multiplex approach would be a suitable to target both clusters at the same time or to target one miRNA and its paralog simultaneously. Resulting possible phenotype will be assessed and the impact on the proteome would be investigated using HPLC-MS/MS followed up by siRNA knockdowns or CRISPR/Cas9 knockouts.

7.3 Genome-wide "loss of gene function" studies in Chinese Hamster Ovary cells using a CRISPR/Cas9 library

It was shown that the delivery of sgRNAs using a lentiviral system is not suitable for CHO-K1 cells. In general cells are transduced and showed several integration events however the coverage of the whole sgRNA-library cannot be assured using a viral delivery system. Furthermore, it was shown that PEI based transfection results in high transfection efficiencies which could ensure coverage but cells exhibit several plasmid integrations. Nucleofection seemed to be an efficient way to ensure good coverage as well as 1-2 copies per cell. The aim of the sgRNA-library is to deliver one sgRNA per cell to ensure an efficient screen for genes which could possible lead to a beneficial phenotype. Future experiments will include:

- Enrichment of sgRNAs which led to survival and outgrow of subpopulations and subsequent identification using NGS. Apoptosis is well understood and we hypothesised that correlation with adaption and survival of subpopulations after treatment in high salt concentrations can be related.

The overall goal of the sgRNA-library is to perform a genome wide "loss of gene function" study. The mixed population of CHO cells expressing ideally one copy per cell will be assessed under different stress conditions which are prevalent in a bioprocess environment.

- Hyperosmolality can potentially be used to identifiy genes which lead to survival of high-stress condition such as the addition of pH adjustant during fed-batch.

Identified genes leading to outgrow and survival can be overexpressed or knocked out to validate function and engineer cells towards stress resistance.

- Cell sorting using an FITC-labelled antibody was proven to be efficient in enrichment for high-producing cells. Next step will be the identification of gene knockouts which led to increased productivity or secretion. Therefore, NGS will be used to identify depleted or enriched sgRNAs. Subsequent overexpression or knockout of genes can be used as validation.
- In addition, genes involved in viral replication and attachment could be identified by using Adeno-associated viruses (AAV). As our experiments showed CHO cells are resistant to viral infections. However, subpopulations show susceptibility to transduction. To investigate genes involved in this process, CHO cells expressing the sgRNA-library will be treated with AAV containing GFP and positive transfected cells will be isolated using FACS. Cells which favourably integrated the viral DNA will be analysed by NGS and genes responsible for higher levels of integrations can subsequently be identified.

If new genes were discovered which are responsible for survival of stress conditions e.g. apoptosis or hypoxia, these genes will be validated by siRNAs or CRISPR/Cas9 knockouts. A CRISPR/Cas9 multiplex approach would be suitable as well to target several genes which have shown to lead to a beneficial phenotype. Last step will be the generation of knockout cell lines which exhibit enhanced features and validation in larger scales.

8.0 Bibliography

8 Bibliography

Abu-Elneel, K., Liu, T., Gazzaniga, F.S., Nishimura, Y., Wall, D.P., Geschwind, D.H., Lao, K. and Kosik, K.S. 2008. Heterogeneous dysregulation of microRNAs across the autism spectrum. *Neurogenetics,* 9(3), pp.153-161.

Agrawal, R., Pandey, P., Jha, P., Dwivedi, V., Sarkar, C. and Kulshreshtha, R. 2014. Hypoxic signature of microRNAs in glioblastoma: Insights from small RNA deep sequencing. *BMC Genomics,* 15pp.686-2164-15-686.

Agrotis, A. and Ketteler, R. 2015. A new age in functional genomics using CRISPR/Cas9 in arrayed library screening. *Frontiers in Genetics,* 6pp.10.3389/fgene.2015.00300.

Ali, N., Karlsson, C., Aspling, M., Hu, G., Hacohen, N., Scadden, D.T. and Larsson, J. 2009. Forward RNAi screens in primary human hematopoietic stem/progenitor cells. *Blood,* 113(16), pp.3690-3695.

Altamirano, C., Paredes, C., Cairo, J.J. and Godia, F. 2000. Improvement of CHO cell culture medium formulation: Simultaneous substitution of glucose and glutamine. *Biotechnology Progress,* 16(1), pp.69-75.

Ambros, V. 2003. MicroRNA pathways in flies and worms: Growth, death, fat, stress, and timing. *Cell,* 113(6), pp.673-676.

Ambros, V., Bartel, B., Bartel, D.P., Burge, C.B., Carrington, J.C., Chen, X., Dreyfuss, G., Eddy, S.R., Griffiths-Jones, S., Marshall, M., Matzke, M., Ruvkun, G. and Tuschl, T. 2003. A uniform system for microRNA annotation. *RNA (New York, N.Y.),* 9(3), pp.277-279.

Ameres, S.L. and Zamore, P.D. 2013. Diversifying microRNA sequence and function. *Nature Reviews.Molecular Cell Biology,* 14(8), pp.475-488.

Andersen, D.C., Bridges, T., Gawlitzek, M. and Hoy, C. 2000. Multiple cell culture factors can affect the glycosylation of asn-184 in CHO-produced tissue-type plasminogen activator. *Biotechnology and Bioengineering,* 70(1), pp.25-31.

Baek, E., Noh, S.M. and Lee, G.M. 2017. Anti-apoptosis engineering for improved protein production from CHO cells. *Methods in Molecular Biology (Clifton, N.J.),* 1603pp.71-85.

Bandi, N. and Vassella, E. 2011. miR-34a and miR-15a/16 are co-regulated in non-small cell lung cancer and control cell cycle progression in a synergistic and rb-dependent manner. *Molecular Cancer,* 10pp.55-4598-10-55.

Barnabe, N. and Butler, M. 1994. Effect of temperature on nucleotide pools and monoclonal antibody production in a mouse hybridoma. *Biotechnology and Bioengineering,* 44(10), pp.1235-1245.

Barnes, L.M., Moy, N. and Dickson, A.J. 2006. Phenotypic variation during cloning procedures: Analysis of the growth behavior of clonal cell lines. *Biotechnology and Bioengineering,* 94(3), pp.530-537.

Barron, N., Kumar, N., Sanchez, N., Doolan, P., Clarke, C., Meleady, P., O'Sullivan, F. and Clynes, M. 2011. Engineering CHO cell growth and recombinant protein productivity by overexpression of miR-7. *Journal of Biotechnology,* 151(2), pp.204-211.

Barron, N., Sanchez, N., Kelly, P. and Clynes, M. 2011. MicroRNAs: Tiny targets for engineering CHO cell phenotypes? *Biotechnology Letters,* 33(1), pp.11-21.

Bartel, D.P. 2009. MicroRNAs: Target recognition and regulatory functions. *Cell,* 136(2), pp.215-233.

Bassik, M.C., Lebbink, R.J., Churchman, L.S., Ingolia, N.T., Patena, W., LeProust, E.M., Schuldiner, M., Weissman, J.S. and McManus, M.T. 2009. Rapid creation and quantitative monitoring of high coverage shRNA libraries. *Nature Methods,* 6(6), pp.443-445.

Baycin-Hizal, D., Tabb, D.L., Chaerkady, R., Chen, L., Lewis, N.E., Nagarajan, H., Sarkaria, V., Kumar, A., Wolozny, D., Colao, J., Jacobson, E., Tian, Y., O'Meally, R.N., Krag, S.S., Cole, R.N., Palsson, B.O., Zhang, H. and Betenbaugh, M. 2012. Proteomic analysis of chinese hamster ovary cells. *Journal of Proteome Research,* 11(11), pp.5265-5276.

Becker, J., Hackl, M., Rupp, O., Jakobi, T., Schneider, J., Szczepanowski, R., Bekel, T., Borth, N., Goesmann, A., Grillari, J., Kaltschmidt, C., Noll, T., Puhler, A., Tauch, A. and Brinkrolf, K. 2011. Unraveling the chinese hamster ovary cell line transcriptome by next-generation sequencing. *Journal of Biotechnology,* 156(3), pp.227-235.

Betel, D., Koppal, A., Agius, P., Sander, C. and Leslie, C. 2010. Comprehensive modeling of microRNA targets predicts functional non-conserved and non-canonical sites. *Genome Biology,* 11(8), pp.R90-2010-11-8-r90. Epub 2010 Aug 27.

Birch, J.R. and Racher, A.J. 2006. Antibody production. *Advanced Drug Delivery Reviews,* 58(5–6), pp.671-685.

Bork, K., Horstkorte, R. and Weidemann, W. 2009. Increasing the sialylation of therapeutic glycoproteins: The potential of the sialic acid biosynthetic pathway. *Journal of Pharmaceutical Sciences,* 98(10), pp.3499-3508.

Born, T.L., Frost, J.A., Schonthal, A., Prendergast, G.C. and Feramisco, J.R. 1994. c-myc cooperates with activated ras to induce the cdc2 promoter. *Molecular and Cellular Biology,* 14(9), pp.5710-5718.

Borth, N., Mattanovich, D., Kunert, R. and Katinger, H. 2005. Effect of increased expression of protein disulfide isomerase and heavy chain binding protein on antibody secretion in a recombinant CHO cell line. *Biotechnology Progress,* 21(1), pp.106-111.

Bretones, G., Delgado, M.D. and Leon, J. 2015. Myc and cell cycle control. *Biochimica Et Biophysica Acta,* 1849(5), pp.506-516.

Brezinsky, S.C., Chiang, G.G., Szilvasi, A., Mohan, S., Shapiro, R.I., MacLean, A., Sisk, W. and Thill, G. 2003. A simple method for enriching populations of transfected CHO cells for cells of higher specific productivity. *Journal of Immunological Methods,* 277(1-2), pp.141-155.

Brezinsky, S.C., Chiang, G.G., Szilvasi, A., Mohan, S., Shapiro, R.I., MacLean, A., Sisk, W. and Thill, G. 2003. A simple method for enriching populations of transfected CHO cells for cells of higher specific productivity. *Journal of Immunological Methods,* 277(1-2), pp.141-155.

Brown, A.J., Sweeney, B., Mainwaring, D.O. and James, D.C. 2014. Synthetic promoters for CHO cell engineering. *Biotechnology and Bioengineering,* 111(8), pp.1638-1647.

Bushman, F., Lewinski, M., Ciuffi, A., Barr, S., Leipzig, J., Hannenhalli, S. and Hoffmann, C. 2005. Genome-wide analysis of retroviral DNA integration. *Nature Reviews.Microbiology,* 3(11), pp.848-858.

Canver, M.C., Bauer, D.E., Dass, A., Yien, Y.Y., Chung, J., Masuda, T., Maeda, T., Paw, B.H. and Orkin, S.H. 2014. Characterization of genomic deletion efficiency mediated by clustered regularly interspaced palindromic repeats (CRISPR)/Cas9 nuclease system in mammalian cells. *The Journal of Biological Chemistry,* 289(31), pp.21312-21324.

Carillo, S., Mittermayr, S., Farrell, A., Albrecht, S. and Bones, J. 2017. Glycosylation analysis of therapeutic glycoproteins produced in CHO cells. *Methods in Molecular Biology (Clifton, N.J.),* 1603pp.227-241.

Carte, J., Wang, R., Li, H., Terns, R.M. and Terns, M.P. 2008. Cas6 is an endoribonuclease that generates guide RNAs for invader defense in prokaryotes. *Genes & Development,* 22(24), pp.3489-3496.

Carter-Franklin, J.N., Victa, C., McDonald, P. and Fahrner, R. 2007. Fragments of protein A eluted during protein A affinity chromatography. *Journal of Chromatography.A,* 1163(1-2), pp.105-111.

Challagundla, K.B., Sun, X.X., Zhang, X., DeVine, T., Zhang, Q., Sears, R.C. and Dai, M.S. 2011. Ribosomal protein L11 recruits miR-24/miRISC to repress c-myc expression in response to ribosomal stress. *Molecular and Cellular Biology,* 31(19), pp.4007-4021.

Chang, H., Yi, B., Ma, R., Zhang, X., Zhao, H. and Xi, Y. 2016. CRISPR/cas9, a novel genomic tool to knock down microRNA in vitro and in vivo. *Scientific Reports,* 6pp.22312.

Chang, K.W., Kao, S.Y., Wu, Y.H., Tsai, M.M., Tu, H.F., Liu, C.J., Lui, M.T. and Lin, S.C. 2013. Passenger strand miRNA miR-31* regulates the phenotypes of oral cancer cells by targeting RhoA. *Oral Oncology,* 49(1), pp.27-33.

Chatterjee, S., Fasler, M., Büssing, I. and Großhans, H. 2011. *Target-Mediated Protection of Endogenous MicroRNAs in C. elegans.*

Chekulaeva, M. and Filipowicz, W. 2009. Mechanisms of miRNA-mediated post-transcriptional regulation in animal cells. *Current Opinion in Cell Biology,* 21(3), pp.452-460.

Chen, J., Tetrault, J. and Ley, A. 2008. Comparison of standard and new generation hydrophobic interaction chromatography resins in the monoclonal antibody purification process. *Journal of Chromatography.A,* 1177(2), pp.272-281.

Chen, K., Liu, Q., Xie, L., Sharp, P.A. and Wang, D.I. 2001. Engineering of a mammalian cell line for reduction of lactate formation and high monoclonal antibody production. *Biotechnology and Bioengineering,* 72(1), pp.55-61.

Cheng, A.M., Byrom, M.W., Shelton, J. and Ford, L.P. 2005. Antisense inhibition of human miRNAs and indications for an involvement of miRNA in cell growth and apoptosis. *Nucleic Acids Research,* 33(4), pp.1290-1297.

Chhabra, R., Adlakha, Y.K., Hariharan, M., Scaria, V. and Saini, N. 2009. Upregulation of miR-23a-27a-24-2 cluster induces caspase-dependent and -independent apoptosis in human embryonic kidney cells. *PloS One,* 4(6), pp.e5848.

Chhabra, R., Dubey, R. and Saini, N. 2010. Cooperative and individualistic functions of the microRNAs in the miR-23a~27a~24-2 cluster and its implication in human diseases. *Molecular Cancer,* 9pp.232-4598-9-232.

Chhabra, R., Dubey, R. and Saini, N. 2010. Cooperative and individualistic functions of the microRNAs in the miR-23a~27a~24-2 cluster and its implication in human diseases. *Molecular Cancer,* 9pp.232-4598-9-232.

Cho, R.J., Campbell, M.J., Winzeler, E.A., Steinmetz, L., Conway, A., Wodicka, L., Wolfsberg, T.G., Gabrielian, A.E., Landsman, D., Lockhart, D.J. and Davis, R.W. 1998. A genome-wide transcriptional analysis of the mitotic cell cycle. *Molecular Cell,* 2(1), pp.65-73.

Cho, S.W., Kim, S., Kim, Y., Kweon, J., Kim, H.S., Bae, S. and Kim, J.S. 2014. Analysis of off-target effects of CRISPR/Cas-derived RNA-guided endonucleases and nickases. *Genome Research,* 24(1), pp.132-141.

Christian, B.E. and Spremulli, L.L. 2012. Mechanism of protein biosynthesis in mammalian mitochondria. *Biochimica Et Biophysica Acta,* 1819(9-10), pp.1035-1054.

Chung, J.Y., Lim, S.W., Hong, Y.J., Hwang, S.O. and Lee, G.M. 2004. Effect of doxycycline-regulated calnexin and calreticulin expression on specific thrombopoietin productivity of recombinant chinese hamster ovary cells. *Biotechnology and Bioengineering,* 85(5), pp.539-546.

Chylinski, K., Le Rhun, A. and Charpentier, E. 2013. The tracrRNA and Cas9 families of type II CRISPR-cas immunity systems. *RNA Biology,* 10(5), pp.726-737.

Cimmino, A., Calin, G.A., Fabbri, M., Iorio, M.V., Ferracin, M., Shimizu, M., Wojcik, S.E., Aqeilan, R.I., Zupo, S., Dono, M., Rassenti, L., Alder, H., Volinia, S., Liu, C.G., Kipps, T.J., Negrini, M. and Croce, C.M. 2005. miR-15 and miR-16 induce apoptosis by targeting BCL2. *Proceedings of the National Academy of Sciences of the United States of America,* 102(39), pp.13944-13949.

Clarke, C., Henry, M., Doolan, P., Kelly, S., Aherne, S., Sanchez, N., Kelly, P., Kinsella, P., Breen, L., Madden, S.F., Zhang, L., Leonard, M., Clynes, M., Meleady, P. and Barron, N. 2012. Integrated miRNA, mRNA and protein expression analysis reveals the role of post-transcriptional regulation in controlling CHO cell growth rate. *BMC Genomics,* 13pp.656-2164-13-656.

Clincke, M.F., Molleryd, C., Zhang, Y., Lindskog, E., Walsh, K. and Chotteau, V. 2013. Very high density of CHO cells in perfusion by ATF or TFF in WAVE bioreactor. part I. effect of the cell density on the process. *Biotechnology Progress,* 29(3), pp.754-767.

CMC Biotech Working Group. 2009. A-mab: A case study in bioprocess development.

Coleman, O., Henry, M., Clynes, M. and Meleady, P. 2017. Filter-aided sample preparation (FASP) for improved proteome analysis of recombinant chinese hamster ovary cells. *Methods in Molecular Biology (Clifton, N.J.),* 1603pp.187-194.

Cong, L., Ran, F.A., Cox, D., Lin, S., Barretto, R., Habib, N., Hsu, P.D., Wu, X., Jiang, W., Marraffini, L.A. and Zhang, F. 2013. Multiplex genome engineering using CRISPR/Cas systems. *Science (New York, N.Y.),* 339(6121), pp.819-823.

Cong, L. and Zhang, F. 2015. Genome engineering using CRISPR-Cas9 system. *Methods in Molecular Biology (Clifton, N.J.),* 1239pp.197-217.

Conner, J., Rixon, F.J. and Brown, S.M. 2005. Herpes simplex virus type 1 strain HSV1716 grown in baby hamster kidney cells has altered tropism for nonpermissive chinese hamster ovary cells compared to HSV1716 grown in vero cells. *Journal of Virology,* 79(15), pp.9970-9981.

Cost, G.J., Freyvert, Y., Vafiadis, A., Santiago, Y., Miller, J.C., Rebar, E., Collingwood, T.N., Snowden, A. and Gregory, P.D. 2010. BAK and BAX deletion using zinc-finger nucleases yields apoptosis-resistant CHO cells. *Biotechnology and Bioengineering,* 105(2), pp.330-340.

Curtis, S., Lee, K., Blank, G.S., Brorson, K. and Xu, Y. 2003. Generic/matrix evaluation of SV40 clearance by anion exchange chromatography in flow-through mode. *Biotechnology and Bioengineering,* 84(2), pp.179-186.

Cyranoski, D. 2016. CRISPR gene-editing tested in a person for the first time. *Nature,* 539(7630), pp.479.

Czajkowsky, D.M., Hu, J., Shao, Z. and Pleass, R.J. 2012. Fc-fusion proteins: New developments and future perspectives. *EMBO Molecular Medicine,* 4(10), pp.1015-1028.

Dâ€™Alessio, C. and Dahms, N.M. 2015. Glucosidase II and MRH-domain containing proteins in the secretory pathway. *Current Protein & Peptide Science,* 16(1), pp.31-48.

Dang, C.V. 2011. Therapeutic targeting of myc-reprogrammed cancer cell metabolism. *Cold Spring Harbor Symposia on Quantitative Biology,* 76pp.369-374.

Datta, P., Linhardt, R.J. and Sharfstein, S.T. 2013. An 'omics approach towards CHO cell engineering. *Biotechnology and Bioengineering,* 110(5), pp.1255-1271.

Davie, J.R. 2003. Inhibition of histone deacetylase activity by butyrate. *The Journal of Nutrition,* 133(7 Suppl), pp.2485S-2493S.

Davies, S.L., Lovelady, C.S., Grainger, R.K., Racher, A.J., Young, R.J. and James, D.C. 2013. Functional heterogeneity and heritability in CHO cell populations. *Biotechnology and Bioengineering,* 110(1), pp.260-274.

Davis, R., Schooley, K., Rasmussen, B., Thomas, J. and Reddy, P. 2000. Effect of PDI overexpression on recombinant protein secretion in CHO cells. *Biotechnology Progress,* 16(5), pp.736-743.

Deberardinis, R.J., Sayed, N., Ditsworth, D. and Thompson, C.B. 2008. Brick by brick: Metabolism and tumor cell growth. *Current Opinion in Genetics & Development,* 18(1), pp.54-61.

Decker, C.J. and Parker, R. 1995. Diversity of cytoplasmic functions for the 3' untranslated region of eukaryotic transcripts. *Current Opinion in Cell Biology,* 7(3), pp.386-392.

Deltcheva, E., Chylinski, K., Sharma, C.M., Gonzales, K., Chao, Y., Pirzada, Z.A., Eckert, M.R., Vogel, J. and Charpentier, E. 2011. CRISPR RNA maturation by trans-encoded small RNA and host factor RNase III. *Nature,* 471(7340), pp.602-607.

Demeulemeester, J., De Rijck, J., Gijsbers, R. and Debyser, Z. 2015. Retroviral integration: Site matters: Mechanisms and consequences of retroviral integration site selection. *BioEssays : News and Reviews in Molecular, Cellular and Developmental Biology,* 37(11), pp.1202-1214.

Derouazi, M., Martinet, D., Besuchet Schmutz, N., Flaction, R., Wicht, M., Bertschinger, M., Hacker, D.L., Beckmann, J.S. and Wurm, F.M. 2006. Genetic characterization of CHO production host DG44 and derivative recombinant cell lines. *Biochemical and Biophysical Research Communications,* 340(4), pp.1069-1077.

Detrait, E.R., Bowers, W.J., Halterman, M.W., Giuliano, R.E., Bennice, L., Federoff, H.J. and Richfield, E.K. 2002. Reporter gene transfer induces apoptosis in primary cortical neurons. *Molecular Therapy : The Journal of the American Society of Gene Therapy,* 5(6), pp.723-730.

Didiano, D. and Hobert, O. 2006. Perfect seed pairing is not a generally reliable predictor for miRNA-target interactions. *Nature Structural & Molecular Biology,* 13(9), pp.849-851.

DiMasi, J.A. and Grabwoski, H.G. 2007. The cost of biopharmaceutical R&D: Is biotech different? 28pp.469.

Doench, J.G. and Sharp, P.A. 2004. Specificity of microRNA target selection in translational repression. *Genes & Development,* 18(5), pp.504-511.

Doolan, P., Meleady, P., Barron, N., Henry, M., Gallagher, R., Gammell, P., Melville, M., Sinacore, M., McCarthy, K., Leonard, M., Charlebois, T. and Clynes, M. 2010. Microarray and proteomics expression profiling identifies several candidates, including the valosin-containing protein (VCP), involved in regulating high cellular growth rate in production CHO cell lines. *Biotechnology and Bioengineering,* 106(1), pp.42-56.

Druz, A., Betenbaugh, M. and Shiloach, J. 2012. Glucose depletion activates mmu-miR-466h-5p expression through oxidative stress and inhibition of histone deacetylation. *Nucleic Acids Research,* 40(15), pp.7291-7302.

Druz, A., Chu, C., Majors, B., Santuary, R., Betenbaugh, M. and Shiloach, J. 2011. A novel microRNA mmu-miR-466h affects apoptosis regulation in mammalian cells. *Biotechnology and Bioengineering,* 108(7), pp.1651-1661.

Druz, A., Son, Y.J., Betenbaugh, M. and Shiloach, J. 2013. Stable inhibition of mmu-miR-466h-5p improves apoptosis resistance and protein production in CHO cells. *Metabolic Engineering,* 16pp.87-94.

Dweep, H., Sticht, C., Pandey, P. and Gretz, N. 2011. miRWalk--database: Prediction of possible miRNA binding sites by "walking" the genes of three genomes. *Journal of Biomedical Informatics,* 44(5), pp.839-847.

Ebert, M.S., Neilson, J.R. and Sharp, P.A. 2007. MicroRNA sponges: Competitive inhibitors of small RNAs in mammalian cells. *Nature Methods,* 4(9), pp.721-726.

Ebert, M.S. and Sharp, P.A. 2010. MicroRNA sponges: Progress and possibilities. *RNA (New York, N.Y.),* 16(11), pp.2043-2050.

Ebina, H., Misawa, N., Kanemura, Y. and Koyanagi, Y. 2013. Harnessing the CRISPR/Cas9 system to disrupt latent HIV-1 provirus. *Scientific Reports,* 3pp.2510.

Elliott, S., Lorenzini, T., Asher, S., Aoki, K., Brankow, D., Buck, L., Busse, L., Chang, D., Fuller, J., Grant, J., Hernday, N., Hokum, M., Hu, S., Knudten, A., Levin, N., Komorowski, R., Martin, F., Navarro, R., Osslund, T., Rogers, G., Rogers, N., Trail, G. and Egrie, J. 2003. Enhancement of therapeutic protein in vivo activities through glycoengineering. *Nature Biotechnology,* 21(4), pp.414-421.

Emmerling, V.V., Fischer, S., Stiefel, F., Holzmann, K., Handrick, R., Hesse, F., Horer, M., Kochanek, S. and Otte, K. 2016. Temperature-sensitive miR-483 is a conserved regulator of recombinant protein and viral vector production in mammalian cells. *Biotechnology and Bioengineering,* 113(4), pp.830-841.

Fahrner, R.L., Knudsen, H.L., Basey, C.D., Galan, W., Feuerhelm, D., Vanderlaan, M. and Blank, G.S. 2001. Industrial purification of pharmaceutical antibodies: Development, operation, and validation of chromatography processes. *Biotechnology & Genetic Engineering Reviews,* 18pp.301-327.

Fischer, S., Marquart, K.F., Pieper, L.A., Fieder, J., Gamer, M., Gorr, I., Schulz, P. and Bradl, H. 2017. miRNA engineering of CHO cells facilitates production of difficult-to-express proteins and increases success in cell line development. *Biotechnology and Bioengineering,* 114(7), pp.1495-1510.

Fischer, S., Paul, A.J., Wagner, A., Mathias, S., Geiss, M., Schandock, F., Domnowski, M., Zimmermann, J., Handrick, R., Hesse, F. and Otte, K. 2015. miR-2861 as novel HDAC5 inhibitor in CHO cells enhances productivity while maintaining product quality. *Biotechnology and Bioengineering,* 112(10), pp.2142-2153.

Fischer, S., Handrick, R. and Otte, K. 2015. *The art of CHO cell engineering: A comprehensive retrospect and future perspectives.*

Fischer, S., Mathias, S., Schaz, S., Emmerling, V.V., Buck, T., Kleemann, M., Hackl, M., Grillari, J., Aschrafi, A., Handrick, R. and Otte, K. 2015. *Enhanced protein production by microRNA-30 family in CHO cells is mediated by the modulation of the ubiquitin pathway.*

Fonfara, I., Le Rhun, A., Chylinski, K., Makarova, K.S., Lecrivain, A.L., Bzdrenga, J., Koonin, E.V. and Charpentier, E. 2014. Phylogeny of Cas9 determines functional exchangeability of dual-RNA and Cas9 among orthologous type II CRISPR-cas systems. *Nucleic Acids Research,* 42(4), pp.2577-2590.

Friedman, R.C., Farh, K.K., Burge, C.B. and Bartel, D.P. 2009. Most mammalian mRNAs are conserved targets of microRNAs. *Genome Research,* 19(1), pp.92-105.

Fromm, B., Billipp, T., Peck, L.E., Johansen, M., Tarver, J.E., King, B.L., Newcomb, J.M., Sempere, L.F., Flatmark, K., Hovig, E. and Peterson, K.J. 2015. A uniform system for the annotation of vertebrate microRNA genes and the evolution of the human microRNAome. *Annual Review of Genetics,* 49pp.213-242.

Fu, Y., Foden, J.A., Khayter, C., Maeder, M.L., Reyon, D., Joung, J.K. and Sander, J.D. 2013. High-frequency off-target mutagenesis induced by CRISPR-cas nucleases in human cells. *Nature Biotechnology,* 31(9), pp.822-826.

Fukuta, K., Abe, R., Yokomatsu, T., Kono, N., Asanagi, M., Omae, F., Minowa, M.T., Takeuchi, M. and Makino, T. 2000. Remodeling of sugar chain structures of human interferon-gamma. *Glycobiology,* 10(4), pp.421-430.

Gallagher, C. and Kelly, P.S. 2017. Selection of high-producing clones using FACS for CHO cell line development. *Methods in Molecular Biology (Clifton, N.J.),* 1603pp.143-152.

Gammell, P. 2007. MicroRNAs: Recently discovered key regulators of proliferation and apoptosis in animal cells: Identification of miRNAs regulating growth and survival. *Cytotechnology,* 53(1-3), pp.55-63.

Gammell, P., Barron, N., Kumar, N. and Clynes, M. 2007. Initial identification of low temperature and culture stage induction of miRNA expression in suspension CHO-K1 cells. *Journal of Biotechnology,* 130(3), pp.213-218.

Gammell, P., Barron, N., Kumar, N. and Clynes, M. 2007. Initial identification of low temperature and culture stage induction of miRNA expression in suspension CHO-K1 cells. *Journal of Biotechnology,* 130(3), pp.213-218.

Gao, P., Tchernyshyov, I., Chang, T.C., Lee, Y.S., Kita, K., Ochi, T., Zeller, K.I., De Marzo, A.M., Van Eyk, J.E., Mendell, J.T. and Dang, C.V. 2009. c-myc suppression of miR-23a/b enhances mitochondrial glutaminase expression and glutamine metabolism. *Nature,* 458(7239), pp.762-765.

Garneau, J.E., Dupuis, M.E., Villion, M., Romero, D.A., Barrangou, R., Boyaval, P., Fremaux, C., Horvath, P., Magadan, A.H. and Moineau, S. 2010. The CRISPR/Cas bacterial immune system cleaves bacteriophage and plasmid DNA. *Nature,* 468(7320), pp.67-71.

Gawlitzek, M., Estacio, M., Furch, T. and Kiss, R. 2009. Identification of cell culture conditions to control N-glycosylation site-occupancy of recombinant glycoproteins expressed in CHO cells. *Biotechnology and Bioengineering,* 103(6), pp.1164-1175.

Gawlitzek, M., Ryll, T., Lofgren, J. and Sliwkowski, M.B. 2000. Ammonium alters N-glycan structures of recombinant TNFR-IgG: Degradative versus biosynthetic mechanisms. *Biotechnology and Bioengineering,* 68(6), pp.637-646.

Gawlitzek, M., Ryll, T., Lofgren, J. and Sliwkowski, M.B. 2000. Ammonium alters N-glycan structures of recombinant TNFR-IgG: Degradative versus biosynthetic mechanisms. *Biotechnology and Bioengineering,* 68(6), pp.637-646.

Gaziel-Sovran, A., Segura, M.F., Di Micco, R., Collins, M.K., Hanniford, D., Vega-Saenz de Miera, E., Rakus, J.F., Dankert, J.F., Shang, S., Kerbel, R.S., Bhardwaj, N., Shao, Y., Darvishian, F., Zavadil, J., Erlebacher, A., Mahal, L.K., Osman, I. and Hernando, E. 2011. miR-30b/30d regulation of GalNAc transferases enhances invasion and immunosuppression during metastasis. *Cancer Cell,* 20(1), pp.104-118.

Ghanem, N., Salilew-Wondim, D., Gad, A., Tesfaye, D., Phatsara, C., Tholen, E., Looft, C., Schellander, K. and Hoelker, M. 2011. Bovine blastocysts with developmental competence to term share similar expression of developmentally important genes although derived from different culture environments. *Reproduction (Cambridge, England),* 142(4), pp.551-564.

Ghazalpour, A., Bennett, B., Petyuk, V.A., Orozco, L., Hagopian, R., Mungrue, I.N., Farber, C.R., Sinsheimer, J., Kang, H.M., Furlotte, N., Park, C.C., Wen, P.Z., Brewer, H., Weitz, K., Camp, D.G.,2nd, Pan, C., Yordanova, R., Neuhaus, I., Tilford, C., Siemers, N., Gargalovic, P., Eskin, E., Kirchgessner, T., Smith, D.J., Smith, R.D. and Lusis, A.J. 2011. Comparative analysis of proteome and transcriptome variation in mouse. *PLoS Genetics,* 7(6), pp.e1001393.

Ghose, S., Tao, Y., Conley, L. and Cecchini, D. 2013. Purification of monoclonal antibodies by hydrophobic interaction chromatography under no-salt conditions. *Mabs,* 5(5), pp.795-800.

Ghosh, R. and Girigoswami, K. 2008. NADH dehydrogenase subunits are overexpressed in cells exposed repeatedly to H2O2.

Gilbert, L.A., Horlbeck, M.A., Adamson, B., Villalta, J.E., Chen, Y., Whitehead, E.H., Guimaraes, C., Panning, B., Ploegh, H.L., Bassik, M.C., Qi, L.S., Kampmann, M. and Weissman, J.S. 2014. Genome-scale CRISPR-mediated control of gene repression and activation. *Cell,* 159(3), pp.647-661.

Glacken, M.W., Fleischaker, R.J. and Sinskey, A.J. 1986. Reduction of waste product excretion via nutrient control: Possible strategies for maximizing product and cell yields on serum in cultures of mammalian cells. *Biotechnology and Bioengineering,* 28(9), pp.1376-1389.

Gomez, M.I., Lee, A., Reddy, B., Muir, A., Soong, G., Pitt, A., Cheung, A. and Prince, A. 2004. Staphylococcus aureus protein A induces airway epithelial inflammatory responses by activating TNFR1. *Nature Medicine,* 10(8), pp.842-848.

Goswami, J., Sinskey, A.J., Steller, H., Stephanopoulos, G.N. and Wang, D.I. 1999. Apoptosis in batch cultures of chinese hamster ovary cells. *Biotechnology and Bioengineering,* 62(6), pp.632-640.

Griffith, A., Kelly, P.S., Vencken, S., Lao, N.T., Greene, C.M., Clynes, M. and Barron, N. 2018. miR-CATCH identifies biologically active miRNA regulators of the pro-survival gene XIAP, in chinese hamster ovary cells. *Biotechnology Journal,* 13(3), pp.e1700299.

Grimson, A., Farh, K.K., Johnston, W.K., Garrett-Engele, P., Lim, L.P. and Bartel, D.P. 2007. MicroRNA targeting specificity in mammals: Determinants beyond seed pairing. *Molecular Cell,* 27(1), pp.91-105.

Grissa, I., Vergnaud, G. and Pourcel, C. 2007. The CRISPRdb database and tools to display CRISPRs and to generate dictionaries of spacers and repeats. *BMC Bioinformatics,* 8pp.172.

Gu, S., Jin, L., Zhang, Y., Huang, Y., Zhang, F., Valdmanis, P.N. and Kay, M.A. 2012. The loop position of shRNAs and pre-miRNAs is critical for the accuracy of dicer processing in vivo. *Cell,* 151(4), pp.900-911.

Guttilla, I.K. and White, B.A. 2009. Coordinate regulation of FOXO1 by miR-27a, miR-96, and miR-182 in breast cancer cells. *The Journal of Biological Chemistry,* 284(35), pp.23204-23216.

Hackl, M., Jakobi, T., Blom, J., Doppmeier, D., Brinkrolf, K., Szczepanowski, R., Bernhart, S.H., Siederdissen, C.H., Bort, J.A.H., Wieser, M., Kunert, R., Jeffs, S., Hofacker, I.L., Goesmann, A., PÃ¼hler, A., Borth, N. and Grillari, J. 2011. Next-generation sequencing of the chinese hamster ovary microRNA transcriptome: Identification, annotation and profiling of microRNAs as targets for cellular engineering(). *Journal of Biotechnology,* 153(1-2), pp.62-75.

Haft, D.H., Selengut, J., Mongodin, E.F. and Nelson, K.E. 2005. A guild of 45 CRISPR-associated (cas) protein families and multiple CRISPR/Cas subtypes exist in prokaryotic genomes. *PLoS Computational Biology,* 1(6), pp.e60.

Hale, C.R., Zhao, P., Olson, S., Duff, M.O., Graveley, B.R., Wells, L., Terns, R.M. and Terns, M.P. 2009. RNA-guided RNA cleavage by a CRISPR RNA-cas protein complex. *Cell,* 139(5), pp.945-956.

Hamilton, W.G. and Ham, R.G. 1977. Clonal growth of chinese hamster cell lines in protein-free media. *In Vitro,* 13(9), pp.537-547.

Hammond, S.M., Bernstein, E., Beach, D. and Hannon, G.J. 2000. An RNA-directed nuclease mediates post-transcriptional gene silencing in drosophila cells. *Nature,* 404(6775), pp.293-296.

Han, Y.K., Kim, Y.G., Kim, J.Y. and Lee, G.M. 2010. Hyperosmotic stress induces autophagy and apoptosis in recombinant chinese hamster ovary cell culture. *Biotechnology and Bioengineering,* 105(6), pp.1187-1192.

Hansen, H.A. and Emborg, C. 1994. Influence of ammonium on growth, metabolism, and productivity of a continuous suspension chinese hamster ovary cell culture. *Biotechnology Progress,* 10(1), pp.121-124.

Hargrove, J.L. and Schmidt, F.H. 1989. The role of mRNA and protein stability in gene expression. *FASEB Journal : Official Publication of the Federation of American Societies for Experimental Biology,* 3(12), pp.2360-2370.

He, X.Z., Que, A.H. and Mo, J.J. 2009. Analysis of charge heterogeneities in mAbs using imaged CE. *Electrophoresis,* 30(5), pp.714-722.

Hefzi, H., Ang, K.S., Hanscho, M., Bordbar, A., Ruckerbauer, D., Lakshmanan, M., Orellana, C.A., Baycin-Hizal, D., Huang, Y., Ley, D., Martinez, V.S., Kyriakopoulos, S., Jimenez, N.E., Zielinski, D.C., Quek, L.E., Wulff, T., Arnsdorf, J., Li, S., Lee, J.S., Paglia, G., Loira, N., Spahn, P.N., Pedersen, L.E., Gutierrez, J.M., King, Z.A., Lund, A.M., Nagarajan, H., Thomas, A., Abdel-Haleem, A.M., Zanghellini, J., Kildegaard, H.F., Voldborg, B.G., Gerdtzen, Z.P., Betenbaugh, M.J., Palsson, B.O., Andersen, M.R., Nielsen, L.K., Borth, N., Lee, D.Y. and

Lewis, N.E. 2016. A consensus genome-scale reconstruction of chinese hamster ovary cell metabolism. *Cell Systems,* 3(5), pp.434-443.e8.

Hernandez Bort, J.A., Hackl, M., Hoflmayer, H., Jadhav, V., Harreither, E., Kumar, N., Ernst, W., Grillari, J. and Borth, N. 2012. Dynamic mRNA and miRNA profiling of CHO-K1 suspension cell cultures. *Biotechnology Journal,* 7(4), pp.500-515.

Hjelm, H., Hjelm, K. and Sjoquist, J. 1972. Protein A from staphylococcus aureus. its isolation by affinity chromatography and its use as an immunosorbent for isolation of immunoglobulins. *FEBS Letters,* 28(1), pp.73-76.

Hober, S., Nord, K. and Linhult, M. 2007. Protein A chromatography for antibody purification. *Journal of Chromatography.B, Analytical Technologies in the Biomedical and Life Sciences,* 848(1), pp.40-47.

Holzel, M., Rohrmoser, M., Schlee, M., Grimm, T., Harasim, T., Malamoussi, A., Gruber-Eber, A., Kremmer, E., Hiddemann, W., Bornkamm, G.W. and Eick, D. 2005. Mammalian WDR12 is a novel member of the Pes1-Bop1 complex and is required for ribosome biogenesis and cell proliferation. *The Journal of Cell Biology,* 170(3), pp.367-378.

Horowitz, R.E., Arjona, C.M., Bang, Y.J. and Storms, D.S. 2009. A novel approach to rapid feed strategy optimisation. *IN:* A novel approach to rapid feed strategy optimisation.

Horvath, P., Romero, D.A., Coute-Monvoisin, A.C., Richards, M., Deveau, H., Moineau, S., Boyaval, P., Fremaux, C. and Barrangou, R. 2008. Diversity, activity, and evolution of CRISPR loci in streptococcus thermophilus. *Journal of Bacteriology,* 190(4), pp.1401-1412.

Hossler, P., Khattak, S.F. and Li, Z.J. 2009. Optimal and consistent protein glycosylation in mammalian cell culture. *Glycobiology,* 19(9), pp.936-949.

Hossler, P., Khattak, S.F. and Li, Z.J. 2009. Optimal and consistent protein glycosylation in mammalian cell culture. *Glycobiology,* 19(9), pp.936-949.

Hsu, P.D., Scott, D.A., Weinstein, J.A., Ran, F.A., Konermann, S., Agarwala, V., Li, Y., Fine, E.J., Wu, X., Shalem, O., Cradick, T.J., Marraffini, L.A., Bao, G. and Zhang, F. 2013. DNA targeting specificity of RNA-guided Cas9 nucleases. *Nature Biotechnology,* 31(9), pp.827-832.

Hu, X., Wang, Y., Liang, H., Fan, Q., Zhu, R., Cui, J., Zhang, W., Zen, K., Zhang, C.Y., Hou, D., Zhou, Z. and Chen, X. 2017. miR-23a/b promote tumor growth and suppress apoptosis by targeting PDCD4 in gastric cancer. *Cell Death & Disease,* 8(10), pp.e3059-. Epub 2017 Oct 5 doi:10.1038/cddis.2017.447.

Huang, Y.M., Hu, W., Rustandi, E., Chang, K., Yusuf-Makagiansar, H. and Ryll, T. 2010. Maximizing productivity of CHO cell-based fed-batch culture using chemically defined media conditions and typical manufacturing equipment. *Biotechnology Progress,* 26(5), pp.1400-1410.

Humphreys, D.T., Westman, B.J., Martin, D.I. and Preiss, T. 2005. MicroRNAs control translation initiation by inhibiting eukaryotic initiation factor 4E/cap and poly(A) tail function. *Proceedings of the National Academy of Sciences of the United States of America,* 102(47), pp.16961-16966.

Huntzinger, E. and Izaurralde, E. 2011. Gene silencing by microRNAs: Contributions of translational repression and mRNA decay. *Nature Reviews.Genetics,* 12(2), pp.99-110.

Hutchinson N. and Bird P. 2015. Automation of a single-use final bulk filtration step: Enhancing operational flexibility and facilitating compliant, Right–First-time manufacturing. *BioProcess International,*

Hwang, W.Y., Fu, Y., Reyon, D., Maeder, M.L., Tsai, S.Q., Sander, J.D., Peterson, R.T., Yeh, J.R. and Joung, J.K. 2013. Efficient genome editing in zebrafish using a CRISPR-cas system. *Nature Biotechnology,* 31(3), pp.227-229.

Ingolia, N.T., Ghaemmaghami, S., Newman, J.R. and Weissman, J.S. 2009. Genome-wide analysis in vivo of translation with nucleotide resolution using ribosome profiling. *Science (New York, N.Y.),* 324(5924), pp.218-223.

International Conference on Harmonisation. 23 September 1999. Viral safety evaluation of biotechnology products derived from cell lines of human or animal originq5a(r1)

International Conference on Harmonisation. 2015. ICH guideline Q9 on quality risk management (ICH-Q9).

International Conference on Harmonisation. 2009. ICH Q8, pharmeceutical Development International Conference on Harmonisation. 2009. Pharmaceutical quality systems.

International Conference on Harmonisation. 1999. Specifications:Test procedures and acceptance criteria for biotechnological/biological productsq6b

Ishino, Y., Shinagawa, H., Makino, K., Amemura, M. and Nakata, A. 1987. Nucleotide sequence of the iap gene, responsible for alkaline phosphatase isozyme conversion in escherichia coli, and identification of the gene product. *Journal of Bacteriology,* 169(12), pp.5429-5433.

Jadhav, V., Hackl, M., Bort, J.A., Wieser, M., Harreither, E., Kunert, R., Borth, N. and Grillari, J. 2012. A screening method to assess biological effects of microRNA overexpression in chinese hamster ovary cells. *Biotechnology and Bioengineering,* 109(6), pp.1376-1385.

Jadhav, V., Hackl, M., Druz, A., Shridhar, S., Chung, C.Y., Heffner, K.M., Kreil, D.P., Betenbaugh, M., Shiloach, J., Barron, N., Grillari, J. and Borth, N. 2013. CHO microRNA engineering is growing up: Recent successes and future challenges. *Biotechnology Advances,* 31(8), pp.1501-1513.

Jadhav, V., Hackl, M., Klanert, G., Hernandez Bort, J.A., Kunert, R., Grillari, J. and Borth, N. 2014. Stable overexpression of miR-17 enhances recombinant protein production of CHO cells. *Journal of Biotechnology,* 175pp.38-44.

Jansen, R., Embden, J.D., Gaastra, W. and Schouls, L.M. 2002. Identification of genes that are associated with DNA repeats in prokaryotes. *Molecular Microbiology,* 43(6), pp.1565-1575.

Jazdzewski, K., Murray, E.L., Franssila, K., Jarzab, B., Schoenberg, D.R. and de la Chapelle, A. 2008. Common SNP in pre-miR-146a decreases mature miR expression and predisposes to papillary thyroid carcinoma. *Proceedings of the National Academy of Sciences of the United States of America,* 105(20), pp.7269-7274.

Jiang, Q., Meng, X., Meng, L., Chang, N., Xiong, J., Cao, H. and Liang, Z. 2014. Small indels induced by CRISPR/Cas9 in the 5' region of microRNA lead to its depletion and drosha processing retardance. *RNA Biology,* 11(10), pp.1243-1249.

Jiang, Z. and Sharfstein, S.T. 2008. Sodium butyrate stimulates monoclonal antibody over-expression in CHO cells by improving gene accessibility. *Biotechnology and Bioengineering,* 100(1), pp.189-194.

Jinek, M., Chylinski, K., Fonfara, I., Hauer, M., Doudna, J.A. and Charpentier, E. 2012. A programmable dual-RNA-guided DNA endonuclease in adaptive bacterial immunity. *Science (New York, N.Y.),* 337(6096), pp.816-821.

Josse, L., Smales, C.M. and Tuite, M.F. 2012. Engineering the chaperone network of CHO cells for optimal recombinant protein production and authenticity. *Methods in Molecular Biology (Clifton, N.J.),* 824pp.595-608.

Kaas, C.S., Kristensen, C., Betenbaugh, M.J. and Andersen, M.R. 2015. Sequencing the CHO DXB11 genome reveals regional variations in genomic stability and haploidy. *BMC Genomics,* 16pp.160-015-1391-x.

Kao, F.T. and Puck, T.T. 1968. Genetics of somatic mammalian cells, VII. induction and isolation of nutritional mutants in chinese hamster cells. *Proceedings of the National Academy of Sciences of the United States of America,* 60(4), pp.1275-1281.

Kao, F.T. and Puck, T.T. 1967. Genetics of somatic mammalian cells. IV. properties of chinese hamster cell mutants with respect to the requirement for proline. *Genetics,* 55(3), pp.513-524.

Kaufmann, H., Mazur, X., Fussenegger, M. and Bailey, J.E. 1999. Influence of low temperature on productivity, proteome and protein phosphorylation of CHO cells. *Biotechnology and Bioengineering,* 63(5), pp.573-582.

Kelly, P. 2014. *Enhancing CHO cell productivity thriugh stable depletion of microRNA-23.* PhD thesis. Dublin City University.

Kelly, P.S., Breen, L., Gallagher, C., Kelly, S., Henry, M., Lao, N.T., Meleady, P., O'Gorman, D., Clynes, M. and Barron, N. 2015. Re-programming CHO cell metabolism using miR-23 tips the balance towards a highly productive phenotype. *Biotechnology Journal,* 10(7), pp.1029-1040.

Kelly, P.S., Breen, L., Gallagher, C., Kelly, S., Henry, M., Lao, N.T., Meleady, P., O'Gorman, D., Clynes, M. and Barron, N. 2015. Re-programming CHO cell metabolism using miR-23 tips

the balance towards a highly productive phenotype. *Biotechnology Journal,* 10(7), pp.1029-1040.

Kelly, P.S., Gallagher, C., Clynes, M. and Barron, N. 2015. Conserved microRNA function as a basis for chinese hamster ovary cell engineering. *Biotechnology Letters,* 37(4), pp.787-798.

Kim, J., Woo, A.J., Chu, J., Snow, J.W., Fujiwara, Y., Kim, C.G., Cantor, A.B. and Orkin, S.H. 2010. A myc network accounts for similarities between embryonic stem and cancer cell transcription programs. *Cell,* 143(2), pp.313-324.

Kim, M., O'Callaghan, P.M., Droms, K.A. and James, D.C. 2011. A mechanistic understanding of production instability in CHO cell lines expressing recombinant monoclonal antibodies. *Biotechnology and Bioengineering,* 108(10), pp.2434-2446.

Kim, N.S. and Lee, G.M. 2002. Inhibition of sodium butyrate-induced apoptosis in recombinant chinese hamster ovary cells by constitutively expressing antisense RNA of caspase-3. *Biotechnology and Bioengineering,* 78(2), pp.217-228.

Kim, N.S. and Lee, G.M. 2000. Overexpression of bcl-2 inhibits sodium butyrate-induced apoptosis in chinese hamster ovary cells resulting in enhanced humanized antibody production. *Biotechnology and Bioengineering,* 71(3), pp.184-193.

Kim, S.H. and Lee, G.M. 2007. Down-regulation of lactate dehydrogenase-A by siRNAs for reduced lactic acid formation of chinese hamster ovary cells producing thrombopoietin. *Applied Microbiology and Biotechnology,* 74(1), pp.152-159.

Kim, S.J., Kim, N.S., Ryu, C.J., Hong, H.J. and Lee, G.M. 1998. Characterization of chimeric antibody producing CHO cells in the course of dihydrofolate reductase-mediated gene amplification and their stability in the absence of selective pressure. *Biotechnology and Bioengineering,* 58(1), pp.73-84.

Kito, M., Itami, S., Fukano, Y., Yamana, K. and Shibui, T. 2002. Construction of engineered CHO strains for high-level production of recombinant proteins. *Applied Microbiology and Biotechnology,* 60(4), pp.442-448.

Kluiver, J., Gibcus, J.H., Hettinga, C., Adema, A., Richter, M.K., Halsema, N., Slezak-Prochazka, I., Ding, Y., Kroesen, B.J. and van den Berg, A. 2012. Rapid generation of microRNA sponges for microRNA inhibition. *PloS One,* 7(1), pp.e29275.

Kochanowski, N., Siriez, G., Roosens, S. and Malphettes, L. 2011. Medium and feed optimization for fed-batch production of a monoclonal antibody in CHO cells. *BMC Proceedings,* 5 Suppl 8pp.P75-6561-5-S8-P75. eCollection 2011.

Koike-Yusa, H., Li, Y., Tan, E.P., Velasco-Herrera Mdel, C. and Yusa, K. 2014. Genome-wide recessive genetic screening in mammalian cells with a lentiviral CRISPR-guide RNA library. *Nature Biotechnology,* 32(3), pp.267-273.

Koles, K., van Berkel, P.H., Mannesse, M.L., Zoetemelk, R., Vliegenthart, J.F. and Kamerling, J.P. 2004. Influence of lactation parameters on the N-glycosylation of recombinant human C1 inhibitor isolated from the milk of transgenic rabbits. *Glycobiology,* 14(11), pp.979-986.

Kozomara, A. and Griffiths-Jones, S. 2014. miRBase: Annotating high confidence microRNAs using deep sequencing data. *Nucleic Acids Research,* 42(Database issue), pp.D68-73.

Kuhn, D.E., Martin, M.M., Feldman, D.S., Terry, A.V., Nuovo, G.J. and Elton, T.S. 2008. Experimental validation of miRNA targets. *Methods (San Diego, Calif.),* 44(1), pp.47-54.

Kulkarni, V., Naqvi, A.R., Uttamani, J.R. and Nares, S. 2016. MiRNA-target interaction reveals cell-specific post-transcriptional regulation in mammalian cell lines. *International Journal of Molecular Sciences,* 17(1), pp.10.3390/ijms17010072.

Kunin, V., Sorek, R. and Hugenholtz, P. 2007. Evolutionary conservation of sequence and secondary structures in CRISPR repeats. *Genome Biology,* 8(4), pp.R61.

Kurcon, T., Liu, Z., Paradkar, A.V., Vaiana, C.A., Koppolu, S., Agrawal, P. and Mahal, L.K. 2015. miRNA proxy approach reveals hidden functions of glycosylation. *Proceedings of the National Academy of Sciences of the United States of America,* 112(23), pp.7327-7332.

Kuystermans, D., Krampe, B., Swiderek, H. and Al-Rubeai, M. 2007. Using cell engineering and omic tools for the improvement of cell culture processes. *Cytotechnology,* 53(1-3), pp.3-22.

Lopez, J., Poitevin, A., Mendoza-Martinez, V., Parez-Plasencia, C. and Garcia-Carranci¡, A. 2012. Cancer-initiating cells derived from established cervical cell lines exhibit stem-cell markers and increased radioresistance. *BMC Cancer,* 12pp.48-2407-12-48.

Lafontaine, D.L. 2015. Noncoding RNAs in eukaryotic ribosome biogenesis and function. *Nature Structural & Molecular Biology,* 22(1), pp.11-19.

Lagos-Quintana, M., Rauhut, R., Yalcin, A., Meyer, J., Lendeckel, W. and Tuschl, T. 2002. Identification of tissue-specific microRNAs from mouse. *Current Biology : CB,* 12(9), pp.735-739.

Lal, A., Navarro, F., Maher, C.A., Maliszewski, L.E., Yan, N., O'Day, E., Chowdhury, D., Dykxhoorn, D.M., Tsai, P., Hofmann, O., Becker, K.G., Gorospe, M., Hide, W. and Lieberman, J. 2009. miR-24 inhibits cell proliferation by targeting E2F2, MYC, and other cell-cycle genes via binding to "seedless" 3'UTR microRNA recognition elements. *Molecular Cell,* 35(5), pp.610-625.

Landauer, K. 2014. Designing media for animal cell culture: CHO cells, the industrial standard. *Methods in Molecular Biology (Clifton, N.J.),* 1104pp.89-103.

Lao, M.S. and Toth, D. 1997. Effects of ammonium and lactate on growth and metabolism of a recombinant chinese hamster ovary cell culture. *Biotechnology Progress,* 13(5), pp.688-691.

Le Fourn, V., Girod, P., Buceta, M., Regamey, A. and Mermod, N. 2014. CHO cell engineering to prevent polypeptide aggregation and improve therapeutic protein secretion. *Metabolic Engineering,* 21pp.91-102.

Lee, J.H., Jeong, Y.R., Kim, Y.G. and Lee, G.M. 2017. Understanding of decreased sialylation of fc-fusion protein in hyperosmotic recombinant chinese hamster ovary cell culture: N-glycosylation gene expression and N-linked glycan antennary profile. *Biotechnology and Bioengineering,* 114(8), pp.1721-1732.

Lee, J.S., Kallehauge, T.B., Pedersen, L.E. and Kildegaard, H.F. 2015. Site-specific integration in CHO cells mediated by CRISPR/Cas9 and homology-directed DNA repair pathway. *Scientific Reports,* 5pp.8572.

Lee, R.C., Feinbaum, R.L. and Ambros, V. 1993. The C. elegans heterochronic gene lin-4 encodes small RNAs with antisense complementarity to lin-14. *Cell,* 75(5), pp.843-854.

Lee, Y., Ahn, C., Han, J., Choi, H., Kim, J., Yim, J., Lee, J., Provost, P., Radmark, O., Kim, S. and Kim, V.N. 2003. The nuclear RNase III drosha initiates microRNA processing. *Nature,* 425(6956), pp.415-419.

Lee, Y., Kim, M., Han, J., Yeom, K.H., Lee, S., Baek, S.H. and Kim, V.N. 2004. MicroRNA genes are transcribed by RNA polymerase II. *The EMBO Journal,* 23(20), pp.4051-4060.

Lewis, B.P., Shih, I.H., Jones-Rhoades, M.W., Bartel, D.P. and Burge, C.B. 2003. Prediction of mammalian microRNA targets. *Cell,* 115(7), pp.787-798.

Li, F., Hashimura, Y., Pendleton, R., Harms, J., Collins, E. and Lee, B. 2006. A systematic approach for scale-down model development and characterization of commercial cell culture processes. *Biotechnology Progress,* 22(3), pp.696-703.

Li, F., Vijayasankaran, N., Shen, A.(.)., Kiss, R. and Amanullah, A. 2010. Cell culture processes for monoclonal antibody production. *Mabs,* 2(5), pp.466-477.

Li, X., Hong, L., Zhao, Y., Jin, H., Fan, R., Du, R., Xia, L., Luo, G. and Fan, D. 2007. A new apoptosis inhibitor, CIAPIN1 (cytokine-induced apoptosis inhibitor 1), mediates multidrug resistance in leukemia cells by regulating MDR-1, bcl-2, and bax. *Biochemistry and Cell Biology = Biochimie Et Biologie Cellulaire,* 85(6), pp.741-750.

Liang, P., Xu, Y., Zhang, X., Ding, C., Huang, R., Zhang, Z., Lv, J., Xie, X., Chen, Y., Li, Y., Sun, Y., Bai, Y., Songyang, Z., Ma, W., Zhou, C. and Huang, J. 2015. CRISPR/Cas9-mediated gene editing in human tripronuclear zygotes. *Protein & Cell,* 6(5), pp.363-372.

Liang, T., Yu, J., Liu, C. and Guo, L. 2014. An exploration of evolution, maturation, expression and function relationships in mir-23 approximately 27 approximately 24 cluster. *PloS One,* 9(8), pp.e106223.

Liang, W., Yang, C., Peng, J., Qian, Y. and Wang, Z. 2015. The expression of HSPD1, SCUBE3, CXCL14 and its relations with the prognosis in osteosarcoma. *Cell Biochemistry and Biophysics,* 73(3), pp.763-768.

Lim, S.F., Chuan, K.H., Liu, S., Loh, S.O., Chung, B.Y., Ong, C.C. and Song, Z. 2006. RNAi suppression of bax and bak enhances viability in fed-batch cultures of CHO cells. *Metabolic Engineering,* 8(6), pp.509-522.

Liu, Y.C., Li, F., Handler, J., Huang, C.R., Xiang, Y., Neretti, N., Sedivy, J.M., Zeller, K.I. and Dang, C.V. 2008. Global regulation of nucleotide biosynthetic genes by c-myc. *PloS One,* 3(7), pp.e2722.

Liu, Y.P., Schopman, N.C. and Berkhout, B. 2013. Dicer-independent processing of short hairpin RNAs. *Nucleic Acids Research,* 41(6), pp.3723-3733.

Livak, K.J. and Schmittgen, T.D. 2001. Analysis of relative gene expression data using real-time quantitative PCR and the 2(-delta delta C(T)) method. *Methods (San Diego, Calif.),* 25(4), pp.402-408.

Lodish, H.F., Zhou, B., Liu, G. and Chen, C.Z. 2008. Micromanagement of the immune system by microRNAs. *Nature Reviews.Immunology,* 8(2), pp.120-130.

Lund, E., Guttinger, S., Calado, A., Dahlberg, J.E. and Kutay, U. 2004. Nuclear export of microRNA precursors. *Science (New York, N.Y.),* 303(5654), pp.95-98.

Lynch, S.M., McKenna, M.M., Walsh, C.P. and McKenna, D.J. 2016. miR-24 regulates CDKN1B/p27 expression in prostate cancer. *The Prostate,* 76(7), pp.637-648.

Ma, H., Wu, Y., Choi, J.G. and Wu, H. 2013. Lower and upper stem-single-stranded RNA junctions together determine the drosha cleavage site. *Proceedings of the National Academy of Sciences of the United States of America,* 110(51), pp.20687-20692.

Ma, N., Ellet, J., Okediadi, C., Hermes, P., McCormick, E. and Casnocha, S. 2009. A single nutrient feed supports both chemically defined NS0 and CHO fed-batch processes: Improved productivity and lactate metabolism. *Biotechnology Progress,* 25(5), pp.1353-1363.

Maccani, A., Ernst, W. and Grabherr, R. 2013. Whole genome sequencing improves estimation of nuclear DNA content of chinese hamster ovary cells. *Cytometry.Part A : The Journal of the International Society for Analytical Cytology,* 83(10), pp.893-895.

Maier, T., Guell, M. and Serrano, L. 2009. Correlation of mRNA and protein in complex biological samples. *FEBS Letters,* 583(24), pp.3966-3973.

Makarova, K.S., Grishin, N.V., Shabalina, S.A., Wolf, Y.I. and Koonin, E.V. 2006. A putative RNA-interference-based immune system in prokaryotes: Computational analysis of the predicted enzymatic machinery, functional analogies with eukaryotic RNAi, and hypothetical mechanisms of action. *Biology Direct,* 1pp.7.

Mali, P., Yang, L., Esvelt, K.M., Aach, J., Guell, M., DiCarlo, J.E., Norville, J.E. and Church, G.M. 2013. RNA-guided human genome engineering via Cas9. *Science (New York, N.Y.),* 339(6121), pp.823-826.

Mandenius, C.F. and Brundin, A. 2008. Bioprocess optimization using design-of-experiments methodology. *Biotechnology Progress,* 24(6), pp.1191-1203.

Mannava, S., Grachtchouk, V., Wheeler, L.J., Im, M., Zhuang, D., Slavina, E.G., Mathews, C.K., Shewach, D.S. and Nikiforov, M.A. 2008. Direct role of nucleotide metabolism in C-MYC-dependent proliferation of melanoma cells. *Cell Cycle (Georgetown, Tex.),* 7(15), pp.2392-2400.

Marraffini, L.A. and Sontheimer, E.J. 2010. Self versus non-self discrimination during CRISPR RNA-directed immunity. *Nature,* 463(7280), pp.568-571.

Mastrangelo, A.J., Hardwick, J.M., Bex, F. and Betenbaugh, M.J. 2000. Part I. bcl-2 and bcl-x(L) limit apoptosis upon infection with alphavirus vectors. *Biotechnology and Bioengineering,* 67(5), pp.544-554.

Meleady, P., Doolan, P., Henry, M., Barron, N., Keenan, J., O'Sullivan, F., Clarke, C., Gammell, P., Melville, M.W., Leonard, M. and Clynes, M. 2011. Sustained productivity in recombinant chinese hamster ovary (CHO) cell lines: Proteome analysis of the molecular basis for a process-related phenotype. *BMC Biotechnology,* 11pp.78-6750-11-78.

Meleady, P., Gallagher, M., Clarke, C., Henry, M., Sanchez, N., Barron, N. and Clynes, M. 2012. Impact of miR-7 over-expression on the proteome of chinese hamster ovary cells. *Journal of Biotechnology,* 160(3-4), pp.251-262.

Meleady, P., Hoffrogge, R., Henry, M., Rupp, O., Bort, J.H., Clarke, C., Brinkrolf, K., Kelly, S., Muller, B., Doolan, P., Hackl, M., Beckmann, T.F., Noll, T., Grillari, J., Barron, N., Puhler, A., Clynes, M. and Borth, N. 2012. Utilization and evaluation of CHO-specific sequence databases for mass spectrometry based proteomics. *Biotechnology and Bioengineering,* 109(6), pp.1386-1394.

Mertens-Talcott, S.U., Chintharlapalli, S., Li, X. and Safe, S. 2007. The oncogenic microRNA-27a targets genes that regulate specificity protein transcription factors and the G2-M checkpoint in MDA-MB-231 breast cancer cells. *Cancer Research,* 67(22), pp.11001-11011.

Meuwly, F., Ruffieux, P.-., Kadouri, A. and von Stockar, U. 2007. Packed-bed bioreactors for mammalian cell culture: Bioprocess and biomedical applications. *Biotechnology Advances,* 25(1), pp.45-56.

Mi, S., Lu, J., Sun, M., Li, Z., Zhang, H., Neilly, M.B., Wang, Y., Qian, Z., Jin, J., Zhang, Y., Bohlander, S.K., Le Beau, M.M., Larson, R.A., Golub, T.R., Rowley, J.D. and Chen, J. 2007. MicroRNA expression signatures accurately discriminate acute lymphoblastic leukemia from acute myeloid leukemia. *Proceedings of the National Academy of Sciences of the United States of America,* 104(50), pp.19971-19976.

Miluzio, A., Beugnet, A., Volta, V. and Biffo, S. 2009. Eukaryotic initiation factor 6 mediates a continuum between 60S ribosome biogenesis and translation. *EMBO Reports,* 10(5), pp.459-465.

Minch, S.L., Kallio, P.T. and Bailey, J.E. 1995. Tissue plasminogen activator coexpressed in chinese hamster ovary cells with alpha(2,6)-sialyltransferase contains NeuAc alpha(2,6)gal beta(1,4)glc-N-AcR linkages. *Biotechnology Progress,* 11(3), pp.348-351.

Mishra, P.J., Humeniuk, R., Mishra, P.J., Longo-Sorbello, G.S.A., Banerjee, D. and Bertino, J.R. 2007. A miR-24 microRNA binding-site polymorphism in dihydrofolate reductase gene leads to methotrexate resistance. *Proceedings of the National Academy of Sciences of the United States of America,* 104(33), pp.13513-13518.

Mishra, P.J., Song, B., Mishra, P.J., Wang, Y., Humeniuk, R., Banerjee, D., Merlino, G., Ju, J. and Bertino, J.R. 2009. MiR-24 tumor suppressor activity is regulated independent of p53 and through a target site polymorphism. *PloS One,* 4(12), pp.e8445.

Mitchell-Logean, C. and Murhammer, D.W. 1997. Bcl-2 expression in spodoptera frugiperda sf-9 and trichoplusia ni BTI-tn-5B1-4 insect cells: Effect on recombinant protein expression and cell viability. *Biotechnology and Bioengineering,* 56(4), pp.380-390.

Miyamoto, S., Chiorini, J.A., Urcelay, E. and Safer, B. 1996. Regulation of gene expression for translation initiation factor eIF-2 alpha: Importance of the 3' untranslated region. *The Biochemical Journal,* 315 (Pt 3)(Pt 3), pp.791-798.

Mohan, C., Park, S.H., Chung, J.Y. and Lee, G.M. 2007. Effect of doxycycline-regulated protein disulfide isomerase expression on the specific productivity of recombinant CHO cells: Thrombopoietin and antibody. *Biotechnology and Bioengineering,* 98(3), pp.611-615.

Mohr, S.E. and Perrimon, N. 2012. RNAi screening: New approaches, understandings and organisms. *Wiley Interdisciplinary Reviews.RNA,* 3(2), pp.145-158.

Moore, A., Mercer, J., Dutina, G., Donahue, C.J., Bauer, K.D., Mather, J.P., Etcheverry, T. and Ryll, T. 1997. Effects of temperature shift on cell cycle, apoptosis and nucleotide pools in CHO cell batch cultues. *Cytotechnology,* 23(1-3), pp.47-54.

Mori, K., Iida, S., Yamane-Ohnuki, N., Kanda, Y., Kuni-Kamochi, R., Nakano, R., Imai-Nishiya, H., Okazaki, A., Shinkawa, T., Natsume, A., Niwa, R., Shitara, K. and Satoh, M. 2007. Non-fucosylated therapeutic antibodies: The next generation of therapeutic antibodies. *Cytotechnology,* 55(2-3), pp.109-114.

Moritz, B., Becker, P.B. and Gopfert, U. 2015. CMV promoter mutants with a reduced propensity to productivity loss in CHO cells. *Scientific Reports,* 5pp.16952.

Musto, A., Navarra, A., Vocca, A., Gargiulo, A., Minopoli, G., Romano, S., Romano, M.F., Russo, T. and Parisi, S. 2015. miR-23a, miR-24 and miR-27a protect differentiating ESCs from BMP4-induced apoptosis. *Cell Death and Differentiation,* 22(6), pp.1047-1057.

Muthing, J., Kemminer, S.E., Conradt, H.S., Sagi, D., Nimtz, M., Karst, U. and Peter-Katalinic, J. 2003. Effects of buffering conditions and culture pH on production rates and glycosylation of clinical phase I anti-melanoma mouse IgG3 monoclonal antibody R24. *Biotechnology and Bioengineering,* 83(3), pp.321-334.

Nam, J.W., Rissland, O.S., Koppstein, D., Abreu-Goodger, C., Jan, C.H., Agarwal, V., Yildirim, M.A., Rodriguez, A. and Bartel, D.P. 2014. Global analyses of the effect of different cellular contexts on microRNA targeting. *Molecular Cell,* 53(6), pp.1031-1043.

Noèlia Sanchez 2013. *miRNAs as tools to improve CHO cell bioprocess phenotypes.* PhD thesis. Dublin City University. Doras: http://doras.dcu.ie/17716/

Noguchi, S., Yasui, Y., Iwasaki, J., Kumazaki, M., Yamada, N., Naito, S. and Akao, Y. 2013. Replacement treatment with microRNA-143 and -145 induces synergistic inhibition of the growth of human bladder cancer cells by regulating PI3K/Akt and MAPK signaling pathways. *Cancer Letters,* 328(2), pp.353-361.

O'Geen, H., Yu, A.S. and Segal, D.J. 2015. *How specific is CRISPR/Cas9 really?*

Obaya, A.J., Kotenko, I., Cole, M.D. and Sedivy, J.M. 2002. The proto-oncogene c-myc acts through the cyclin-dependent kinase (cdk) inhibitor p27(Kip1) to facilitate the activation of Cdk4/6 and early G(1) phase progression. *The Journal of Biological Chemistry,* 277(34), pp.31263-31269.

Osterlehner, A., Simmeth, S. and Gopfert, U. 2011. Promoter methylation and transgene copy numbers predict unstable protein production in recombinant chinese hamster ovary cell lines. *Biotechnology and Bioengineering,* 108(11), pp.2670-2681.

Osthus, R.C., Shim, H., Kim, S., Li, Q., Reddy, R., Mukherjee, M., Xu, Y., Wonsey, D., Lee, L.A. and Dang, C.V. 2000. Deregulation of glucose transporter 1 and glycolytic gene expression by c-myc. *The Journal of Biological Chemistry,* 275(29), pp.21797-21800.

Park, H., Kim, I.H., Kim, I.Y., Kim, K.H. and Kim, H.J. 2000. Expression of carbamoyl phosphate synthetase I and ornithine transcarbamoylase genes in chinese hamster ovary dhfr-cells decreases accumulation of ammonium ion in culture media. *Journal of Biotechnology,* 81(2-3), pp.129-140.

Pasquinelli, A.E. 2012. MicroRNAs and their targets: Recognition, regulation and an emerging reciprocal relationship. *Nature Reviews.Genetics,* 13(4), pp.271-282.

Patel, M.I., Tuckerman, R. and Dong, Q. 2005. A pitfall of the 3-(4,5-dimethylthiazol-2-yl)-5(3-carboxymethonyphenol)-2-(4-sulfophenyl)-2H-tetra zolium (MTS) assay due to evaporation in wells on the edge of a 96 well plate. *Biotechnology Letters,* 27(11), pp.805-808.

Patel, T.P., Parekh, R.B., Moellering, B.J. and Prior, C.P. 1992. Different culture methods lead to differences in glycosylation of a murine IgG monoclonal antibody. *The Biochemical Journal,* 285 (Pt 3)(Pt 3), pp.839-845.

Paul S. Kelly 2014. *Enhancing CHO cel productivity through the stable depletion of microRNA-23.* Dublin City University. Doras: http://doras.dcu.ie/20181/

Pelletier, M.F., Marcil, A., Sevigny, G., Jakob, C.A., Tessier, D.C., Chevet, E., Menard, R., Bergeron, J.J. and Thomas, D.Y. 2000. The heterodimeric structure of glucosidase II is required for its activity, solubility, and localization in vivo. *Glycobiology,* 10(8), pp.815-827.

Peng, R.W., Abellan, E. and Fussenegger, M. 2011. Differential effect of exocytic SNAREs on the production of recombinant proteins in mammalian cells. *Biotechnology and Bioengineering,* 108(3), pp.611-620.

Peng, R.W. and Fussenegger, M. 2009. Molecular engineering of exocytic vesicle traffic enhances the productivity of chinese hamster ovary cells. *Biotechnology and Bioengineering,* 102(4), pp.1170-1181.

Perez-Roger, I., Kim, S.H., Griffiths, B., Sewing, A. and Land, H. 1999. Cyclins D1 and D2 mediate myc-induced proliferation via sequestration of p27(Kip1) and p21(Cip1). *The EMBO Journal,* 18(19), pp.5310-5320.

Pichler, J., Galosy, S., Mott, J. and Borth, N. 2011. Selection of CHO host cell subclones with increased specific antibody production rates by repeated cycles of transient transfection and cell sorting. *Biotechnology and Bioengineering,* 108(2), pp.386-394.

Porkka, K.P., Pfeiffer, M.J., Waltering, K.K., Vessella, R.L., Tammela, T.L. and Visakorpi, T. 2007. MicroRNA expression profiling in prostate cancer. *Cancer Research,* 67(13), pp.6130-6135.

Pratt, A.J. and MacRae, I.J. 2009. The RNA-induced silencing complex: A versatile gene-silencing machine. *The Journal of Biological Chemistry,* 284(27), pp.17897-17901.

Puck, T.T., Cieciura, S.J. and Robinson, A. 1958. Genetics of somatic mammalian cells. III. long-term cultivation of euploid cells from human and animal subjects. *The Journal of Experimental Medicine,* 108(6), pp.945-956.

Qin, W., Shi, Y., Zhao, B., Yao, C., Jin, L., Ma, J. and Jin, Y. 2010. miR-24 regulates apoptosis by targeting the open reading frame (ORF) region of FAF1 in cancer cells. *PloS One,* 5(2), pp.e9429.

Raju, T.S. 2008. Terminal sugars of fc glycans influence antibody effector functions of IgGs. *Current Opinion in Immunology,* 20(4), pp.471-478.

Rathore, A.S. 2009. Roadmap for implementation of quality by design (QbD) for biotechnology products. *Trends in Biotechnology,* 27(9), pp.546-553.

Rathore, A.S. and Winkle, H. 2009. Quality by design for biopharmaceuticals. *Nature Biotechnology,* 27(1), pp.26-34.

Rodriguez, E. 1970. *Journal of Clinical Research & Bioethics,* (2), pp.1-4.

Rodriguez, T.H., Poertner, R. and Frahm, B. 2015. Considerations for cell passaging in cell culture seed trains. *BMC Proceedings,* 9(Suppl 9), pp.P43-6561-9-S9-P43.

Rohrmoser, M., Holzel, M., Grimm, T., Malamoussi, A., Harasim, T., Orban, M., Pfisterer, I., Gruber-Eber, A., Kremmer, E. and Eick, D. 2007. Interdependence of Pes1, Bop1, and WDR12 controls nucleolar localization and assembly of the PeBoW complex required for maturation of the 60S ribosomal subunit. *Molecular and Cellular Biology,* 27(10), pp.3682-3694.

Ronda, C., Pedersen, L.E., Hansen, H.G., Kallehauge, T.B., Betenbaugh, M.J., Nielsen, A.T. and Kildegaard, H.F. 2014. Accelerating genome editing in CHO cells using CRISPR Cas9 and CRISPy, a web-based target finding tool. *Biotechnology and Bioengineering,* 111(8), pp.1604-1616.

Root, D.E., Hacohen, N., Hahn, W.C., Lander, E.S. and Sabatini, D.M. 2006. Genome-scale loss-of-function screening with a lentiviral RNAi library. *Nature Methods,* 3(9), pp.715-719.

Rosati, A., Graziano, V., De Laurenzi, V., Pascale, M. and Turco, M.C. 2011. BAG3: A multifaceted protein that regulates major cell pathways. *Cell Death & Disease,* 2pp.e141.

Rosen, M.B., Schmid, J.R., Corton, J.C., Zehr, R.D., Das, K.P., Abbott, B.D. and Lau, C. 2010. Gene expression profiling in wild-type and PPARÎ±-null mice exposed to perfluorooctane sulfonate reveals PPARÎ±-independent effects. *PPAR Research,* 2010pp.10.1155/2010/794739.

Rothman, R.J., Perussia, B., Herlyn, D. and Warren, L. 1989. Antibody-dependent cytotoxicity mediated by natural killer cells is enhanced by castanospermine-induced alterations of IgG glycosylation. *Molecular Immunology,* 26(12), pp.1113-1123.

Rouiller, Y., Solacroup, T., Deparis, V., Barbafieri, M., Gleixner, R., Broly, H. and Eon-Duval, A. 2012. Application of quality by design to the characterization of the cell culture process of an fc-fusion protein. *European Journal of Pharmaceutics and Biopharmaceutics : Official Journal of Arbeitsgemeinschaft Fur Pharmazeutische Verfahrenstechnik e.V,* 81(2), pp.426-437.

Running Deer, J. and Allison, D.S. 2004. High-level expression of proteins in mammalian cells using transcription regulatory sequences from the chinese hamster EF-1alpha gene. *Biotechnology Progress,* 20(3), pp.880-889.

Saini, H.K., Griffiths-Jones, S. and Enright, A.J. 2007. Genomic analysis of human microRNA transcripts. *Proceedings of the National Academy of Sciences of the United States of America,* 104(45), pp.17719-17724.

Sanchez, N., Gallagher, M., Lao, N., Gallagher, C., Clarke, C., Doolan, P., Aherne, S., Blanco, A., Meleady, P., Clynes, M. and Barron, N. 2013. MiR-7 triggers cell cycle arrest at the G1/S transition by targeting multiple genes including Skp2 and Psme3. *PloS One,* 8(6), pp.e65671.

Sanchez, N., Kelly, P., Gallagher, C., Lao, N.T., Clarke, C., Clynes, M. and Barron, N. 2014. CHO cell culture longevity and recombinant protein yield are enhanced by depletion of miR-7 activity via sponge decoy vectors. *Biotechnology Journal,* 9(3), pp.396-404.

Sauerwald, T.M., Betenbaugh, M.J. and Oyler, G.A. 2002. Inhibiting apoptosis in mammalian cell culture using the caspase inhibitor XIAP and deletion mutants. *Biotechnology and Bioengineering,* 77(6), pp.704-716.

Sauerwald, T.M., Oyler, G.A. and Betenbaugh, M.J. 2003. Study of caspase inhibitors for limiting death in mammalian cell culture. *Biotechnology and Bioengineering,* 81(3), pp.329-340.

Saumet, A., Vetter, G., Bouttier, M., Portales-Casamar, E., Wasserman, W.W., Maurin, T., Mari, B., Barbry, P., Vallar, L., Friederich, E., Arar, K., Cassinat, B., Chomienne, C. and Lecellier, C.H. 2009. Transcriptional repression of microRNA genes by PML-RARA increases expression of key cancer proteins in acute promyelocytic leukemia. *Blood,* 113(2), pp.412-421.

Sautter, K. and Enenkel, B. 2005. Selection of high-producing CHO cells using NPT selection marker with reduced enzyme activity. *Biotechnology and Bioengineering,* 89(5), pp.530-538.

Sayed, D., Hong, C., Chen, I.Y., Lypowy, J. and Abdellatif, M. 2007. MicroRNAs play an essential role in the development of cardiac hypertrophy. *Circulation Research,* 100(3), pp.416-424.

Schimke, R.T. 1984. Gene amplification in cultured animal cells. *Cell,* 37(3), pp.705-713.

Schmelzer, A.E. and Miller, W.M. 2002. Hyperosmotic stress and elevated pCO2 alter monoclonal antibody charge distribution and monosaccharide content. *Biotechnology Progress,* 18(2), pp.346-353.

Schröder, M. and Kaufman, R.J. 2005. *ER stress and the unfolded protein response.*

Schuster-Bockler, B., Conrad, D. and Bateman, A. 2010. Dosage sensitivity shapes the evolution of copy-number varied regions. *PloS One,* 5(3), pp.e9474.

Schwanhausser, B., Busse, D., Li, N., Dittmar, G., Schuchhardt, J., Wolf, J., Chen, W. and Selbach, M. 2011. Global quantification of mammalian gene expression control. *Nature,* 473(7347), pp.337-342.

Schwank, G., Koo, B.K., Sasselli, V., Dekkers, J.F., Heo, I., Demircan, T., Sasaki, N., Boymans, S., Cuppen, E., van der Ent, C.K., Nieuwenhuis, E.E., Beekman, J.M. and Clevers, H. 2013. Functional repair of CFTR by CRISPR/Cas9 in intestinal stem cell organoids of cystic fibrosis patients. *Cell Stem Cell,* 13(6), pp.653-658.

Schwarz, D.S., Hutvagner, G., Du, T., Xu, Z., Aronin, N. and Zamore, P.D. 2003. Asymmetry in the assembly of the RNAi enzyme complex. *Cell,* 115(2), pp.199-208.

Shalem, O., Sanjana, N.E., Hartenian, E., Shi, X., Scott, D.A., Mikkelsen, T.S., Heckl, D., Ebert, B.L., Root, D.E., Doench, J.G. and Zhang, F. 2014. Genome-scale CRISPR-Cas9 knockout screening in human cells. *Science (New York, N.Y.),* 343(6166), pp.84-87.

Shalem, O., Sanjana, N.E. and Zhang, F. 2015. High-throughput functional genomics using CRISPR-Cas9. *Nature Reviews.Genetics,* 16(5), pp.299-311.

Shan, S.W., Fang, L., Shatseva, T., Rutnam, Z.J., Yang, X., Du, W., Lu, W.Y., Xuan, J.W., Deng, Z. and Yang, B.B. 2013. Mature miR-17-5p and passenger miR-17-3p induce hepatocellular carcinoma by targeting PTEN, GalNT7 and vimentin in different signal pathways. *Journal of Cell Science,* 126(Pt 6), pp.1517-1530.

Sharma, V., Ichikawa, M., He, P., Scott, D.A., Bravo, Y., Dahl, R., Ng, B.G., Cosford, N.D. and Freeze, H.H. 2011. Phosphomannose isomerase inhibitors improve N-glycosylation in selected phosphomannomutase-deficient fibroblasts. *The Journal of Biological Chemistry,* 286(45), pp.39431-39438.

Shu, J., Xia, Z., Li, L., Liang, E.T., Slipek, N., Shen, D., Foo, J., Subramanian, S. and Steer, C.J. 2012. Dose-dependent differential mRNA target selection and regulation by let-7a-7f and miR-17-92 cluster microRNAs. *RNA Biology,* 9(10), pp.1275-1287.

Shukla, A.A., Hubbard, B., Tressel, T., Guhan, S. and Low, D. 2007. Downstream processing of monoclonal antibodies--application of platform approaches. *Journal of Chromatography.B, Analytical Technologies in the Biomedical and Life Sciences,* 848(1), pp.28-39.

Simon, M.T., Ng, B.G., Friederich, M.W., Wang, R.Y., Boyer, M., Kircher, M., Collard, R., Buckingham, K.J., Chang, R., Shendure, J., Nickerson, D.A., Bamshad, M.J., University of Washington Center for Mendelian Genomics, Van Hove, J.L.K., Freeze, H.H. and Abdenur, J.E. 2017. Activation of a cryptic splice site in the mitochondrial elongation factor GFM1 causes combined OXPHOS deficiency(). *Mitochondrion,* 34pp.84-90.

Singh, R. and Saini, N. 2012. Downregulation of BCL2 by miRNAs augments drug-induced apoptosis--a combined computational and experimental approach. *Journal of Cell Science,* 125(Pt 6), pp.1568-1578.

Smale, S.T. and Kadonaga, J.T. 2003. The RNA polymerase II core promoter. *Annual Review of Biochemistry,* 72pp.449-479.

Sommeregger, W., Mayrhofer, P., Steinfellner, W., Reinhart, D., Henry, M., Clynes, M., Meleady, P. and Kunert, R. 2016. Proteomic differences in recombinant CHO cells producing two similar antibody fragments. *Biotechnology and Bioengineering,* 113(9), pp.1902-1912.

Squatrito, M., Mancino, M., Donzelli, M., Areces, L.B. and Draetta, G.F. 2004. EBP1 is a nucleolar growth-regulating protein that is part of pre-ribosomal ribonucleoprotein complexes. *Oncogene,* 23(25), pp.4454-4465.

Squatrito, M., Mancino, M., Sala, L. and Draetta, G.F. 2006. Ebp1 is a dsRNA-binding protein associated with ribosomes that modulates eIF2alpha phosphorylation. *Biochemical and Biophysical Research Communications,* 344(3), pp.859-868.

Starega-Roslan, J., Galka-Marciniak, P. and Krzyzosiak, W.J. 2015. Nucleotide sequence of miRNA precursor contributes to cleavage site selection by dicer. *Nucleic Acids Research,* 43(22), pp.10939-10951.

Starega-Roslan, J., Witkos, T.M., Galka-Marciniak, P. and Krzyzosiak, W.J. 2015. Sequence features of drosha and dicer cleavage sites affect the complexity of IsomiRs. *International Journal of Molecular Sciences,* 16(4), pp.8110-8127.

Stranger, B.E., Forrest, M.S., Dunning, M., Ingle, C.E., Beazley, C., Thorne, N., Redon, R., Bird, C.P., de Grassi, A., Lee, C., Tyler-Smith, C., Carter, N., Scherer, S.W., Tavare, S., Deloukas, P., Hurles, M.E. and Dermitzakis, E.T. 2007. Relative impact of nucleotide and copy number variation on gene expression phenotypes. *Science (New York, N.Y.),* 315(5813), pp.848-853.

Strotbek, M., Florin, L., Koenitzer, J., Tolstrup, A., Kaufmann, H., Hausser, A. and Olayioye, M.A. 2013. Stable microRNA expression enhances therapeutic antibody productivity of chinese hamster ovary cells. *Metabolic Engineering,* 20pp.157-166.

Strutzenberger, K., Borth, N., Kunert, R., Steinfellner, W. and Katinger, H. 1999. Changes during subclone development and ageing of human antibody-producing recombinant CHO cells. *Journal of Biotechnology,* 69(2-3), pp.215-226.

Sun, G., Yan, J., Noltner, K., Feng, J., Li, H., Sarkis, D.A., Sommer, S.S. and Rossi, J.J. 2009. SNPs in human miRNA genes affect biogenesis and function. *Rna,* 15(9), pp.1640-1651.

Sung, Y.H., Lee, J.S., Park, S.H., Koo, J. and Lee, G.M. 2007. Influence of co-down-regulation of caspase-3 and caspase-7 by siRNAs on sodium butyrate-induced apoptotic cell death of chinese hamster ovary cells producing thrombopoietin. *Metabolic Engineering,* 9(5-6), pp.452-464.

Sung, Y.H., Song, Y.J., Lim, S.W., Chung, J.Y. and Lee, G.M. 2004. Effect of sodium butyrate on the production, heterogeneity and biological activity of human thrombopoietin by recombinant chinese hamster ovary cells. *Journal of Biotechnology,* 112(3), pp.323-335.

Thomas, J.A., Ott, D.E. and Gorelick, R.J. 2007. Efficiency of human immunodeficiency virus type 1 postentry infection processes: Evidence against disproportionate numbers of defective virions. *Journal of Virology,* 81(8), pp.4367-4370.

Thompson, L.H. and Baker, R.M. 1973. Isolation of mutants of cultured mammalian cells. *Methods in Cell Biology,* 6pp.209-281.

Toussaint, C., Henry, O. and Durocher, Y. 2016. Metabolic engineering of CHO cells to alter lactate metabolism during fed-batch cultures. *Journal of Biotechnology,* 217pp.122-131.

Trombetta, E.S., Simons, J.F. and Helenius, A. 1996. Endoplasmic reticulum glucosidase II is composed of a catalytic subunit, conserved from yeast to mammals, and a tightly bound noncatalytic HDEL-containing subunit. *The Journal of Biological Chemistry,* 271(44), pp.27509-27516.

Trummer, E., Fauland, K., Seidinger, S., Schriebl, K., Lattenmayer, C., Kunert, R., Vorauer-Uhl, K., Weik, R., Borth, N., Katinger, H. and Muller, D. 2006. Process parameter shifting: Part II. biphasic cultivation-A tool for enhancing the volumetric productivity of batch processes using epo-fc expressing CHO cells. *Biotechnology and Bioengineering,* 94(6), pp.1045-1052.

Tsai, S.Q., Wyvekens, N., Khayter, C., Foden, J.A., Thapar, V., Reyon, D., Goodwin, M.J., Aryee, M.J. and Joung, J.K. 2014. Dimeric CRISPR RNA-guided FokI nucleases for highly specific genome editing. *Nature Biotechnology,* 32(6), pp.569-576.

Urlaub, G., Kas, E., Carothers, A.M. and Chasin, L.A. 1983. Deletion of the diploid dihydrofolate reductase locus from cultured mammalian cells. *Cell,* 33(2), pp.405-412.

Veerappa, A.M., Murthy, M.N., Vishweswaraiah, S., Lingaiah, K., Suresh, R.V., Nachappa, S.A., Prashali, N., Yadav, S.N., Srikanta, M.A., Manjegowda, D.S., Seshachalam, K.B. and Ramachandra, N.B. 2014. Copy number variations burden on miRNA genes reveals layers of complexities involved in the regulation of pathways and phenotypic expression. *PloS One,* 9(2), pp.e90391.

Ventura, A., Young, A.G., Winslow, M.M., Lintault, L., Meissner, A., Erkeland, S.J., Newman, J., Bronson, R.T., Crowley, D., Stone, J.R., Jaenisch, R., Sharp, P.A. and Jacks, T. 2008. Targeted deletion reveals essential and overlapping functions of the miR-17 through 92 family of miRNA clusters. *Cell,* 132(5), pp.875-886.

Vidali, G., Boffa, L.C., Bradbury, E.M. and Allfrey, V.G. 1978. Butyrate suppression of histone deacetylation leads to accumulation of multiacetylated forms of histones H3 and H4 and increased DNase I sensitivity of the associated DNA sequences. *Proceedings of the National Academy of Sciences of the United States of America,* 75(5), pp.2239-2243.

Vives, J., Juanola, S., Cairó, J.J. and Gòdia, F. 2003. Metabolic engineering of apoptosis in cultured animal cells: Implications for the biotechnology industry. *Metabolic Engineering,* 5(2), pp.124-132.

Vlach, J., Hennecke, S., Alevizopoulos, K., Conti, D. and Amati, B. 1996. Growth arrest by the cyclin-dependent kinase inhibitor p27Kip1 is abrogated by c-myc. *The EMBO Journal,* 15(23), pp.6595-6604.

Walsh, G. 2014. Biopharmaceutical benchmarks 2014. *Nature Biotechnology,* 32(10), pp.992-1000.

Wang, J., Haubrock, M., Cao, K.M., Hua, X., Zhang, C.Y., Wingender, E. and Li, J. 2011. Regulatory coordination of clustered microRNAs based on microRNA-transcription factor regulatory network. *BMC Systems Biology,* 5pp.199-0509-5-199.

Wang, L., Hu, H., Yang, J., Wang, F., Kaisermayer, C. and Zhou, P. 2012. High yield of human monoclonal antibody produced by stably transfected drosophila schneider 2 cells in perfusion culture using wave bioreactor. *Molecular Biotechnology,* 52(2), pp.170-179.

Wang, Q., Yin, B., Chung, C.Y. and Betenbaugh, M.J. 2017. Glycoengineering of CHO cells to improve product quality. *Methods in Molecular Biology (Clifton, N.J.),* 1603pp.25-44.

Wang, T., Wei, J.J., Sabatini, D.M. and Lander, E.S. 2014. Genetic screens in human cells using the CRISPR/Cas9 system. *Science (New York, N.Y.),* 343(6166), pp.80-84.

Wang, W., Singh, S., Zeng, D.L., King, K. and Nema, S. 2007. Antibody structure, instability, and formulation. *Journal of Pharmaceutical Sciences,* 96(1), pp.1-26.

Wang, Y., Luo, J., Zhang, H. and Lu, J. 2016. microRNAs in the same clusters evolve to coordinately regulate functionally related genes. *Molecular Biology and Evolution,* 33(9), pp.2232-2247.

Warburg, O. 1956. On respiratory impairment in cancer cells. *Science (New York, N.Y.),* 124(3215), pp.269-270.

Wei, Y.Y., Naderi, S., Meshram, M., Budman, H., Scharer, J.M., Ingalls, B.P. and McConkey, B.J. 2011. Proteomics analysis of chinese hamster ovary cells undergoing apoptosis during prolonged cultivation. *Cytotechnology,* 63(6), pp.663-677.

Wlaschin, K.F. and Hu, W.S. 2007. Engineering cell metabolism for high-density cell culture via manipulation of sugar transport. *Journal of Biotechnology,* 131(2), pp.168-176.

Wolter, T. and Richter, A. 2005. Assays for controlling host-cell impurities in biopharmaceuticals. *BioProcess International,*

Wu, F., Zikusoka, M., Trindade, A., Dassopoulos, T., Harris, M.L., Bayless, T.M., Brant, S.R., Chakravarti, S. and Kwon, J.H. 2008. MicroRNAs are differentially expressed in ulcerative colitis and alter expression of macrophage inflammatory peptide-2 alpha. *Gastroenterology,* 135(5), pp.1624-1635.e24.

Wu, X., Kriz, A.J. and Sharp, P.A. 2014. Target specificity of the CRISPR-Cas9 system. *Quantitative Biology,* 2(2), pp.59-70.

Wu, X., Kriz, A.J. and Sharp, P.A. 2014. Target specificity of the CRISPR-Cas9 system. *Quantitative Biology,* 2(2), pp.59-70.

Wu, Y., Liang, D., Wang, Y., Bai, M., Tang, W., Bao, S., Yan, Z., Li, D. and Li, J. 2013. Correction of a genetic disease in mouse via use of CRISPR-Cas9. *Cell Stem Cell,* 13(6), pp.659-662.

Wurm, M.F. 2013. CHO Quasispecies—Implications for manufacturing processes. 1(3), pp.298.

Wurm, F.M. 2004. Production of recombinant protein therapeutics in cultivated mammalian cells. *Nature Biotechnology,* 22(11), pp.1393-1398.

Wurm, F.M. and Wurm, M.J. 2017. Cloning of CHO cells, productivity and genetic. *Processes,* 5(2)

Xie, L., Zhou, W. and Robinson, D. 2003. Protein production by large-scale mammalian cell culture. *New Comprehensive Biochemistry,* 38pp.605-623.

Xie, M., Wang, X.L., Ji, Y.Q., Li, J., Meng, Z.J., Shi, L. and Yuan, Y.K. 2005. Study on the relationship between level of CD58 expression in peripheral blood mononuclear cell and severity of HBV infection. *Chinese Medical Journal,* 118(24), pp.2072-2076.

Xu, L., Chen, Z., Xue, F., Chen, W., Ma, R., Cheng, S. and Cui, P. 2015. MicroRNA-24 inhibits growth, induces apoptosis, and reverses radioresistance in laryngeal squamous cell carcinoma by targeting X-linked inhibitor of apoptosis protein. *Cancer Cell International,* 15pp.10.1186/s12935-015-0217-x.

Xu, X., Nagarajan, H., Lewis, N.E., Pan, S., Cai, Z., Liu, X., Chen, W., Xie, M., Wang, W., Hammond, S., Andersen, M.R., Neff, N., Passarelli, B., Koh, W., Fan, H.C., Wang, J., Gui, Y., Lee, K.H., Betenbaugh, M.J., Quake, S.R., Famili, I., Palsson, B.O. and Wang, J. 2011. The genomic sequence of the chinese hamster ovary (CHO)-K1 cell line. *Nature Biotechnology,* 29(8), pp.735-741.

Yallop, C., NÃ¸rby, P., Jensen, R., Reinbach, H. and Svendsen, I. 2003. Characterisation of G418-induced metabolic load in recombinant CHO and BHK cells: Effect on the activity and expression of central metabolic enzymes. *Cytotechnology,* 42(2), pp.87-99.

Yang, J., Wang, N., Chen, D., Yu, J., Pan, Q., Wang, D., Liu, J., Shi, X., Dong, X., Cao, H., Li, L. and Li, L. 2017. The impact of GFP reporter gene transduction and expression on

metabolomics of placental mesenchymal stem cells determined by UHPLC-Q/TOF-MS. *Stem Cells International,* 2017pp.10.1155/2017/3167985.

Yang, S., Wang, K., Qian, C., Song, Z., Pu, P., Zhang, A., Wang, W., Niu, H., Li, X., Qi, X., Zhu, Y. and Wang, Y. 2012. A predicted miR-27a-mediated network identifies a signature of glioma. *Oncology Reports,* 28(4), pp.1249-1256.

Yang, X., Du, W.W., Li, H., Liu, F., Khorshidi, A., Rutnam, Z.J. and Yang, B.B. 2013. Both mature miR-17-5p and passenger strand miR-17-3p target TIMP3 and induce prostate tumor growth and invasion. *Nucleic Acids Research,* 41(21), pp.9688-9704.

Yang, Y., Mariati, Chusainow, J. and Yap, M.G. 2010. DNA methylation contributes to loss in productivity of monoclonal antibody-producing CHO cell lines. *Journal of Biotechnology,* 147(3-4), pp.180-185.

Yin, B., Gao, Y., Chung, C.Y., Yang, S., Blake, E., Stuczynski, M.C., Tang, J., Kildegaard, H.F., Andersen, M.R., Zhang, H. and Betenbaugh, M.J. 2015. Glycoengineering of chinese hamster ovary cells for enhanced erythropoietin N-glycan branching and sialylation. *Biotechnology and Bioengineering,* 112(11), pp.2343-2351.

Yin, H., Xue, W., Chen, S., Bogorad, R.L., Benedetti, E., Grompe, M., Koteliansky, V., Sharp, P.A., Jacks, T. and Anderson, D.G. 2014. Genome editing with Cas9 in adult mice corrects a disease mutation and phenotype. *Nature Biotechnology,* 32(6), pp.551-553.

Yoon, S.K., Hwang, S.O. and Lee, G.M. 2004. Enhancing effect of low culture temperature on specific antibody productivity of recombinant chinese hamster ovary cells: Clonal variation. *Biotechnology Progress,* 20(6), pp.1683-1688.

Yoon, S.K., Song, J.Y. and Lee, G.M. 2003. Effect of low culture temperature on specific productivity, transcription level, and heterogeneity of erythropoietin in chinese hamster ovary cells. *Biotechnology and Bioengineering,* 82(3), pp.289-298.

Yu, J., Wang, F., Yang, G.H., Wang, F.L., Ma, Y.N., Du, Z.W. and Zhang, J.W. 2006. Human microRNA clusters: Genomic organization and expression profile in leukemia cell lines. *Biochemical and Biophysical Research Communications,* 349(1), pp.59-68.

Zagari, F., Jordan, M., Stettler, M., Broly, H. and Wurm, F.M. 2013. Lactate metabolism shift in CHO cell culture: The role of mitochondrial oxidative activity. *New Biotechnology,* 30(2), pp.238-245.

Zetsche, B., Gootenberg, J.S., Abudayyeh, O.O., Slaymaker, I.M., Makarova, K.S., Essletzbichler, P., Volz, S.E., Joung, J., van der Oost, J., Regev, A., Koonin, E.V. and Zhang, F. 2015. Cpf1 is a single RNA-guided endonuclease of a class 2 CRISPR-cas system. *Cell,* 163(3), pp.759-771.

Zhang, F., Frost, A.R., Blundell, M.P., Bales, O., Antoniou, M.N. and Thrasher, A.J. 2010. A ubiquitous chromatin opening element (UCOE) confers resistance to DNA Methylationâ€“mediated silencing of lentiviral vectors. *Molecular Therapy,* 18(9), pp.1640-1649.

Zhang, F., Sun, X., Yi, X. and Zhang, Y. 2006. Metabolic characteristics of recombinant chinese hamster ovary cells expressing glutamine synthetase in presence and absence of glutamine. *Cytotechnology,* 51(1), pp.21-28.

Zhang, X., Garcia, I.F., Baldi, L., Hacker, D.L. and Wurm, F.M. 2010. Hyperosmolarity enhances transient recombinant protein yield in chinese hamster ovary cells. *Biotechnology Letters,* 32(11), pp.1587-1592.

Zhang, Y., Lu, Y., Zhou, H., Lee, M., Liu, Z., Hassel, B.A. and Hamburger, A.W. 2008. Alterations in cell growth and signaling in ErbB3 binding protein-1 (Ebp1) deficient mice. *BMC Cell Biology,* 9pp.69-2121-9-69.

Zhang, Y., Wang, J.H., Lu, Q. and Wang, Y.J. 2012. Bag3 promotes resistance to apoptosis through bcl-2 family members in non-small cell lung cancer. *Oncology Reports,* 27(1), pp.109-113.

Zhang, Y.F., Li, X.H., Shi, Y.Q., Wu, Y.Y., Li, N., He, Q., Ji, Q., Wang, R.Q., Yang, S.M. and Fang, D.C. 2011. CIAPIN1 confers multidrug resistance through up-regulation of MDR-1 and bcl-L in LoVo/Adr cells and is independent of p53. *Oncology Reports,* 25(4), pp.1091-1098.

Zhang, Y., Stobbe, P., Silvander, C.O. and Chotteau, V. 2015. Very high cell density perfusion of CHO cells anchored in a non-woven matrix-based bioreactor. *Journal of Biotechnology,* 213pp.28-41.

Zhao, Y., Dai, Z., Liang, Y., Yin, M., Ma, K., He, M., Ouyang, H. and Teng, C.B. 2014. Sequence-specific inhibition of microRNA via CRISPR/CRISPRi system. *Scientific Reports,* 4pp.3943.

9.0 Supplements

9 Supplemental Figures

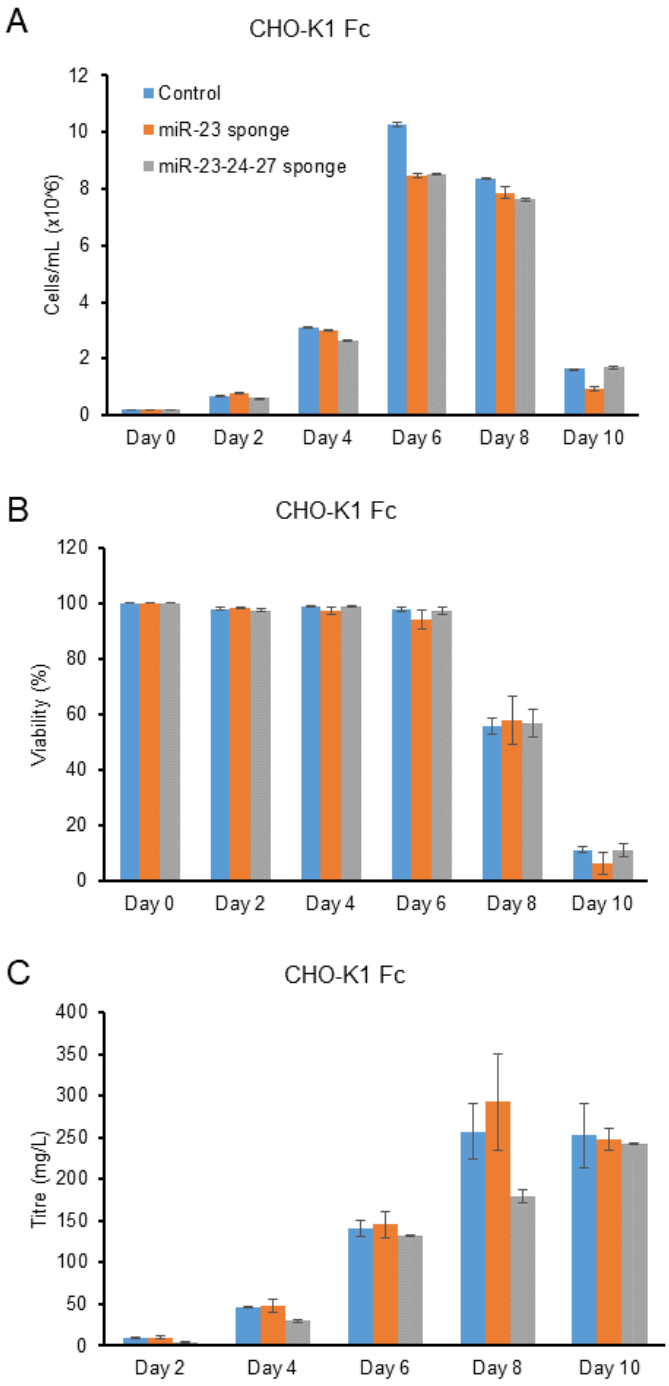

Figure S 1: Impact of stable depletion of the miR-23-24-27 cluster and miR-23 on CHO-K1 expressing a Fc fusion protein compared to the control. Cells transfected with eiter a control sponge, miR-23 sponge or a miR-23-24-27 sponge were grown in batch cultivation. A) Viable cell density. B) Viability of cultures. C) Titre assessed by ELISA. (n=3).

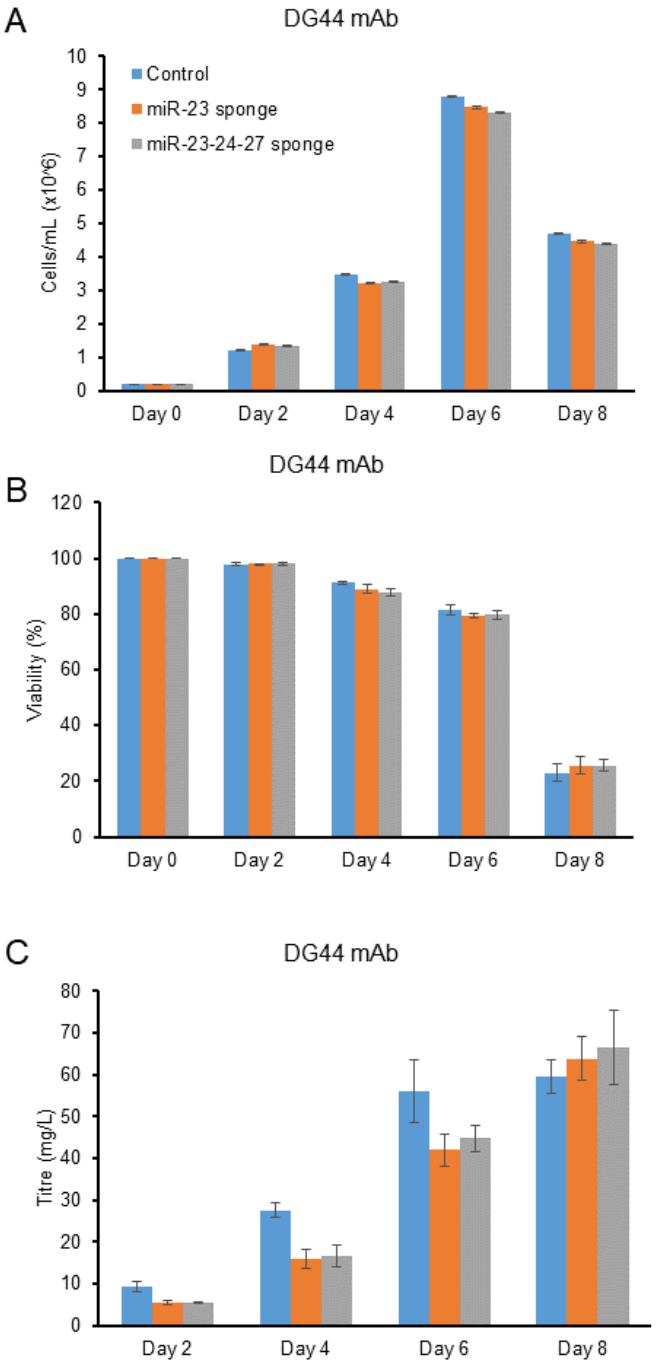

Figure S 2: Impact of stable depletion of the miR-23-24-27 cluster and miR-23 on DG44 producing a difficult express mAb compared to the control. Cells transfected with eiter a control sponge, miR-23 sponge or a miR-23-24-27 sponge were grown in batch cultivation. A) Viable cell density. B) Viability of cultures. C) Titre assessed by ELISA. (n=3).

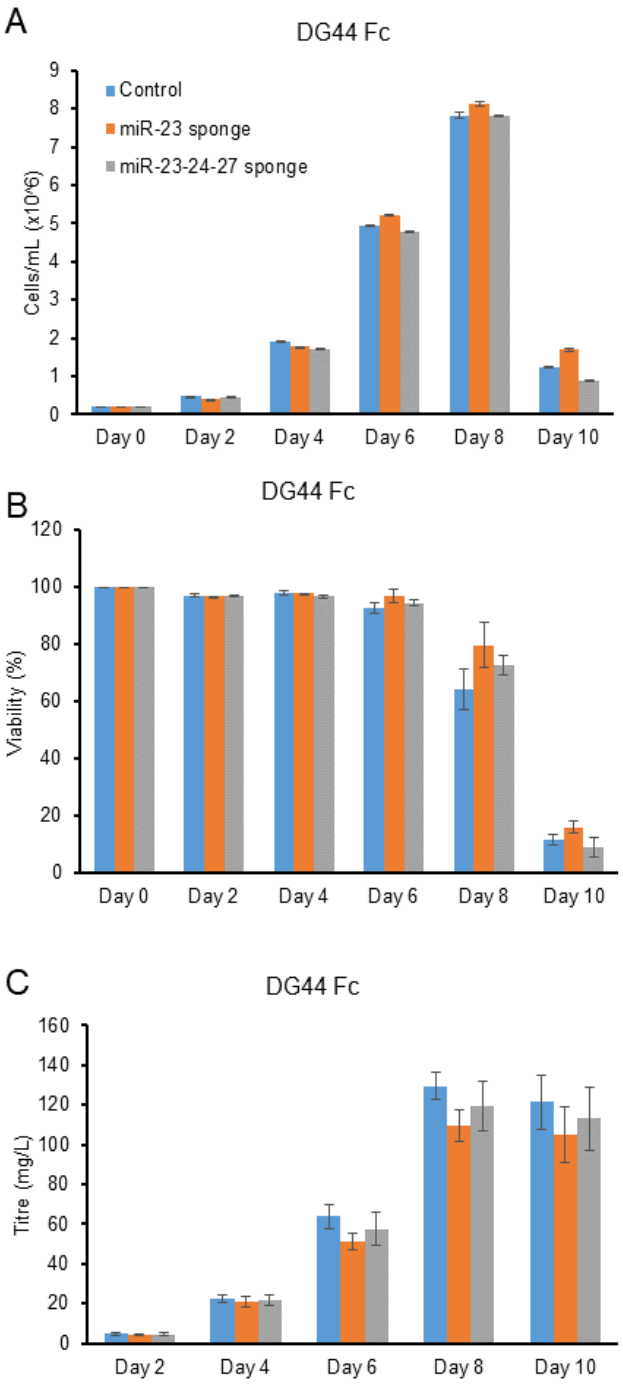

Figure S 3: Impact of stable depletion of the miR-23-24-27 cluster and miR-23 on DG44 expressing a Fc fusion compared to the control. Cells transfected with eiter a control sponge, miR-23 sponge or a miR-23-24-27 sponge were grown in batch cultivation. A) Viable cell density. B) Viability of cultures. C) Titre assessed by ELISA. No phenotype was observed (n=3).

A

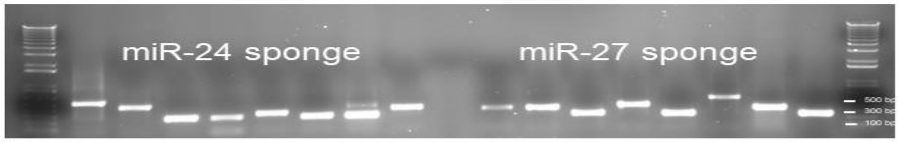

B

miR-24_3--12 binding sites

GCTTCCGCCGGAGGTGGAGGAGCAGGATGATGGCACGCTGCCCATGTCTTGTGCCCAGGAGAG
CGGGATGGACCGTCACCCTGCAGCCTGTGCTTCTGCTAGGATCAATGTGTAGGCGGCCGCTCGA
GTCTAGGGTCCCCCTGTTCCTGACTACTGAGCCAAATTCCTGTTCCTGACTACTGAGCCAGGGTC
CCCCTGTTCCTGACTACTGAGCCAAATTCCTGTTCCTGACTACTGAGCCAGGGTCCCCCTGTTCC
TGACTACTGAGCCAAATTCCTGTTCCTGACTACTGAGCCAGGGTCCCCCTGTTCCTGACTACTGA
GCCAAATTCCTGTTCCTGACTACTGAGCCAGGGTCCCCCTGTTCCTGACTACTGAGCCAAATTCC
TGTTCCTGACTACTGAGCCAGGGTCCCCCTGTTCCTGATACTGAGCCAAATTCCTGTTCCTGACT
ACTGAGCCAGGGTCCCCCTGTTCCTGACTACTGAGCCAAATTCCTGTTCCTGACTACTGAGCCAG
GGTCCCATCGGAATTCTCGATGCATGCCTCGACTGTGCCTTCTAGTTGCCAGCCATCTGTTGTTT
GCCCCTCCCCCGTGCCTT

miR-27_2--12 binding sites miR-27

GCTTCCGCCGGAGGTGGAGGAGCAGGATGATGGCACGCTGCCCATGTCTTGTGCCCAGGAGAG
CGGGATGGACCGTCACCCTGCAGCCTGTGCTTCTGCTAGGATCAATGTGTAGGCGGCCGCTCGA
GTCTAGGGTCCCCAGAACTTGTAACTGTGAAAATTCAGAACTTGTAACTGTGAAGGGTCCCCAGA
ACTTGTAACTGTGAAAATTCAGAACTTGTAACTGTGAAGGGTCCCCAGAACTTGTAACTGTGAAAA
TTCAGAACTTGTAACTGTGAAGGGTCCCCAGAACTTGTAACTGTGAAAATTCAGAACTTGTAACTG
TGAAGGGTCCCCAGAACTTGTAACTGTGAAAATTCAGAACTTGTAACTGTGAAGGGTCCCCAGAA
CTTGTAACTGTGAAAATTCAGAACTTGTAACTGTGAAGGGTCCCCAGAACTTGTAACTGTGAAAAT
TCAGAACTTGTAACTGTGAAGGGTCCCATCGGAATTCTCGATGCATGCCTCGACTGTGCCTTCTA
GTTGCCAGCCATCTGTTGTT

Figure S 4: Sequencing of sponge constructs after cloning and selection. Primers targeting up and downstream the MBS ligation side were used and PCR products were sent for Sanger sequencing. Higher amplicon sizes represent higher number of MBS. For experiments insertions exhibiting 10-14 MBS were considered.

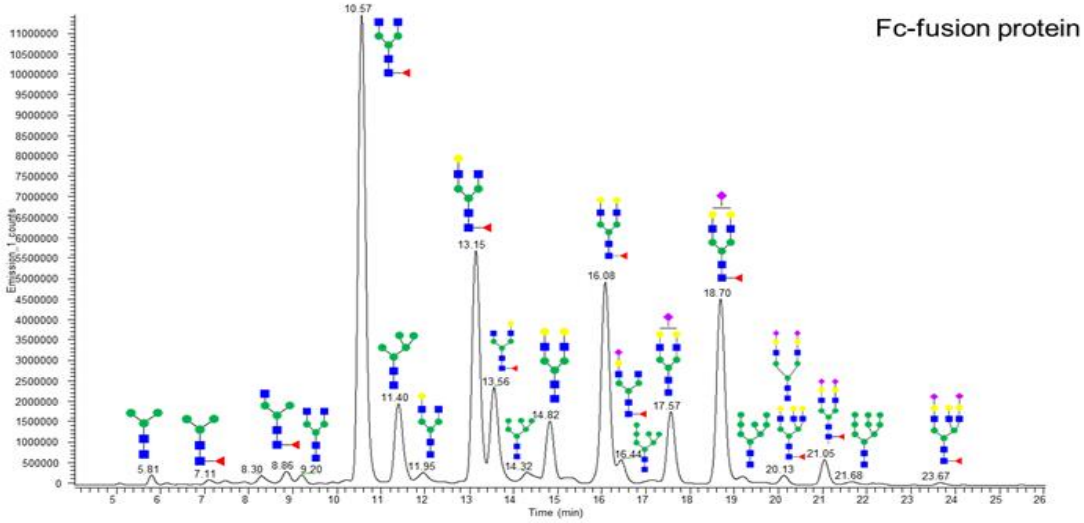

Glycan	Nomenclature	Retention time	Observed mass	Charge state	Δppm
	M3	5.81	1029.3909	+1	0.7
	FM3	7.13	1175.4486	+1	1.2
	A1F	8.91	688.7612	+2	2.3
	A2	9.22	717.2719	+2	2.1
	A2F	10.62	790.2995	+2	0.2
	M5	11.44	676.2446	+2	1.1
	A2G1	11.89	798.2981	+2	1.6
	A2G1F/A2G1'F	13.15/13.57	871.3259	+2	0.2
	M6	14.35	757.2711	+2	1.1
	A2G2	14.86	879.3242	+2	1.1
	A2G2F	16.10	952.3520	+2	0.1
	A2G1S1F	16.44	1016.8754	+2	1.9
	M7	16.66	838.2979	+2	1.5
	A2G2S1	17.57	1024.8719	+2	1.0
	A2G2S1F	18.69	1097.8997	+2	0.1
	M8	19.18	919.3249	+2	2.0
	A3G3F	20.15	1134.9201	+2	1.6
	A2G2S2	20.15	1170.4199	+2	1.1
	A2G2S2F	21.04	1243.4480	+2	0.3
	M9	21.61	1000.3509	+2	1.4
	A3G3S2F	23.10	1426.0151	+2	1.0

Figure S 5: Different glycosylation species identified after the depletion of each individual miRNA using sponge on the Fc-fusion protein expressed by CHO-S. The Fc fusion was purified by protein A chromatography and analysed for changes in glycosylation species. LC/LFR-MS/MS was used according to Carillo and colleagues (Carillo et al., 2017) as part of a collaboration with NIBRT.

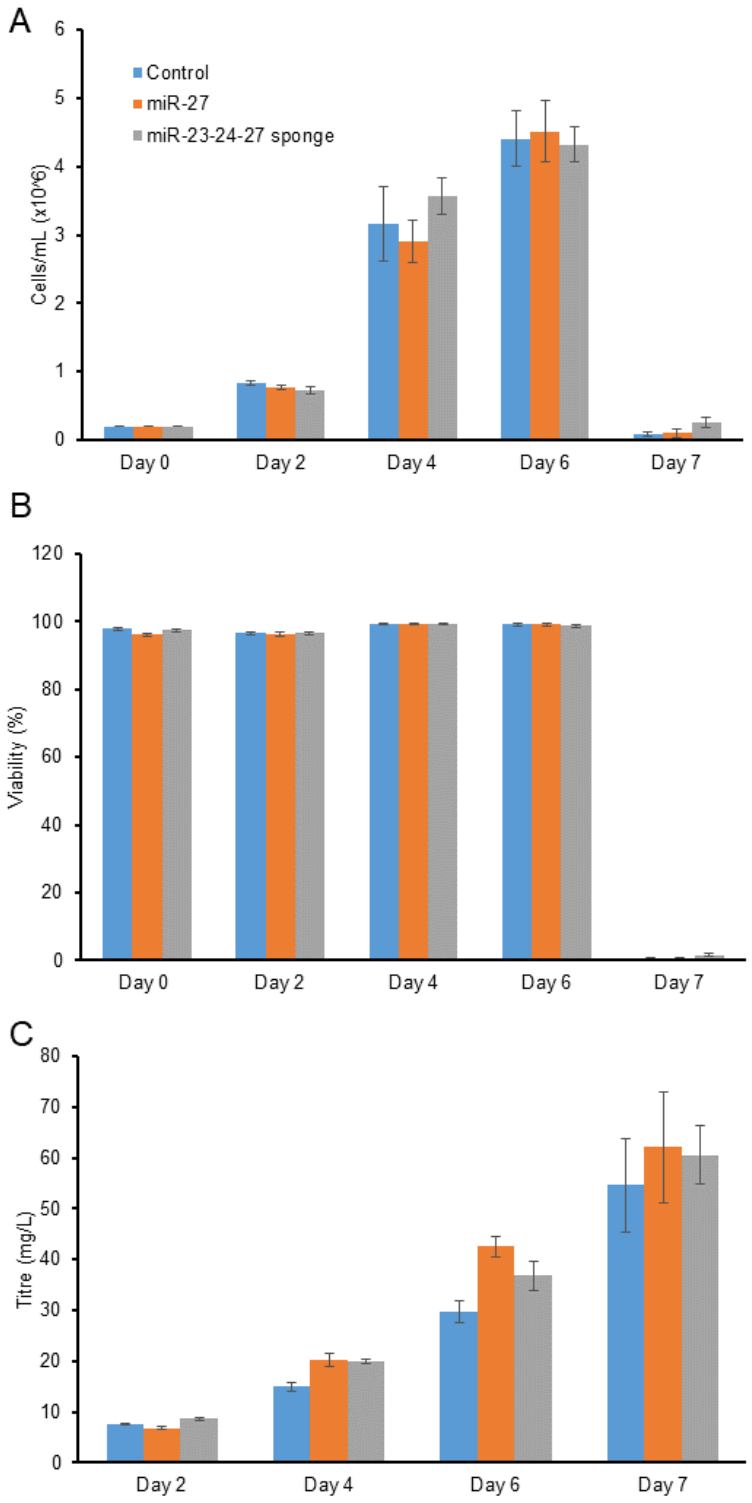

Figure S 6: Impact of depletion of miR-27 and miR-23-24-27 on CHO-K1 mAb. Cells transfected with eiter a control sponge, miR-27 sponge or a miR-23-24-27 sponge were grown in batch cultivation. A) Viable cell density. B) Viability of cultures. C) Titre assessed by ELISA. (n=3).

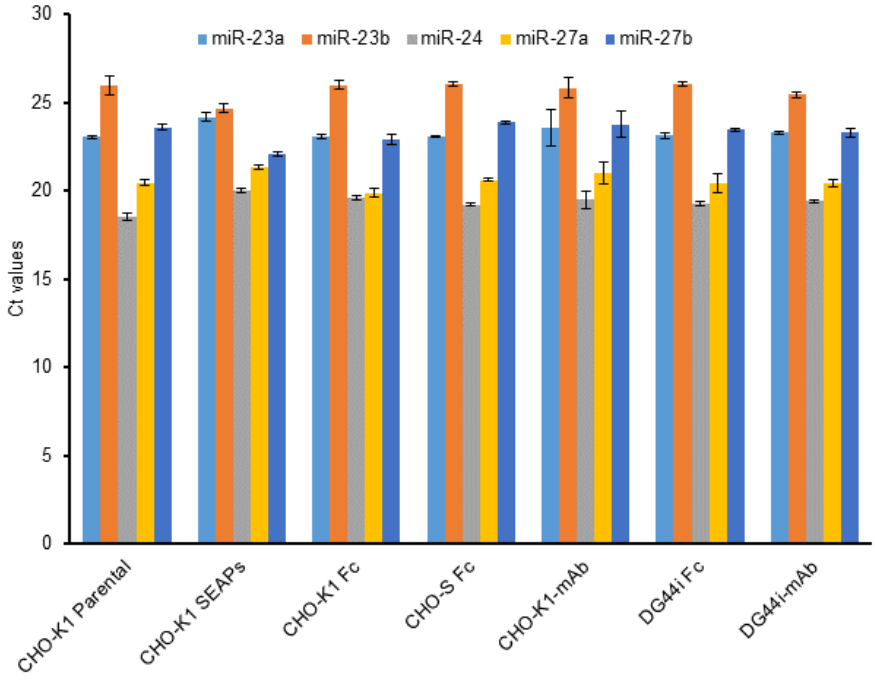

Figure S 7: Expression of all members of the miR-23a and miR-23b cluster in a panel of CHO cell lines. Total RNA was extracted from cells grown in exponential growth phase and reverse transcribed into cDNA using looped RT primers. TaqMan® miRNA assays for miR-23a, miR-23b, miR-27a, miR-27b and miR-24 was performed using the TaqMan® probe and corresponding forward/reverse primer implemented in the kit. If Ct-values are compared miR-24 together with miR-27a are the highest expressed members of the clusters. MiR-23b, miR-23a and miR-27b are in general lower expressed (n=3).

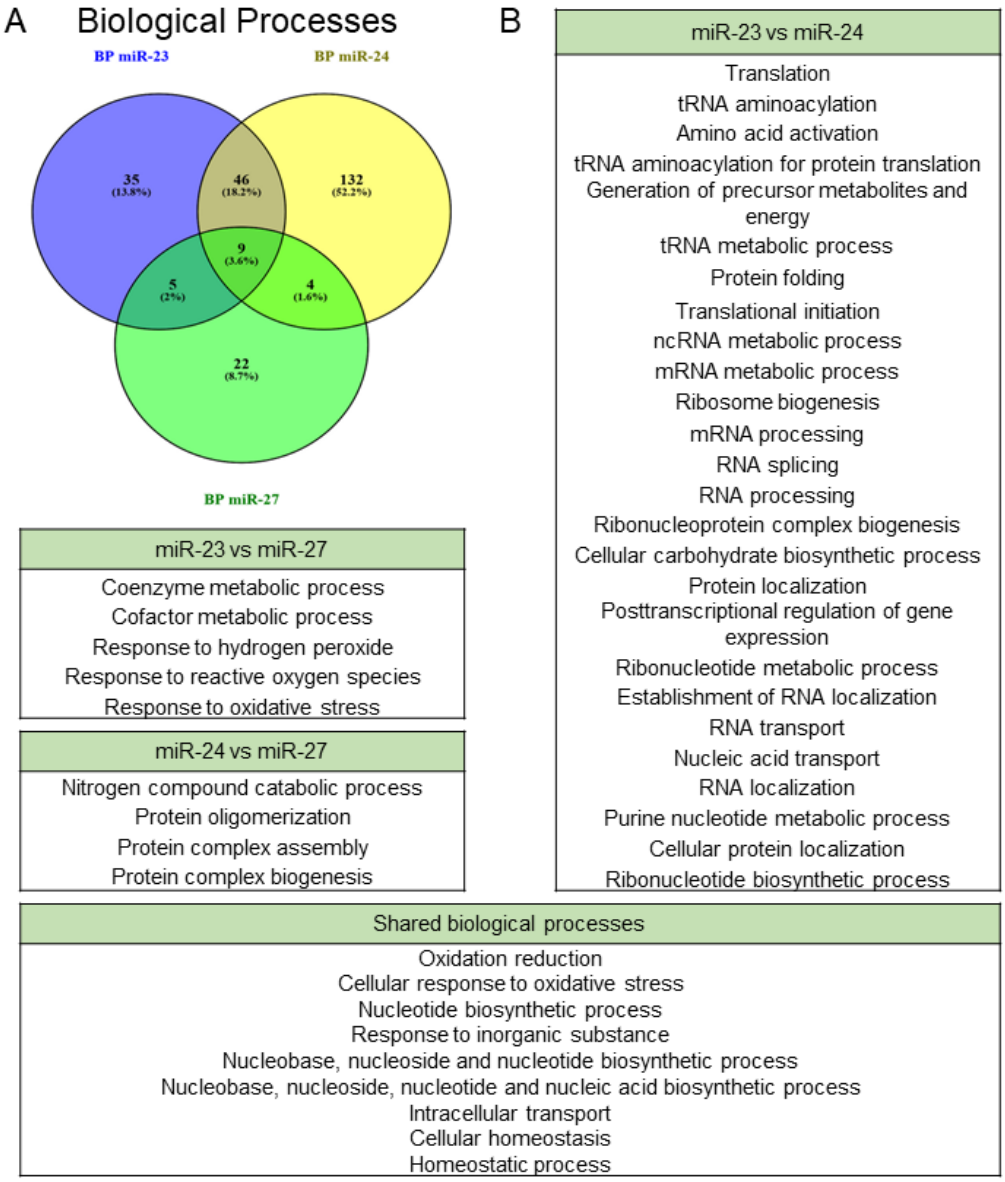

Figure S 8: Analysis of shared and individual biological processes in which miR-23, miR-24 and miR-27 are potentially involved. DAVID was used for functional annotation and analysis of overrepresented pathways. Subsequently shared targets were analysed for miR-23 compared to miR-24 and miR-27. Aditionally miR-24 was compared with miR-27. Furthermore, pathways targeted by all three miRNAs were analysed. Shared biological processes seemed to be related to oxidative stress and synthesis of nucleotide precursors.

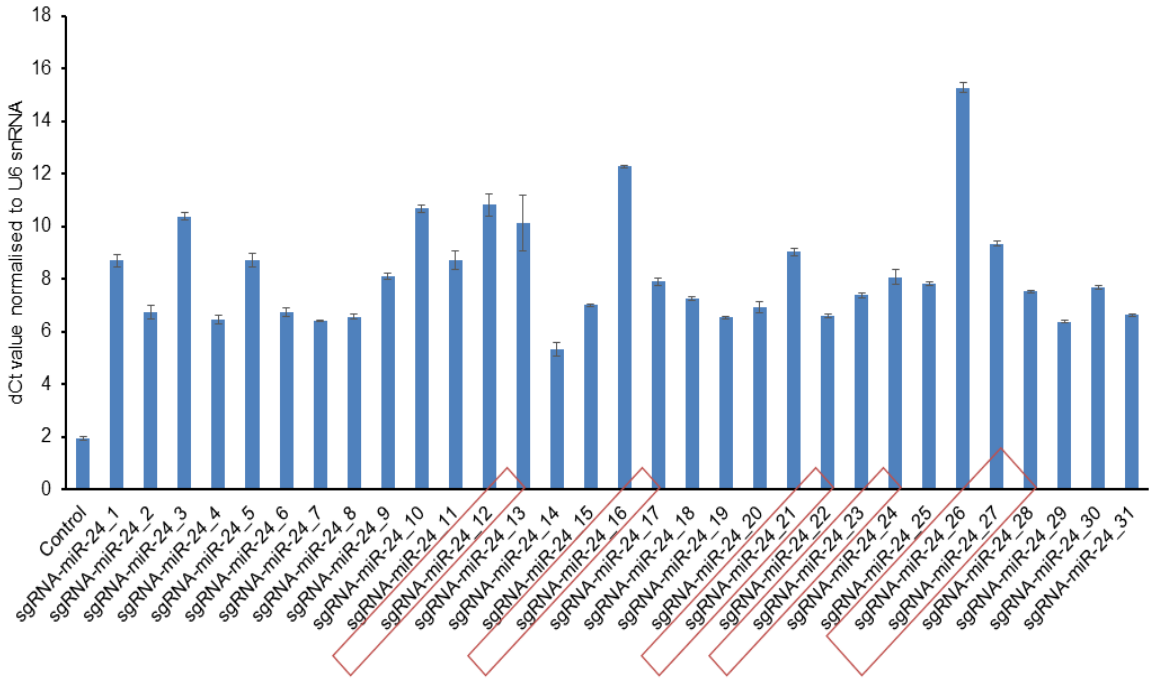

Figure S 9: Screen of single cell clones derived from a miR-24 mixed population targeted by CRISPR/Cas9. Single cell clones were isolated using limited dilution cloning and analysed for expression using Taqman® assays. Total RNA was extracted from cells grown in exponential growth phase and reverse transcribed into cDNA using looped RT primers. TaqMan® miRNA assays for miR-24 was performed using the TaqMan® probe and corresponding forward/reverse primer implemented in the kit. Higher Ct-values indicate a lower expression of the miRNA.

	Depletion of miR-27		
BP	Proteins	P-value	False discovery rate
Regulation of cell proliferation	10	4,0E-7	2,2E-4
Regulation of apoptosis	10	4,8E-7	1,3E-4
Regulation of programmed cell death	10	5,2E-7	9,6E-5
Regulation of cell death	10	5,3E-7	7,4E-5
Cellular response to oxidative stress	4	2,8E-5	3,1E-3
Response to oxidative stress	5	7,0E-5	6,4E-3
Negative regulation of apoptosis	6	1,0E-4	8,1E-3
Negative regulation of programmed cell death	6	1,1E-4	7,6E-3
Negative regulation of cell death	6	1,1E-4	6,8E-3
Anti-apoptosis	5	1,7E-4	9,3E-3
Positive regulation of cell proliferation	6	2,1E-4	1,1E-2

Figure S 10: Depletion of miR-27 in CHO-S Fc and pathway analysis showed several proteins upregulated which are involved in apoptosis. Differential protein expression was assessed by label-free mass spectrometry and analysed for overrepresented pathways using DAVID. Depletion of miR-27 indicated an involvement in apoptosis.

10 Supplemental Tables

CHO-K1 mAb sgRNA-miR-24 (CRISPR) – Proteomic Profiling

Gene ID	Name	More abundant in	Fold-change	Anova
*	Histone H3.1t [Cricetulus griseus]	Control	1.42	0.03321
AACS	Acetoacetyl-CoA synthetase [Cricetulus griseus]	Control	1.43	0.001761
AASDHPPT	L-aminoadipate-semialdehyde dehydrogenase-phosphopantetheinyl transferase [Cricetulus griseus]	Control	1.4	0.018226
ACAT2	Acetyl-CoA acetyltransferase, cytosolic [Cricetulus griseus]	Control	1.31	0.024372
ACLY	ATP-citrate synthase [Cricetulus griseus]	Control	1.26	0.012851
ACO1	Cytoplasmic aconitate hydratase [Cricetulus griseus]	Control	1.27	0.022283
ACOT7	Cytosolic acyl coenzyme A thioester hydrolase [Cricetulus griseus]	Control	1.21	0.009395
ACSL4	Long-chain-fatty-acid--CoA ligase 4 [Cricetulus griseus]	Control	1.31	0.001129
ACTL1	Long-chain-fatty-acid--CoA ligase 1 [Cricetulus griseus]	Control	1.37	0.031514
ACTR1A	Alpha-centractin [Cricetulus griseus]	Control	1.23	0.023381
ACTR2	Actin-related protein 2 [Cricetulus griseus]	Control	1.37	0.013113

AGFG2	Arf-GAP domain and FG repeats-containing protein 2 [Cricetulus griseus]	Control	1.49	0.014589
AKAP12	A-kinase anchor protein 12 [Cricetulus griseus]	Control	1.7	0.007255
ALDH1A1	Retinal dehydrogenase 1 [Cricetulus griseus]	Control	2.05	0.015479
ARF5	ADP-ribosylation factor 5 [Cricetulus griseus]	Control	1.46	0.001182
ARFGAP3	ADP-ribosylation factor GTPase-activating protein 3 [Cricetulus griseus]	Control	1.38	0.000963
ARPC4	Actin-related protein 2/3 complex subunit 4 [Cricetulus griseus]	Control	1.55	0.002764
ASAH1	Acid ceramidase [Cricetulus griseus]	Control	1.23	0.011193
ASF1B	Histone chaperone ASF1B [Cricetulus griseus]	Control	2.14	0.020449
ATP6AP2	PREDICTED: renin receptor isoform X1 [Cricetulus griseus]	Control	1.41	0.011032
BAIAP2	Brain-specific angiogenesis inhibitor 1-associated protein 2 [Cricetulus griseus]	Control	1.23	0.029518
BST2	bone marrow stromal antigen 2 [Cricetulus griseus]	Control	1.3	0.023368
C3PO	RecName: Full=Translin; AltName: Full=Component 3 of promoter of RISC; Short=C3PO	Control	1.53	0.00217
CACNA2D1	Voltage-dependent calcium channel subunit alpha-2/delta-1 [Cricetulus griseus]	Control	1.29	0.016252
CALD1	Non-muscle caldesmon [Cricetulus griseus]	Control	1.22	0.01587
CALR	Calreticulin [Cricetulus griseus]	Control	1.31	0.009298

CAP1	Adenylyl cyclase-associated protein 1 [Cricetulus griseus]	Control	1.33	0.001156
CCT3	T-complex protein 1 subunit gamma [Cricetulus griseus]	Control	1.4	0.009084
CD36	Platelet glycoprotein 4 [Cricetulus griseus]	Control	2.32	0.021724
CD44	CD44 antigen [Cricetulus griseus]	Control	1.46	0.021956
CDC16	Cell division cycle protein 16-like [Cricetulus griseus]	Control	1.26	0.006452
CDC23	Cell division cycle protein 23-like, partial [Cricetulus griseus]	Control	1.35	0.001377
CDK6	Cell division protein kinase 6 [Cricetulus griseus]	Control	1.21	0.002425
CHCHD2	Coiled-coil-helix-coiled-coil-helix domain-containing protein 2, mitochondrial [Cricetulus griseus]	Control	1.61	0.009001
CHUK	Inhibitor of nuclear factor kappa-B kinase subunit alpha [Cricetulus griseus]	Control	1.4	0.023165
CLU	Clusterin [Cricetulus griseus]	Control	1.61	0.006931
CN166	UPF0568 protein C14orf166-like [Cricetulus griseus]	Control	1.3	0.00416
CNN3	Calponin-3 [Cricetulus griseus]	Control	1.29	9.77E-05
CORO1C	Coronin-1C [Cricetulus griseus]	Control	1.24	0.036848
CPNE3	Copine-3 [Cricetulus griseus]	Control	1.27	0.007471
CSDE1	PREDICTED: cold shock domain-containing protein E1 isoform X2 [Cricetulus griseus]	Control	1.22	0.023011

CTLA2B	Protein CTLA-2-beta [Cricetulus griseus]	Control	1.78	0.030514
CTNND1	Catenin delta-1 [Cricetulus griseus]	Control	1.25	0.006596
CUL1	Cullin-1 [Cricetulus griseus]	Control	1.21	0.012532
CUL3	Cullin-3 [Cricetulus griseus]	Control	1.45	0.004734
DDB1	DNA damage-binding protein 1 [Cricetulus griseus]	Control	1.27	0.007691
DDOST	Dolichyl-diphosphooligosaccharide--protein glycosyltransferase 48 kDa subunit [Cricetulus griseus]	Control	1.38	0.001328
DHFR	Dihydrofolate reductase [Cricetulus griseus]	Control	1.36	0.01055
DHRS1	Dehydrogenase/reductase SDR family member 1 [Cricetulus griseus]	Control	1.41	0.016992
DHX15	Putative pre-mRNA-splicing factor ATP-dependent RNA helicase DHX15 [Cricetulus griseus]	Control	1.28	0.008177
DLST	Dihydrolipoyllysine-residue succinyltransferase component of 2-oxoglutarate dehydrogenase complex, mitochondrial [Cricetulus griseus]	Control	1.28	0.010147
DNM2	Dynamin [Cricetulus griseus]	Control	1.21	0.0085
DPY30	Protein dpy-30-like [Cricetulus griseus]	Control	1.34	0.034863
DSTN	Destrin [Cricetulus griseus]	Control	1.54	0.035397
EDF1	Endothelial differentiation-related factor 1 [Cricetulus griseus]	Control	1.69	0.034099

EML2	Echinoderm microtubule-associated protein-like 2 [Cricetulus griseus]	Control	1.28	0.011091
ERP29	Endoplasmic reticulum protein ERp29 [Cricetulus griseus]	Control	1.37	0.018304
FKBP9	FK506-binding protein 9 [Cricetulus griseus]	Control	1.21	0.005384
GALNT2	Polypeptide N-acetylgalactosaminyltransferase 2 [Cricetulus griseus]	Control	1.34	0.016705
GCN1	Translational activator GCN1 [Cricetulus griseus]	Control	1.31	0.009776
GDI2	Rab GDP dissociation inhibitor beta [Cricetulus griseus]	Control	1.23	0.014774
GJA1	Gap junction alpha-1 protein [Cricetulus griseus]	Control	1.23	0.009077
GLG1	latent TGF-beta complexed protein (LTCP) [Cricetulus griseus]	Control	1.56	0.004873
GMDS	GDP-mannose 4,6 dehydratase [Cricetulus griseus]	Control	1.27	0.028927
GNAI2	guanine nucleotide-binding protein G(i) subunit alpha-2 [Cricetulus griseus]	Control	1.23	0.00106
GNAI3	guanine nucleotide-binding protein G(k) subunit alpha [Cricetulus griseus]	Control	1.32	0.011954
GNB2	Guanine nucleotide-binding protein G(I)/G(S)/G(T) subunit beta-2 [Cricetulus griseus]	Control	1.31	0.012915
GNPDA1	Glucosamine-6-phosphate isomerase 1, partial [Cricetulus griseus]	Control	1.98	0.00218

GOLIM4	Golgi integral membrane protein 4 [Cricetulus griseus]	Control	1.45	0.029387
GPC1	Glypican-1 [Cricetulus griseus]	Control	1.48	0.000206
GSTM3	Glutathione S-transferase Mu 5 [Cricetulus griseus]	Control	1.38	0.002922
GSTT2	Glutathione S-transferase theta-2 [Cricetulus griseus]	Control	1.38	0.018941
HECTD1	E3 ubiquitin-protein ligase HECTD1 [Cricetulus griseus]	Control	1.72	0.010965
HIST1H2AG	Histone H2A type 1 [Cricetulus griseus]	Control	1.23	0.014551
HMGCS1	Hydroxymethylglutaryl-CoA synthase, cytoplasmic [Cricetulus griseus]	Control	1.35	0.000757
HNRNPD	PREDICTED: heterogeneous nuclear ribonucleoprotein D0 isoform X3, partial [Cricetulus griseus]	Control	1.33	0.012981
HNRNPK	PREDICTED: heterogeneous nuclear ribonucleoprotein K isoform X5, partial [Cricetulus griseus]	Control	2.29	0.017203
IDH3A	Isocitrate dehydrogenase [NAD] subunit alpha, mitochondrial [Cricetulus griseus]	Control	1.32	0.017268
IDI1	Isopentenyl-diphosphate Delta-isomerase 1 [Cricetulus griseus]	Control	1.27	0.009032
KCNAB2	Voltage-gated potassium channel subunit beta-2 [Cricetulus griseus]	Control	1.46	0.009464
KIDINS220	Kinase D-interacting substrate of 220 kDa [Cricetulus griseus]	Control	1.34	0.018381

KIF1B	Kinesin-like protein KIF1C [Cricetulus griseus]	Control	1.51	0.000601
KIF1BP	KIF1-binding protein [Cricetulus griseus]	Control	1.56	0.029917
KPNA2	Importin subunit alpha-2 [Cricetulus griseus]	Control	1.33	0.011142
KPNA6	Importin subunit alpha-7 [Cricetulus griseus]	Control	1.32	0.001128
LAMC1	Laminin subunit gamma-1 [Cricetulus griseus]	Control	1.22	0.010014
LIMS1	LIM and senescent cell antigen-like-containing domain protein 1 [Cricetulus griseus]	Control	1.22	0.019254
LMAN1	Protein ERGIC-53 [Cricetulus griseus]	Control	1.27	0.000625
LMNB1	Lamin-L(I) [Cricetulus griseus]	Control	1.35	0.021303
MAGOH	Protein mago nashi-like [Cricetulus griseus]	Control	1.23	0.002573
MAN2A1	Alpha-mannosidase 2 [Cricetulus griseus]	Control	1.38	0.038155
MAN2C1	Alpha-mannosidase 2C1 [Cricetulus griseus]	Control	1.34	0.000945
MANF	Mesencephalic astrocyte-derived neurotrophic factor [Cricetulus griseus]	Control	1.22	0.013162
MAPRE1	Microtubule-associated protein RP/EB family member 1 [Cricetulus griseus]	Control	1.41	0.015235
MCM2	DNA replication licensing factor MCM2 [Cricetulus griseus]	Control	1.37	0.006212
MRPL21	39S ribosomal protein L21, mitochondrial [Cricetulus griseus]	Control	1.27	0.014106

NAA15	NMDA receptor-regulated protein 1 [Cricetulus griseus]	Control	1.48	0.002675
NAGA	Alpha-N-acetylgalactosaminidase [Cricetulus griseus]	Control	1.27	0.00978
NASP	PREDICTED: nuclear autoantigenic sperm protein isoform X1 [Cricetulus griseus]	Control	2.86	0.025303
NCAM1	Neural cell adhesion molecule 1 [Cricetulus griseus]	Control	1.29	0.006087
NDC80	Kinetochore protein NDC80-like [Cricetulus griseus]	Control	1.43	0.01866
NPC2	Epididymal secretory protein E1 [Cricetulus griseus]	Control	1.23	0.030912
NQO1	NAD(P)H dehydrogenase [quinone] 1 [Cricetulus griseus]	Control	1.45	0.003176
NUFIP2	Nuclear fragile X mental retardation-interacting protein 2 [Cricetulus griseus]	Control	1.56	0.039179
NUP37	Nucleoporin Nup37 [Cricetulus griseus]	Control	1.29	0.038329
NUP54	Nucleoporin p54 [Cricetulus griseus]	Control	1.62	0.011231
OCIAD2	OCIA domain-containing protein 2 [Cricetulus griseus]	Control	1.88	0.007278
PCYOX1	Prenylcysteine oxidase [Cricetulus griseus]	Control	1.24	0.007896
PDCD10	Programmed cell death protein 10 [Cricetulus griseus]	Control	1.53	0.024899
PDIA5	Protein disulfide-isomerase A5 [Cricetulus griseus]	Control	1.3	0.04612
PDIA6	Protein disulfide-isomerase A6 [Cricetulus griseus]	Control	1.41	0.006104

PDWD1	Peptidylprolyl isomerase domain and WD repeat-containing protein 1 [Cricetulus griseus]	Control	1.61	0.009743
PLEC	Plectin-1 [Cricetulus griseus]	Control	1.24	0.001179
PLS3	RecName: Full=Plastin-3; AltName: Full=T-plastin	Control	1.39	0.00678
PPP1R12A	Protein phosphatase 1 regulatory subunit 12A [Cricetulus griseus]	Control	1.21	0.025775
PPP2CB	Serine/threonine-protein phosphatase 2A catalytic subunit beta isoform, partial [Cricetulus griseus]	Control	1.21	0.033596
PPP6C	Serine/threonine-protein phosphatase 6 catalytic subunit [Cricetulus griseus]	Control	1.43	0.022204
PREP	Prolyl endopeptidase [Cricetulus griseus]	Control	1.3	0.021064
PRKACA	cAMP-dependent protein kinase catalytic subunit alpha [Cricetulus griseus]	Control	1.64	0.033851
PRUNE2	Protein prune-like 2 [Cricetulus griseus]	Control	1.24	0.02083
PSMA2	Proteasome subunit alpha type-2 [Cricetulus griseus]	Control	1.49	0.014121
PSMD1	26S proteasome non-ATPase regulatory subunit 1 [Cricetulus griseus]	Control	1.22	0.007224
PTPN11	Tyrosine-protein phosphatase non-receptor type 11 [Cricetulus griseus]	Control	1.56	0.046553
PXDN	Peroxidasin-like [Cricetulus griseus]	Control	1.54	0.017734
PYCR2	Pyrroline-5-carboxylate reductase 2 [Cricetulus griseus]	Control	1.26	0.009166

RAB1B	Ras-related protein Rab-1B [Cricetulus griseus]	Control	1.47	0.004065
RAB35	Ras-related protein Rab-35 [Cricetulus griseus]	Control	1.5	0.014282
RECQL	ATP-dependent DNA helicase Q1 [Cricetulus griseus]	Control	1.53	0.011103
RFC5	Replication factor C subunit 5 [Cricetulus griseus]	Control	1.23	0.005033
RPA1	PREDICTED: replication protein A 70 kDa DNA-binding subunit isoform X1 [Cricetulus griseus]	Control	1.27	0.022337
RPL29	60S ribosomal protein L29 [Cricetulus griseus]	Control	1.28	0.012051
RPN1	Dolichyl-diphosphooligosaccharide--protein glycosyltransferase subunit 1 [Cricetulus griseus]	Control	1.27	0.006898
RPN2	Dolichyl-diphosphooligosaccharide--protein glycosyltransferase subunit 2 [Cricetulus griseus]	Control	1.27	0.012258
RPS16	PREDICTED: 40S ribosomal protein S16 isoform X2 [Cricetulus griseus]	Control	1.49	0.016712
RPS6	PREDICTED: 40S ribosomal protein S6 isoform X1 [Cricetulus griseus]	Control	1.29	0.00015
RPS9	40S ribosomal protein S9 [Cricetulus griseus]	Control	1.25	0.016141
SAR1B	GTP-binding protein SAR1b [Cricetulus griseus]	Control	1.24	0.034956
SBSN	Suprabasin [Cricetulus griseus]	Control	1.57	0.007512
SCD2	Acyl-CoA desaturase 2 [Cricetulus griseus]	Control	1.66	0.027411
SEC13	Protein SEC13-like [Cricetulus griseus]	Control	1.21	0.030987

SEC23A	Protein transport protein Sec23A [Cricetulus griseus]	Control	1.34	0.023133
SEC24D	Protein transport protein Sec24D [Cricetulus griseus]	Control	1.27	0.00712
SEPT11	Septin-11 [Cricetulus griseus]	Control	1.46	0.027881
SEPT8	Septin-8 [Cricetulus griseus]	Control	1.35	0.009728
SERPINB6	Serpin B6 [Cricetulus griseus]	Control	1.28	0.006652
SLC25A10	Mitochondrial dicarboxylate carrier [Cricetulus griseus]	Control	1.23	0.00179
SLC25A13	Calcium-binding mitochondrial carrier protein Aralar2 [Cricetulus griseus]	Control	1.35	0.005871
SNRPB2	U2 small nuclear ribonucleoprotein B'' [Cricetulus griseus]	Control	1.21	0.024064
SRP68	Signal recognition particle 68 kDa protein [Cricetulus griseus]	Control	1.34	0.013687
TK1	Thymidine kinase, cytosolic [Cricetulus griseus]	Control	1.9	0.033041
TOP2A	DNA topoisomerase 2-alpha [Cricetulus griseus]	Control	1.23	0.014307
TPM2	PREDICTED: tropomyosin beta chain isoform X1 [Cricetulus griseus]	Control	1.47	0.031053
TTC37	Tetratricopeptide repeat protein 37 [Cricetulus griseus]	Control	1.31	0.010334
TUBB5	beta-tubulin isotype I [Cricetulus griseus]	Control	1.33	0.023229

UBC	Ubiquitin [Cricetulus griseus]	Control	1.73	0.019879
UBE2C	Ubiquitin-conjugating enzyme E2 C [Cricetulus griseus]	Control	1.23	0.029222
UGGT1	UDP-glucose:glycoprotein glucosyltransferase 1 [Cricetulus griseus]	Control	1.33	0.005405
UNC45A	Protein unc-45-like A [Cricetulus griseus]	Control	1.27	0.024863
VAT1	Synaptic vesicle membrane protein VAT-1-like [Cricetulus griseus]	Control	1.26	0.011097
WDR43	WD repeat-containing protein 43 [Cricetulus griseus]	Control	1.22	0.028529
YKT6	Synaptobrevin-like YKT6 [Cricetulus griseus]	Control	1.8	0.006997
YWHAB	14-3-3 protein beta/alpha [Cricetulus griseus]	Control	1.79	0.01887
ZFAND5	AN1-type zinc finger protein 5 [Cricetulus griseus]	Control	1.95	0.008301
*	hypothetical protein I79_001369 [Cricetulus griseus]	CRISPR	1.36	0.000599
AARS	Alanyl-tRNA synthetase, cytoplasmic [Cricetulus griseus]	CRISPR	1.24	0.002764
AARS	Alanyl-tRNA synthetase, cytoplasmic [Cricetulus griseus]	CRISPR	1.33	0.001675
ACAA1B	3-ketoacyl-CoA thiolase B, peroxisomal, partial [Cricetulus griseus]	CRISPR	1.64	0.00816
ACADVL	Very long-chain specific acyl-CoA dehydrogenase, mitochondrial [Cricetulus griseus]	CRISPR	1.3	0.025717
ACTN4	Alpha-actinin-4 [Cricetulus griseus]	CRISPR	1.24	0.012471

ADK	Adenosine kinase [Cricetulus griseus]	CRISPR	1.37	0.001233
ADPRH	[Protein ADP-ribosylarginine] hydrolase [Cricetulus griseus]	CRISPR	1.22	0.010897
ADSL	mutant adenylosuccinate lyase [Cricetulus griseus]	CRISPR	1.22	0.025559
ADSS	adenylosuccinate synthetase isozyme 2 [Cricetulus griseus]	CRISPR	1.45	0.030153
AIP	AH receptor-interacting protein [Cricetulus griseus]	CRISPR	1.21	0.034149
AIRE	Autoimmune regulator [Cricetulus griseus]	CRISPR	1.42	0.029258
APIP	APAF1-interacting protein [Cricetulus griseus]	CRISPR	1.49	0.028185
APOOL	Apolipoprotein O-like [Cricetulus griseus]	CRISPR	1.23	0.01292
ATAD3A	ATPase family AAA domain-containing protein 3 [Cricetulus griseus]	CRISPR	1.27	0.007938
ATIC	Bifunctional purine biosynthesis protein PURH [Cricetulus griseus]	CRISPR	1.29	0.01346
BAG6	Large proline-rich protein BAT3 [Cricetulus griseus]	CRISPR	1.24	0.003435
BCLAF1	Bcl-2-associated transcription factor 1 [Cricetulus griseus]	CRISPR	1.28	0.00557
BRIX1	Brix domain-containing protein 2 [Cricetulus griseus]	CRISPR	1.27	0.02393
BYSL	Bystin [Cricetulus griseus]	CRISPR	1.45	0.002827
CALU	Calumenin [Cricetulus griseus]	CRISPR	1.52	0.009195
CAPN2	Calpain-2 catalytic subunit [Cricetulus griseus]	CRISPR	1.31	0.008083

CCDC86	Coiled-coil domain-containing protein 86 [Cricetulus griseus]	CRISPR	1.25	0.004686
CES1	Liver carboxylesterase 4 [Cricetulus griseus]	CRISPR	1.23	0.007857
CHORDC1	Cysteine and histidine-rich domain-containing protein 1 [Cricetulus griseus]	CRISPR	1.24	0.000391
CHTF18	Chromosome transmission fidelity protein 18-like [Cricetulus griseus]	CRISPR	1.31	0.001018
CPT2	Carnitine O-palmitoyltransferase 2, mitochondrial [Cricetulus griseus]	CRISPR	1.21	0.009102
CTTN	Src substrate cortactin [Cricetulus griseus]	CRISPR	1.26	0.013676
CYC1	Cytochrome c1, heme protein, mitochondrial [Cricetulus griseus]	CRISPR	1.24	0.038317
DCTN1	Dynactin subunit 1 [Cricetulus griseus]	CRISPR	1.41	0.019829
DCTN1	Dynactin subunit 1 [Cricetulus griseus]	CRISPR	1.31	0.02996
DDX10	putative ATP-dependent RNA helicase DDX10 [Cricetulus griseus]	CRISPR	1.28	0.008085
DDX21	Nucleolar RNA helicase 2 [Cricetulus griseus]	CRISPR	1.44	0.0003
DDX27	putative ATP-dependent RNA helicase DDX27 [Cricetulus griseus]	CRISPR	1.3	0.016398
DDX39A	ATP-dependent RNA helicase DDX39 [Cricetulus griseus]	CRISPR	1.25	0.004534
DDX46	putative ATP-dependent RNA helicase DDX46 [Cricetulus griseus]	CRISPR	1.3	0.018143

DHX30	Putative ATP-dependent RNA helicase DHX30 [Cricetulus griseus]	CRISPR	1.26	0.000854
DHX9	PREDICTED: ATP-dependent RNA helicase A isoform X2 [Cricetulus griseus]	CRISPR	1.21	0.006301
DKC1	H/ACA ribonucleoprotein complex subunit 4 [Cricetulus griseus]	CRISPR	1.72	0.033292
DNAJA3	DnaJ-like subfamily A member 3, mitochondrial [Cricetulus griseus]	CRISPR	1.38	0.038158
DNAJC8	DnaJ-like subfamily C member 8 [Cricetulus griseus]	CRISPR	1.21	0.012468
EBNA1BP2	putative rRNA-processing protein EBP2 [Cricetulus griseus]	CRISPR	1.33	0.023375
EDC4	Enhancer of mRNA-decapping protein 4 [Cricetulus griseus]	CRISPR	1.39	0.030688
EEF1B2	Elongation factor 1-beta [Cricetulus griseus]	CRISPR	1.27	0.019678
EFHD2	EF-hand domain-containing protein D2 [Cricetulus griseus]	CRISPR	1.27	0.011877
EHD3	EH domain-containing protein 3 [Cricetulus griseus]	CRISPR	1.25	0.036722
EIF2S1	Eukaryotic translation initiation factor 2 subunit 1 [Cricetulus griseus]	CRISPR	1.21	0.005102
EIF3G	Eukaryotic translation initiation factor 3 subunit G [Cricetulus griseus]	CRISPR	1.23	0.023204
EIF3I	Eukaryotic translation initiation factor 3 subunit I [Cricetulus griseus]	CRISPR	1.32	0.025181

EIF5A2	Eukaryotic translation initiation factor 5A-2 [Cricetulus griseus]	CRISPR	1.33	0.011208
EIF6	Eukaryotic translation initiation factor 6 [Cricetulus griseus]	CRISPR	1.25	0.042275
ESF1	ESF1-like [Cricetulus griseus]	CRISPR	1.25	0.018449
EXOSC2	Exosome complex exonuclease RRP4 [Cricetulus griseus]	CRISPR	1.21	0.021361
FAM103A1	Protein FAM103A1 [Cricetulus griseus]	CRISPR	1.23	0.045944
FAM98B	Protein FAM98B [Cricetulus griseus]	CRISPR	1.29	0.003239
FARSB	Phenylalanyl-tRNA synthetase beta chain [Cricetulus griseus]	CRISPR	1.56	0.006058
FBL	rRNA 2'-O-methyltransferase fibrillarin [Cricetulus griseus]	CRISPR	1.24	0.007149
FBXO6	F-box only protein 6 [Cricetulus griseus]	CRISPR	1.37	0.020647
FH	Fumarate hydratase, mitochondrial [Cricetulus griseus]	CRISPR	1.33	0.003742
FLNB	Filamin-B [Cricetulus griseus]	CRISPR	1.27	0.006279
FTSJ3	Putative rRNA methyltransferase 3 [Cricetulus griseus]	CRISPR	1.49	0.018471
FXR1	RecName: Full=Fragile X mental retardation syndrome-related protein 1	CRISPR	1.27	0.012796
FXR2	Fragile X mental retardation syndrome-related protein 2 [Cricetulus griseus]	CRISPR	1.22	0.016988

GARS	Glycyl-tRNA synthetase [Cricetulus griseus]	CRISPR	1.21	0.015705
GLRX3	Glutaredoxin-3 [Cricetulus griseus]	CRISPR	1.39	0.006653
GNL1	Guanine nucleotide-binding protein-like 1, partial [Cricetulus griseus]	CRISPR	1.41	0.002033
GSPT2	Eukaryotic peptide chain release factor GTP-binding subunit ERF3B [Cricetulus griseus]	CRISPR	1.42	0.010913
GTF2F1	General transcription factor IIF subunit 1 [Cricetulus griseus]	CRISPR	1.31	0.025717
H2AFV	Histone H2A.V [Cricetulus griseus]	CRISPR	1.25	0.019768
HADHA	Trifunctional enzyme subunit alpha, mitochondrial [Cricetulus griseus]	CRISPR	1.22	0.015423
HIBADH	3-hydroxyisobutyrate dehydrogenase, mitochondrial [Cricetulus griseus]	CRISPR	1.36	0.013455
HMGB1	PREDICTED: high mobility group protein B1 isoform X2 [Cricetulus griseus]	CRISPR	1.25	0.000256
HMGN5	Nucleosome-binding protein 1 [Cricetulus griseus]	CRISPR	1.28	0.018927
HNRNPA2B1	Heterogeneous nuclear ribonucleoproteins A2/B1 [Cricetulus griseus]	CRISPR	1.33	0.021037
HNRNPAB	Heterogeneous nuclear ribonucleoprotein A/B [Cricetulus griseus]	CRISPR	1.21	0.013762
HP1BP3	Heterochromatin protein 1-binding protein 3 [Cricetulus griseus]	CRISPR	1.36	0.030462

HSD17B10	3-hydroxyacyl-CoA dehydrogenase type-2 [Cricetulus griseus]	CRISPR	1.25	0.005037
HSP90AA1	heat shock protein HSP 90-alpha [Cricetulus griseus]	CRISPR	1.21	0.015809
HSP90AB1	Heat shock protein HSP 90-beta [Cricetulus griseus]	CRISPR	1.49	0.034098
HSPD1	60 kDa heat shock protein, mitochondrial [Cricetulus griseus]	CRISPR	1.24	0.023391
HUWE1	E3 ubiquitin-protein ligase HUWE1, partial [Cricetulus griseus]	CRISPR	1.24	0.044871
IARS	PREDICTED: isoleucine--tRNA ligase, cytoplasmic isoform X2 [Cricetulus griseus]	CRISPR	1.28	0.015959
IARS	PREDICTED: isoleucine--tRNA ligase, cytoplasmic isoform X2 [Cricetulus griseus]	CRISPR	1.23	0.001292
ILF2	Interleukin enhancer-binding factor 2 [Cricetulus griseus]	CRISPR	1.25	0.014053
ILF3	Interleukin enhancer-binding factor 3 [Cricetulus griseus]	CRISPR	1.23	0.002212
KLC1	Kinesin light chain 1 [Cricetulus griseus]	CRISPR	1.21	0.025125
KPNB1	Importin subunit beta-1 [Cricetulus griseus]	CRISPR	1.21	0.027856
LANCL1	LanC-like protein 1, partial [Cricetulus griseus]	CRISPR	1.42	0.040789
LETM1	LETM1 and EF-hand domain-containing protein 1, mitochondrial, partial [Cricetulus griseus]	CRISPR	1.43	0.001145
LHPP	Inorganic pyrophosphatase [Cricetulus griseus]	CRISPR	1.21	0.003911

LONP1	Lon protease-like, mitochondrial [Cricetulus griseus]	CRISPR	1.34	0.003481
LRPPRC	Leucine-rich PPR motif-containing protein, mitochondrial [Cricetulus griseus]	CRISPR	1.28	0.000808
LRRFIP1	Leucine-rich repeat flightless-interacting protein 1 [Cricetulus griseus]	CRISPR	1.27	0.00672
MAP1B	Microtubule-associated protein 1B [Cricetulus griseus]	CRISPR	1.3	0.00378
MCM4	DNA replication licensing factor MCM4 [Cricetulus griseus]	CRISPR	1.22	0.04087
MEMO1	PREDICTED: protein MEMO1 isoform X2 [Cricetulus griseus]	CRISPR	1.96	0.026159
MPHOSPH10	U3 small nucleolar ribonucleoprotein protein MPP10 [Cricetulus griseus]	CRISPR	1.35	0.015285
MPST	3-mercaptopyruvate sulfurtransferase [Cricetulus griseus]	CRISPR	1.58	0.007714
MRPL18	39S ribosomal protein L18, mitochondrial [Cricetulus griseus]	CRISPR	1.26	0.011376
MRPS22	28S ribosomal protein S22, mitochondrial [Cricetulus griseus]	CRISPR	1.56	0.008447
MRPS6	28S ribosomal protein S6, mitochondrial [Cricetulus griseus]	CRISPR	1.36	0.007319
MRPS7	28S ribosomal protein S7, mitochondrial [Cricetulus griseus]	CRISPR	1.24	2.82E-05
MSI2	RNA-binding protein Musashi-like 2 [Cricetulus griseus]	CRISPR	1.62	0.023029

MYBBP1A	Myb-binding protein 1A [Cricetulus griseus]	CRISPR	1.33	0.008405
NAA50	N-acetyltransferase NAT13 [Cricetulus griseus]	CRISPR	1.33	0.013926
NAXE	Apolipoprotein A-I-binding protein [Cricetulus griseus]	CRISPR	1.28	0.007794
NDUFA8	NADH dehydrogenase [ubiquinone] 1 alpha subcomplex subunit 8 [Cricetulus griseus]	CRISPR	1.45	0.001742
NDUFB8	NADH dehydrogenase [ubiquinone] 1 beta subcomplex subunit 8, mitochondrial [Cricetulus griseus]	CRISPR	1.39	0.005821
NDUFS1	NADH-ubiquinone oxidoreductase 75 kDa subunit, mitochondrial [Cricetulus griseus]	CRISPR	1.38	0.002623
NDUFS2	NADH dehydrogenase [ubiquinone] iron-sulfur protein 2, mitochondrial [Cricetulus griseus]	CRISPR	1.39	0.002759
NDUFS3	NADH dehydrogenase [ubiquinone] iron-sulfur protein 3, mitochondrial [Cricetulus griseus]	CRISPR	1.27	0.028795
NDUFS6	NADH dehydrogenase [ubiquinone] iron-sulfur protein 6, mitochondrial [Cricetulus griseus]	CRISPR	1.22	0.021147
NDUFV1	NADH dehydrogenase [ubiquinone] flavoprotein 1, mitochondrial [Cricetulus griseus]	CRISPR	1.26	0.000198
NDUFV3	NADH dehydrogenase [ubiquinone] flavoprotein 3, mitochondrial [Cricetulus griseus]	CRISPR	1.27	0.003061
NIF3L1	NIF3-like protein 1 [Cricetulus griseus]	CRISPR	1.36	0.003077
NIFK	MKI67 FHA domain-interacting nucleolar phosphoprotein [Cricetulus griseus]	CRISPR	1.21	0.015381

NOL11	Nucleolar protein 11 [Cricetulus griseus]	CRISPR	1.59	0.011023
NOP2	Putative ribosomal RNA methyltransferase NOP2 [Cricetulus griseus]	CRISPR	1.25	0.007907
NOP56	Nucleolar protein 56 [Cricetulus griseus]	CRISPR	1.28	0.011064
NUDC	Nuclear migration protein nudC [Cricetulus griseus]	CRISPR	1.27	0.024114
OPA1	Dynamin-like 120 kDa protein, mitochondrial [Cricetulus griseus]	CRISPR	1.43	0.000515
P4HB	protein disulfide-isomerase precursor [Cricetulus griseus]	CRISPR	1.29	0.022742
PA2G4	Proliferation-associated protein 2G4 [Cricetulus griseus]	CRISPR	1.34	0.001522
PAK2	Serine/threonine-protein kinase PAK 2 [Cricetulus griseus]	CRISPR	1.29	0.001131
PALM	Paralemmin [Cricetulus griseus]	CRISPR	1.22	0.004249
PALM2	A-kinase anchor protein 2 [Cricetulus griseus]	CRISPR	1.44	0.010043
PARN	Poly(A)-specific ribonuclease PARN [Cricetulus griseus]	CRISPR	1.44	0.007075
PDCD6IP	Programmed cell death 6-interacting protein [Cricetulus griseus]	CRISPR	1.22	0.00084
PEBP1	Phosphatidylethanolamine-binding protein 1 [Cricetulus griseus]	CRISPR	1.31	0.030115
PFKL	6-phosphofructokinase, liver type [Cricetulus griseus]	CRISPR	1.23	0.014398

PGLS	6-phosphogluconolactonase [Cricetulus griseus]	CRISPR	1.4	0.00773
PITPNA	Phosphatidylinositol transfer protein alpha isoform [Cricetulus griseus]	CRISPR	2.25	0.005313
PITRM1	Presequence protease, mitochondrial [Cricetulus griseus]	CRISPR	1.21	0.020618
PLAA	Phospholipase A-2-activating protein [Cricetulus griseus]	CRISPR	1.22	0.005832
PLIN2	Adipophilin [Cricetulus griseus]	CRISPR	1.55	0.005063
POLRMT	DNA-directed RNA polymerase, mitochondrial [Cricetulus griseus]	CRISPR	1.45	0.048488
PPFIBP1	Liprin-beta-1 [Cricetulus griseus]	CRISPR	1.52	0.031311
PPM1F	Protein phosphatase 1F [Cricetulus griseus]	CRISPR	1.38	0.001041
PPM1G	Protein phosphatase 1G [Cricetulus griseus]	CRISPR	1.23	0.0337
PPP1R10	Serine/threonine-protein phosphatase 1 regulatory subunit 10 [Cricetulus griseus]	CRISPR	1.45	0.009177
PRDX5	Peroxiredoxin-5, mitochondrial [Cricetulus griseus]	CRISPR	1.24	0.015035
PRMT5	Protein arginine N-methyltransferase 5 [Cricetulus griseus]	CRISPR	1.39	0.043131
PRPF8	Pre-mRNA-processing-splicing factor 8 [Cricetulus griseus]	CRISPR	1.21	0.005923
PSMB2	Proteasome subunit beta type-2 [Cricetulus griseus]	CRISPR	1.33	0.005688

PSMD2	26S proteasome non-ATPase regulatory subunit 2 [Cricetulus griseus]	CRISPR	1.28	0.006574
PSMD6	26S proteasome non-ATPase regulatory subunit 6 [Cricetulus griseus]	CRISPR	1.25	0.031914
PSME1	PREDICTED: proteasome activator complex subunit 1 isoform X2 [Cricetulus griseus]	CRISPR	1.22	0.000405
PSMF1	Proteasome inhibitor PI31 subunit [Cricetulus griseus]	CRISPR	1.3	0.024361
PSPC1	Paraspeckle component 1 [Cricetulus griseus]	CRISPR	1.27	0.019659
PTBP1	Polypyrimidine tract-binding protein 1 [Cricetulus griseus]	CRISPR	1.21	0.00645
PYCR1	Pyrroline-5-carboxylate reductase 1, mitochondrial [Cricetulus griseus]	CRISPR	1.23	0.000878
RACK1	Guanine nucleotide-binding protein subunit beta-2-like 1 [Cricetulus griseus]	CRISPR	1.45	0.025487
RCC2	Protein RCC2 [Cricetulus griseus]	CRISPR	1.34	0.002603
RCN2	Reticulocalbin-2 [Cricetulus griseus]	CRISPR	1.3	0.039155
RCN3	Reticulocalbin-3 [Cricetulus griseus]	CRISPR	1.27	0.010397
RIOX2	Myc-induced nuclear antigen [Cricetulus griseus]	CRISPR	1.24	0.024601
RNPEP	Aminopeptidase B [Cricetulus griseus]	CRISPR	1.3	0.010691
RPL23	60S ribosomal protein L23 [Cricetulus griseus]	CRISPR	1.3	0.042536
RPL32	60S ribosomal protein L32 [Cricetulus griseus]	CRISPR	1.35	0.001604

RPL4	60S ribosomal protein L4 [Cricetulus griseus]	CRISPR	1.31	0.030893
RPL7A	60S ribosomal protein L7a [Cricetulus griseus]	CRISPR	1.29	0.017233
RPLP0	60S acidic ribosomal protein P0 [Cricetulus griseus]	CRISPR	1.25	0.002178
RPS20	40S ribosomal protein S20 [Cricetulus griseus]	CRISPR	1.26	0.004883
RTCB	PREDICTED: tRNA-splicing ligase RtcB homolog [Cricetulus griseus]	CRISPR	1.24	0.001332
RUVBL2	RuvB-like 2 [Cricetulus griseus]	CRISPR	1.22	6.34E-05
SAMHD1	SAM domain and HD domain-containing protein 1 [Cricetulus griseus]	CRISPR	1.47	0.028087
SDHB	Succinate dehydrogenase [ubiquinone] iron-sulfur subunit, mitochondrial [Cricetulus griseus]	CRISPR	1.4	0.001606
SET	Protein SET [Cricetulus griseus]	CRISPR	1.82	0.005147
SHMT2	Serine hydroxymethyltransferase, mitochondrial [Cricetulus griseus]	CRISPR	1.33	0.006493
SKIV2L	Helicase SKI2W [Cricetulus griseus]	CRISPR	1.21	0.010774
SLK	STE20-like serine/threonine-protein kinase [Cricetulus griseus]	CRISPR	1.27	0.026675
SMC3	Structural maintenance of chromosomes protein 3 [Cricetulus griseus]	CRISPR	1.31	0.001503
STUB1	STIP1-likey and U box-containing protein 1 [Cricetulus griseus]	CRISPR	1.24	0.005487
SUN2	Protein unc-84-like B [Cricetulus griseus]	CRISPR	1.29	0.012685

SUPT6H	Transcription elongation factor SPT6 [Cricetulus griseus]	CRISPR	1.4	0.008911
SUPV3L1	ATP-dependent RNA helicase SUPV3L1, mitochondrial [Cricetulus griseus]	CRISPR	1.28	0.012164
SURF6	Surfeit locus protein 6 [Cricetulus griseus]	CRISPR	1.44	0.023124
TCOF1	Treacle protein [Cricetulus griseus]	CRISPR	1.47	0.03177
TFRC	Transferrin receptor protein 1 [Cricetulus griseus]	CRISPR	1.21	0.029422
TGM2	Protein-glutamine gamma-glutamyltransferase 2 [Cricetulus griseus]	CRISPR	1.3	0.02635
TMEM43	Transmembrane protein 43 [Cricetulus griseus]	CRISPR	2.54	0.002434
TPD52L2	Uncharacterized protein C20orf135-like [Cricetulus griseus]	CRISPR	1.24	0.00328
TTLL12	Tubulin--tyrosine ligase-like protein 12 [Cricetulus griseus]	CRISPR	1.35	0.003879
TUFM	Elongation factor Tu, mitochondrial [Cricetulus griseus]	CRISPR	1.21	0.018946
U2AF2	PREDICTED: splicing factor U2AF 65 kDa subunit isoform X1, partial [Cricetulus griseus]	CRISPR	1.41	0.01606
UQCRC7	Cytochrome b-c1 complex subunit 7, partial [Cricetulus griseus]	CRISPR	1.88	0.032707
USP15	Ubiquitin carboxyl-terminal hydrolase 15 [Cricetulus griseus]	CRISPR	1.24	0.003445

VMN2R1	GMP synthase [glutamine-hydrolyzing] [Cricetulus griseus]	CRISPR	1.26	0.010444
VWA8	Uncharacterized protein KIAA0564-like [Cricetulus griseus]	CRISPR	1.21	0.001299
WDR12	Ribosome biogenesis protein WDR12 [Cricetulus griseus]	CRISPR	1.25	0.036868
WDR81	WD repeat-containing protein 81 [Cricetulus griseus]	CRISPR	1.24	0.021081
YARS	Tyrosyl-tRNA synthetase, cytoplasmic [Cricetulus griseus]	CRISPR	1.27	0.034077

CHO-K1 mAb sgRNA-miR-24 (CRISPR)/ predicted and validated targets

Gene ID	Predicted/Validated	miR-24-3p	miR-24-5p
TMEM43	Predicted	X	
PPFIBP1	Predicted/Validated	X	
SAMHD1	Predicted	X	
BYSL	Predicted	X	X
SURF6	Predicted	X	
PALM2	Predicted	X	
LETM1	Predicted	X	
LANCL1	Predicted	X	
PGLS	Predicted	X	
GLRX3	Predicted	X	
PPM1F	Predicted	X	
NDUFS1	Predicted	X	X
ADK	Predicted	X	
HP1BP3	Predicted	X	
NIF3L1	Predicted	X	
TTLL12	Predicted	X	

RCC2	Predicted	X	
EBNA1BP2	Predicted	X	
PSMB2	Predicted	X	
NAA50	Predicted	X	
MYBBP1A	Predicted	X	
EIF5A2	Predicted	X	
EIF3I	Predicted	X	
RPL4	Predicted	X	
GTF2F1	Predicted	X	
CAPN2	Predicted	X	
MAP1B	Predicted	X	X
PSMF1	Predicted	X	X
TGM2	Predicted	X	
RCN2	Predicted	X	
RPL23	Predicted	X	
RNPEP	Predicted	X	
DDX46	Predicted	X	
SUN2	Predicted	X	

ATIC	Predicted	X	
PAK2	Predicted	X	
LRPPRC	Predicted	X	
FLNB	Predicted	X	X
BRIX1	Predicted	X	
NDUFV3	Predicted	X	X
RCN3	Predicted	X	
ATAD3A	Predicted	X	X
DHX30	Predicted	X	
H2AFV	Predicted	X	
ESF1	Predicted	X	X
EHD3	Predicted	X	X
ACTN4	Predicted	X	
CHORDC1	Predicted	X	
AARS	Predicted	X	
TPD52L2	Predicted	X	
RTCB	Predicted	X	
APOOL	Predicted	X	

PPM1G	Predicted	X	
ILF3	Predicted	X	X
ADSL	Predicted	X	
PLAA	Predicted	X	
PALM	Predicted	X	
MCM4	Predicted	X	
EXOSC2	Predicted	X	
EIF2S1	Predicted	X	
LHPP	Predicted	X	
WDR12	Predicted	X	
DNAJA3	Predicted	X	
TMEM43	Predicted	X	
PPFIBP1	Predicted	X	
SAMHD1	Predicted	X	
BYSL	Predicted	X	
SURF6	Predicted	X	
PALM2	Predicted	X	
LETM1	Predicted	X	

LANCL1	Predicted	X		
PGLS	Predicted	X		
GLRX3	Predicted	X		
PPM1F	Predicted	X		
NDUFS1	Predicted	X		
ADK	Predicted	X		
HP1BP3	Predicted	X		
NIF3L1	Predicted	X		
TTLL12	Predicted	X		
RCC2	Predicted	X		
EBNA1BP2	Predicted	X		
PSMB2	Predicted	X		
NAA50	Predicted	X		
MYBBP1A	Predicted	X		
EIF5A2	Predicted	X		
EIF3I	Predicted	X		
RPL4	Predicted	X		
GTF2F1	Predicted	X		

CAPN2	Predicted	X	
MAP1B	Predicted	X	
PSMF1	Predicted	X	
TGM2	Predicted	X	
RCN2	Predicted	X	
RPL23	Predicted	X	
RNPEP	Predicted	X	
DDX46	Predicted	X	
SUN2	Predicted	X	
ATIC	Predicted	X	
PAK2	Predicted	X	
LRPPRC	Predicted	X	
FLNB	Predicted	X	
BRIX1	Predicted	X	
NDUFV3	Predicted	X	
RCN3	Predicted	X	
ATAD3A	Predicted	X	
DHX30	Predicted	X	

H2AFV	Predicted	X	
ESF1	Predicted	X	
EHD3	Predicted	X	
ACTN4	Predicted	X	
CHORDC1	Predicted	X	
AARS	Predicted	X	
TPD52L2	Predicted	X	
RTCB	Predicted	X	
APOOL	Predicted	X	
PPM1G	Predicted	X	
ILF3	Predicted	X	
ADSL	Predicted	X	
PLAA	Predicted	X	
PALM	Predicted	X	
MCM4	Predicted	X	
EXOSC2	Predicted	X	
EIF2S1	Predicted	X	
LHPP	Predicted	X	

WDR12	Predicted	X	
DNAJA3	Predicted	X	
PITPNA	Predicted		X
FARSB	Predicted		X
CALU	Predicted		X
DDX21	Predicted		X
SHMT2	Predicted		X
PEBP1	Predicted		X
FAM98B	Predicted		X
DDX10	Predicted		X
BCLAF1	Predicted		X
MRPL18	Predicted		X
CTTN	Predicted		X
USP15	Predicted		X
HSP90AA1	Predicted		X
TFRC	Predicted		X
NARS	Predicted/Validated	X	
PPM1F	Predicted/Validated	X	X

NCBP2	Predicted/Validated	X	
NOP56	Predicted/Validated	X	
PA2G4	Predicted/Validated	X	
PCK2	Predicted/Validated	X	
CCDC58	Predicted/Validated	X	

CHO-K1 mAb sgRNA-miR-24 (RNASeq)

Gene ID	Log2 fold change	Anova	Abundance Control	Abundance CRISPR
A2ML1	0.812235	0.008235	7076.79	5692.44
AATK	0.485439	0.002864	2563.3	2161.07
ABCA1	0.467905	0.03518	20.36	40.39
ABCC2	-1.2543	0.004506	200.36	310.85
ABCD1	0.387186	0.003813	1457.01	1077.48
ABCD2	-0.44258	0.024434	14.57	30.62
ABHD11	-0.43211	2.01E-05	23.03	38.31
ABHD2	0.372604	0.000252	43.21	23.64
ACAA2	0.662733	0.007831	772.31	603.71
ACACB	-0.68446	0.002069	350.55	246.32
ACKR3	1.238888	0.001798	106.52	70.25
ACO2	-0.3143	1.07E-06	5.77	25.76
ACP5	-0.48017	2.05E-42	490.59	353.85
ACSBG1	-0.24601	0.019032	627.74	826.16
ACY3	0.352191	0.009111	968.28	1256.31

ADAMTS7	0.290051	1.63E-12	68.37	97.22
ADCK1	-0.63283	0.016616	592.06	931.83
ADCY6	0.500092	0.010372	168.52	231.87
ADD2	4.331363	8.23E-11	7420.41	6281.97
ADH5	0.34556	0.039527	5944.91	9388.88
ADSSL1	0.694325	0.004071	522.88	413.69
AGAP1	0.537581	0.006976	179.96	282.82
AHCYL1	-0.27158	3.35E-07	98.49	62.39
AHNAK	0.712402	0.04843	1191.87	902.27
AKR1B8	0.373602	0.008264	1189.76	1858.95
ALDH4A1	0.334598	4.34E-05	6086.49	7562.61
ALS2CL	0.324978	0.006791	30.37	47.45
ANGPT4	0.985762	0.027952	179.56	251.1
ANKH	0.386293	0.007521	453.68	336.15
ANKRD13A	0.311653	0.000716	51.66	84.64
ANKRD27	0.371663	0.010835	3327.33	2678.57
ANKRD39	0.630641	0.00101	194.36	280.55
ANXA1	-0.43409	0.03289	412.34	247.3

APLP2	-0.45408	0.019856	17.57	31.47
AQP10	-0.35291	3.07E-15	503.77	1087.18
AQP3	0.819515	0.001268	719.13	1001.95
ARAP3	0.563271	0.01847	70.19	109.2
ARFRP1	-0.40189	0.034638	607.26	497.35
ARHGAP22	1.033536	0.009895	622.18	495.23
ARHGAP24	-0.90182	0.001903	72.71	106.49
ARHGAP27	0.931419	0.000402	131.95	89.44
ARHGEF17	0.281863	0.000825	8.69	21.41
ARL4C	0.299904	0.012477	20.66	5.65
ARNTL2	1.061464	0.044597	1433.79	1219.06
ARTN	0.728132	0.015615	349.65	553.18
ASAP3	0.609258	8.65E-24	37.3	20.75
ATF3	-0.7113	0.045149	616.17	747.4
ATF4	-0.26675	0.035851	99.49	68.07
ATF5	-0.53501	0.039954	1260.07	1576.36
ATG14	-0.7203	0.012353	1306.52	1681.5
ATG2B	0.307582	0.002383	406.28	320.61

ATP2B4	0.474301	0.028159	227.71	169.1
ATP4A	-1.44323	0.041544	20.33	7.39
ATP6V1G1	0.729517	0.006432	3926.4	5535.83
ATP8B2	-0.43862	0.000376	7076.79	5692.44
BCL9L	0.424764	0.008235	2563.3	2161.07
BCO2	-0.79384	0.002864	20.36	40.39
BEND4	-0.27323	0.03518	200.36	310.85
BEST1	0.691279	0.004506	1457.01	1077.48
BMF	0.352665	0.003813	14.57	30.62
BMP1	0.337314	0.024434	23.03	38.31
BNIP3	-0.34303	2.01E-05	43.21	23.64
BRAT1	0.363191	0.000252	772.31	603.71
BZRAP1	-0.42947	0.007831	350.55	246.32
C1QTNF1	-1.06532	0.002069	106.52	70.25
C3	-0.87355	0.001798	5.77	25.76
CACNA1C	0.455732	1.07E-06	490.59	353.85
CAD	-0.35711	2.05E-42	627.74	826.16
CAPN5	0.427929	0.019032	968.28	1256.31

CAPN9	0.686353	0.009111	68.37	97.22
CARD10	0.606556	1.63E-12	592.06	931.83
CASKIN1	-0.60833	0.016616	168.52	231.87
CCBE1	-0.62337	0.010372	7420.41	6281.97
CCDC137	-0.28011	8.23E-11	5944.91	9388.88
CCDC65	-0.32599	0.039527	522.88	413.69
CCKAR	-0.76667	0.004071	179.96	282.82
CCND1	0.519264	0.006976	98.49	62.39
CCNE1	-1.12639	3.35E-07	1191.87	902.27
CCNI	0.787593	0.04843	1189.76	1858.95
CCS	-0.37606	0.008264	6086.49	7562.61
CD40LG	0.46381	4.34E-05	30.37	47.45
CD47	0.510398	0.006791	179.56	251.1
CDC42BPB	0.337871	0.027952	453.68	336.15
CDC42EP2	0.780657	0.007521	51.66	84.64
CDCA4	0.708383	0.000716	3327.33	2678.57
CDH16	-0.59164	0.010835	194.36	280.55
CDON	0.431125	0.00101	412.34	247.3

CDS1	-0.50644	0.03289	17.57	31.47
CHD7	-0.78861	0.019856	503.77	1087.18
CIB2	-0.58474	3.07E-15	719.13	1001.95
CIRBP	0.309752	0.001268	70.19	109.2
CNBP	-0.59962	0.01847	607.26	497.35
CNKSR1	-0.83136	0.034638	622.18	495.23
CNN3	-0.31792	0.009895	72.71	106.49
COL16A1	0.602875	0.001903	131.95	89.44
COL17A1	0.516172	0.000402	8.69	21.41
COL27A1	1.696222	0.000825	20.66	5.65
COL3A1	1.173342	0.012477	1433.79	1219.06
COL4A1	2.136309	0.044597	349.65	553.18
COL6A1	1.556977	0.015615	37.3	20.75
CORNIFIN-A	-1.77186	8.65E-24	616.17	747.4
CPT1A	0.376488	0.045149	99.49	68.07
CRB3	-0.47546	0.035851	1260.07	1576.36
CREB1	0.305551	0.039954	1306.52	1681.5
CREB3	0.646881	0.012353	406.28	320.61

CRIP1	0.366888	0.002383	227.71	169.1
CSE1L	-0.31315	0.028159	20.33	7.39
CSF3	-0.93873	0.041544	3926.4	5535.83
CSTF2	-0.27011	0.006432	7076.79	5692.44
CTNND1	0.270156	0.000376	2563.3	2161.07
CTSE	0.874699	0.008235	20.36	40.39
CTU2	0.324535	0.002864	200.36	310.85
CYR61	-0.86395	0.03518	1457.01	1077.48
DAB2IP	-0.45097	0.004506	14.57	30.62
DCTPP1	-0.36935	0.003813	23.03	38.31
DDX27	-0.3488	0.024434	43.21	23.64
DENND1C	-0.45457	2.01E-05	772.31	603.71
DENND3	0.351901	0.000252	350.55	246.32
DFNA5	0.414422	0.007831	106.52	70.25
DGAT1	1.011326	0.002069	5.77	25.76
DGAT2	-0.56365	0.001798	490.59	353.85
DGKD	0.311809	1.07E-06	627.74	826.16
DLG1	0.512812	2.05E-42	968.28	1256.31

DNAJB13	-1.26434	0.019032	68.37	97.22
DNAJC14	0.604542	0.009111	592.06	931.83
DNMT3A	0.397099	1.63E-12	168.52	231.87
DNTTIP1	-1.11019	0.016616	7420.41	6281.97
DST	0.520615	0.010372	5944.91	9388.88
DTX4	-1.81275	8.23E-11	522.88	413.69
DUSP16	-0.43716	0.039527	179.96	282.82
DUSP8	-0.80569	0.004071	98.49	62.39
DYNC1H1	0.29862	0.006976	1191.87	902.27
DZIP1	0.484625	3.35E-07	1189.76	1858.95
EIF4E2	0.895989	0.04843	6086.49	7562.61
EIF4G3	1.018229	0.008264	30.37	47.45
EMP1	0.430022	4.34E-05	179.56	251.1
ENDOD1	0.627488	0.006791	453.68	336.15
ENDOV	0.32394	0.027952	51.66	84.64
ENOSF1	0.490311	0.007521	3327.33	2678.57
ENTPD5	0.375798	0.000716	194.36	280.55
EPAS1	-5.17427	0.010835	412.34	247.3

EPHB3	-0.49113	0.00101	17.57	31.47
EPS8	0.40262	0.03289	503.77	1087.18
ERRFI1	0.404	0.019856	719.13	1001.95
ESYT2	0.38125	3.07E-15	70.19	109.2
ETS2	-0.36209	0.001268	607.26	497.35
ETV1	0.509657	0.01847	622.18	495.23
EXO1	-0.43174	0.034638	72.71	106.49
EXOC3	0.346905	0.009895	131.95	89.44
EXTL1	-0.59626	0.001903	8.69	21.41
F2RL2	0.513566	0.000402	20.66	5.65
FABP4	0.653895	0.000825	1433.79	1219.06
FADS3	0.435676	0.012477	349.65	553.18
FAH	0.341604	0.044597	37.3	20.75
FAM102A	0.330038	0.015615	616.17	747.4
FAM115A	0.456543	8.65E-24	99.49	68.07
FAM13C	-1.83393	0.045149	1260.07	1576.36
FAM161A	-0.24017	0.035851	1306.52	1681.5
FAM167B	-0.69933	0.039954	406.28	320.61

FAM20C	-0.50039	0.012353	227.71	169.1
FAM83A	1.190008	0.002383	20.33	7.39
FAXDC2	0.549456	0.028159	3926.4	5535.83
FBLIM1	0.281327	0.041544	7076.79	5692.44
FBXL18	0.365647	0.006432	2563.3	2161.07
FBXO32	0.666871	0.000376	20.36	40.39
FBXW7	0.964333	0.008235	200.36	310.85
FER1L5	0.287784	0.002864	1457.01	1077.48
FGFR2	-3.28894	0.03518	14.57	30.62
FIBP	0.305093	0.004506	23.03	38.31
FLNC	0.324697	0.003813	43.21	23.64
FMNL3	0.33706	0.024434	772.31	603.71
FN1	0.760327	2.01E-05	350.55	246.32
FOLR1	-1.81709	0.000252	106.52	70.25
FOSL1	0.374402	0.007831	5.77	25.76
FSTL1	0.233109	0.002069	490.59	353.85
FTH1	0.659128	0.001798	627.74	826.16
FTSJ3	-1.68137	1.07E-06	968.28	1256.31

FUK	-0.3497	2.05E-42	68.37	97.22
GALNT2	0.462951	0.019032	592.06	931.83
GARS	-0.28357	0.009111	168.52	231.87
GBA2	0.497137	1.63E-12	7420.41	6281.97
GCAT	0.404976	0.016616	5944.91	9388.88
GGCX	0.267706	0.010372	522.88	413.69
GLIPR2	0.306832	8.23E-11	179.96	282.82
GLS2	-0.79758	0.039527	98.49	62.39
GNPTAB	-0.33432	0.004071	1191.87	902.27
GPATCH8	-0.42583	0.006976	1189.76	1858.95
GPD1	1.453052	3.35E-07	6086.49	7562.61
GPD2	-0.36237	0.04843	30.37	47.45
GPNMB	-0.34137	0.008264	179.56	251.1
GPR108	-0.7042	4.34E-05	453.68	336.15
GPR133	-1.68851	0.006791	51.66	84.64
GPR176	-0.73599	0.027952	3327.33	2678.57
GPR182	0.5979	0.007521	194.36	280.55
GPR56	0.502342	0.000716	412.34	247.3

GPS2	-0.87345	0.010835	17.57	31.47
GPSM1	-0.53148	0.00101	503.77	1087.18
GRAMD1B	1.653203	0.03289	719.13	1001.95
GRAMD4	0.513153	0.019856	70.19	109.2
GRIA4	-0.36166	3.07E-15	607.26	497.35
GRIP2	0.505002	0.001268	622.18	495.23
GSDMD	0.987189	0.01847	72.71	106.49
GSN	0.351863	0.034638	131.95	89.44
GTF3C2	0.875765	0.009895	8.69	21.41
GTPBP6	-0.40556	0.001903	20.66	5.65
GYS1	0.310706	0.000402	1433.79	1219.06
HAUS8	0.364633	0.000825	349.65	553.18
HDAC4	0.351422	0.012477	37.3	20.75
HDAC7	0.384787	0.044597	616.17	747.4
HERC3	-0.42562	0.015615	99.49	68.07
HIP1	0.277872	8.65E-24	1260.07	1576.36
HIPK2	0.793127	0.045149	1306.52	1681.5
HK2	-0.35915	0.035851	406.28	320.61

HMGCR	0.248385	0.039954	227.71	169.1
HMGCS2	0.648475	0.012353	20.33	7.39
HMOX1	0.742432	0.002383	3926.4	5535.83
HNF4A	-0.67171	0.028159	7076.79	5692.44
HOMER1	-0.50407	0.041544	2563.3	2161.07
HOXC6	0.359422	0.006432	20.36	40.39
HOXC8	-0.50174	0.000376	200.36	310.85
HPSE	-0.3656	0.008235	1457.01	1077.48
HSPG2	0.265989	0.002864	14.57	30.62
HTR6	-0.63422	0.03518	23.03	38.31
HUNK	0.774776	0.004506	43.21	23.64
HYAL2	-0.57503	0.003813	772.31	603.71
IARS	-0.31235	0.024434	350.55	246.32
IER5L	0.882492	2.01E-05	106.52	70.25
IFFO2	0.475239	0.000252	5.77	25.76
IGDCC3	-0.7692	0.007831	490.59	353.85
IGDCC4	-0.56934	0.002069	627.74	826.16
IKBKAP	-0.23432	0.001798	968.28	1256.31

IMP3	0.583391	1.07E-06	68.37	97.22
INPP5J	-0.48659	2.05E-42	592.06	931.83
IP6K3	-1.51769	0.019032	168.52	231.87
IQGAP2	0.379908	0.009111	7420.41	6281.97
IRS2	0.555096	1.63E-12	5944.91	9388.88
ITGA2B	-0.83457	0.016616	522.88	413.69
ITGB4	0.3224	0.010372	179.96	282.82
ITPR3	0.45155	8.23E-11	98.49	62.39
JADE1	-0.42703	0.039527	1191.87	902.27
JAK3	0.456521	0.004071	1189.76	1858.95
JUN	-0.55307	0.006976	6086.49	7562.61
KANK2	0.376212	3.35E-07	30.37	47.45
KANSL2	-0.24224	0.04843	179.56	251.1
KCNK5	0.513713	0.008264	453.68	336.15
KCNS2	1.577716	4.34E-05	51.66	84.64
KCTD12	0.367852	0.006791	3327.33	2678.57
KCTD15	-0.76392	0.027952	194.36	280.55
KCTD21	0.511734	0.007521	412.34	247.3

KIAA0319	-0.45052	0.000716	17.57	31.47
KIAA1522	-0.40188	0.010835	503.77	1087.18
KIF27	-0.88872	0.00101	719.13	1001.95
KIRREL	0.24478	0.03289	70.19	109.2
KLHDC1	-0.51376	0.019856	607.26	497.35
KLHL21	-0.3711	3.07E-15	622.18	495.23
KLHL22	0.375451	0.001268	72.71	106.49
KMT2A	0.444194	0.01847	131.95	89.44
KMT2C	0.424529	0.034638	8.69	21.41
KRT80	-0.47918	0.009895	20.66	5.65
LARS	-0.35944	0.001903	1433.79	1219.06
LASP1	0.386554	0.000402	349.65	553.18
LAYN	0.643106	0.000825	37.3	20.75
LGALS1	1.181909	0.012477	616.17	747.4
LGR6	-0.44647	0.044597	99.49	68.07
LIMA1	0.357068	0.015615	1260.07	1576.36
LIPA	0.368245	8.65E-24	1306.52	1681.5
LMBR1L	0.757323	0.045149	406.28	320.61

LOC100689270	0.272288	0.035851	227.71	169.1
LOC100750560	0.475289	0.039954	20.33	7.39
LOC100750688	0.398999	0.012353	3926.4	5535.83
LOC100750719	0.356338	0.002383	7076.79	5692.44
LOC100750843	1.017969	0.028159	2563.3	2161.07
LOC100751267	-2.50978	0.041544	20.36	40.39
LOC100752605	0.789775	0.006432	200.36	310.85
LOC100752702	0.695703	0.000376	1457.01	1077.48
LOC100752852	-0.32401	0.008235	14.57	30.62
LOC100753154	-0.32449	0.002864	23.03	38.31
LOC100753183	0.565097	0.03518	43.21	23.64
LOC100753203	0.464849	0.004506	772.31	603.71
LOC100753390	0.421115	0.003813	350.55	246.32
LOC100753628	-0.79257	0.024434	106.52	70.25
LOC100753650	0.308198	2.01E-05	5.77	25.76
LOC100753871	0.281209	0.000252	490.59	353.85
LOC100754104	0.531868	0.007831	627.74	826.16
LOC100754429	0.624484	0.002069	968.28	1256.31

LOC100754526	0.313135	0.001798	68.37	97.22
LOC100754646	-1.56592	1.07E-06	592.06	931.83
LOC100755494	-2.36432	2.05E-42	168.52	231.87
LOC100756292	0.476098	0.019032	7420.41	6281.97
LOC100756494	-1.28467	0.009111	5944.91	9388.88
LOC100756672	-0.35238	1.63E-12	522.88	413.69
LOC100756967	0.336979	0.016616	179.96	282.82
LOC100757535	-0.27887	0.010372	98.49	62.39
LOC100757664	0.516981	8.23E-11	1191.87	902.27
LOC100757825	-0.32805	0.039527	1189.76	1858.95
LOC100757863	0.898288	0.004071	6086.49	7562.61
LOC100758352	-0.51205	0.006976	30.37	47.45
LOC100758409	0.344744	3.35E-07	179.56	251.1
LOC100759179	0.695578	0.04843	453.68	336.15
LOC100759598	0.567214	0.008264	51.66	84.64
LOC100760306	0.780732	4.34E-05	3327.33	2678.57
LOC100761082	-1.17915	0.006791	194.36	280.55
LOC100762429	0.863855	0.027952	412.34	247.3

LOC100762503	2.036139	0.007521	17.57	31.47
LOC100762980	1.546724	0.000716	503.77	1087.18
LOC100763569	0.387315	0.010835	719.13	1001.95
LOC100764240	0.468802	0.00101	70.19	109.2
LOC100764436	-0.32974	0.03289	607.26	497.35
LOC100765869	0.707596	0.019856	622.18	495.23
LOC100766020	-0.84744	3.07E-15	72.71	106.49
LOC100766243	0.645212	0.001268	131.95	89.44
LOC100766840	0.361769	0.01847	8.69	21.41
LOC100767397	1.068817	0.034638	20.66	5.65
LOC100767511	1.309742	0.009895	1433.79	1219.06
LOC100767645	0.588983	0.001903	349.65	553.18
LOC100767691	1.393346	0.000402	37.3	20.75
LOC100768011	2.269969	0.000825	616.17	747.4
LOC100768019	0.541282	0.012477	99.49	68.07
LOC100768454	0.486824	0.044597	1260.07	1576.36
LOC100768487	0.387642	0.015615	1306.52	1681.5
LOC100768534	0.331004	8.65E-24	406.28	320.61

LOC100768732	1.171037	0.045149	227.71	169.1
LOC100768899	-0.79823	0.035851	20.33	7.39
LOC100768961	0.88518	0.039954	3926.4	5535.83
LOC100769643	-0.35501	0.012353	7076.79	5692.44
LOC100769997	1.109077	0.002383	2563.3	2161.07
LOC100770111	0.488838	0.028159	20.36	40.39
LOC100770228	0.318044	0.041544	200.36	310.85
LOC100770323	-0.38076	0.006432	1457.01	1077.48
LOC100770632	0.46057	0.000376	14.57	30.62
LOC100770794	-0.43627	0.008235	23.03	38.31
LOC100770841	0.582796	0.002864	43.21	23.64
LOC100771510	0.280032	0.03518	772.31	603.71
LOC100771813	-2.33696	0.004506	350.55	246.32
LOC100772312	-1.00465	0.003813	106.52	70.25
LOC100772325	1.1543	0.024434	5.77	25.76
LOC100772483	0.723871	2.01E-05	490.59	353.85
LOC100772624	-0.42985	0.000252	627.74	826.16
LOC100772948	-0.66002	0.007831	968.28	1256.31

LOC100773017	-0.45722	0.002069	68.37	97.22
LOC100773107	0.441871	0.001798	592.06	931.83
LOC100773301	-0.45367	1.07E-06	168.52	231.87
LOC100773569	0.837716	2.05E-42	7420.41	6281.97
LOC100773725	0.537708	0.019032	5944.91	9388.88
LOC100773785	-0.31353	0.009111	522.88	413.69
LOC100774337	0.397813	1.63E-12	179.96	282.82
LOC100774451	0.490335	0.016616	98.49	62.39
LOC100774515	0.64344	0.010372	1191.87	902.27
LOC100774629	-0.71517	8.23E-11	1189.76	1858.95
LOC100774659	0.404432	0.039527	6086.49	7562.61
LOC100774914	-1.0484	0.004071	30.37	47.45
LOC103158575	-0.93143	0.006976	179.56	251.1
LOC103158589	0.667938	3.35E-07	453.68	336.15
LOC103158648	1.162566	0.04843	51.66	84.64
LOC103158703	2.395627	0.008264	3327.33	2678.57
LOC103158724	0.864212	4.34E-05	194.36	280.55
LOC103158729	-0.87103	0.006791	412.34	247.3

LOC103158731	0.392697	0.027952	17.57	31.47
LOC103158749	-0.33488	0.007521	503.77	1087.18
LOC103158782	0.970759	0.000716	719.13	1001.95
LOC103158821	0.376259	0.010835	70.19	109.2
LOC103158822	0.400236	0.00101	607.26	497.35
LOC103158840	0.526191	0.03289	622.18	495.23
LOC103158906	-0.38679	0.019856	72.71	106.49
LOC103158907	-0.80478	3.07E-15	131.95	89.44
LOC103158935	3.053748	0.001268	8.69	21.41
LOC103159029	-0.48181	0.01847	20.66	5.65
LOC103159166	-0.41098	0.034638	1433.79	1219.06
LOC103159462	-0.52182	0.009895	349.65	553.18
LOC103159467	1.403451	0.001903	37.3	20.75
LOC103159578	1.051093	0.000402	616.17	747.4
LOC103159771	-0.34617	0.000825	99.49	68.07
LOC103160298	-0.6311	0.012477	1260.07	1576.36
LOC103160606	0.942138	0.044597	1306.52	1681.5
LOC103160739	0.669903	0.015615	406.28	320.61

LOC103161096	0.627933	8.65E-24	227.71	169.1
LOC103161097	0.740045	0.045149	20.33	7.39
LOC103161223	1.025204	0.035851	3926.4	5535.83
LOC103161382	0.45784	0.039954	7076.79	5692.44
LOC103161428	1.152744	0.012353	2563.3	2161.07
LOC103161455	1.36857	0.002383	20.36	40.39
LOC103161733	-1.00066	0.028159	200.36	310.85
LOC103161831	1.047627	0.041544	1457.01	1077.48
LOC103162177	-0.4632	0.006432	14.57	30.62
LOC103162198	0.993474	0.000376	23.03	38.31
LOC103162849	0.668556	0.008235	43.21	23.64
LOC103162851	0.930666	0.002864	772.31	603.71
LOC103162884	-1.07559	0.03518	350.55	246.32
LOC103162906	0.498778	0.004506	106.52	70.25
LOC103163028	0.72285	0.003813	5.77	25.76
LOC103163200	-0.62145	0.024434	490.59	353.85
LOC103163374	-1.25439	2.01E-05	627.74	826.16
LOC103163594	1.425435	0.000252	968.28	1256.31

LOC103163628	2.410664	0.007831	68.37	97.22
LOC103163823	0.740002	0.002069	592.06	931.83
LOC103163825	0.740532	0.001798	168.52	231.87
LOC103163866	0.635887	1.07E-06	7420.41	6281.97
LOC103163905	-0.7395	2.05E-42	5944.91	9388.88
LOC103164085	-0.36609	0.019032	522.88	413.69
LOC103164093	1.303953	0.009111	179.96	282.82
LOC103164151	1.374021	1.63E-12	98.49	62.39
LOC103164153	0.569981	0.016616	1191.87	902.27
LOC103164186	-2.42693	0.010372	1189.76	1858.95
LOC103164219	0.337014	8.23E-11	6086.49	7562.61
LOC103164247	0.864932	0.039527	30.37	47.45
LOC103164338	0.75266	0.004071	179.56	251.1
LOC103164432	0.498343	0.006976	453.68	336.15
LOC103164434	0.444701	3.35E-07	51.66	84.64
LOC103164479	0.905789	0.04843	3327.33	2678.57
LOC103164483	0.836451	0.008264	194.36	280.55
LOC103164570	1.108182	4.34E-05	412.34	247.3

LOC103164585	1.863466	0.006791	17.57	31.47
LOC103164586	1.087147	0.027952	503.77	1087.18
LPIN3	-0.36348	0.007521	719.13	1001.95
LPL	0.47887	0.000716	70.19	109.2
LRIG1	0.370298	0.010835	607.26	497.35
LRP10	0.298661	0.00101	622.18	495.23
LRPAP1	0.392946	0.03289	72.71	106.49
LRPPRC	-0.34677	0.019856	131.95	89.44
LRRN3	0.686543	3.07E-15	8.69	21.41
LRWD1	0.936936	0.001268	20.66	5.65
LSMEM1	-0.46283	0.01847	1433.79	1219.06
LTBP1	0.438481	0.034638	349.65	553.18
MADD	0.527226	0.009895	37.3	20.75
MAN1C1	0.633307	0.001903	616.17	747.4
MAP3K10	-0.32907	0.000402	99.49	68.07
MAP3K14	0.455647	0.000825	1260.07	1576.36
MAPK8	1.151056	0.012477	1306.52	1681.5
38777	0.521448	0.044597	406.28	320.61

MAST1	-0.78763	0.015615	227.71	169.1
MB	-0.77931	8.65E-24	20.33	7.39
MBD6	-0.28942	0.045149	3926.4	5535.83
MEDAG	0.398884	0.035851	7076.79	5692.44
MESDC1	-0.33079	0.039954	2563.3	2161.07
METTL7B	0.560045	0.012353	20.36	40.39
MFF	0.558969	0.002383	200.36	310.85
MICAL2	0.619419	0.028159	1457.01	1077.48
MIR23B	6.091509	0.041544	14.57	30.62
MLPH	0.774353	0.006432	23.03	38.31
MMD	0.465227	0.000376	43.21	23.64
MMP14	0.359336	0.008235	772.31	603.71
MMP17	-0.93633	0.002864	350.55	246.32
MMP28	0.815489	0.03518	106.52	70.25
MOGAT3	1.200788	0.004506	5.77	25.76
MRGBP	0.753712	0.003813	490.59	353.85
MRPL4	-0.41846	0.024434	627.74	826.16
MSN	0.428194	2.01E-05	968.28	1256.31

MTSS1	0.578105	0.000252	68.37	97.22
MVP	0.330212	0.007831	592.06	931.83
MYBBP1A	-0.2775	0.002069	168.52	231.87
MYBL2	-0.40137	0.001798	7420.41	6281.97
MYH9	0.223272	1.07E-06	5944.91	9388.88
MYLK2	0.565741	2.05E-42	522.88	413.69
MYLPF	-0.57273	0.019032	179.96	282.82
MYO10	0.677362	0.009111	98.49	62.39
MYOF	0.376021	1.63E-12	1191.87	902.27
MYZAP	1.476586	0.016616	1189.76	1858.95
N4BP1	-0.43378	0.010372	6086.49	7562.61
NCKAP5L	0.473701	8.23E-11	30.37	47.45
NCOR2	0.276904	0.039527	179.56	251.1
NDRG1	0.76393	0.004071	453.68	336.15
NEO1	0.325697	0.006976	51.66	84.64
NFAT5	0.623163	3.35E-07	3327.33	2678.57
NHLRC2	0.345115	0.04843	194.36	280.55
NHSL2	1.145188	0.008264	412.34	247.3

NLRC5	-2.0276	4.34E-05	17.57	31.47
NPDC1	-0.43375	0.006791	503.77	1087.18
NQO1	0.552379	0.027952	719.13	1001.95
NRSN2	-0.36227	0.007521	70.19	109.2
NSDHL	0.57344	0.000716	607.26	497.35
NT5DC3	-0.4	0.010835	622.18	495.23
NTAN1	0.407495	0.00101	72.71	106.49
NUDT22	-0.43362	0.03289	131.95	89.44
NUFIP1	-0.45265	0.019856	8.69	21.41
NUPR1	0.744065	3.07E-15	20.66	5.65
NUTM1	-0.34261	0.001268	1433.79	1219.06
NXPE4	0.871258	0.01847	349.65	553.18
OLFM1	0.387879	0.034638	37.3	20.75
OLFML2B	-0.77162	0.009895	616.17	747.4
OSTF1	0.283907	0.001903	99.49	68.07
OXSR1	-0.30292	0.000402	1260.07	1576.36
PAK6	1.295712	0.000825	1306.52	1681.5
PANK2	0.464452	0.012477	406.28	320.61

PAQR5	-0.48299	0.044597	227.71	169.1
PARVA	0.37605	0.015615	20.33	7.39
PCIF1	-0.82483	8.65E-24	3926.4	5535.83
PDCD6	0.472816	0.045149	7076.79	5692.44
PDE1C	-7.9132	0.035851	2563.3	2161.07
PDE2A	0.899	0.039954	20.36	40.39
PDGFRA	0.554967	0.012353	200.36	310.85
PDGFRB	1.399838	0.002383	1457.01	1077.48
PDIA6	0.273147	0.028159	14.57	30.62
PDXDC1	0.409353	0.041544	23.03	38.31
PDZD4	-1.22424	0.006432	43.21	23.64
PHLDB1	0.323713	0.000376	772.31	603.71
PHLPP2	0.545634	0.008235	350.55	246.32
PHOSPHO1	1.249053	0.002864	106.52	70.25
PHYHIPL	-1.83116	0.03518	5.77	25.76
PICALM	0.902056	0.004506	490.59	353.85
PIGG	0.393337	0.003813	627.74	826.16
PIK3CB	-0.58477	0.024434	968.28	1256.31

PIP4K2B	0.298813	2.01E-05	68.37	97.22
PIPOX	0.987589	0.000252	592.06	931.83
PKD2	0.367427	0.007831	168.52	231.87
PKP1	-1.25161	0.002069	7420.41	6281.97
PLBD2	-0.2946	0.001798	5944.91	9388.88
PLCG1	-0.32792	1.07E-06	522.88	413.69
PLEC	0.465937	2.05E-42	179.96	282.82
PLXDC1	1.598545	0.019032	98.49	62.39
PLXNA1	0.401492	0.009111	1191.87	902.27
PNKD	0.414503	1.63E-12	1189.76	1858.95
PNLIPRP1	-0.2605	0.016616	6086.49	7562.61
POLB	-0.30579	0.010372	30.37	47.45
POLE2	-0.44501	8.23E-11	179.56	251.1
POLR1A	-0.23393	0.039527	453.68	336.15
POLR3H	-0.38424	0.004071	51.66	84.64
PPARG	0.467913	0.006976	3327.33	2678.57
PPP1R2	0.664318	3.35E-07	194.36	280.55
PRAMEF12	4.879678	0.04843	412.34	247.3

PRKAG2	-0.55254	0.008264	17.57	31.47
PRKCA	0.427013	4.34E-05	503.77	1087.18
PRNP	-1.10915	0.006791	719.13	1001.95
PRPS1	-0.27948	0.027952	70.19	109.2
PSAT1	-0.33297	0.007521	607.26	497.35
PSMB8	-0.44738	0.000716	622.18	495.23
PSMC5	-1.1004	0.010835	72.71	106.49
PTCD2	-0.4217	0.00101	131.95	89.44
PTCH2	-0.28746	0.03289	8.69	21.41
PTGFRN	0.400917	0.019856	20.66	5.65
PTGR1	-0.40932	3.07E-15	1433.79	1219.06
PTK2	0.934534	0.001268	349.65	553.18
PTPN13	0.36284	0.01847	37.3	20.75
PTPN18	-0.88133	0.034638	616.17	747.4
PTPRM	0.575629	0.009895	99.49	68.07
PTPRO	0.284745	0.001903	1260.07	1576.36
PTPRZ1	0.593719	0.000402	1306.52	1681.5
PTRF	0.393371	0.000825	406.28	320.61

PXDN	0.303985	0.012477	227.71	169.1
PXK	-0.43185	0.044597	20.33	7.39
RAD51D	-0.31974	0.015615	3926.4	5535.83
RANGAP1	-0.44935	8.65E-24	7076.79	5692.44
RASGRP4	-0.44881	0.045149	2563.3	2161.07
RBMX2	-0.36997	0.035851	20.36	40.39
RBPJL	-1.00908	0.039954	200.36	310.85
RBX1	0.312578	0.012353	1457.01	1077.48
RCC2	-0.28556	0.002383	14.57	30.62
RDH13	-0.34664	0.028159	23.03	38.31
RELB	-0.62927	0.041544	43.21	23.64
RELT	-0.36434	0.006432	772.31	603.71
RETSAT	0.372565	0.000376	350.55	246.32
RGL2	-0.26716	0.008235	106.52	70.25
RGS19	-0.52319	0.002864	5.77	25.76
RNASEH2B	1.044553	0.03518	490.59	353.85
RNF114	-0.83001	0.004506	627.74	826.16
RNF166	0.277855	0.003813	968.28	1256.31

RNF170	-0.55349	0.024434	68.37	97.22
RNF216	0.285542	2.01E-05	592.06	931.83
RPS6KL1	-0.40995	0.000252	168.52	231.87
RREB1	0.47257	0.007831	7420.41	6281.97
RRN3	0.323229	0.002069	5944.91	9388.88
RRP12	-0.38602	0.001798	522.88	413.69
RRP9	-0.33171	1.07E-06	179.96	282.82
RTN4IP1	-0.93874	2.05E-42	98.49	62.39
RXRA	0.363273	0.019032	1191.87	902.27
SAMHD1	-0.40156	0.009111	1189.76	1858.95
SART1	-0.28114	1.63E-12	6086.49	7562.61
SBK1	-0.47929	0.016616	30.37	47.45
SCGB1A1	0.958656	0.010372	179.56	251.1
SDK2	0.405537	8.23E-11	453.68	336.15
SEMA3C	-0.74753	0.039527	51.66	84.64
SEMA6B	-0.32984	0.004071	3327.33	2678.57
SEPHS2	-0.31764	0.006976	194.36	280.55
37135	-0.90046	3.35E-07	412.34	247.3

40787	0.465981	0.04843	17.57	31.47
37865	-1.54865	0.008264	503.77	1087.18
SERPINH1	0.453712	4.34E-05	719.13	1001.95
SFXN5	0.560778	0.006791	70.19	109.2
SH2B3	0.480202	0.027952	607.26	497.35
SH3BP4	0.266219	0.007521	622.18	495.23
SH3GLB1	0.354165	0.000716	72.71	106.49
SH3PXD2A	0.378422	0.010835	131.95	89.44
SHD	-0.53828	0.00101	8.69	21.41
SHROOM3	0.291544	0.03289	20.66	5.65
SIGMAR1	-0.50134	0.019856	1433.79	1219.06
SIPA1L2	0.55035	3.07E-15	349.65	553.18
SIRT4	0.472976	0.001268	37.3	20.75
SIVA1	0.647551	0.01847	616.17	747.4
SLC15A5	0.634791	0.034638	99.49	68.07
SLC1A3	-0.49282	0.009895	1260.07	1576.36
SLC22A18	0.895334	0.001903	1306.52	1681.5
SLC23A1	-0.33937	0.000402	406.28	320.61

SLC25A30	-0.32394	0.000825	227.71	169.1
SLC25A32	-0.32778	0.012477	20.33	7.39
SLC25A33	-0.42962	0.044597	3926.4	5535.83
SLC25A44	-0.41704	0.015615	7076.79	5692.44
SLC25A45	0.395802	8.65E-24	2563.3	2161.07
SLC3A2	-0.33054	0.045149	20.36	40.39
SLC6A6	0.567841	0.035851	200.36	310.85
SLC7A5	-0.34822	0.039954	1457.01	1077.48
SLIT1	0.398171	0.012353	14.57	30.62
SLURP1	-0.4599	0.002383	23.03	38.31
SMARCD2	-1.15243	0.028159	43.21	23.64
SNX16	-0.41175	0.041544	772.31	603.71
SNX21	-0.29573	0.006432	350.55	246.32
SNX33	0.703475	0.000376	106.52	70.25
SOD2	-0.2489	0.008235	5.77	25.76
SORBS1	0.866336	0.002864	490.59	353.85
SORCS2	0.316488	0.03518	627.74	826.16
SPATC1L	0.339152	0.004506	968.28	1256.31

SPR	0.341497	0.003813	68.37	97.22
SPRED2	0.553944	0.024434	592.06	931.83
SPTA1	-1.47012	2.01E-05	168.52	231.87
SPTBN1	0.373367	0.000252	7420.41	6281.97
SPTBN5	0.447895	0.007831	5944.91	9388.88
SREBF2	0.370089	0.002069	522.88	413.69
SRGAP3	0.665602	0.001798	179.96	282.82
SRM	-0.38743	1.07E-06	98.49	62.39
ST3GAL1	0.495378	2.05E-42	1191.87	902.27
ST3GAL3	0.702618	0.019032	1189.76	1858.95
STAB2	-0.64841	0.009111	6086.49	7562.61
STK10	0.392487	1.63E-12	30.37	47.45
STRBP	-0.46922	0.016616	179.56	251.1
STYK1	1.258077	0.010372	453.68	336.15
SULF2	2.724332	8.23E-11	51.66	84.64
SWSAP1	0.613063	0.039527	3327.33	2678.57
SYCP3	-0.52552	0.004071	194.36	280.55
SYNE3	0.833729	0.006976	412.34	247.3

SYNPO2	-0.83363	3.35E-07	17.57	31.47
SYTL4	0.66287	0.04843	503.77	1087.18
TAF10	0.382954	0.008264	719.13	1001.95
TANC1	0.574852	4.34E-05	70.19	109.2
TBC1D16	-0.83259	0.006791	607.26	497.35
TBCCD1	-0.37623	0.027952	622.18	495.23
TCF7	0.612683	0.007521	72.71	106.49
TCN2	-0.95654	0.000716	131.95	89.44
TDGF1	0.385851	0.010835	8.69	21.41
TERT	0.400668	0.00101	20.66	5.65
TESK2	-0.4203	0.03289	1433.79	1219.06
THBS1	0.968187	0.019856	349.65	553.18
TLE3	0.525706	3.07E-15	37.3	20.75
TLR1	-1.13286	0.001268	616.17	747.4
TMBIM1	0.356512	0.01847	99.49	68.07
TMBIM6	0.27122	0.034638	1260.07	1576.36
TMC1	0.552726	0.009895	1306.52	1681.5
TMC4	-0.56265	0.001903	406.28	320.61

TMEM240	-0.28872	0.000402	227.71	169.1
TMEM245	0.444777	0.000825	20.33	7.39
TMEM25	0.630167	0.012477	3926.4	5535.83
TMEM51	0.575057	0.044597	7076.79	5692.44
TMOD1	-1.18003	0.015615	2563.3	2161.07
TNFAIP2	0.471916	8.65E-24	20.36	40.39
TNKS	0.703878	0.045149	200.36	310.85
TNS1	1.327192	0.035851	1457.01	1077.48
TNS3	0.7203	0.039954	14.57	30.62
TPCN1	0.310424	0.012353	23.03	38.31
TREH	0.370574	0.002383	43.21	23.64
TRERF1	0.343976	0.028159	772.31	603.71
TRIM35	0.410377	0.041544	350.55	246.32
TRIM54	-0.33503	0.006432	106.52	70.25
TRIM8	0.286288	0.000376	5.77	25.76
TRIOBP	0.512485	0.008235	490.59	353.85
TRIP10	-0.89922	0.002864	627.74	826.16
TRMT61B	-0.31439	0.03518	968.28	1256.31

TSC1	0.263634	0.004506	68.37	97.22
TSPAN11	1.088778	0.003813	592.06	931.83
TSPAN3	1.039814	0.024434	168.52	231.87
TTN	-0.36391	2.01E-05	7420.41	6281.97
TUFT1	-0.61286	0.000252	5944.91	9388.88
TULP2	-0.32492	0.007831	522.88	413.69
TXNDC17	-0.50255	0.002069	179.96	282.82
UBR5	0.323425	0.001798	98.49	62.39
UCP2	-0.79579	1.07E-06	1191.87	902.27
VANGL2	-0.42502	2.05E-42	1189.76	1858.95
VARS	-0.34559	0.019032	6086.49	7562.61
VCAN	0.712189	0.009111	30.37	47.45
VMP1	0.926339	1.63E-12	179.56	251.1
VWA7	-0.36748	0.016616	453.68	336.15
WARS	0.315501	0.010372	51.66	84.64
WBP2NL	-1.87187	8.23E-11	3327.33	2678.57
WDFY4	0.898595	0.039527	194.36	280.55
WDR12	-0.36613	0.004071	412.34	247.3

WDR43	-0.6218	0.006976	17.57	31.47
WNT4	0.687391	3.35E-07	503.77	1087.18
XAB2	-0.45938	0.04843	719.13	1001.95
ZBTB2	-0.30796	0.008264	70.19	109.2
ZBTB47	-4.44721	4.34E-05	607.26	497.35
ZCCHC24	-0.29752	0.006791	622.18	495.23
ZDHHC24	-0.47172	0.027952	72.71	106.49
ZDHHC7	0.816782	0.007521	131.95	89.44
ZFHX2	-0.32112	0.000716	8.69	21.41
ZFHX3	-0.76508	0.010835	20.66	5.65
ZHX3	-0.36169	0.00101	1433.79	1219.06
ZMAT2	-0.43165	0.03289	349.65	553.18
ZMIZ1	0.591245	0.019856	37.3	20.75
ZNF334	-0.63152	3.07E-15	616.17	747.4
ZNF358	-0.79451	0.001268	99.49	68.07
ZNF395	0.421706	0.01847	1260.07	1576.36
ZNF7	0.374907	0.034638	1306.52	1681.5
ZXDC	1.265381	0.009895	406.28	320.61

ZZEF1	0.357985	0.001903	227.71	169.1

CHO-S Fc miR-24 (Sponge) – Proteomic Profiling

Gene ID	Name	More abundant in	Fold-change	Anova
ACADVL	Very long-chain specific acyl-CoA dehydrogenase, mitochondrial [Cricetulus griseus]	Control	1.33	0.006855
ACSL1	Long-chain-fatty-acid--CoA ligase 1 [Cricetulus griseus]	Control	1.78	0.014342
ACTB	Actin, cytoplasmic 1 [Cricetulus griseus]	Control	1.4	0.000662
ACTN1	Alpha-actinin-1 [Cricetulus griseus]	Control	1.29	0.020151
AFAP1	Actin filament-associated protein 1 [Cricetulus griseus]	Control	2.2	0.002112
AHNAK2	Protein AHNAK2 [Cricetulus griseus]	Control	2.08	0.000334
AIMP2	Aminoacyl tRNA synthetase complex-interacting multifunctional protein 2 [Cricetulus griseus]	Control	1.49	0.048247
ALCAM	CD166 antigen [Cricetulus griseus]	Control	3.13	1.63E-06
ARF4	ADP-ribosylation factor 4 [Cricetulus griseus]	Control	1.45	0.009632
ARHGAP1	Rho GTPase-activating protein 1 [Cricetulus griseus]	Control	1.62	0.036126
ARHGEF2	Rho guanine nucleotide exchange factor 2 [Cricetulus griseus]	Control	1.57	0.015172

ARPC4	Actin-related protein 2/3 complex subunit 4 [Cricetulus griseus]	Control	1.5	0.001712
CAP1	Adenylyl cyclase-associated protein 1 [Cricetulus griseus]	Control	1.74	0.013458
CARMIL1	Leucine-rich repeat-containing protein 16A [Cricetulus griseus]	Control	3.18	0.013164
CASP12	Caspase-12, partial [Cricetulus griseus]	Control	1.63	0.014284
CCT7	T-complex protein 1 subunit eta [Cricetulus griseus]	Control	1.56	0.048791
CCT8	T-complex protein 1 subunit theta [Cricetulus griseus]	Control	1.51	0.027222
CD36	Platelet glycoprotein 4 [Cricetulus griseus]	Control	7	3.58E-06
CDK1	Cell division control protein 2-like [Cricetulus griseus]	Control	1.68	0.002758
CHD4	Chromodomain-helicase-DNA-binding protein 4 [Cricetulus griseus]	Control	1.42	0.049299
CKAP5	Cytoskeleton-associated protein 5 [Cricetulus griseus]	Control	1.86	0.010288
CLIC4	Chloride intracellular channel protein 4 [Cricetulus griseus]	Control	1.28	0.031041
CNN2	Calponin-2 [Cricetulus griseus]	Control	2.03	0.000837
COPA	Coatomer subunit alpha [Cricetulus griseus]	Control	1.56	0.016266

CORO1C	Coronin-1C [Cricetulus griseus]	Control	1.43	0.012681
CSPG4	Chondroitin sulfate proteoglycan 4 [Cricetulus griseus]	Control	1.68	2.53E-05
CTLA2B	Protein CTLA-2-beta [Cricetulus griseus]	Control	14.58	0.000369
CTLA2B	Protein CTLA-2-beta [Cricetulus griseus]	Control	2.37	0.003369
CTSZ	Cathepsin Z [Cricetulus griseus]	Control	1.43	0.009848
CYFIP1	Cytoplasmic FMR1-interacting protein 1 [Cricetulus griseus]	Control	1.61	0.001795
DAB2	Disabled-like 2 [Cricetulus griseus]	Control	1.57	0.005282
DCTN2	Dynactin subunit 2 [Cricetulus griseus]	Control	1.3	0.002976
DLAT	Dihydrolipoyllysine-residue acetyltransferase component of pyruvate dehydrogenase complex, mitochondrial [Cricetulus griseus]	Control	1.48	0.004367
DLG1	Disks large-like 1 [Cricetulus griseus]	Control	1.36	0.025768
DSTN	Destrin [Cricetulus griseus]	Control	1.85	0.002351
DYNC1H1	Cytoplasmic dynein 1 heavy chain 1, partial [Cricetulus griseus]	Control	1.44	0.007737
EIF4A1	Eukaryotic initiation factor 4A-I [Cricetulus griseus]	Control	1.2	0.084736
ENO1	PREDICTED: alpha-enolase isoform X2 [Cricetulus griseus]	Control	2.43	0.021904

EPHA2	Ephrin type-A receptor 2 [Cricetulus griseus]	Control	1.57	0.000114
ETF1	Eukaryotic peptide chain release factor subunit 1 [Cricetulus griseus]	Control	1.34	0.008763
FAAH	Fatty-acid amide hydrolase 1 [Cricetulus griseus]	Control	1.71	0.006811
FASN	Fatty acid synthase [Cricetulus griseus]	Control	1.71	0.002266
FERMT2	Fermitin family-like 2 [Cricetulus griseus]	Control	1.69	0.007001
FLNB	Filamin-B [Cricetulus griseus]	Control	2.29	0.00924
GALNT2	PREDICTED: polypeptide N-acetylgalactosaminyltransferase 2 [Cricetulus griseus]	Control	1.67	0.005331
GAPDH	glyceraldehyde-3-phosphate dehydrogenase [Cricetulus griseus]	Control	1.5	0.000611
GDI2	Rab GDP dissociation inhibitor beta [Cricetulus griseus]	Control	1.33	0.00019
GLG1	latent TGF-beta complexed protein (LTCP) [Cricetulus griseus]	Control	1.32	0.004413
GLO1	Lactoylglutathione lyase [Cricetulus griseus]	Control	1.53	0.017488
GPC1	Glypican-1 [Cricetulus griseus]	Control	1.62	8.76E-05
GPDH	Glycerol-3-phosphate dehydrogenase [NAD+], cytoplasmic [Cricetulus griseus]	Control	2	0.00016

GSTM6	Glutathione S-transferase Mu 6 [Cricetulus griseus]	Control	1.72	0.016092
GSTM7	Glutathione S-transferase Mu 7 [Cricetulus griseus]	Control	1.89	0.010407
HDGFL2	Hepatoma-derived growth factor-related protein 2 [Cricetulus griseus]	Control	1.72	0.015263
HDLBP	Vigilin [Cricetulus griseus]	Control	1.55	0.004727
HMGCS1	Hydroxymethylglutaryl-CoA synthase, cytoplasmic [Cricetulus griseus]	Control	1.59	0.000349
IDH1	Isocitrate dehydrogenase [NADP] cytoplasmic [Cricetulus griseus]	Control	1.92	0.002038
IPO4	Importin-4 [Cricetulus griseus]	Control	1.82	0.029183
IPO5	Importin-5 [Cricetulus griseus]	Control	1.65	0.030691
ITGA3	Integrin alpha-3 [Cricetulus griseus]	Control	2.11	0.000909
ITGA5	Integrin alpha-5 [Cricetulus griseus]	Control	1.51	0.007201
ITGAV	Integrin alpha-V [Cricetulus griseus]	Control	1.5	0.020807
ITGB1	Integrin beta-1 [Cricetulus griseus]	Control	1.44	0.000265
KIF5B	PREDICTED: kinesin-1 heavy chain isoform X2 [Cricetulus griseus]	Control	1.3	0.004739
KLC1	Kinesin light chain 1 [Cricetulus griseus]	Control	1.78	0.016381
KPNB1	Importin subunit beta-1 [Cricetulus griseus]	Control	1.29	0.008704

LAMP2	lysosome-associated membrane glycoprotein 2 precursor [Cricetulus griseus]	Control	1.47	0.012262
LAP3	Cytosol aminopeptidase [Cricetulus griseus]	Control	1.38	0.039703
LDHA	L-lactate dehydrogenase A chain [Cricetulus griseus]	Control	2.22	0.006102
LDLR	RecName: Full=Low-density lipoprotein receptor; Short=LDL receptor; Flags: Precursor	Control	1.36	0.021391
LGALS1	Lectin galactoside-binding soluble 1	Control	1.58	0.001334
LGALS3	Galectin-3 [Cricetulus griseus]	Control	1.37	0.003448
LOC100757491	Histone H3 [Cricetulus griseus]	Control	12.04	0.017064
MAP1S	Microtubule-associated protein 1S [Cricetulus griseus]	Control	1.26	0.027674
MEMO1	PREDICTED: protein MEMO1 isoform X2 [Cricetulus griseus]	Control	1.6	0.027637
MFGE8	PREDICTED: lactadherin isoform X1 [Cricetulus griseus]	Control	1.37	0.023936
MMS19	MMS19 nucleotide excision repair protein-like [Cricetulus griseus]	Control	2.28	0.019004
MPP1	55 kDa erythrocyte membrane protein [Cricetulus griseus]	Control	1.54	0.001624
MTHFD1	C-1-tetrahydrofolate synthase, cytoplasmic [Cricetulus griseus]	Control	1.14	0.040844

MVP	Major vault protein [Cricetulus griseus]	Control	1.64	0.013223
MYADM	Myeloid-associated differentiation marker [Cricetulus griseus]	Control	1.27	0.004059
MYH10	Myosin-10 [Cricetulus griseus]	Control	2.31	1.83E-05
MYH9	PREDICTED: myosin-9 isoform X2 [Cricetulus griseus]	Control	2.83	5.63E-06
MYL12B	Myosin regulatory light chain 12B [Cricetulus griseus]	Control	1.9	0.000293
MYL6	Myosin light polypeptide 6 [Cricetulus griseus]	Control	1.42	0.000236
MYO1C	Myosin-Ic [Cricetulus griseus]	Control	1.52	0.011441
MYOF	Myoferlin [Cricetulus griseus]	Control	1.42	0.013826
NDRG3	Protein NDRG3 [Cricetulus griseus]	Control	2.7	0.004605
NDUFA8	NADH dehydrogenase [ubiquinone] 1 alpha subcomplex subunit 8 [Cricetulus griseus]	Control	1.54	0.018605
NDUFS1	NADH-ubiquinone oxidoreductase 75 kDa subunit, mitochondrial [Cricetulus griseus]	Control	2.56	0.038355
NDUFV1	NADH dehydrogenase [ubiquinone] flavoprotein 1, mitochondrial [Cricetulus griseus]	Control	1.38	0.003759
NHLRC2	NHL repeat-containing protein 2 [Cricetulus griseus]	Control	1.34	0.000227

P4HB	protein disulfide-isomerase precursor [Cricetulus griseus]	Control	1.92	0.030905
PCCA	Propionyl-CoA carboxylase alpha chain, mitochondrial [Cricetulus griseus]	Control	2	3.01E-05
PCNA	proliferating cell nuclear antigen [Cricetulus griseus]	Control	1.51	0.010597
PDLIM7	PDZ and LIM domain protein 7 [Cricetulus griseus]	Control	1.87	0.001146
PGAM1	Phosphoglycerate mutase 1 [Cricetulus griseus]	Control	1.39	0.007127
PLA2G4E	EH domain-containing protein 4 [Cricetulus griseus]	Control	1.78	0.000654
PLAA	Phospholipase A-2-activating protein [Cricetulus griseus]	Control	1.36	0.056936
PLEC	Plectin-1 [Cricetulus griseus]	Control	1.5	0.011258
PLEC	hypothetical protein I79_015376 [Cricetulus griseus]	Control	1.5	9.38E-05
PLIN3	Mannose-6-phosphate receptor-binding protein 1 [Cricetulus griseus]	Control	2.06	0.005715
PRKACA	cAMP-dependent protein kinase catalytic subunit alpha [Cricetulus griseus]	Control	2.37	0.023361
PRKAR1A	cAMP-dependent protein kinase type I-alpha regulatory subunit [Cricetulus griseus]	Control	2.31	0.022856

PSMB7	Proteasome subunit beta type-7 [Cricetulus griseus]	Control	1.27	0.01611
PSMC4	26S protease regulatory subunit 6B, partial [Cricetulus griseus]	Control	1.61	0.041244
PSMD2	26S proteasome non-ATPase regulatory subunit 2 [Cricetulus griseus]	Control	1.37	0.011375
PSMG1	Proteasome assembly chaperone 1 [Cricetulus griseus]	Control	1.5	0.028846
PTBP3	Regulator of differentiation 1 [Cricetulus griseus]	Control	1.84	0.0123
PTGFRN	Prostaglandin F2 receptor negative regulator [Cricetulus griseus]	Control	1.65	0.000482
RAB11B	Ras-related protein Rab-11B [Cricetulus griseus]	Control	1.47	0.007697
RAB2B	Ras-related protein Rab-2B [Cricetulus griseus]	Control	1.37	0.011692
RAB5C	Ras-related protein Rab-5C [Cricetulus griseus]	Control	1.45	0.004813
RANSET2	Ribonuclease T2 [Cricetulus griseus]	Control	2.01	0.002388
RPLP0	60S acidic ribosomal protein P0 [Cricetulus griseus]	Control	1.45	0.008041
RRM2	Ribonucleoside-diphosphate reductase subunit M2 [Cricetulus griseus]	Control	2.15	0.000477
S100A16	Protein S100-A16 [Cricetulus griseus]	Control	1.81	0.00206

S100A5	Protein S100-A5 [Cricetulus griseus]	Control	1.93	0.000367
S100A6	Protein S100-A6 [Cricetulus griseus]	Control	1.32	0.019891
SEPT6	Septin-6 [Cricetulus griseus]	Control	2.05	0.000125
SF1	PREDICTED: splicing factor 1 [Cricetulus griseus]	Control	1.32	0.037637
SF3A3	Splicing factor 3A subunit 3 [Cricetulus griseus]	Control	1.46	0.039789
SLC1A4	neutral amino acid transporter type 1 [Cricetulus griseus]	Control	1.58	0.00493
SLC25A20	Mitochondrial carnitine/acylcarnitine carrier protein [Cricetulus griseus]	Control	2.18	0.040367
SLC25A24	Calcium-binding mitochondrial carrier protein SCaMC-1 [Cricetulus griseus]	Control	2.06	0.007961
SNX9	Sorting nexin-9 [Cricetulus griseus]	Control	1.49	0.002421
SPTAN1	Spectrin alpha chain, brain [Cricetulus griseus]	Control	1.79	0.037511
SPTBN1	Spectrin beta chain, brain 1 [Cricetulus griseus]	Control	1.65	0.000175
STUB1	STIP1-likey and U box-containing protein 1 [Cricetulus griseus]	Control	1.77	0.001039
TGM2	Protein-glutamine gamma-glutamyltransferase 2 [Cricetulus griseus]	Control	1.47	0.006735

TPP2	PREDICTED: tripeptidyl-peptidase 2 isoform X6 [Cricetulus griseus]	Control	1.44	0.010295
TRA2B	Transformer-2 protein-like beta [Cricetulus griseus]	Control	1.28	0.00668
TUBB4A	Tubulin beta-4 chain [Cricetulus griseus]	Control	1.47	0.010237
UBE2C	Ubiquitin-conjugating enzyme E2 C [Cricetulus griseus]	Control	1.52	0.001476
UGDH	UDP-glucose 6-dehydrogenase [Cricetulus griseus]	Control	1.8	0.002139
USP10	Ubiquitin carboxyl-terminal hydrolase 10 [Cricetulus griseus]	Control	1.33	0.015262
USP15	Ubiquitin carboxyl-terminal hydrolase 15 [Cricetulus griseus]	Control	1.42	0.001316
UTP15	U3 small nucleolar RNA-associated protein 15-like [Cricetulus griseus]	Control	1.29	0.032082
VNN1	Pantetheinase [Cricetulus griseus]	Control	2.07	0.000488
VPS35	Vacuolar protein sorting-associated protein 35 [Cricetulus griseus]	Control	1.44	0.038762
VWA5A	von Willebrand factor A domain-containing protein 5A [Cricetulus griseus]	Control	1.72	8.09E-05
WDR1	PREDICTED: WD repeat-containing protein 1 isoform X2 [Cricetulus griseus]	Control	1.6	0.001642
YWHAH	14-3-3 protein eta [Cricetulus griseus]	Control	1.47	0.009735

*	Glycosyltransferase 25 family member 1 [Cricetulus griseus]	mIR-24	1.36	0.012099
ABCE1	ATP-binding cassette sub-family E member 1 [Cricetulus griseus]	mIR-24	1.26	0.004335
ABCF1	ATP-binding cassette sub-family F member 1 [Cricetulus griseus]	mIR-24	1.54	0.017853
ACAD9	Acyl-CoA dehydrogenase family member 9, mitochondrial [Cricetulus griseus]	mIR-24	1.47	0.009745
ACAT1	Acetyl-CoA acetyltransferase, mitochondrial [Cricetulus griseus]	mIR-24	1.3	0.011472
ADRM1	Proteasomal ubiquitin receptor ADRM1 [Cricetulus griseus]	mIR-24	1.29	0.015862
AFG3L2	AFG3-like protein 2 [Cricetulus griseus]	mIR-24	1.58	0.006681
AHCY	Adenosylhomocysteinase [Cricetulus griseus]	mIR-24	1.31	0.001541
AHCYL1	Putative adenosylhomocysteinase 2 [Cricetulus griseus]	mIR-24	1.43	0.01648
AHSA1	Activator of 90 kDa heat shock protein ATPase-like 1 [Cricetulus griseus]	mIR-24	1.27	0.027662
AIMP1	multisynthetase complex auxiliary component p43 [Cricetulus griseus]	mIR-24	1.54	0.031332
AIRE	Autoimmune regulator [Cricetulus griseus]	mIR-24	1.42	0.018937
AKR1B1	Aldose reductase [Cricetulus griseus]	mIR-24	1.34	0.000104

AKR1B10	Aldo-keto reductase family 1 member B10 [Cricetulus griseus]	mIR-24	3.08	0.000317
AKR1B8	aldose reductase-related protein 2 [Cricetulus griseus]	mIR-24	1.96	0.000183
ALDH2	Aldehyde dehydrogenase, mitochondrial [Cricetulus griseus]	mIR-24	1.36	8.59E-05
ALDH7A1	Alpha-aminoadipic semialdehyde dehydrogenase [Cricetulus griseus]	mIR-24	1.3	0.02933
ALDOA	Fructose-bisphosphate aldolase A [Cricetulus griseus]	mIR-24	1.32	0.033149
ANXA1	Annexin A1 [Cricetulus griseus]	mIR-24	1.5	0.013146
ANXA11	Annexin A11 [Cricetulus griseus]	mIR-24	1.4	0.007018
APEX1	DNA-(apurinic or apyrimidinic site) lyase [Cricetulus griseus]	mIR-24	1.53	0.001498
ASUN	Cell cycle regulator Mat89Bb-like [Cricetulus griseus]	mIR-24	2.49	0.000379
ATAD3A	ATPase family AAA domain-containing protein 3 [Cricetulus griseus]	mIR-24	1.42	0.003156
ATP2A1	Sarcoplasmic/endoplasmic reticulum calcium ATPase 1 [Cricetulus griseus]	mIR-24	1.31	0.007275
ATP2A2	Sarcoplasmic/endoplasmic reticulum calcium ATPase 2 [Cricetulus griseus]	mIR-24	1.41	0.026601
ATP5B	ATP synthase subunit beta, mitochondrial [Cricetulus griseus]	mIR-24	1.33	0.032882

ATP5C1	ATP synthase subunit gamma, mitochondrial [Cricetulus griseus]	mIR-24	1.35	0.002065
ATP5D	ATP synthase subunit delta, mitochondrial [Cricetulus griseus]	mIR-24	1.28	0.070538
ATP5F1	PREDICTED: ATP synthase F(0) complex subunit B1, mitochondrial isoform X1 [Cricetulus griseus]	mIR-24	1.29	0.000639
ATP5H	ATP synthase subunit d, mitochondrial [Cricetulus griseus]	mIR-24	1.29	0.017302
ATXN2	Ataxin-2, partial [Cricetulus griseus]	mIR-24	1.28	0.016439
ATXN2L	PREDICTED: ataxin-2-like protein isoform X13 [Cricetulus griseus]	mIR-24	1.26	0.018663
BAG3	BAG family molecular chaperone regulator 3 [Cricetulus griseus]	mIR-24	1.52	0.005742
BUB3	Mitotic checkpoint protein BUB3 [Cricetulus griseus]	mIR-24	1.3	0.028922
BZW2	Basic leucine zipper and W2 domain-containing protein 2 [Cricetulus griseus]	mIR-24	1.42	0.000283
CALR	Calreticulin [Cricetulus griseus]	mIR-24	1.3	0.000276
CALU	Calumenin [Cricetulus griseus]	mIR-24	1.71	0.002119
CAND1	Cullin-associated NEDD8-dissociated protein 1 [Cricetulus griseus]	mIR-24	1.31	0.011178
CANX	Calnexin [Cricetulus griseus]	mIR-24	1.48	0.002229

CAT	Catalase [Cricetulus griseus]	mIR-24	1.35	0.002814
CBR3	Carbonyl reductase [NADPH] 3 [Cricetulus griseus]	mIR-24	1.26	0.010759
CCT8	T-complex protein 1 subunit theta [Cricetulus griseus]	mIR-24	1.3	0.001556
CEBPZ	CCAAT/enhancer-binding protein zeta [Cricetulus griseus]	mIR-24	1.69	0.011993
CLPP	Putative ATP-dependent Clp protease proteolytic subunit, mitochondrial [Cricetulus griseus]	mIR-24	1.46	0.039538
CMAS	N-acylneuraminate cytidylyltransferase [Cricetulus griseus]	mIR-24	2.05	1.84E-05
CNBP	Cellular nucleic acid-binding protein [Cricetulus griseus]	mIR-24	1.85	0.004321
CSE1L	Exportin-2 [Cricetulus griseus]	mIR-24	1.36	0.026768
CSNK2B	Casein kinase II subunit beta [Cricetulus griseus]	mIR-24	1.37	0.001843
CSTF2	Cleavage stimulation factor 64 kDa subunit [Cricetulus griseus]	mIR-24	1.7	0.007249
CTSA	Lysosomal protective protein [Cricetulus griseus]	mIR-24	1.32	0.015781
DAP3	28S ribosomal protein S29, mitochondrial [Cricetulus griseus]	mIR-24	1.49	0.009249
DDB1	DNA damage-binding protein 1 [Cricetulus griseus]	mIR-24	1.31	0.001222

DDX1	ATP-dependent RNA helicase DDX1 [Cricetulus griseus]	mIR-24	1.26	0.000182
DDX19A	ATP-dependent RNA helicase DDX19A [Cricetulus griseus]	mIR-24	1.28	0.010245
DDX21	Nucleolar RNA helicase 2 [Cricetulus griseus]	mIR-24	1.3	0.003036
DDX39B	Spliceosome RNA helicase BAT1 [Cricetulus griseus]	mIR-24	1.3	0.015989
DDX3X	ATP-dependent RNA helicase DDX3X [Cricetulus griseus]	mIR-24	1.32	3.81E-05
DDX47	putative ATP-dependent RNA helicase DDX47 [Cricetulus griseus]	mIR-24	1.76	0.000812
DDX5	putative ATP-dependent RNA helicase DDX5 [Cricetulus griseus]	mIR-24	2.01	0.012501
DDX56	putative ATP-dependent RNA helicase DDX56 [Cricetulus griseus]	mIR-24	1.57	0.008844
DHFR	Dihydrofolate reductase [Cricetulus griseus]	mIR-24	4.22	0.000152
DNAJA2	PREDICTED: dnaJ homolog subfamily A member 2 isoform X2 [Cricetulus griseus]	mIR-24	1.37	0.002452
DNAJC11	DnaJ-like subfamily C member 11 [Cricetulus griseus]	mIR-24	1.29	0.011819
DNAJC8	DnaJ-like subfamily C member 8 [Cricetulus griseus]	mIR-24	1.31	0.012966

DNTTIP2	Deoxynucleotidyltransferase terminal-interacting protein 2 [Cricetulus griseus]	mIR-24	1.46	0.011345
DPP7	Dipeptidyl-peptidase 2 [Cricetulus griseus]	mIR-24	1.28	0.012718
DRG1	Developmentally-regulated GTP-binding protein 1 [Cricetulus griseus]	mIR-24	1.43	0.026052
EEF1D	Elongation factor 1-delta [Cricetulus griseus]	mIR-24	1.39	0.019266
EEF1G	Elongation factor 1-gamma [Cricetulus griseus]	mIR-24	1.4	0.027449
EEF2	Elongation factor 2 [Cricetulus griseus]	mIR-24	1.23	0.000277
EFHD2	EF-hand domain-containing protein D2 [Cricetulus griseus]	mIR-24	1.45	0.003517
EHD1	EH domain-containing protein 1 [Cricetulus griseus]	mIR-24	1.49	0.000101
EIF2B4	Translation initiation factor eIF-2B subunit delta [Cricetulus griseus]	mIR-24	1.36	0.013214
EIF2S2	Eukaryotic translation initiation factor 2 subunit 2 [Cricetulus griseus]	mIR-24	1.19	0.062663
EIF3G	Eukaryotic translation initiation factor 3 subunit G [Cricetulus griseus]	mIR-24	2.01	0.004199
EIF3L	Eukaryotic translation initiation factor 3 subunit L [Cricetulus griseus]	mIR-24	1.4	0.001022
EIF5A2	Eukaryotic translation initiation factor 5A-2 [Cricetulus griseus]	mIR-24	1.39	0.01664

EIF5B	Eukaryotic translation initiation factor 5B [Cricetulus griseus]	mIR-24	1.41	0.003758
EIF6	Eukaryotic translation initiation factor 6 [Cricetulus griseus]	mIR-24	1.4	0.001529
ELP1	Elongator complex protein 1 [Cricetulus griseus]	mIR-24	1.29	0.001873
ELP3	Elongator complex protein 3 [Cricetulus griseus]	mIR-24	1.38	0.021238
EML4	Echinoderm microtubule-associated protein-like 4, partial [Cricetulus griseus]	mIR-24	1.87	0.009485
EPDR1	Mammalian ependymin-related protein 1 [Cricetulus griseus]	mIR-24	1.76	0.000419
EPHX1	Epoxide hydrolase 1 [Cricetulus griseus]	mIR-24	1.34	0.009354
ERP29	Endoplasmic reticulum protein ERp29 [Cricetulus griseus]	mIR-24	1.36	0.017371
ESD	S-formylglutathione hydrolase [Cricetulus griseus]	mIR-24	1.32	0.018366
EXOSC9	Exosome complex exonuclease RRP45 [Cricetulus griseus]	mIR-24	1.42	0.016084
FKBP10	FK506-binding protein 10 [Cricetulus griseus]	mIR-24	1.39	0.003103
FKBP4	FK506-binding protein 4 [Cricetulus griseus]	mIR-24	1.28	0.000155
FLNC	Filamin-C [Cricetulus griseus]	mIR-24	4.09	7.87E-05

FTSJ3	Putative rRNA methyltransferase 3 [Cricetulus griseus]	mIR-24	1.35	0.023726
GAA	PREDICTED: lysosomal alpha-glucosidase isoform X2 [Cricetulus griseus]	mIR-24	1.41	0.003153
GALK1	Galactokinase [Cricetulus griseus]	mIR-24	1.28	0.008349
GART	Trifunctional purine biosynthetic protein adenosine-3 [Cricetulus griseus]	mIR-24	1.31	0.000991
GFM1	Elongation factor G, mitochondrial [Cricetulus griseus]	mIR-24	1.35	0.008702
GOT1	Aspartate aminotransferase, cytoplasmic [Cricetulus griseus]	mIR-24	1.31	0.009104
GOT2	Aspartate aminotransferase, mitochondrial [Cricetulus griseus]	mIR-24	1.3	0.02913
GPI	glucose phosphate isomerase [Cricetulus griseus]	mIR-24	1.36	0.024393
GRPEL1	GrpE protein-like 1, mitochondrial [Cricetulus griseus]	mIR-24	1.28	0.006868
GSPT1	Eukaryotic peptide chain release factor GTP-binding subunit ERF3B [Cricetulus griseus]	mIR-24	1.32	0.000724
GSTA3	Glutathione S-transferase alpha-3 [Cricetulus griseus]	mIR-24	1.5	0.00032
GSTA4	Glutathione S-transferase A4 [Cricetulus griseus]	mIR-24	1.5	0.00082

GSTP1	Glutathione S-transferase P [Cricetulus griseus]	mIR-24	1.37	0.005148
GTPBP4	Nucleolar GTP-binding protein 1 [Cricetulus griseus]	mIR-24	1.44	0.001507
H1F0	Histone H1.0 [Cricetulus griseus]	mIR-24	1.34	0.003095
HARS2	putative histidyl-tRNA synthetase, mitochondrial [Cricetulus griseus]	mIR-24	1.32	0.000492
HEATR1	hypothetical protein I79_015294 [Cricetulus griseus]	mIR-24	1.54	0.000842
HEBP1	Heme-binding protein 1 [Cricetulus griseus]	mIR-24	1.63	0.01115
HMGCS2	Hydroxymethylglutaryl-CoA synthase, mitochondrial [Cricetulus griseus]	mIR-24	1.62	0.010528
HNRNPA1	Putative heterogeneous nuclear ribonucleoprotein A1-like protein 3 [Cricetulus griseus]	mIR-24	1.46	0.004402
HNRNPA2B1	Heterogeneous nuclear ribonucleoproteins A2/B1 [Cricetulus griseus]	mIR-24	1.44	0.007648
HNRNPA3	PREDICTED: heterogeneous nuclear ribonucleoprotein A3 isoform X2 [Cricetulus griseus]	mIR-24	1.3	0.019314
HNRNPAB	Heterogeneous nuclear ribonucleoprotein A/B [Cricetulus griseus]	mIR-24	1.4	0.003547
HNRNPM	Heterogeneous nuclear ribonucleoprotein M [Cricetulus griseus]	mIR-24	1.32	0.000462

HNRNPR	Heterogeneous nuclear ribonucleoprotein R [Cricetulus griseus]	mIR-24	1.4	0.021491
HNRNPU	PREDICTED: heterogeneous nuclear ribonucleoprotein U, partial [Cricetulus griseus]	mIR-24	1.27	0.007209
HNRNPUL2	Heterogeneous nuclear ribonucleoprotein U-like protein 2 [Cricetulus griseus]	mIR-24	1.44	0.015738
HSD17B10	3-hydroxyacyl-CoA dehydrogenase type-2 [Cricetulus griseus]	mIR-24	1.49	0.000441
HSP90B1	Endoplasmin [Cricetulus griseus]	mIR-24	1.23	0.001374
HSPA4	Heat shock 70 kDa protein 4, partial [Cricetulus griseus]	mIR-24	1.44	0.015464
HSPA5	78 kDa glucose-regulated protein precursor [Cricetulus griseus]	mIR-24	1.34	0.00864
HSPA9	stress-70 protein, mitochondrial [Cricetulus griseus]	mIR-24	1.29	0.000673
HSPE1	PREDICTED: 10 kDa heat shock protein, mitochondrial [Cricetulus griseus]	mIR-24	1.3	0.011299
HUWE1	E3 ubiquitin-protein ligase HUWE1, partial [Cricetulus griseus]	mIR-24	1.29	0.002081
IARS	PREDICTED: isoleucine--tRNA ligase, cytoplasmic isoform X2 [Cricetulus griseus]	mIR-24	1.63	0.006384
ILF3	Interleukin enhancer-binding factor 3 [Cricetulus griseus]	mIR-24	1.71	0.019111

IMPDH1	Inosine-5'-monophosphate dehydrogenase 1 [Cricetulus griseus]	mIR-24	1.28	0.001861
IMPDH2	RecName: Full=Inosine-5'-monophosphate dehydrogenase 2; Short=IMP dehydrogenase 2; Short=IMPD 2; Short=IMPDH 2; AltName: Full=IMPDH-II	mIR-24	1.36	0.007728
ISYNA1	Inositol-3-phosphate synthase 1 [Cricetulus griseus]	mIR-24	1.4	0.001108
ITPR3	Inositol 1,4,5-trisphosphate receptor type 3 [Cricetulus griseus]	mIR-24	1.98	0.000222
KARS	Lysyl-tRNA synthetase [Cricetulus griseus]	mIR-24	1.33	0.001164
KHSRP	Far upstream element-binding protein 2 [Cricetulus griseus]	mIR-24	1.32	0.004545
KLHDC4	Kelch domain-containing protein 4 [Cricetulus griseus]	mIR-24	1.63	0.030509
LAMC1	Laminin subunit gamma-1 [Cricetulus griseus]	mIR-24	1.32	0.007947
LARS	Leucyl-tRNA synthetase, cytoplasmic [Cricetulus griseus]	mIR-24	1.34	0.011782
LARS	Leucyl-tRNA synthetase, cytoplasmic [Cricetulus griseus]	mIR-24	1.34	0.000158
LBHD1	hypothetical protein I79_016739 [Cricetulus griseus]	mIR-24	1.46	0.018541
LBR	Lamin-B receptor [Cricetulus griseus]	mIR-24	1.32	0.001199

LCT	Lactase-phlorizin hydrolase [Cricetulus griseus]	mIR-24	1.66	0.034181
LOC100772531	Suppressor of SWI4 1-like [Cricetulus griseus]	mIR-24	1.52	0.012511
LONP1	Lon protease-like, mitochondrial [Cricetulus griseus]	mIR-24	1.32	0.00272
LRPPRC	Leucine-rich PPR motif-containing protein, mitochondrial [Cricetulus griseus]	mIR-24	1.35	0.000234
LTA4H	Leukotriene A-4 hydrolase [Cricetulus griseus]	mIR-24	1.4	0.008993
LUC7L3	PREDICTED: luc7-like protein 3 isoform X1 [Cricetulus griseus]	mIR-24	1.29	0.019802
LYAR	Cell growth-regulating nucleolar protein [Cricetulus griseus]	mIR-24	2.77	0.020454
MATR3	Matrin-3 [Cricetulus griseus]	mIR-24	1.38	0.001022
MCM5	DNA replication licensing factor MCM5 [Cricetulus griseus]	mIR-24	3.56	3.89E-05
MDH2	Malate dehydrogenase, mitochondrial, partial [Cricetulus griseus]	mIR-24	1.27	0.013815
MRPS27	28S ribosomal protein S27, mitochondrial [Cricetulus griseus]	mIR-24	1.62	0.012011
MRPS35	28S ribosomal protein S35, mitochondrial [Cricetulus griseus]	mIR-24	2.14	0.000934
MRPS9	28S ribosomal protein S9, mitochondrial [Cricetulus griseus]	mIR-24	1.51	0.032616

MRTO4	mRNA turnover protein 4-like, partial [Cricetulus griseus]	mIR-24	1.34	0.004978
MYBBP1A	Myb-binding protein 1A [Cricetulus griseus]	mIR-24	1.37	0.002094
NAA15	NMDA receptor-regulated protein 1 [Cricetulus griseus]	mIR-24	1.3	0.012901
NAA50	N-acetyltransferase NAT13 [Cricetulus griseus]	mIR-24	1.35	8.16E-05
NARS	Asparaginyl-tRNA synthetase, cytoplasmic [Cricetulus griseus]	mIR-24	1.43	0.003182
NASP	PREDICTED: nuclear autoantigenic sperm protein isoform X1 [Cricetulus griseus]	mIR-24	1.34	0.001532
NAT10	N-acetyltransferase 10 [Cricetulus griseus]	mIR-24	1.48	0.001676
NCLN	Nicalin [Cricetulus griseus]	mIR-24	1.53	0.008406
NIFK	MKI67 FHA domain-interacting nucleolar phosphoprotein [Cricetulus griseus]	mIR-24	1.64	0.031959
NME2	Nucleoside diphosphate kinase B [Cricetulus griseus]	mIR-24	1.34	0.001638
NOC2L	Nucleolar complex protein 2-like [Cricetulus griseus]	mIR-24	1.56	0.036155
NOL10	Nucleolar protein 10 [Cricetulus griseus]	mIR-24	1.8	0.003445
NOLC1	Nucleolar phosphoprotein p130 [Cricetulus griseus]	mIR-24	1.55	0.000564

NOMO1	PREDICTED: nodal modulator 1 isoform X2, partial [Cricetulus griseus]	mIR-24	1.37	0.000969
NOP2	Putative ribosomal RNA methyltransferase NOP2 [Cricetulus griseus]	mIR-24	1.27	0.015608
NPM1	Nucleophosmin [Cricetulus griseus]	mIR-24	1.33	0.00651
NSUN2	tRNA (cytosine-5-)-methyltransferase NSUN2 [Cricetulus griseus]	mIR-24	1.47	0.004212
NT5C2	Cytosolic purine 5'-nucleotidase [Cricetulus griseus]	mIR-24	1.28	0.021542
NUCB1	Nucleobindin-1 [Cricetulus griseus]	mIR-24	2.67	0.04012
NUDC	Nuclear migration protein nudC [Cricetulus griseus]	mIR-24	1.29	0.009453
NUMA1	Nuclear mitotic apparatus protein 1 [Cricetulus griseus]	mIR-24	1.38	0.015185
NUP153	Nuclear pore complex protein Nup153 [Cricetulus griseus]	mIR-24	1.35	0.01522
NUP93	Nuclear pore complex protein Nup93 [Cricetulus griseus]	mIR-24	1.36	0.003455
PA2G4	Proliferation-associated protein 2G4 [Cricetulus griseus]	mIR-24	1.29	0.002106
PARP1	poly [ADP-ribose] polymerase 1 [Cricetulus griseus]	mIR-24	1.37	0.000557
PCBP1	Poly(rC)-binding protein 1 [Cricetulus griseus]	mIR-24	1.45	0.00115

PCK2	Phosphoenolpyruvate carboxykinase [GTP], mitochondrial [Cricetulus griseus]	mIR-24	1.4	0.012219
PCYT2	Ethanolamine-phosphate cytidylyltransferase [Cricetulus griseus]	mIR-24	2.03	0.040112
PDIA4	Protein disulfide-isomerase A4 [Cricetulus griseus]	mIR-24	1.36	0.01444
PFAS	Phosphoribosylformylglycinamidine synthase [Cricetulus griseus]	mIR-24	1.56	0.004929
PGD	6-phosphogluconate dehydrogenase, decarboxylating [Cricetulus griseus]	mIR-24	1.29	0.001711
PHB	Prohibitin [Cricetulus griseus]	mIR-24	1.32	0.019767
PHB2	Prohibitin-2 [Cricetulus griseus]	mIR-24	1.53	0.014341
PLCD1	1-phosphatidylinositol-4,5-bisphosphate phosphodiesterase delta-1 [Cricetulus griseus]	mIR-24	1.55	0.031416
PLOD1	Procollagen-lysine,2-oxoglutarate 5-dioxygenase 1 [Cricetulus griseus]	mIR-24	1.51	0.013623
PMPCA	PREDICTED: mitochondrial-processing peptidase subunit alpha isoform X1 [Cricetulus griseus]	mIR-24	1.53	0.002638
PNN	Pinin [Cricetulus griseus]	mIR-24	1.37	0.000221
POLDIP3	Polymerase delta-interacting protein 3, partial [Cricetulus griseus]	mIR-24	1.46	0.008521
PPFIBP1	Liprin-beta-1 [Cricetulus griseus]	mIR-24	2.96	2.37E-05

PPM1G	Protein phosphatase 1G [Cricetulus griseus]	mIR-24	1.45	0.009857
PPP2R1A	Serine/threonine-protein phosphatase 2A 65 kDa regulatory subunit A alpha isoform, partial [Cricetulus griseus]	mIR-24	1.32	0.016659
PRDX1	thioredoxin peroxidase II [Cricetulus griseus]	mIR-24	1.31	0.005345
PRDX3	Thioredoxin-dependent peroxide reductase, mitochondrial [Cricetulus griseus]	mIR-24	1.43	0.000715
PRKCSH	Glucosidase 2 subunit beta [Cricetulus griseus]	mIR-24	1.32	0.024168
PRMT1	Protein arginine N-methyltransferase 1 [Cricetulus griseus]	mIR-24	1.45	0.022119
PRPS2	Ribose-phosphate pyrophosphokinase 2 [Cricetulus griseus]	mIR-24	1.37	0.030915
PSMA1	Proteasome subunit alpha type-1 [Cricetulus griseus]	mIR-24	1.37	0.012945
PSMA3	Proteasome subunit alpha type-3 [Cricetulus griseus]	mIR-24	1.58	2.98E-05
PSMA7	Proteasome subunit alpha type-7, partial [Cricetulus griseus]	mIR-24	1.44	0.000213
PSMB4	Proteasome subunit beta type-4 [Cricetulus griseus]	mIR-24	1.36	0.031699
PSME2	Proteasome activator complex subunit 2 [Cricetulus griseus]	mIR-24	1.3	0.011584

PSPH	Phosphoserine phosphatase [Cricetulus griseus]	mIR-24	1.37	0.008783
PUM3	Pumilio domain-containing protein KIAA0020-like [Cricetulus griseus]	mIR-24	1.57	0.002624
RACK1	Guanine nucleotide-binding protein subunit beta-2-like 1 [Cricetulus griseus]	mIR-24	1.31	0.008033
RAD23B	PREDICTED: LOW QUALITY PROTEIN: UV excision repair protein RAD23 homolog B isoform X2 [Cricetulus griseus]	mIR-24	1.26	0.011592
RALY	RNA-binding protein Raly [Cricetulus griseus]	mIR-24	1.39	0.00679
RANBP2	E3 SUMO-protein ligase RanBP2 [Cricetulus griseus]	mIR-24	1.4	0.006817
RBM14	RNA-binding protein 14 [Cricetulus griseus]	mIR-24	1.28	0.009196
RCC1	Regulator of chromosome condensation [Cricetulus griseus]	mIR-24	1.26	0.011764
RCC2	Protein RCC2 [Cricetulus griseus]	mIR-24	1.29	0.011654
RCN3	Reticulocalbin-3 [Cricetulus griseus]	mIR-24	1.62	0.000845
RINL	Ras and Rab interactor-like protein [Cricetulus griseus]	mIR-24	1.32	0.000117
RNMT	mRNA cap guanine-N7 methyltransferase [Cricetulus griseus]	mIR-24	1.28	0.0077
RP7	60S ribosomal protein L7 [Cricetulus griseus]	mIR-24	1.27	0.001628

RPL10	60S ribosomal protein L10 [Cricetulus griseus]	mIR-24	1.47	0.030368
RPL13	60S ribosomal protein L13 [Cricetulus griseus]	mIR-24	1.32	0.000879
RPL13A	60S ribosomal protein L13a [Cricetulus griseus]	mIR-24	1.3	0.026852
RPL15	60S ribosomal protein L15 [Cricetulus griseus]	mIR-24	1.28	0.005215
RPL17	60S ribosomal protein L17 [Cricetulus griseus]	mIR-24	1.38	0.008468
RPL18A	PREDICTED: 60S ribosomal protein L18a isoform X2 [Cricetulus griseus]	mIR-24	1.26	0.038705
RPL23A	60S ribosomal protein L23a [Cricetulus griseus]	mIR-24	1.3	0.02266
RPL3	60S ribosomal protein L3 [Cricetulus griseus]	mIR-24	1.22	0.020758
RPL36A	60S ribosomal protein L36a [Cricetulus griseus]	mIR-24	1.28	0.004358
RPN1	Dolichyl-diphosphooligosaccharide--protein glycosyltransferase subunit 1 [Cricetulus griseus]	mIR-24	1.35	0.001804
RPS11	40S ribosomal protein S11 [Cricetulus griseus]	mIR-24	1.48	0.001304
RPS18	40S ribosomal protein S18 [Cricetulus griseus]	mIR-24	1.3	0.015964

RPS23	40S ribosomal protein S23 [Cricetulus griseus]	mIR-24	1.37	0.01405
RPS3A	40S ribosomal protein S3a [Cricetulus griseus]	mIR-24	1.3	0.001585
RPS4	40S ribosomal protein S4 [Cricetulus griseus]	mIR-24	1.32	0.005539
RPS6	PREDICTED: 40S ribosomal protein S6 isoform X1 [Cricetulus griseus]	mIR-24	1.81	0.00682
RRM1	Ribonucleoside-diphosphate reductase large subunit [Cricetulus griseus]	mIR-24	1.82	0.007666
RRP12	RRP12-like protein [Cricetulus griseus]	mIR-24	1.38	0.008418
RRP9	U3 small nucleolar RNA-interacting protein 2 [Cricetulus griseus]	mIR-24	1.56	0.01127
RUVBL1	RuvB-like 1 [Cricetulus griseus]	mIR-24	1.58	0.005994
RUVBL2	RuvB-like 2 [Cricetulus griseus]	mIR-24	1.52	0.003174
SEC22B	Vesicle-trafficking protein SEC22b [Cricetulus griseus]	mIR-24	1.29	0.009604
SERBP1	PREDICTED: plasminogen activator inhibitor 1 RNA-binding protein isoform X1 [Cricetulus griseus]	mIR-24	1.36	0.007496
SF3B1	Splicing factor 3B subunit 1 [Cricetulus griseus]	mIR-24	1.67	0.014404
SF3B2	Splicing factor 3B subunit 2 [Cricetulus griseus]	mIR-24	1.42	0.007007

SFPQ	Splicing factor, proline- and glutamine-rich [Cricetulus griseus]	mIR-24	1.35	0.012404
SFXN1	Sideroflexin-1 [Cricetulus griseus]	mIR-24	1.31	0.024124
SLC7A11	Cystine/glutamate transporter [Cricetulus griseus]	mIR-24	2.59	0.001724
SLK	STE20-like serine/threonine-protein kinase [Cricetulus griseus]	mIR-24	1.46	0.00836
SND1	nuclease domain-containing protein 1 [Cricetulus griseus]	mIR-24	1.41	0.00885
SNRNP70	U1 small nuclear ribonucleoprotein 70 kDa [Cricetulus griseus]	mIR-24	1.34	0.002377
SNRPA1	U2 small nuclear ribonucleoprotein A' [Cricetulus griseus]	mIR-24	1.29	0.00788
SNRPB2	U2 small nuclear ribonucleoprotein B'' [Cricetulus griseus]	mIR-24	1.35	0.000558
SNRPD2	Small nuclear ribonucleoprotein Sm D2 [Cricetulus griseus]	mIR-24	1.26	0.007542
SNRPN	Small nuclear ribonucleoprotein-associated protein N [Cricetulus griseus]	mIR-24	1.42	0.000441
SNX2	Sorting nexin-2 [Cricetulus griseus]	mIR-24	1.32	0.022697
SORD	Sorbitol dehydrogenase [Cricetulus griseus]	mIR-24	1.34	0.000987
SRP68	Signal recognition particle 68 kDa protein [Cricetulus griseus]	mIR-24	1.33	0.005184

SRPRB	Signal recognition particle receptor subunit beta [Cricetulus griseus]	mIR-24	1.33	0.003504
SRSF1	Splicing factor, arginine/serine-rich 1 [Cricetulus griseus]	mIR-24	1.51	0.005298
STIP1	Stress-induced-phosphoprotein 1 [Cricetulus griseus]	mIR-24	1.19	0.011514
STK38L	Serine/threonine-protein kinase 38-like [Cricetulus griseus]	mIR-24	2.85	8.53E-05
STOML2	Stomatin-like protein 2 [Cricetulus griseus]	mIR-24	1.48	0.024219
SUPT16H	FACT complex subunit SPT16 [Cricetulus griseus]	mIR-24	1.29	0.000632
TARDBP	TAR DNA-binding protein 43 [Cricetulus griseus]	mIR-24	1.3	0.00873
TARS	Threonyl-tRNA synthetase, cytoplasmic [Cricetulus griseus]	mIR-24	1.31	0.000868
TCOF1	Treacle protein [Cricetulus griseus]	mIR-24	1.35	0.031868
THOP1	Thimet oligopeptidase [Cricetulus griseus]	mIR-24	1.43	0.01074
TIMM44	PREDICTED: mitochondrial import inner membrane translocase subunit TIM44 [Cricetulus griseus]	mIR-24	1.51	0.019012
TIMM8A	Mitochondrial import inner membrane translocase subunit Tim8 A [Cricetulus griseus]	mIR-24	1.67	0.024256

TKT	PREDICTED: transketolase isoform X2 [Cricetulus griseus]	mIR-24	1.26	0.002741
TPD52L2	Uncharacterized protein C20orf135-like [Cricetulus griseus]	mIR-24	1.32	0.001167
TPM3	Tropomyosin alpha-3 chain [Cricetulus griseus]	mIR-24	1.27	0.006601
TRAP1	Heat shock protein 75 kDa, mitochondrial [Cricetulus griseus]	mIR-24	1.34	0.0013
TRMT1L	TRM1-like protein [Cricetulus griseus]	mIR-24	1.52	0.003691
TSFM	Elongation factor Ts, mitochondrial [Cricetulus griseus]	mIR-24	1.31	0.00579
TSTS	RecName: Full=Thiosulfate sulfurtransferase; AltName: Full=Rhodanese	mIR-24	1.61	0.000119
TTLL12	Tubulin--tyrosine ligase-like protein 12 [Cricetulus griseus]	mIR-24	1.45	0.000194
TUFM	Elongation factor Tu, mitochondrial [Cricetulus griseus]	mIR-24	1.35	0.002292
UBAP2L	Ubiquitin-associated protein 2-like [Cricetulus griseus]	mIR-24	1.43	0.021691
UPF1	Regulator of nonsense transcripts 1 [Cricetulus griseus]	mIR-24	1.38	0.006308
USP5	Ubiquitin carboxyl-terminal hydrolase 5 [Cricetulus griseus]	mIR-24	1.4	0.015407

VARS	Valyl-tRNA synthetase [Cricetulus griseus]	mIR-24	1.31	0.003383
VCP	Transitional endoplasmic reticulum ATPase [Cricetulus griseus]	mIR-24	1.35	0.00528
VDAC2	Voltage-dependent anion-selective channel protein 2 [Cricetulus griseus]	mIR-24	1.29	0.009657
WARS	PREDICTED: tryptophan--tRNA ligase, cytoplasmic isoform X2 [Cricetulus griseus]	mIR-24	1.52	0.007185
WDR12	Ribosome biogenesis protein WDR12 [Cricetulus griseus]	mIR-24	1.31	0.012643
WDR5	WD repeat-containing protein 5 [Cricetulus griseus]	mIR-24	1.61	0.004475
XPNPEP1	Xaa-Pro aminopeptidase 1 [Cricetulus griseus]	mIR-24	1.42	0.0179
XPO5	Exportin-5 [Cricetulus griseus]	mIR-24	3.41	0.000122
YARS	Tyrosyl-tRNA synthetase, cytoplasmic [Cricetulus griseus]	mIR-24	1.27	0.006098
YTHDF1	YTH domain family protein 1 [Cricetulus griseus]	mIR-24	1.47	0.002222
ZC3H14	Zinc finger CCCH domain-containing protein 14 [Cricetulus griseus]	mIR-24	2	0.032746
ZC3H4	Zinc finger CCCH domain-containing protein 4, partial [Cricetulus griseus]	mIR-24	1.4	0.010908

ZCCHC3	Zinc finger CCHC domain-containing protein 3 [Cricetulus griseus]	mIR-24	1.86	0.00191
ZPR1	Zinc finger protein ZPR1 [Cricetulus griseus]	mIR-24	1.91	0.020843